MECHANISMS OF CONVECTIVE DRYING IN THICK BEDS OF SOLIDS

BY

ABDULAZIZ ALI ALMUBARAK

Doctor of Philosophy

THE UNIVERSITY OF ASTON IN BIRMINGHAM

October 1995

The University of Aston in Birmingham

Mechanisms of Convective Drying in Thick Beds of Solids

ABDULAZIZ ALI ALMUBARAK

Doctor of Philosophy October 1995

SUMMARY

The literature on heat and mass transfer mechanisms in the convective drying of thick beds of solids has been critically reviewed. Related mathematical models of heat transfer are also considered.

Experimental and theoretical studies were made of the temperature distribution within beds, and of drying rates, with various materials undergoing convective drying. The experimental work covered thick beds of hygroscopic and non-hygroscopic materials (glass beads of different diameters, polystyrene pellets, activated alumina and wood powder) at air temperatures of 54 °C to 84 °C. Tests were carried out in a laboratory drying apparatus comprising a wind tunnel through which the air, of controlled temperature and humidity, was passed over a sample suspended from a balance. Thermocouples were inserted at different depths within the sample bed.

The temperature distribution profiles for both hygroscopic and non-hygroscopic beds exhibited a clear difference between the temperatures at the surface and bottom during the constant rate period. An effective method was introduced for predicting the critical moisture content. During the falling rate period the profiles showed the existence of a receding evaporation plane; this divided the system into a hotter dry zone in the upper section and a wet zone near the bottom. A graphical procedure was established to predict accurately the position of the receding evaporation front at any time.

A new mathematical model, based on the receding evaporation front phenomenon, was proposed to predict temperature distributions throughout a bed during drying. Good agreement was obtained when the model was validated by comparing its predictions with experimental data. The model was also able to predict the duration of each drying stage.

In experiments using sample trays of different diameters, the drying rate was found to increase with a decrease in the effective length of the bed surface. During the constant rate period with trays of a small effective length ,i.e. less than 0.08 m, an 'inversion' in temperature distribution occurred in the bed; the bottom temperature increased and became greater than that of the surface. Experimental measurements were verified in several ways to ensure this phenomenon was real. Theoretical explanations are given for both the effective length and temperature inversion phenomena.

Key words: Temperature Distribution Profiles, Receding Evaporation Front, Convective Drying Rate, Effective Length.

Dedication

To my mother,wife and children,

To the memory of my father missed by us all but never forgotten.

Acknowledgements

I would like to express my gratitude to Dr C.J. Mumford for his valued guidance throughout the course of this work. His comments and suggestions were a great help.

I also wish to thank the following people:

Dr E.L. Smith for his assistance with the mathematical modelling.

Dr D. Walton, Mr M.Santoro and Mr M. Lea for their help during the experimental work and in the construction of the apparatus.

My family for their patience and continual encouragement.

CONTENTS

LIST OF FIGURES

LIST OF TABLES

CHAPTER 1

INTRODUCTION

Drying of solids is an important operation in chemical engineering and the majority of solids being processed undergo a drying operation at some stage. Avoidance of product loss or thermal degradation, and the efficiency of energy utilisation are often prime considerations.. However, the drying of solids provides a technical challenge due to the presence of complex interactions between the simultaneous processes of heat and mass transfer, both on the surface and within the structure of the materials being dried.

Drying is generally defined as the removal of residual water from a moist material by heat. Heat is transferred from the surroundings to the wet solid as a result of convection, conduction or radiation and in some cases, as a result of a combination of these effects. Industrial dryers vary in type and design, depending on the principal method of heat transfer employed, and also the physical form of the solid and its mode of support and/or movement.

In drying by convection, the area covered in the present work, heat is supplied to the wet material by direct contact with hot gas at atmospheric pressure and the evaporated moisture is carried away by the gas. This mechanism is widely used in the food stuffs, pharmaceuticals, fine chemicals, wood, ceramics industries and other applications. Examples of convective dryers, also called direct dryers, are tunnel dryers, tray dryers, spray dryers, kilns, etc.

Drying by conduction means that heat is transferred to the solid indirectly by contact with a heated metal surface and the evaporated moisture is carried away by natural convection, by vacuum operation or by a flow of gas. Conductive drying plays an important role in the production of textiles and paper. Drum, agitated pan and rotary dryers are examples of conductive dryers.

In certain dryers, e.g. infra-red dryers, radiation is the main mode of heat transfer. More often it enhances convective or conductive heat transfer, i.e. it provides a minor enhancement in dryers relying predominantly on these modes of transfer. Infrared radiation is often used in drying coatings, thin sheet and films.

Numerous publications on drying have appeared in the chemical engineering literature. However, relatively few studies describe the mechanisms of drying or discuss the general theory of drying. Various theories have been proposed to describe the simultaneous heat and mass transfer processes. Those widely quoted in the literature are the diffusion theory, the capillary theory, the evaporation-condensation theory and the moving boundary theory. The latter, also termed the receding evaporation front theory, is a relatively new theory in drying. It postulates that during the falling rate period, a receding evaporation front is created which divides the system into a wet region and a dry region. However, whilst this phenomenon may provide an acceptable description of the drying mechanism, little work has been carried out to test it. Further research in this area seems merited. Other theories of drying are reported in the next chapter. From a review of the literature, it seems generally that the theory of drying is still relatively poorly understood and

considerable debate still occurs on the mechanisms of drying.

A knowledge of heat and mass transfer mechanisms during the drying of a thick material bed is essential to optimise the process, to ensure the quality of the final product and to achieve satisfactory design of the dryers.

The drying rate curve is conventionally used to characterise the drying process. It is influenced by the nature of the material to be dried and by hot gas conditions such as temperature, humidity and velocity. It is commonly accepted that the drying rate curve can be roughly divided into two sections: the constant and falling rate periods. The point between the two periods is termed the critical moisture content. The critical moisture content has attracted the attention of authors, and the solution of mathematical models depend in many cases on its values. However, the accurate value of critical moisture content is difficult to determine either theoretically or experimentally.

The temperature distribution profiles may provide more information on heat transfer throughout the bed, and on stages of drying and the receding evaporation front phenomenon. These profiles are discussed in Chapter 5.

In convective drying, the whole resistance to heat and mass transfer can be regarded as residing within a thin film in the vicinity of the surface. This effective film or "boundary layer" is affected by the geometry of the system, the gas velocity and roughness of the surface. Heat and mass transfer coefficients and the characteristics of the boundary layer have a direct effect on the drying rate and the mechanisms of drying. This effect is reviewed

in Chapter 7.

Some of the many mathematical models reported in the drying literature are reviewed in Chapters 2 and 3. These models usually result in empirical formulae and their applicability is limited by the mathematical complexities encountered in their analysis. On the other hand, few models have been proposed for analysing the mechanism of drying thick beds on the basis of the receding evaporation front phenomenon. A further deficiency in the existing research is that many of the proposed models have not been validated with corresponding experimental data, but rather, using the results of other tests. This makes the solutions more difficult, and may compromise their validity and reliability, since the limitations of experimental drying conditions differ from one test to another. The lack of experimental work leads to uncertainty regarding the models' predictions. Therefore, it is desirable to study heat and moisture transfer mechanisms through experimental work on the drying of wet materials, to develop an effective model.

The aim of the present project was to contribute to increased understanding of the mechanisms of convective drying, with the ultimate goal of optimum process and dryer design. This was done through theoretical and experimental work on convective drying of thick beds of hygroscopic and non-hygroscopic materials under various conditions, representing a comprehensive study on temperature distribution within solids and the drying rates of various materials.

For the purpose of this work, an experimental laboratory drying apparatus was constructed. This dryer consisted basically of a wind tunnel through which hot dry air was

passed over the sample. A number of experimental techniques and controls were used to obtain reliable data for analysis and study.

CHAPTER 2

BASIC CONCEPTS AND THEORIES OF DRYING

2.1 THE DRYING PROCESS

Drying, in general, usually refers to the removal of a relatively small amount of liquid, usually water, from a solid. [Drying of gases, or liquids, e.g. by adsorption, involve quite different phenomena, as does pre-drying of a solid by expression or extrusion]. In the drying process, heat has to be supplied to the material so that simultaneous heat and mass transfer occurs. Internal moisture flow may occur by a complex mechanism depending on the structure of the solid body, type of moisture bonding, moisture content, temperature, and pressure in any capillaries and/or pores. External conditions such as temperature, humidity, pressure, relative velocity of the drying medium and area of exposed surface also have an effect on the rate of drying.

The rate at which drying is accomplished is governed by the rates of heat and mass transfer . Heat is transferred from the surroundings to the wet solid as a result of convection, conduction or radiation and in some cases as a result of a combination of these effects. Moisture moves inside the wet material as a liquid and/or vapour and is then transferred as vapour from the surface. The transport of moisture internally within the solid is a function of the physical nature of the solid , the temperature and its moisture content . In convective drying, which is the subject of the present study, mass transfer is in the opposite direction to heat transfer; in conductive drying the directions are the same. This has an important significance in relation to the drying temperature required to achieve a practical residence time.

2.2 RATES OF DRYING

Previous work by Lewis (1), Sherwood (2-4) and many others indicates that the process of drying can be divided into a "constant-rate" period and one or two "falling-rate" periods.

Convective drying data are usually obtained experimentally from test samples exposed to an air or gas flow under conditions which enable the weight of the sample to be recorded over given time intervals and the drying rate expressed as change in moisture content with time. Figure 2.1 shows qualitatively a typical drying rate curve; the nature of the curve depends on the type of solid being dried, and the temperature, velocity and humidity of the gas.

The drying rate is established immediately the solid contacts the drying medium as represented in phase AB, i.e. pre-constant rate period. The initial drying rate and the solid surface temperature increase until the heat transfer rate across the solid-air interface reaches a steady value. This initial period is usually quite short and it is often ignored in the analysis of time of drying.

During the constant rate period, phase BC, the surface of the solid is so wet that a continuous film of water exists on the drying surface. This water is entirely unbound water and exerts a vapour pressure equal to that of pure water at the same temperature. The rate of moisture movement within the solid is sufficient to maintain a saturated condition at the surface. The rate of drying is controlled by the rate of heat transfer to the surface, which

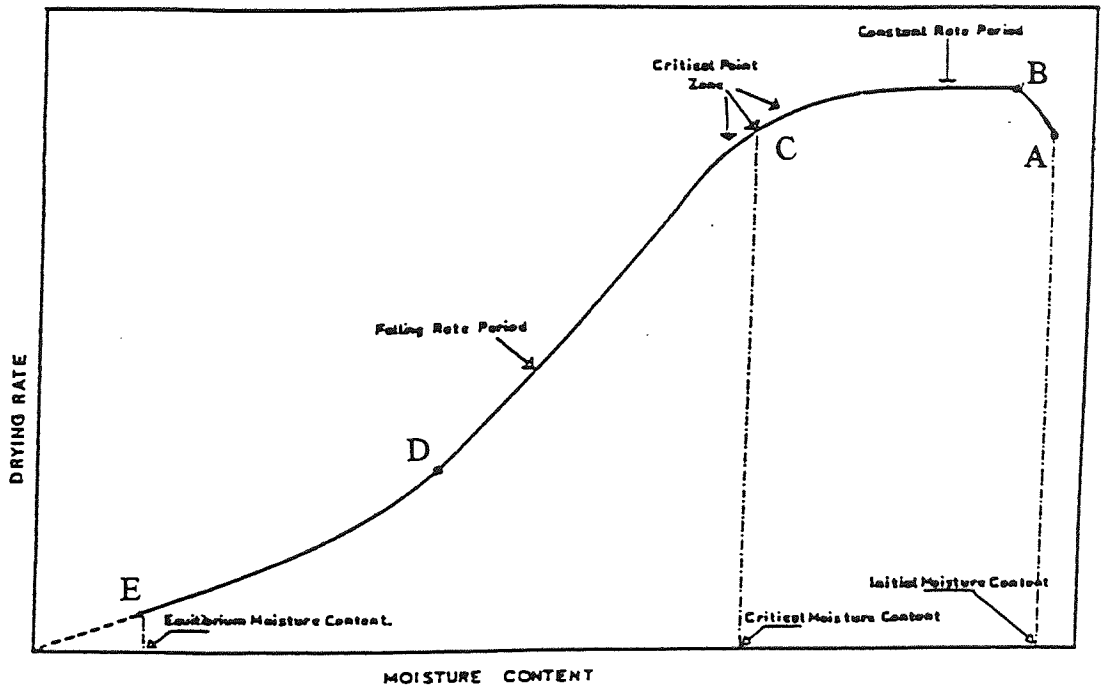

Figure 2.1 A Typical Drying Rate Curve.

provides the latent heat for evaporation of the liquid (5). A dynamic equilibrium is established between the rate of heat supply and the rate of water removal from the surface. The temperature of the saturated surface remains constant. If the heat transfer is mainly by convection, or the effect of heat transfer by conduction and radiation are negligible, the surface temperature approximates to that of the wet bulb temperature of the gas. Under these conditions, the magnitude of the constant-rate period depends on the heat and mass transfer coefficients, geometry of the sample, and the differences in temperature and humidity between the gas stream and the wet surface of the solid. These factors are external variables. The internal variables affecting the internal moisture flow are always assumed to have no effect on the drying rate in the constant rate period (6-8).

Point C in Fig. 2.1 is the "Critical Point". The concentration at this point is termed the Critical Moisture Content. This moisture content is very difficult to predict because of its dependence on the structure of the solid. Therefore, it is usually determined experimentally. At this critical point, there is insufficient water on the surface to form a continuous film. The surface is no longer completely wetted, and the wetted area decreases as discontinuous dry patches are formed on the surface. At this point the drying rate begins to fall, initiating the first falling rate period, phase CD.

During the first falling rate period, the crucial factor influencing the rate of drying is the mechanism by which moisture from inside the material is transferred to the surface. This moisture is transferred mainly by capillary action and exerts its full vapour pressure.

The second falling-rate period begins at point D when the surface is completely dry. The drying rate falls off rapidly. Moisture is held in the finest capillaries and can migrate by moving along the capillary walls or by successive evaporation and condensation between liquid bridges(9). The drying ends at point E in Fig. 2.1 . The moisture content corresponding to this point is the "equilibrium moisture content" and is mainly a property of the solid being dried and of the condition of the gas.

2.3 MOISTURE RETENTION IN SOLIDS

The moisture content of a solid is usually expressed as the mass ratio of moisture to bone-dry material in the solid, i.e. on a 'dry-weight' basis. The moisture contained within a wet solid exerts a vapor pressure to an extent depending upon the nature of moisture retention, the structure of the specific solid and the temperature. A wet solid exposed to a stream of air having constant humidity and temperature, continues to lose moisture until an equilibrium is reached. This moisture content is termed the 'equilibrium moisture content' of the material under the specified conditions. The equilibrium moisture content varies greatly with the type of material for any given percentage relative humidity of air with which it is in contact.

Solids are usually divided into different categories according to their porosity, moisture content, and structure of material, etc. However whilst different classifications can be found in the drying literature (10-14), the most convenient classification is into hygroscopic, non-hygroscopic and colloidal material.

Hygroscopic materials include clay, alumina, silica gel, wood and textiles. These materials possess fine pore spaces and can therefore retain large amounts of bound water. This bound water exerts a vapor pressure less than that of liquid water at the same temperature so that large driving forces, or long residence times, may be required for drying. Shrinkage often occurs in the initial stage of drying this type of solid.

Non-hygroscopic materials include sand, crushed minerals, polymer particles and some ceramics. This type of material has a clearly recognizable porous structure and unbound water moves through capillaries and voids. Thus, such substances are often referred to as 'capillary porous solids'. The medium does not shrink during the drying process.

Colloidal materials include gelatin, agar, soap and some food products. This category of material does not contain pore spaces in its structure. They contain bound water and undergo limited swelling during the drying process.

2.4 THEORETICAL MECHANISMS OF DRYING

Several theories have been proposed to describe the mechanisms of drying in general. Keey (15), Fortes (16), Kisakurek (17), Robbins (18) and Moyne (19) classified classical theories which describe moisture movement in solids. These theories are the diffusion theory, capillary theory and evaporation-condensation theory . However, other theories have been proposed by many researchers and appear in the drying literature; these

also need to be considered and classified when considering the mechanisms of drying. Almost without exception, every researcher relies upon one or more of these theories.

The following section summarises the major theories and classical models which explain the simultaneous heat and moisture transfer processes.

2.4.1 Liquid Diffusion Theory

Lewis (1), Sherwood (2-4), Newman (20) and many other research workers have proposed movement of moisture by liquid diffusion as the principal transfer mechanism in drying. The rate of moisture movement during the falling rate period is expressed by Fick's second law:

$$\frac{\partial C}{\partial t} = D\frac{\partial^2 C}{\partial x^2} \qquad (2.4\text{–}1)$$

The solution of this equation is given by Gilliland (21), Sherwood (22), Crank (23) and others for several boundary conditions for the case of the drying of a slab of thickness 2L from both surfaces, when the diffusivity can be assumed constant and moisture movement is due to diffusion only. A similar solution is also applicable to drying from one side only. Integration of the diffusion equation for several cases can be found in Refs (23 and 24).

Liquid diffusion theory has been subjected to severe criticism. Hougen et al (25) pointed out the limitations in the application of the diffusion equations to drying. They found that the diffusion equation could be applied to the drying of non-granular materials such as soap, glue, gelatine and paste. It could also be applied to the last stage of drying of clay, starch, textiles, wood and paper. In most of the previous work, the diffusion coefficient was assumed to be either constant or linearly dependent on temperature and/or concentration.

Kamei and Shiomi (26) found that the diffusion coefficient of moisture through paper, clay and soap changes somewhat with the temperature of the solid. Van Arsdel (27) presented an approximate numerical procedure for the drying rate calculated with varying diffusion coefficients.

Babbit (28) found that the driving force in diffusion through solids is pressure and not concentration. Clearly these are inter-related but the relationship is rarely linear, owing to the complexities of adsorption and desorption. Using a piece of fibreboard, Babbit demonstrated experimentally that water could flow in response to a vapour gradient and against a water concentration gradient.

The liquid diffusion theory has been described as misleading by Babbit (28), Berger and Pei (29), Ceaglsk and Hougen (30) and many researchers since it has resulted in incorrect predictions and misinterpretation of experimental results. However, moisture movement by liquid diffusion cannot be excluded. Many recent theories take Fick's law as representative for both liquid and vapour movement. The limitations then lie in the

assumption that liquid movement is the only process for moisture transfer in the drying process and the effects of gravity and capillary forces are neglected.

Swanson (31) extended the utility of the diffusion equation by considering the surface film resistance. He found that the resistance of the air film to diffusion is an appreciable portion of the overall resistance. The relative magnitudes of surface and internal resistance in drying are also discussed by Peck et al (32).

2.4.2 Capillary Theory

The fundamentals of capillary flow theory were first laid down by Buckingham (33) in 1907. He introduced the concept of "capillary potential" as the driving force for unsaturated capillary flow. The capillary potential is the pressure difference between water and air at the curved air-water interfaces present in a capillary. A porous solid contains interconnecting pores and channels of varying pore sizes. As water evaporates, a meniscus of liquid water is formed across each pore in the depths of solid. This sets up capillary forces due to the interfacial tension between the water and the solid. These forces provide the driving force for transporting moisture through the pores or voids to the surface.

Gardner (34), Richards (35), Richards and Wilson (36) and Muskat (37) explained the movement of moisture through unsaturated solids in terms of capillary action. Further evidence of the mechanism of capillary action in drying was presented by Ceaglsk and Hougen (30). They provided experimental evidence which showed that the drying rate of a granular solid was determined entirely by the capillary forces and not by diffusion.

Miller and Miller (38, 39) stated that the driving force required for moisture flow is a surface tension gradient and hence is independent of water concentration. Their argument was that both surface tension and viscous flow laws were based on pressure. However the tension was proportional to moisture content only for the homogenous media. Van Vorst (40) described a model for capillary flow based upon a modified Darcy's law. He assumed that the air and the liquid flowed simultaneously in opposite directions and proposed a capillary flow equation containing effective permeabilities for the air and liquid. The capillary relationship was given as:

$$\frac{dp_{fc}}{dx} = Q_L\left(\frac{\mu}{A_c B_L} + \frac{\mu_L}{A_c B_a}\right) + (\rho_L + \rho)g \qquad (2.4\text{-}2)$$

where the symbols are as defined in the Nomenclature. However, no experimental work was done by Van Vorst in order to verify his assumption and to evaluate the assumed permeabilities of the air and liquid.

Other models have been proposed by Martynenko (41), and Kisakurek (42) but their application is limited by the mathematical complexities encountered in their analysis.

2.4.3 Evaporation - Condensation Theory

The evaporation - condensation theory assumes that moisture migration takes place in the pores entirely in the gaseous phase. Water evaporates from the hot side of the pore, migrates under the action of gaseous diffusion and condenses on the cold side, thus transferring its latent heat of evaporation. This mechanism was first utilised by Henry (43)

and later by Cassie et al (44) and others in order to describe the moisture transfer mechanism within textile materials. Henry studied the diffusion of moisture through the pores of cotton bales and assumed the pores to comprise a continuous network of spaces within the solid. For mathematical convenience, it was further assumed that the amount of vapour in the solid varied in a linear manner with both concentration of vapour and temperature.

Moisture movement in the vapour phase was proved by Gurr et al (45) and Kuzmak and Sereda (46, 47) who found that, in an unsaturated porous material such as soil, there is no flow in the liquid phase when water moves due to a temperature gradient. The flow therefore occurs entirely in the vapour phase. However, when there is a pressure gradient, moisture flow occurs in the liquid phase. They also showed that the basic assumption of evaporation - condensation theory was essentially correct even at relatively high pore saturation.

A further refinement of Henry's model was made by Harmathy (48) who developed a theory for a simultaneous heat and mass transfer during the falling rate period of such a system; his model was based on two fundamental assumptions. The first states that all movement of moisture in a porous system takes place in the gaseous phase. The second assumption is that within a porous system the phases are so finely distributed that from the macroscopic view point the system is a quasi-one-phase system. He presented a set of differential equations for continuity of matter, convective mass transport and energy transport. Solving the equations with the appropriate initial and boundary condition yielded the complete moisture content, temperature and pressure history of the system. He

concluded that the evaporation - condensation mechanism is the governing mechanism in drying during the falling rate period.

Recently, Garside, et al (49) investigated the drying of granular fertilisers in several laboratory devices. Spherical granules of various diameters were moulded from moistened ICI No. 2 fertiliser with a solution of radioactive ammonium sulphate. The weight loss of the moisturised granules was continuously measured whilst suspended in a stream of air of controlled temperature and humidity. The experimental results showed that the magnitude of the diffusion coefficients, calculated from the drying rate, and their dependence on porosity were consistent with the mechanism of vapour diffusion. He concluded that moisture transfer in fertiliser of low moisture content is by an evaporation-condensation process.

Garside et al made a theoretical treatment based on numerical integration, by finite difference methods, of the partial differential equation for the moisture transport. The differential equation governing the moisture transfer was written as follows:

$$\frac{\partial C(r,t)}{\partial t} = \frac{DC_1}{T}\left[\frac{\partial^2 P_W(r,t)}{\partial r^2} + \frac{2}{r}\frac{\partial P_W(r,t)}{\partial r}\right] \qquad (2.4\text{-}3)$$

where r is the radius variable, C_1 is constant and P_W is water vapour pressure. The boundary condition at r = 0 was,

$$\frac{\partial P_W(0,t)}{\partial r} = 0 \qquad (2.4\text{-}4)$$

Some agreement was demonstrated between the predicted results and the laboratory measurements.

Some significant points among the theories mentioned above merit further discussion. Liquid-diffusion theory, capillary theory and evaporation-condensation theory have been subjected to severe criticism because of limitations and restrictions in their application to drying processes and their lack of valid physical meaning when applied to a complete drying process. However, these theories are complementary to each other and should be taken as such. Liquid-diffusion theory lends itself more easily to mathematical treatment but predicted moisture distributions are not generally in good agreement with experimental results. However, the capillary, and evaporation-condensation, theories lead to mathematical complexities in analysis which in turn restrict their application.

2.4.4 Receding Evaporation Front Theory

In recent years a new theory of drying has been proposed. This postulates that during the falling rate period, a receding evaporation front is present which divides the system into two regions. In one region the moisture is in vapour form only and this is termed the sorption or 'dry zone'. The other region, termed the 'wet zone', is in the interior of the material and moisture within it is in either a mixed form (vapour and liquid) or in liquid form alone. This concept is widely accepted by Russian authors.

Luikov (50) proposed a two-zone model which assumes the existence of a receding evaporation front inside the body at a certain depth. This front separates the material into a moist zone and an evaporation zone, each with different moisture transfer coefficients. Based on Luikov's analysis, Mikhailov (51) derived equations for a porous body. In the evaporation zone, the moisture transfer was assumed to be in vapour form only. He obtained some solutions for the model and discussed the influence of the parameters included in it. Further details about Luikov's and Mikhailov's work are discussed in Chapter 3. Other models developed by several researchers dealing with this theory are also reported there.

A moving boundary theory provides acceptable descriptions of the drying mechanism and most recent models take into account a moving front during the drying process. Further research on this phenomenon therefore seems useful to cover heat and mass transfer mechanisms and to obtain a clear understanding of the theory of drying.

2.4.5 Thermodynamics Approach

In the last two decades, analyses based upon irreversible thermodynamics have been used to describe mechanisms of drying. From a thermodynamics viewpoint, drying is a process which tends to equilibrium and stops when the chemical potential of the liquid phase is equal to that of the gas phase. This approach was initiated by Cary and Taylor (52,53), who used non-equilibrium irreversible thermodynamics to derive an equation for the drying of soil. They proposed a model for heat and mass transfer in unsaturated porous

media. However, their model does not appear to have been tested by solving the equations with well defined boundary conditions, neither has it been proved experimentally.

Luikov (54,55) derived a system of differential equations representing simultaneous heat and mass transfer in gaseous mixtures and capillary porous bodies such as sand. He based his analysis on the principle of irreversible thermodynamics providing a rigorous means of coupling the fluxes due to a thermal as well as a moisture gradient.

To describe transport phenomena in capillary porous media, Fortes and Okos (56) found some basic differences between the classical approach (mechanistic) and non-equilibrium thermodynamic concepts. The application of irreversible or non-equilibrium thermodynamics to the solution of transport phenomena was based on the following Gibb's equation :

$$TdS = dU + PdV - \Sigma i\ \mu i\ dni \qquad (2.4\text{-}5)$$

which is assumed to be valid for non-equilibrium conditions. They formulated a set of equations for fluxes of heat, vapour and liquid water and applied this to drying sand. Good agreement was obtained.

2.4.6 Other Theories

Various mechanisms of moisture transfer have been identified, as summarised above and it has been seen to be desirable to combine them into a comprehensive theory of drying.

Possibly the first researcher to attempt this approach was Krischer (57). His book, "Die Wissenschaftlichen Grundlagen der Trocknungstechnik", covers all aspects of the drying process. He developed a set of two partial differential equations to describe the coupled heat and mass transfer in hygroscopic media. Krischer's model was based on the assumption that during drying, moisture can migrate in the liquid state by capillary force, and in the vapour state under the influence of a gradient in vapour concentration. The set of equations presented by Krischer are general and may be applicable to many systems of porous media in various stages of drying.

Philip and De Vries (58,59) proposed a theory to describe the transfer of moisture and heat in porous media under a combined moisture and temperature gradient. Heat of wetting of the solid and the transfer of sensible heat were taken into account. They presented a theoretical analysis for a clay loam and sand. Moisture movement was found to be dependent on the boundary conditions for moisture transfer, on the direction of the temperature gradient and on the ratio between the two moisture diffusivities used in the analysis. In a recent paper (60), De Vries attempted to test the theory on the drying of soil. He proved the usefulness of the theory in describing and analysing the experiments.

Recently, Whitaker (61-65) developed a rigorous theory to describe the drying of granular porous media. He attempted to solve equations of momentum, heat and mass transfer for a porous medium at "microscopic" level. A so-called 'volume average method' was then applied in order to obtain "macroscopic" equations. This method was applicable in the discontinuous (pendular) regions and in the continuous (funicular) regions. Solid phase was defined as α, liquid phase as β and vapour (gas) phase as γ, and appropriate boundary

conditions were applied at the interfaces between them. His theory, based on the assumption that a local thermal equilibrium exists, led to a simplification of the equation for energy transport. He presented the following equations,

The mass transfer equation,

$$\frac{\partial Pi}{\partial t} + \nabla(\rho i\, \upsilon i) = 0 \qquad i = 1,2,\ldots \tag{2.4-6}$$

The heat transfer equation,

$$\rho Cp \frac{\partial T}{\partial t} = \lambda \nabla^2 T + \phi \tag{2.4-7}$$

The momentum equation,

$$-\nabla P + \rho g + \mu \nabla^2 \upsilon = 0 \tag{2.4-8}$$

Whitaker and Chou (66) compared predictions from this theory of drying with old experimental results observed by Ceaglsk and Hougen (30) with drying sand. The experimental data, however, were not adequate to validate the model, since drying air velocities were not reported and simultaneous measurements were not made of temperature distributions and saturation distributions. Unfortunately, there was little agreement with experimental results. Therefore, further experimental data are required to test this model.

CHAPTER 3

MECHANISMS OF CONVECTIVE DRYING IN THICK BEDS

3.1 INTRODUCTION

In drying by convection heat is supplied to the wet material by direct contact with a hot gas, normally at atmospheric pressure, and the evaporated moisture is carried away in the exit gas stream. The solid may be exposed in particle, slab or ribbon form, with different methods of promoting solid-gas contact. This form of drying is widely used in the foodstuff industry. Tray dryers, rotary dryers and conveyor, truck, or tunnel dryers are used to dry different types of granular materials. Spray drying is another convective drying process; most pharmaceutical products and fine chemicals are dried by this process (67). Convective drying is predominant in the wood industry, where wood is usually dried in large compartmental kilns. Convective drying is also widely used in the textile and fibres industry. Other materials such as minerals, ceramics, paint pigments and dyes can be dried by convection drying using the various types of dryer described in references (68-70).

The mechanism of drying by convection involves a wet solid being dried by passing a hot gas stream across it, e.g. in a tray dryer, or through it e.g. in a fluidised bed or spray dryer, or in the case of a pneumatic dryer actually conveying the particulate solid in the gas stream. The heated gas serves to transfer heat to the solid by convection and to remove the evaporated vapour. Simultaneous heat and mass transfer occurs within the solid.

Considerable duplication can be found in the literature dealing with the mechanisms

of convective drying . However, little research work has been carried out to study the mechanisms within a thick bed . Experimental and theoretical investigation of drying in a thick bed can provide a clearer picture of moisture movement and heat transfer within the bed. A knowledge of heat and mass transfer mechanisms during the drying of thick beds of various materials is essential to optimize the process, to ensure the quality of the final products and to achieve satisfactory design of the equipment. This can be achieved by experimental and theoretical work on the moisture and temperature distributions throughout thick beds of different materials. In this chapter, the literature on the mechanisms in convective drying are summarised and models to describe the temperature distribution profiles in thick beds of materials are reported.

3.2 HEAT AND MASS TRANSFER MECHANISMS

Early experimental studies in the 1930s (2, 3, 8, 25, 30, 71, 72) dealt with drying of relatively thick beds (0.5 cm - 5 cm) of soap, sand, clay and wood. These studies neglected the effect of heat transfer completely in the descriptions of the mechanisms of drying. The studies assumed the moisture was transferred either by diffusion or by capillary action. This oversimplification, applicable under very specific circumstances, led not only to wrong predictions in some general situations, but also in other cases to misinterpretation of the experimental results.

In an extensive study from 1947 - 1955, Newitt and co-workers (73 - 78) presented a study of the mechanisms of solids drying. Beds of silica flour, sand, and china clay were dried experimentally in copper and glass sample trays. A method of measuring suction

potentials of various materials was developed. Suction potential was a measure of the capillary suction caused by the menisci in the pores, related to the moisture content of the coarse granular solids. This early study discussed the drying rate curve and the stages in the drying process. Various curves of drying rate and suction potential were recorded. The study also supported the capillary theory and confirmed that moisture movement is controlled by the structure of the bed. Newitt and co-workers observed that the rate of drying fell rapidly after the constant rate period and so considered this to be the first falling rate period. A second falling rate period was also observed, during which time the rate decreased slowly until the material approached its equilibrium moisture content under the prevailing conditions.

They also concluded that capillary, gravitational and frictional forces are responsible for the movement of liquid in a solid. In a specific solid bed made up of large particles and pore spaces, the gravitational force would be greater than the capillary force, and frictional effects would be negligible. It was also concluded that the rate of vaporization at any point in the porous structure is controlled by two factors: (i) the difference in vapour pressure between the moisture at that point and the moisture in the drying gas; (ii) the total resistance to vapour flow from the point under consideration to the interface with the gas stream. Actually this is no more than could be predicted from elementary mass transfer theory. They also found that as would be expected, a high gas temperature and high velocity would accelerate the rate of drying in the early stages of drying.

Experimental work on drying balsa wood was carried out by Peck, et al (32) in 1952. Rectangular slabs of balsa wood with thicknesses ranging from 0.2 to 0.85 inch were

suspended from a balance arm which extended into a wind tunnel. Average moisture content versus time was recorded. It was concluded that the log-log plot of drying rate against average concentration of moisture resulted in a straight line. The relation was given as

$$\frac{dX}{dt} = -C\overline{X}^{n} \qquad (3.2\text{-}1)$$

where C is a constant and n was the slope of the log-log plot. The constant rate period could not be distinguished from the falling rate period on the log-log plot, since a straight line was always obtained.

Nissan, et. al. (79) attempted to obtain values for thermal conductivity during the drying of two highly porous one inch thick textiles (Terylene and wool bobbins) in a wind tunnel. Temperature measurements within the bobbins were recorded. The temperature distribution provided a means to estimate the apparent thermal conductivity coefficient of the moist material. They concluded that the thermal conductivity increased towards the surface. Moisture content distribution was not measured. Therefore, doubts remained about the results, since the thermal conductivity coefficient varies with moisture content.

A deep bed (20 - 50 cm) of fine calcium carbonate powder was dried in a wooden tunnel by Toei et al (80). The experiments were carried out at a range of air temperature between 40°C - 110°C and range of air velocity between 1 - 10 m/s. Containers, which could be sub-divided into 9 rings, were designed to enable the measurement of moisture

distribution at different depths after every experiment. It was concluded that the drying period was divided into three periods, i.e. constant rate period and first and second falling rate periods. As would be expected, surface moisture content decreased until it reached the equilibrium moisture content; the evaporating plane then retreated into the bed and the dried-up zone began to extend from the surface.

In a recent study to examine the mechanisms governing liquid movement during the drying of porous solids, Vyas (81) proposed a mathematical model to predict moisture distribution. The movement of moisture in thick porous and granular solids was explained on the basis of capillary theory. The model was applicable for the three drying periods, namely the constant rate, falling rate and receding front. According to the author, the receding front occurs when capillarity is no longer able to bring water to the surface, and the surface will be dried to the corresponding equilibrium moisture content. Vyas provided a general equation for drying rate applicable to all three drying periods. The equation is

$$\frac{\partial W}{\partial t} = \frac{\partial}{\partial x}\left(B\frac{\partial W}{\partial x}\right) \qquad (3.2\text{-}2)$$

where B is the permeability. During the constant rate period, the value of permeability is constant, whereas during the falling rate period it varies with moisture concentration in the drying material. The equation for permeability was given as,

$$B = B_1 e^{2b(W-W_1)} \qquad (3.2\text{-}3)$$

where B_1 is a reference value of permeability at a known value of water concentration W_1; b is a slope of the ln(r) versus W and r is the capillary radius. Equation (3.2-3) was solved by a finite difference method using the following boundary conditions, at x = 1

$$\frac{dW}{dx} = 0 \tag{3.2-4}$$

and at x = 0,

$$\mathbf{m} = \frac{k_c'}{RT}\left(\frac{W}{W_c}\right)^{2/3}\left(P_s - P_{va}\right) \tag{3.2-5}$$

The drying data predicted by theory were compared with the experimental data for fire-resistance brick given by Toei (82). Good agreement was obtained, as shown in Fig. 3.1. In a later paper with Peck and Toei (83), Vyas has shown that information on the pore distribution within a solid is required to help in determination of the permeability as a function of water concentration. One experimental point, at least, is required to determine the value of permeability and to solve the model.

Haertling (84) carried out drying experiments with clay brick of 6 mm thickness and pumice concrete of 9 mm thickness, using air at temperatures between 50°C - 300°C and at a velocity of 5 m/s . Calculated drying rate curves were recorded. Drying rate increased with an increase in air temperature. However, no measurements were made of temperature and moisture distributions throughout the bed.

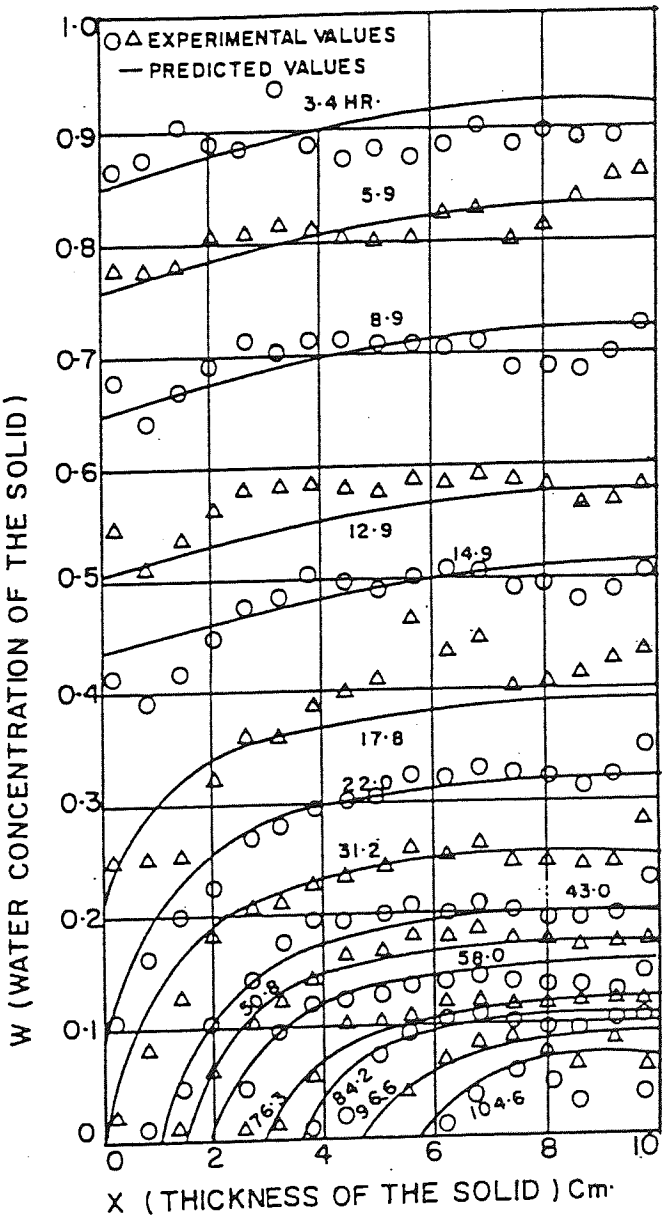

Figure 3.1 Water concentration versus thickness for fire-resistance brick.

An experimental drier apparatus was used by Wang and Brennan (85) to investigate the drying behavior of potato. Slabs of Desiree potato with thicknesses varying from 4 to 10 mm were used. The drying experiments were carried out in air at temperatures between 40°C to 70°C, and at a velocity between 3.30 to 4.5 m/s. It was concluded that dry bulb temperature of the sample had a strong influence on drying behavior. Fig. 3.2 shows the variation of moisture content at different air temperatures. However, the air velocity had little effect on the drying rate. Other studies on potato drying are described in reference (86).

Dressel and Militzer (87) proposed a model for mass transfer within a drying solid. The model was based on the diffusion theory. The differential equation for mass transfer was written as

$$\frac{\partial X}{\partial t} = \frac{x^2 \partial^2}{t \partial x^2}(D * X) \tag{3.2-6}$$

where D* is a normalized effective transfer coefficient equal to $D_{eff}\, t/x^2$. The boundary condition was

$$\frac{\partial X}{\partial x} = \frac{\mathbf{mt}}{\rho D * x^2}(Y_i - Y) \tag{3.2-7}$$

An iterative method was necessary to solve the model. Predictions from the model were not however compared with experimental results.

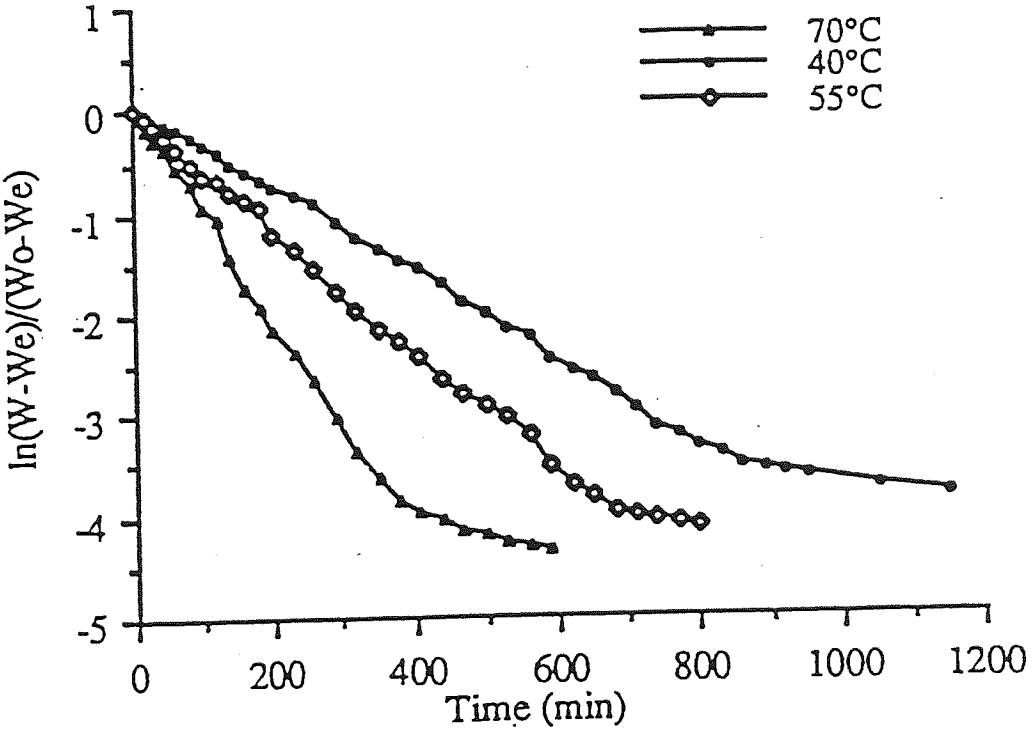

Figure 3.2 Variation of average moisture content of potato versus time at different air temperatures.

Other models (88 - 90) have been proposed to predict moisture movement through a bed of wet material. However, because of lack of validation by experimental data uncertain results were obtained. Therefore, these models can be considered unreliable.

Marc Part (91) put forward a new method for determining the rates of heat, mass and momentum transfers between a porous material and a convective external flow based on the use of two bidimensional computer codes, one involving laminar and turbulent boundary type flow calculation, the other allowing calculation of moisture content evolution in a porous medium. Simulation was performed considering a specific geometrical configuration with initial and boundary conditions. The model gave a method to predict heat and mass transfer coefficients between an external flow and a capillary porous solid. However, no comparison was drawn between the numerical results and experimental data.

In a study on the convective drying of sand, Oliveira (92) supported the proposal of Whitaker and Chou relating to the division of the drying medium into three regions. In Region 1, where the moisture content X is greater than the critical moisture content X_{cr}, the liquid phase is continuous and flows by capillary action. In the constant drying rate period, this region fills all the material. In Region 2 where $0 < X < X_{cr}$, the capillaries become discontinuous and liquid phase transport becomes negligible. This region is near the surface during the first falling rate period. Region 3 appears in the second falling rate period, where moisture content equals zero and water flows only by vapour diffusion. However, the three regions may co-exist in the second falling rate period.

Cunningham and Kelly (93) examined both experimental and theoretical moisture

concentration profiles during the drying of cylindrical beds (9.5 cm diameter and 4.5 cm deep) of glass beads with diameters of 485 μm. A model was developed using equilibrium suction pressure data. The computer model gave good results when validated with experimental data. In order to determine the mass transfer coefficient for the bed surface, the surface moisture content and suction pressure must be determined as a function of the average bed moisture content.

A recent study of the convective drying of a 6 mm layer of natural crumb rubber with hot air passing over the surface, was presented by Cousin et al (94). The evolution of temperature profiles within the solid crumb and profiles of temperature and relative humidity of intergranular air and of water content in the crumb were presented. The results presented were from different experiments. In spite of the precautions taken to control the procedure for the preparation of granules, natural variations in latex could not be avoided. Therefore, the curves of a standard experiment representing the evolution of the different quantities were reconstituted as if the measurements had been made during a single drying experiment. However, there was no scientific analysis of the experimental results.

Moyne and co-workers have published extensively (95 - 100) on the kinetics of high temperature drying of softwood and hardwood. In laboratory work, the researchers dried several types of 27 mm thick softwood and hardwood at temperatures in the range 100°C - 180°C in superheated steam and in moist air. The boards were placed lengthwise on a horizontal plate in a test section of a wind tunnel. Measurements of temperature, pressure and moisture content were recorded. They concluded that in the first period of drying, the temperature at the board surface is close to the boiling point of water (100°C), and the

drying rate is governed by the heat transfer relations. Moisture migration occurred essentially in the liquid phase with capillary pressure as the driving force. During the second period, the moisture at the board surface fell below the fibre saturation point and the temperature increased above the boiling point of water. Simultaneously, the total pressure of the vapour phase inside the wood increased quickly due to the increase of saturated vapour pressure with temperature. The over pressure field within the board shows the existence of pressure gradients which induce new driving forces for mass flow. In spite of the attempt by the researchers to analyze the moisture and temperature flows in the board, they could not give a clear picture of the mechanism of drying in the board, probably because of the complex structure of the wood. In addition, they did not take into account the theory of the receding evaporation front and the two zone model in their analysis, which may give a better explanation of the results obtained.

Schadler and Kast (101, 102) dried non-hygroscopic, capillary porous bodies saturated with liquid at an air temperature in range 30°C to 70°C and at velocities in the range 0.15 - 0.35 m/s . The drying rates for sintered bodies of crushed glass and filterstones of 0.35 mm mean particle size were investigated. Dimensions of the beds were however not reported. Different liquids, e.g. water, benzene, methanol were used. Drying rate curves were calculated and reported. From the investigation of drying rate in the constant rate period it was, as would be expected, possible to predict the critical moisture content. They concluded that due to the high evaporation rates of the liquids, the drying rate varied in a wide range at low air temperature and at low air velocity.

Experimental and theoretical studies of mass transfer phenomena were presented by

Bories, Bacon and Recan (103, 104). The experiments were performed on a dry unsaturated porous medium made of sand in a wind tunnel at an air temperature of 50°C. Moisture distribution profiles were reported. The mass transfer equation was written as follows.

$$(1+\gamma)\frac{\partial W}{\partial t}+\beta\frac{\partial T}{\partial t}=\frac{\partial}{\partial x}\left(D_w+\frac{\partial W}{\partial x}D_T\frac{\partial T}{\partial x}-\frac{\rho_L}{\rho_o}B_{eff}\vec{k}\right) \tag{3.2-8}$$

where B_{eff} is the effective permeability and $\vec{k}$ is the unit vector on the vertical axis of the coordinates system. The coefficients γ and β in Equation (3.2-8), were given by:

$$\gamma=\frac{\left(\psi-\frac{\rho_o}{\rho_L}W\right)D_{AB}}{f.D\frac{P}{P-P_{va}}}-\frac{\rho_v}{\rho_L} \tag{3.2-9}$$

and

$$\beta=\left(\frac{D_T}{f.D\frac{P}{P-P_{va}}}-\frac{1}{T}\frac{\rho_v}{\rho_o}\right)\left(\psi-\frac{\rho_o}{\rho_L}W\right) \tag{3.2-10}$$

where f is a parameter depending on the structure of the porous material. The proposed model was solved by the Galerkin method with a linear finite elements approximation. The numerical results were compared with the experimental data and an agreement was

obtained. The results confirmed the development of a dry zone in the upper part of the sample and a wet zone in the lower part. The researchers concluded that because of the moisture gradient within the bed, the liquid flow moves toward the dry zone, whereas the gas phase flow moves toward the wet zone because of the temperature gradient.

The work of Krischer on moisture transfer in drying materials has been adapted, extended and used for verification purposes in recent work by other researchers. Przesmycki and Strumillo (105) proposed a model for the drying of hygroscopic - porous materials based on Krischer's approach. The model is based upon the phenomenon of recession of the evaporation zone into the body and takes into account shrinkage of the dried body. It was assumed that in the general case, the dried body material could be divided into three zones: dry, evaporation and wet. During the constant rate drying rate period, the wet zone extends throughout the whole body and evaporation takes place from the surface of the drying medium. The other zones subsequently appear during the falling rate periods. In the evaporation zone, moisture transfer occurs in both the liquid and gaseous phases.

It can be concluded that in general there has been little published work on the convective drying of thick beds i.e. beds > 1 mm deep. This work has concentrated mostly on the construction of drying rate curves, identification of the stages of drying, and the mechanisms of moisture transfer relating to specific materials. Theoretical models have been proposed for mass transfer that occur under various drying conditions and for a variety of geometries. However, little experimental and theoretical work has been done on the measurement or prediction of the distribution of temperature and moisture throughout the

wet material. Furthermore, only a few authors have taken into account the two zone model and the receding evaporation front phenomenon which appears in all thick materials during the falling rate period. Obviously, this phenomenon is not yet fully understood. Therefore, experimental work to measure the moisture and temperature distributions in thick beds appeared worthwhile to provide a better understanding of the mechanisms of drying and to assist in the optimum design of convective dryers.

In previous studies, the material to be dried, or the sample container, was always suspended or placed on the base of the wind tunnel so that convective drying occurred from the bed surface. However this method enables heat to be transferred by conduction through the base of the tunnel, or through the sides of the sample container, which affects the temperature distribution throughout the bed and leads to incorrect results. Moreover, the air stream can induce vibration of the suspended sample which will affect the measurement of the weight loss. Therefore, it was deduced that more attention was required to the sample container and its position in the wind tunnel.

Heat and mass transfer coefficients are functions of fluid properties, the system geometry and the flow velocity. Therefore, the geometry of the exposed surface would be expected to have a significant effect on both the drying rate and the temperature distribution profiles within the bed. However, little attention has previously been given to this effect.

In the present research, a comprehensive programme of experimental work was followed to investigate the temperature distribution profiles within thick beds of hygroscopic and non-hygroscopic materials in contact with a flow of air at a fixed

temperature. The average moisture contents were measured and the drying rate curves constructed . This work is discussed in Chapter Five. Chapter Seven describes experimental and analytical work which investigated the influence of geometry of the exposed surface upon the drying rate and the temperature distribution profiles.

3.3 MATHEMATICAL MODELS OF HEAT TRANSFER

As stated in the previous section, early studies completely neglected the effect of the heat transfer process upon the mechanism of drying. Additional models were subsequently proposed, taking into account the effect of heat transfer. Krischer (57) in 1956 was the first to propose a model which included the heat transfer mechanism. He developed a set of two partial differential equations for the coupled rates of heat and mass transfer in hygroscopic media. However, many difficulties were encountered in determining the surface boundary conditions. An assumption was therefore made that at the surface of the drying material, the corresponding equilibrium values of the dependent variables were reached instantaneously at the beginning of the drying process. For this reason, the results were not satisfactory.

As to a general description of heat and mass transfer in unsaturated porous bodies, a major contribution is made by the work of Philip and De Vries (58) on the physics of soil. They incorporated terms in the gradients of temperature for the liquid and vapour movement within porous media. However the defined coefficients required determination by experiments under specific conditions. Hence this approach would become somewhat complicated in describing drying under process conditions.

Based on Krischer's approach, Berger and Pei (29) proposed a model for heat transfer to determine the temperature of the drying material. The differential equation for heat transfer was:

$$\frac{\partial T}{\partial t} = \alpha \frac{\partial^2 T}{\partial x^2} + \frac{\Delta hv}{\rho_s Cp_s}\left[k_c' \left[(\varepsilon - X)\frac{\partial^2 P_{va}}{\partial x^2} - \frac{\partial X}{\partial x}\frac{\partial P_{va}}{\partial x} \right] - (\varepsilon - X)\frac{\partial P_{va}}{\partial t} + P_{va}\frac{\partial X}{\partial t} \right] \quad (3.3\text{-}1)$$

The boundary conditions at the surface x = 0, was

$$h(T_a - T_s) = \Delta hv D_L P_L \frac{\partial X}{\partial x} - \lambda_m \frac{\partial T}{\partial x} \quad (3.3\text{-}2)$$

and that at the lowest part of the bed, x = L was

$$\frac{\partial T}{\partial x} = 0 \quad (3.3\text{-}3)$$

Berger and Pei solved the non-linear algebraic equation by an iterative procedure similar to the method of successive over-relaxation. The temperature of the surface was estimated during the falling rate period. However, the predictions were not validated with experimental data.

A significant limitation in the above models was that they did not take into account the receding evaporation front phenomenon and the existence of the two zones during the

falling rate period. This was probably because the receding front phenomenon was not well known at that time. Unfortunately, even some models proposed recently (106 - 109) attempted to describe temperature distribution profiles in the drying material without considering the moving boundary and two zones theory. These models are therefore misleading and are unreliable to predict the temperature distribution throughout the beds, especially for thick beds. However, they may be acceptable, with some care, to predict an average temperature for drying thin beds, i.e. beds < 1 mm thick..

A few models have recently been proposed on the basis of the receding evaporation front phenomenon to predict the temperature distribution in thick beds. Toei (110), was probably the first to adopt this theory, and proposed a set of equations for both the dry zone and the wet zone. The term "asymptotic temperature" was introduced to describe the temperature of the moving boundary. This temperature was assumed constant during the falling rate period. Toie ignored the temperature distribution in the constant rate period in his calculations. A comparison was made between the analytical solution and experimental results from drying a bed of polymer resin granules. The model did not predict the temperature gradient, in the constant period nor in the wet zone during the falling rate period. Further comparisons with experimental results may be necessary to verify this model.

On the basis of Stefan's model for the freezing water, Luikov (111) proposed a model for heat transfer in capillary porous bodies during the falling rate period. He developed a system of differential equations with complex boundary conditions. The heat transfer equation was written as,

$$Cp\ \rho_s \frac{\partial T}{\partial t} = \frac{\partial}{\partial x}\left(\lambda \frac{\partial T}{\partial x}\right) + \varepsilon * \Delta hv \rho_s \frac{\partial X}{\partial t} \tag{3.3-4}$$

where, ε^*, is a phase conversion factor of liquid into vapour. This conversion factor varies with moisture content continuously and may be written for porous materials as,

$$\varepsilon^*(x,t) = H^*(x) - H^*(x - \beta^* t) \tag{3.3-5}$$

$H^*(x)$ is the single Heaviside function,

$$H^*(x) = \begin{cases} 0 & x \le f(t) \\ 1 & x > f(t) \end{cases} \tag{3.3-6}$$

and β^* is a coefficient defined as

$$\beta^* = \frac{\rho_s P}{\rho_L \varepsilon - \rho_s X} \tag{3.3-7}$$

Because of great difficulties in the solution of the problem, Luikov reduced the differential equation to an ordinary heat transfer relationship. He did not however display the theoretical solution or graphical results for his model. Moreover, no comparison with the experimental results was provided.

Based on Luikov's model, Mikhailov (51, 112) derived differential equations for heat transfer during the falling rate period. The equations were expressed in a non-dimensional form for a half space of the system (x>0) as

$$\frac{\partial T_i(x,F)}{\partial F} = \alpha_i \frac{\partial^2 T_i(x,F)}{\partial x^2} - \varepsilon_i * KO_i \frac{\partial \theta *_i (x,F)}{\partial F} \qquad (3.3\text{-}8)$$

where i = 1 refers to the evaporation zone and i = 2 indicates the moist zone. F is the Fourier number, KO is the Kossovithich number, and the term θ*i (x, F) represents the non-dimensional mass transfer potential. Mikhailov introduced several non-dimensional numbers, which made the solution more complicated. One set of results is shown in Fig. 3.3, which illustrates the effect of variability of Luikov number on non-dimensional temperature. Obviously, the Figure cannot describe the constant rate period and shows the temperature of the surface only. The temperature distribution throughout the whole bed was not predicted by the model. Furthermore, the model was not validated by experimental results.

Oliveria (92) adopted Whitaker's theoretical analysis (66) and proposed a mathematical model for capillary porous materials. One major problem arising in the solution scheme, was the treatment of boundaries between regions, since they are mobile. Another difficulty may arise from not knowing some of the properties of the drying medium. The numerical results were compared with old experimental data, obtained whilst drying sand, by Ceaglsk and Hougen (30, 113) in 1937. Uncertain agreement was obtained.

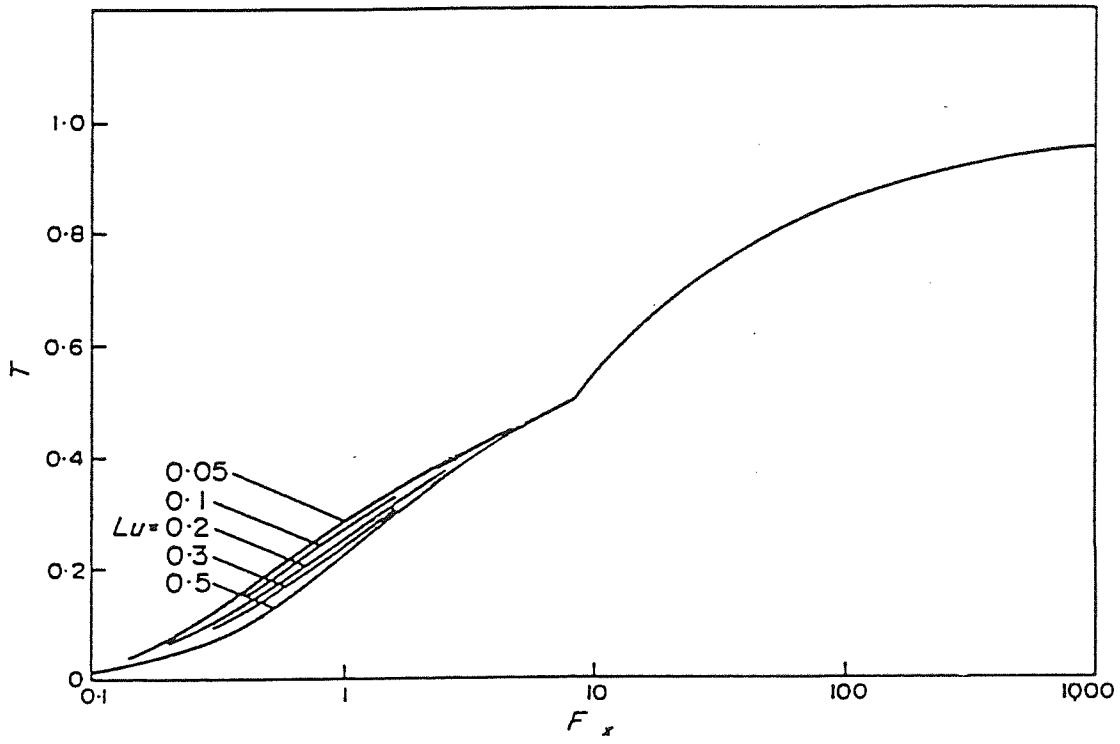

Figure 3.3 The effect of variability of Luikov number, Lu, on non-dimensional temperature; $Lu = \frac{\alpha^*}{\alpha}$.

Szentgyorgyi (114 - 115) described an approximation method for the determination of the temperature distribution profiles within beds of capillary-porous materials. The energy balance equation was written as

$$\rho_s Cp \frac{\partial T}{\partial t} = -\frac{\partial}{\partial x}\left(-\lambda \frac{\partial T}{\partial x}\right) - \Delta hv\, \sigma_v \qquad (3.3\text{-}9)$$

where σ_v is flux of vapour phase moisture.

The heat requirement for heating up the material to be dried and for evaporating the moisture was described as

$$h(Tg - Ts) = \frac{ms}{A} Cpw \frac{dT}{dt} + \Delta hv\, \mathbf{m}(t) \qquad (3.3\text{-}10)$$

On the assumption that the temperature distribution inside the material was uniform, the mean temperature in the first falling rate period as a function of time was given as

$$T = Tg - \left[Tg - T_{wb} + \frac{\Delta hv}{h}(Bt^* - \mathbf{m}_c)\right]$$

$$\exp\left(\frac{-t + t_{cr}}{t^*}\right) + \frac{\Delta hv}{h}(Bt^* - \mathbf{m}(t)) \qquad (3.3\text{-}11)$$

where B = d**m**/dt is constant and t* is the time to reach the equilibrium moisture content. The mean temperatures of the surface and the evaporation front during the second falling

period can be calculated from the following equations.

$$Tg - Ts = \frac{\Delta hv\, \mathbf{m}}{\lambda_d} \frac{\lambda_d}{h} \tag{3.3-12}$$

$$Tg - Tf = \frac{\Delta hv\, \mathbf{m}}{\lambda_d} \left(\frac{\lambda_d}{h} + f(t) \right) \tag{3.3-13}$$

The model was applied to experimental results obtained whilst drying a 100 mm by 100 mm by 30 mm thick gypsum plate at a gas temperature of 80°C. Satisfactory agreement was obtained. Clearly, because of the assumption of a uniform temperature inside the material, Szentgyorgyi could not predict a temperature gradient during the constant rate period and within the wet zone during the second falling rate period. [The model was subsequently tested with results from the present work as described in Chapter 6 and showed little agreement.]

A mathematical model of drying of a hygroscopic-porous material has been proposed by Przesmycki and Strumillo (105). A set of differential balance equations were written for three zones; wet zone, evaporation zone and dried zone. It was assumed that liquid transfer might occur in the evaporation zone, even when liquid continuity does not exist. However, there was no indication as to how the position of the two moving boundaries was determined or when the first or second falling rate period commenced. A test material, clay, of 3 cm depth was dried from an initial moisture content of 0.2 kg H_2O/kg dry solid at an air temperature of 80°C. The temperature distributions within the

tested material, demonstrated satisfactory agreement with the model predictions in the latter stages of drying, as shown in Fig. 3.4.

Chen et al (116, 117) proposed a mathematical model for simulation of dielectric heating-enhanced convective drying in granular products. The movement of bound water and its contribution to moisture transfer within hygroscopic materials was discussed. It was assumed that during the falling rate period there is no significant gradient in temperature across the wet region. Complicated equations with different parameters, involving gas and liquid phase permeabilities, need to be solved before the model can be solved. A comparison of the model with experimental data of Przesmycki (105) was given. Chen encountered difficulties in the solution of the model, because of lack of experimental data and of physical property data. The many assumptions therefore lead to uncertain results.

In summary, all the above models ignored the pre-constant rate period in spite of its importance. Secondly, the temperature distribution within the constant rate period was always assumed as uniform inside the material and equal to the surface temperature. However, as the current research demonstrated, this is not always true. Furthermore, only a few models were proposed on the basis of the phenomenon of the receding evaporation front. All models are unable to predict the temperature distribution within the wet zone. The complicated boundary conditions increased the difficulty in finding solutions for models. Moreover, inadequacies in the application of mathematical numerical methods to solve non-linear differential equations with the moving boundaries was another difficulty. Thus, for purposes of simplification of the solution, more assumptions and other characteristic factors have been introduced into the modified models. This led to uncertain

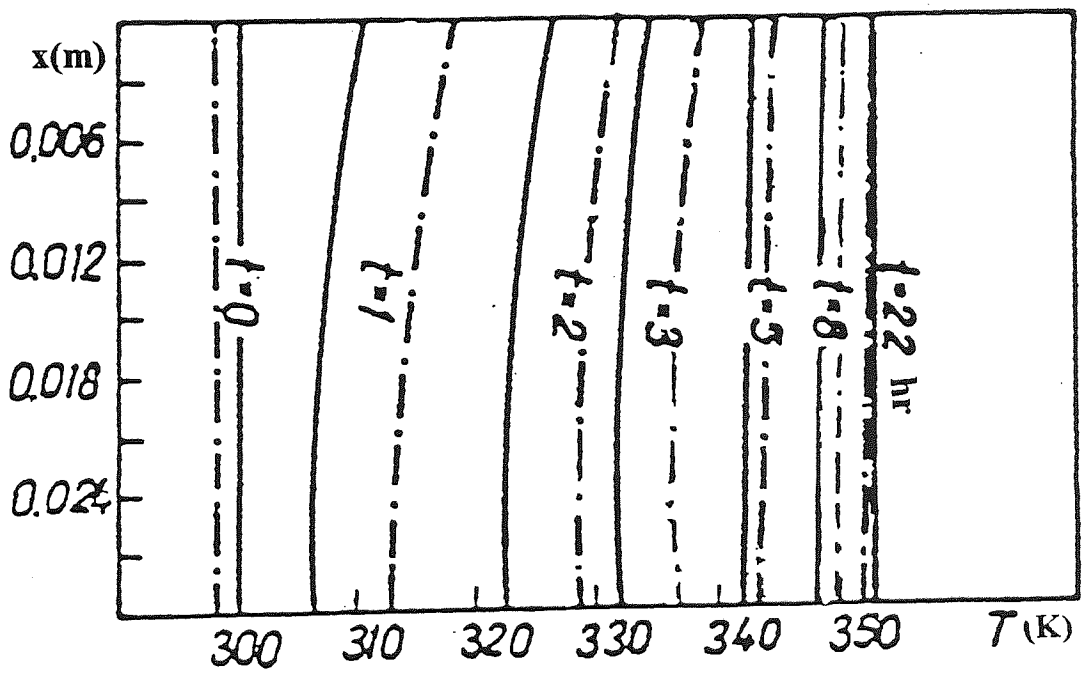

Figure 3.4 The predicted temperature distributions within a bed of clay compared with experimental data (dotted lines); air temperature 80°C .

results being obtained.

Many researchers proposed mathematical models which were not associated with their own experimental work but relied upon the data of others. The model solutions usually differed from the conditions of the laboratory work and from the physical properties of the materials during the experiments. This lack of strictly comparable experimental work led to uncertain accuracy in predictions from the mathematical model.

The physical properties of the materials, and the experimental parameters, e.g. heat and mass transfer coefficients, thermal conductivities, heat capacities, etc., play an important role in the solution of models. The techniques applied to determine these properties and functions has varied from one author to another. In order to obtain more accurate values, more attention must be made to the estimation, or measurement, of these variables.

In general, none of the previous models was successful in providing a clear description and prediction of the temperature distribution profiles in thick wet beds during the various stages of drying. Therefore, it was necessary to study heat and mass transfer mechanisms inside beds of wet material by experiment, to develop an effective model.

CHAPTER 4

EXPERIMENTAL INVESTIGATION

4.1 GENERAL CONSIDERATIONS

Measurement of the moisture content of materials in a laboratory apparatus is a widely-used technique in drying research and technology. Design of the apparatus or dryer for a laboratory scale is mainly based upon the drying kinetics and the particular application. However, in spite of relatively extensive descriptions of experimental work on convective drying in the literature, little information is available explaining the fundamental requirements in the design of the dryer. The scant information on scale-up from laboratory data can be found in references (13, 69, 118).

To obtain reliable results for the convective drying of flat slabs or beds of solids, many factors must be considered for the design of the experimental dryer. These factors include the source of heat to the sample, the gas flow pattern over the sample; the relative size of the sample to the tunnel; the bed depth and the position of the sample inside the dryer.

For the purpose of the present work with beds of hygroscopic and non-hygroscopic solids, an experimental dryer rig was constructed. This dryer consisted basically of a rectangular stainless steel tunnel through which a forced flow of heated air at constant

humidity, velocity and temperature was passed over the sample. An insulated tray containing the sample was positioned centrally in a slot and supported on a metal plate which was suspended from an accurate balance. The loss of weight during the drying process could hence be registered as a function of time. Several thermocouples were inserted through the tray at different depths to measure temperature distribution within the bed. An overall view of the apparatus is shown in Fig. 4.1, and the construction in Fig. 4.2

4.2 THE WIND TUNNEL

Different types of tunnel for the investigation of convective drying of wet materials are described in the literature (97, 119-122). The actual size of the equipment varied depending on the particular application. However, there seems to be little information as to the basis on which the tunnel dimensions were selected.

For the purpose of this work, a fairly uniform flow of air, with a constant velocity, was required over a flat slab. A rectangular stainless steel tunnel joined into diverging and converging conical sections from the two sides was constructed. Figure 4.3 shows the dimensions of the tunnel and the joined sections.

For the characterisation of gas flow, Reynolds number is by far the most important aerodynamic parameter. The air can be considered an incompressible fluid so that,

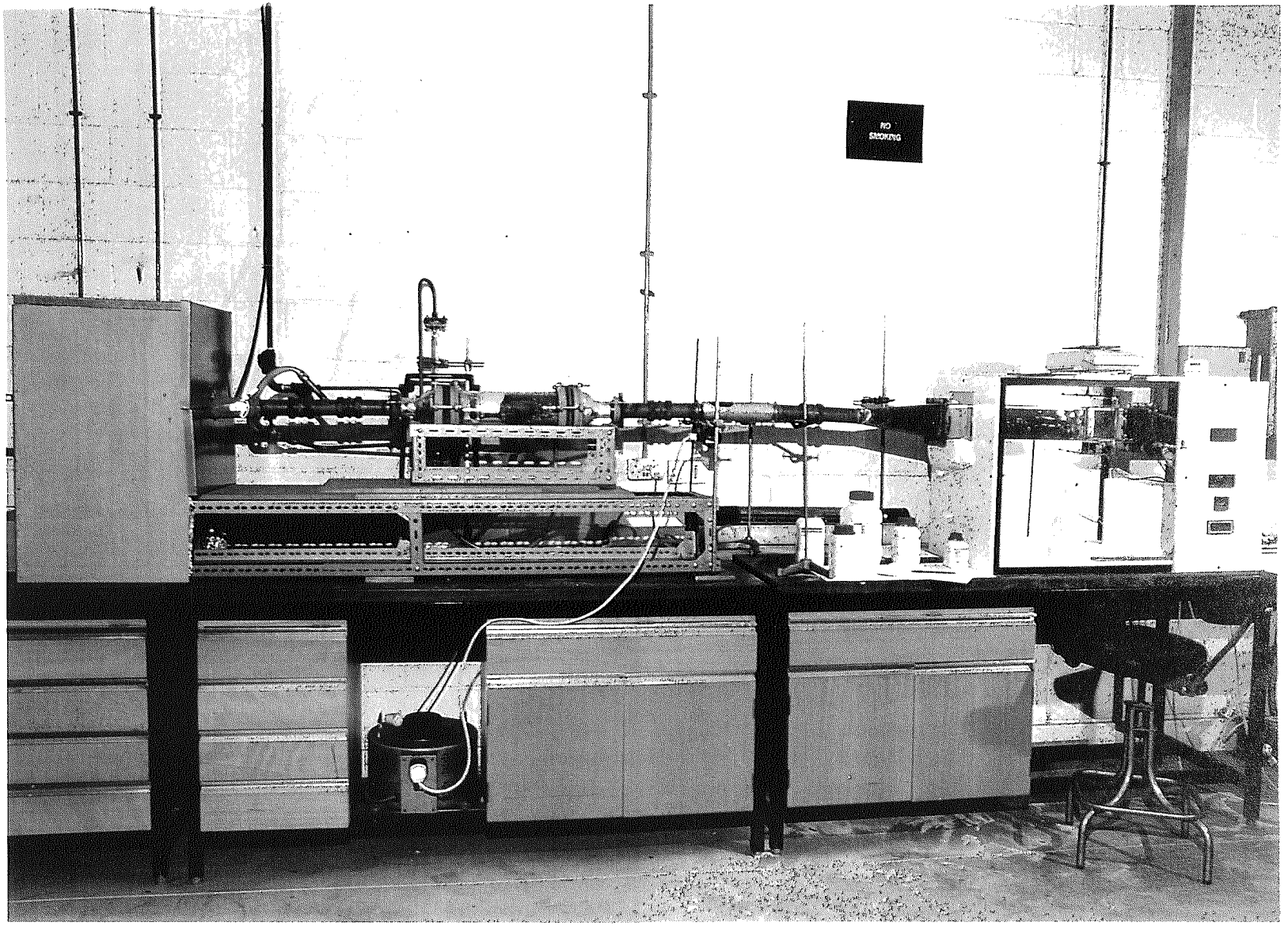

Figure 4.1 Overall view of the dryer rig.

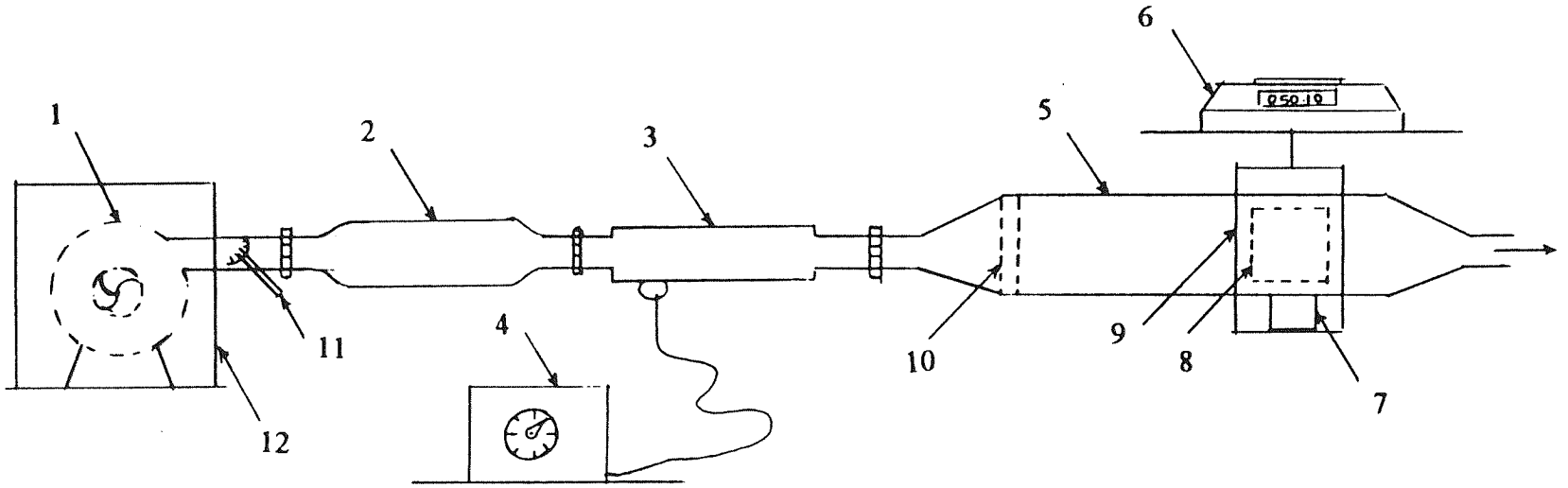

Figure 4.2 Experimental apparatus, 1. fan, 2. pre-drying agent container, 3. electric air heater, 4. voltage regulator, 5. wind tunnel, 6. balance, 7. sample tray, 8. observation port, 9. framework, 10. smoothing grids, 11. regulatory valve, 12. hard board partitions.

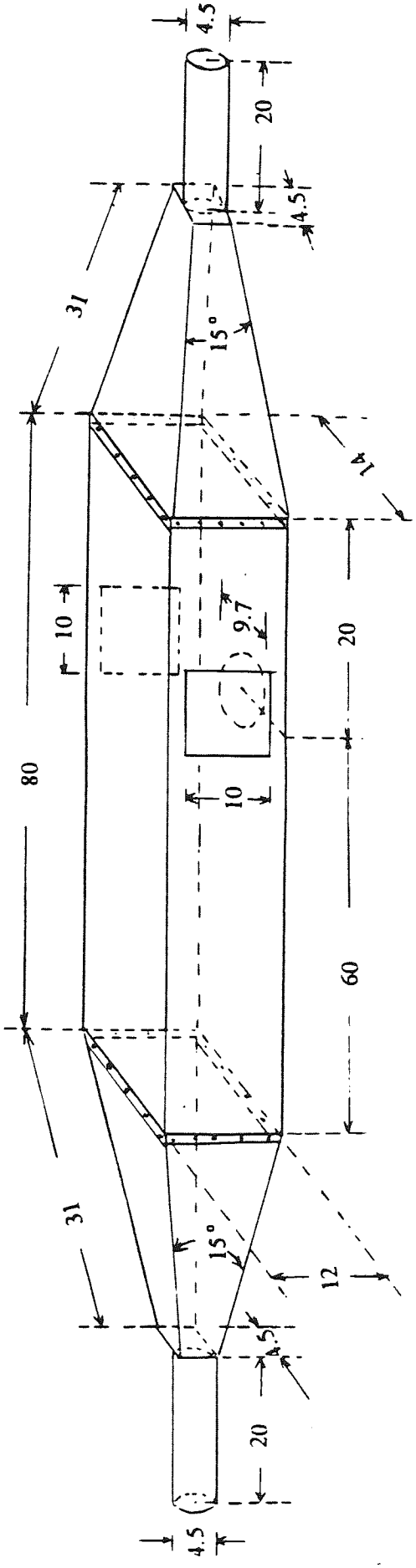

Figure 4.3 Wind tunnel; dimensions in (cm).

$$Re = \frac{\upsilon \rho d}{\mu} \qquad (4.2\text{-}1)$$

The nature of the flow becomes turbulent when values of Re are greater than 4000. Therefore, any value of Re less than 4000 is desirable to obtain a flow rate of uniform profile through the wind tunnel. In Eq. (4.2-1), d is the pipe diameter. However, for non-circular sections, the hydraulic mean diameter ,d_h , may be used instead. Hydraulic mean diameter for a rectangular duct of sides a and b is,

$$d_h = \frac{2ab}{a+b} \qquad (4.2\text{-}2)$$

When a fluid flows over a thin plate, a boundary layer forms over the adjacent surface. The longitudinal velocity rises very steeply from the plate to approximately the stream velocity at the outer boundary of the layer. This gradient in velocity retards the flow of the air stream. The thickness of this boundary layer increases with increasing distance from the leading edge (7, 123) as shown in Fig. 4.4. Near the leading edge, where the thickness of the boundary layer is very small, the flow is laminar. When the thickness of the boundary layer exceeds a critical value, a turbulent flow is induced within it; a laminar sublayer is present within a thin region close to the surface. The formation and the behaviour of the boundary layer are important not only in the flow of fluids, but also in the transfer of heat and mass as discussed in Chapter 7.

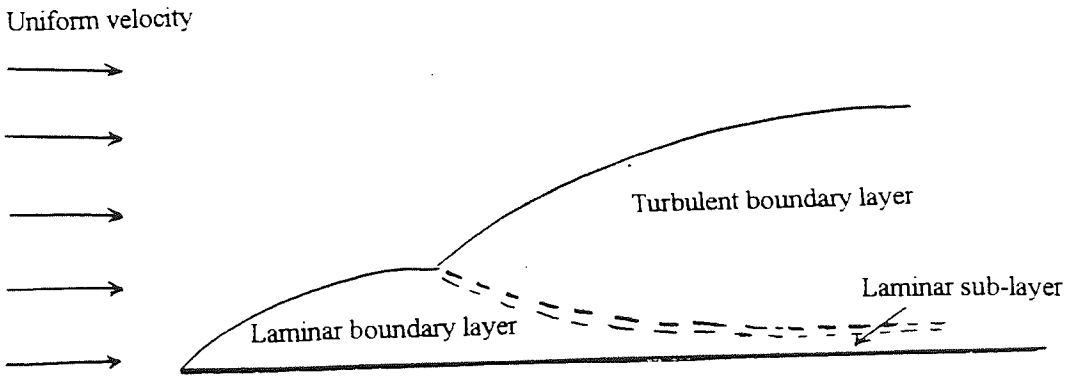

Figure 4.4 Development of boundary layer.

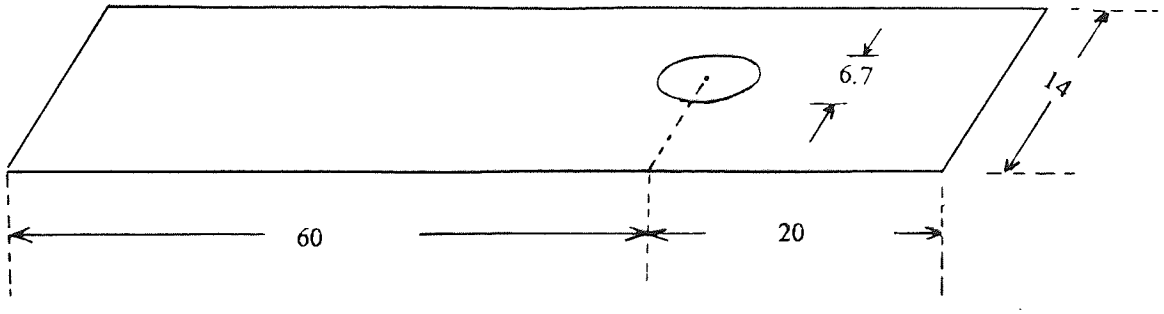

Figure 4.5 A thin stainless steel sheet (with slot for sample tray to fit exactly); dimensions in (cm).

The Reynolds number based on the distance, ℓ, from the leading edge of the plate is expressed as Re, ℓ, defined as,

$$\mathrm{Re}, \ell = \frac{\upsilon \rho \ell}{\mu} \qquad (4.2\text{-}3)$$

The boundary layer is in a turbulent state when $\mathrm{Re}, \ell > 3 \times 10^6$ (123). Equation (4.2-3) was calculated, using the following average operating conditions:

Air velocity	=	0.5 m/s
Density of the drying air	=	0.984 kg/m^3
Viscosity of the drying air	=	2.1142×10^{-5} kg/m.s
The length of the sample plate	=	0.083 m

Thus, the calculation of Re, ℓ gives a value of 1931.5, indicative of a laminar boundary layer.

To avoid extraneous effects of the inner upper wall of the tunnel (wall effect) on the motion of the flow over the sample, it is preferable to have a distance much greater than the thickness of the boundary layer. The thickness of the boundary layer, δ, is defined in reference (7) as,

$$\delta = 4.64 \ell \ (\mathrm{Re}, \ell)^{-0.5} \qquad (4.2\text{-}4)$$

Solution of Eq. (4.2-4) gives a value of thickness of 8.76 mm. Based on this consideration, and using Eq. (4.2-1) and (4.2-2), the cross section of the rectangular duct was evaluated. Thus, the width of the duct was 14 cm and the height was 12 cm.

There is no rigid rule for selecting the length of the tunnel. However, a considerable length is required to obtain a fairly uniform flow of air. Conversely, Lomax (124) has shown that the energy head loss, i.e. the change in pressure drop between two sections in a horizontal pipe, is directly proportional to the mean velocity of flow and the length of the pipe. The energy loss was defined as:

$$h_f = \frac{32\mu l \upsilon}{\rho g d^2} \qquad (4.2\text{-}5)$$

where d is the diameter of pipe and can be substituted by d_h for the rectangular duct. Solving Eq. (4.2-5) by an iterative process assuming different lengths, predicted a negligible magnitude of energy loss for a length less than one metre. Therefore, based on this consideration and for practical reasons, a length of 80 cm was selected for the wind tunnel.

To avoid sudden enlargement because of differences between the size of tube just before the duct and that of the duct, a uniformly diverging conical section was made with an included angle of 15° to act as a calming section and to minimise the pressure drop through the tunnel. This angle was chosen according to Gibson's tests (125, 126) which indicate that the minimum loss occurs when the angle of a conical diffuser is $7.5° < \theta < 35°$. A converging conical duct was built with the same included angle, i.e. 15°, to keep the

pressure drop in the apparatus to a minimum. Moreover, six smoothing grids, 50 mesh x 36SWG - stainless steel, were fitted at the junction of the duct and the diverging section to provide a better velocity distribution. Velocity of air flow was measured above the test section at three positions across the height of the tunnel: near the two inner wall sides of the tunnel and at the middle. The velocity readings were 0.45 m/s near the two sides and 0.55 m/s at the middle, i.e. a fairly uniform air flow with average velocity of 0.5 m/s was obtained.

A circular slot of 9.7 cm diameter was provided in the base of the tunnel through which the sample tray could be inserted. For experiments with a smaller tray diameter, a metal sheet was made of the same material as the tunnel, i.e. polished stainless steel, and with the same dimensions as the tunnel base. This sheet had a circular slot of 6.7 cm to allow the smaller tray diameter to fit as shown in Fig. 4.5. To carry out the experiment with a smaller tray, the converging section of the duct was loosened and the sheet inserted and placed on the tunnel base such that the position of the slot in the sheet coincided with the slot in the tunnel base.

Two glass windows were provided on opposite sides of the test section, through which the material to be dried could be observed. Figure 4.6 shows the wind tunnel and the test section.

To minimise the effect of radiation on the material to be dried, polished stainless steel was selected for the inner wall side of the tunnel, since the emissivity factor of polished stainless steel is 0.074 which is very small. However, the effect of radiation was considered

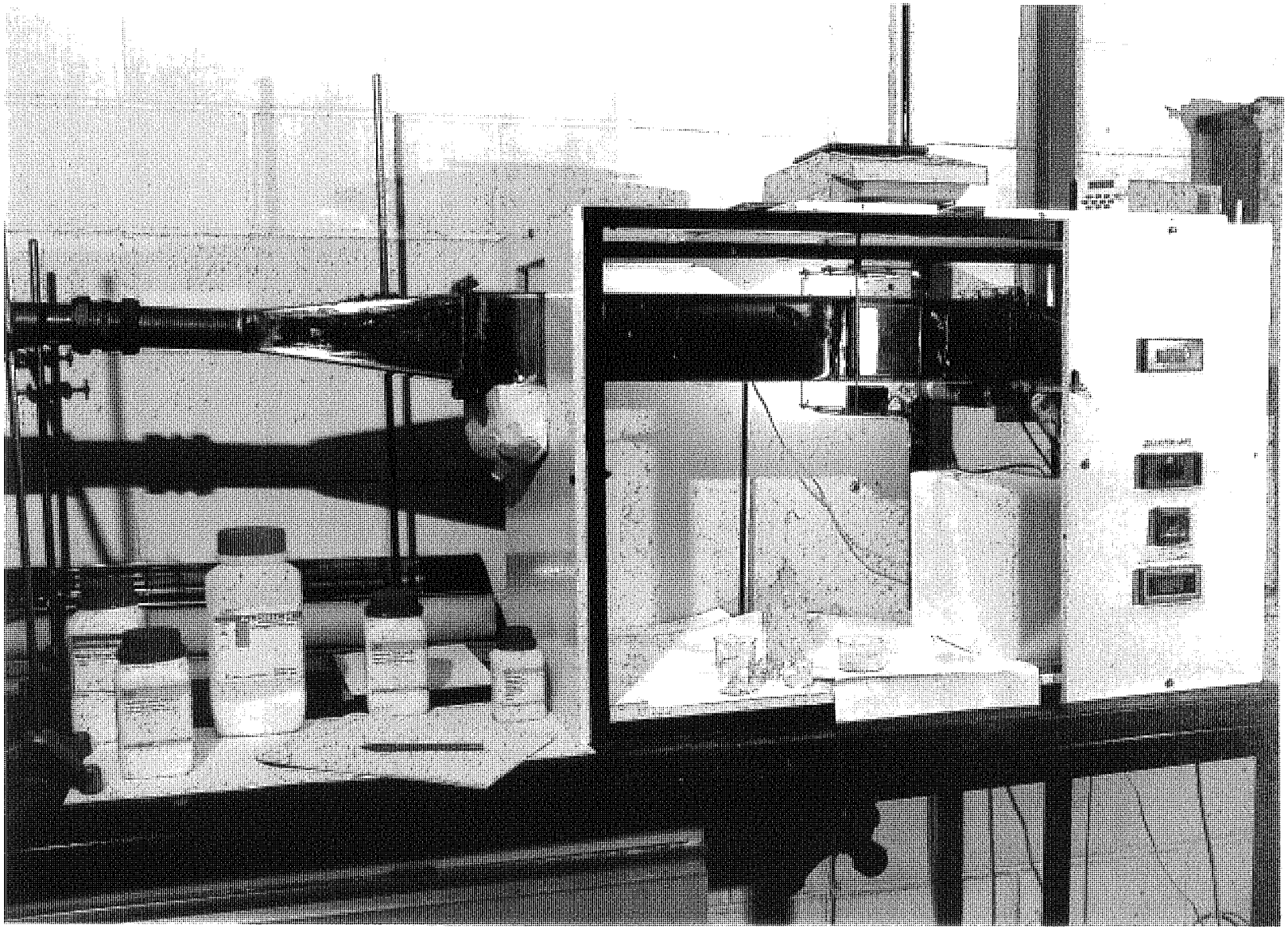

Figure 4.6 The wind tunnel and the test section.

in the calculation of heat transfer coefficients in Chapter 6.

4.3 SAMPLE CONTAINER

Several 1 mm thick glass trays of different diameters and different depths, were designed. The inner wall and the bottom of the sample trays were insulated with either Polychloroprene (neoprene) rubber or latex foam rubber to minimise heat transfer via the glass wall. These types of insulator have very low thermal conductivities (127). Neoprene rubber has a thermal conductivity of 0.0025 W/m.K, whereas the thermal conductivity of latex foam is 0.0009 W/m.K.

Several thermocouples were inserted from one side of the tray at different depths to facilitate measurement of temperature distribution throughout the bed. The distances between thermocouples were not the same for all sample trays. (The distances are reported with the temperature distribution profiles for every experiment.)

Figure 4.7 shows the dimensions and thermocouple positions inside a tray of 8.3 cm diameter and 3.2 cm depth. The dimensions and thicknesses of insulation for other trays are shown in Figures 7.14 - 7.19 in Chapter 7. All trays had a total diameter, i.e. the total of thickness of insulator, thickness of glass wall and inside diameter, of either 9.6 cm or 6.6 cm. This was made to fit in the circular slots of 9.7 cm or 6.7 cm.

A rectangular tray shape 8.3 cm long, 3.7 cm wide and 3.2 cm deep, was designed inside a circular container of 9.6 cm diameter, as shown in Fig. 4.8. Again, this was to

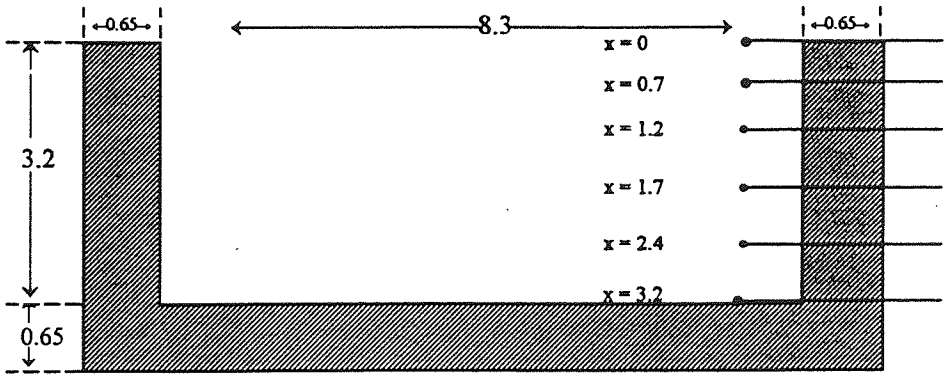

Figure 4.7 A glass sample tray, 8.3 cm internal diameter and 3.2 cm deep; insulated with neoprene rubber; six thermocouples were inserted at different depths; dimensions in (cm).

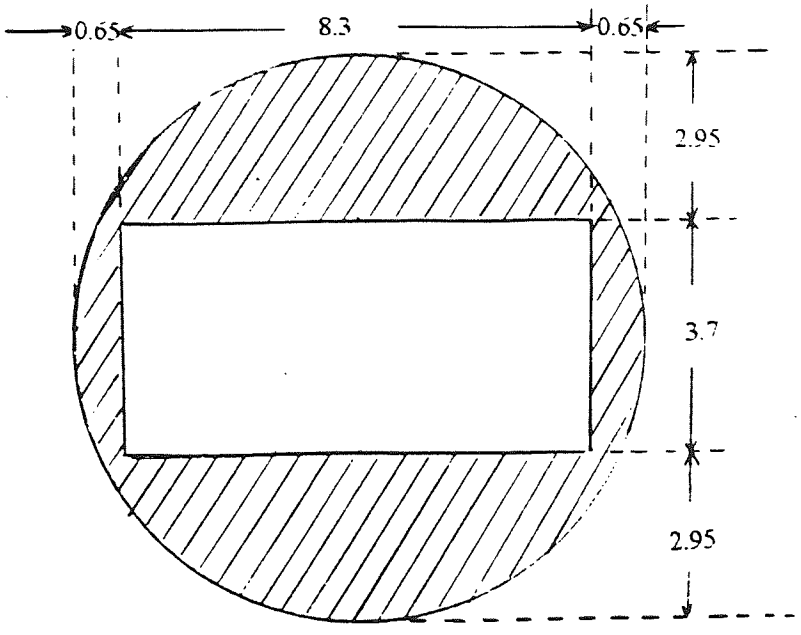

Top view

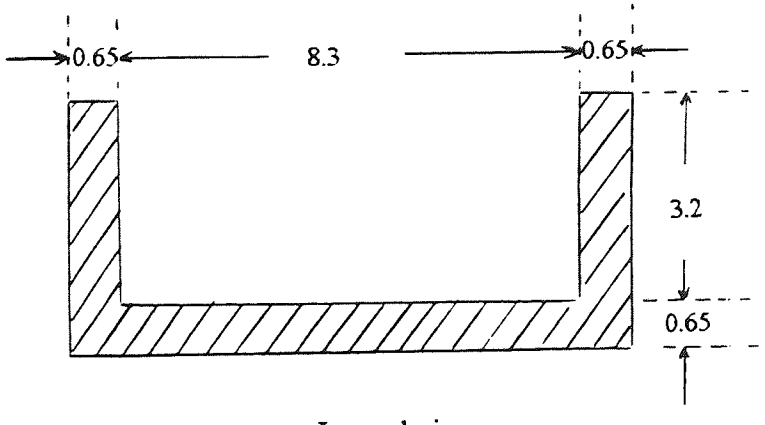

Lateral view

Figure 4.8 A rectangular tray of 8.3 cm long, 3.7 cm width and 3.2 cm deep; insulated with neoprene rubber; dimensions in (cm).

allow this tray to fit properly in the slot. Another rectangular tray 5.3 cm long, 3.7 cm wide and 3.2 cm deep, was made in the same manner.

Attention was paid to the position of the sample tray in the wind tunnel. The tray containing the material was positioned centrally through the slot of the duct, and in such a way that the surface of the sample was flush with the base of the duct. It was also placed on a metal plate which was supported by a linkage (framework) situated around the drying duct and suspended from one arm of the balance. The framework and the whole of the sample tray, except the top, were kept outside the duct to eliminate any heat transfer from the hot air to the wall or bottom of the tray. The arrangement also helped to eliminate any vibration of the framework due to the flowing air which would otherwise have affected the balance readings.

4.4 ANCILLARY EQUIPMENT

A centrifugal fan, Secomak Model 574, with maximum free air delivery rate of 0.142 m^3/s was used for this experimental work. The fan was connected to a regulating valve to control the inlet air velocity to the wind tunnel. To minimize the noise emitted into the laboratory, hardboard partitions lined with an anti-acoustic material were built around the fan.

In order to obtain dry air, a cylindrical pre-dryer was constructed. This dryer consisted of a 45 cm long Q.V.F. horizontal glass pipe of 12 cm OD. It was packed with self-indicating silica gel and calcium alumino-silicate molecular sieve (Type 5A).

An electric air heater, Secomak 571-3 kW, with a maximum outlet temperature of 400°C, was used to heat the dry air to the desired temperature. This was controlled by using a Cressal Torovolt Model 76ZP voltage regulator, connected to the 230 A.C. mains supply. The centrifugal fan, the pre-dryer, the electric air heater and the wind tunnel were interconnected by copper pipe joints. These parts of the dryer were installed horizontally, as in Fig. 4.2 making a total length of 4.27 m.

An Ohaus TS4KD balance was chosen as the best compromise for the precision, sensitivity and capacity required for tray and sample weighing. The balance was dual-range with a capacity of 800/4000 g with readabilities of 0.01/0.1 g respectively. The balance was mounted directly above the tunnel test section on a hardboard structure.

Thermocouples, of welded tip PTFE insulated (Type K), were used to measure the temperatures of the drying air and sample bed. The thermocouples were connected to a thermocouple 12-way selector switch (type K), which enabled readings to be taken from 12 sensors. A digital temperature indicator (type K), which displayed temperatures in degrees centigrade, was used. The inlet and outlet temperatures of the air were measured by two thermocouples fitted inside the wind tunnel. Another thermocouple was fixed just above the slot centre to measure the air temperature (dry bulb temperature) which was passed over the sample. The accuracy of air temperature readings was ± 1°C.

In order to measure the wet-bulb temperature, a covered thermocouple with a fine cotton wick was housed inside a fine tube. One end of the tube was fitted inside the wind tunnel with the thermocouple exposed. The other end was connected externally to a small

reservoir filled with distilled water. The cotton wick hence remained continuously wetted during the experiment. The registered temperature approximated to the wet-bulb temperature. From the dry bulb and wet-bulb temperatures the humidity was estimated using a humidity chart.

An anemometer, TA6000, was inserted through the tunnel slot before and after each experiment to measure the velocity of air. The velocity readings were always within the range 0.45 m/s - 0.55 m/s. All experiments were carried out at an air velocity of approximately 0.5 m/s.

4.5 TESTED MATERIALS

For the purpose of this work, two types of material were selected to be tested experimentally: hygroscopic materials, which hold bound water within their structure, and non-hygroscopic materials, which possess considerable pore spaces and therefore retain unbound water. Glass beads of various diameters (see below) and polystyrene pellets were selected as non-hygroscopic materials. Wood powder and activated alumina were selected as hygroscopic materials.

The glass beads had diameters of approximately 100 μm, 400 μm and 4000 μm diameter respectively. These beads were spherical in shape and inert to water. Particle sizing of the beads was carried out using a Malvern Instruments Master Particle Sizer M3.0. The diameter ranges were found to be,

1. For the glass beads of approximately 100 μm diameter, the actual sizes ranged between 84.3 μm and 112.8 μm.

2. For the glass beads of approximately 400 μm diameter, the size range was between 362.7 μm and 470.2 μm.

3. For the glass beads of approximately 4000 μm diameter, the size ranged between 3890.2 μm and 4122.5 μm.

The polystyrene pellets used were inert and cylindrical. These pellets were subjected to microscopic investigation. The investigation revealed that the pellets were cylindrical in shape, with an average diameter of 300 μm and length of 400 μm.

The activated alumina, Al_2O_3, was a highly hygroscopic solid. This material was neutral type Brockmann I, STD, Ca. 150 mesh. Microscopic investigation revealed particles averaging 90 μm in size.

Wood powder is also a highly hygroscopic solid. This material was investigated using an optical microscopic to estimate the size and shape. This investigation showed that the powder was comprised of non-homogeneous particles with lengths between 100 μm and 300 μm and widths between 45 μm and 120 μm.

4.6 EXPERIMENTAL PROCEDURE

Each experiment was commenced by switching on the centrifugal fan, and then the electric air heater. The voltage regulator was adjusted to provide the desired air temperature. After one hour, the air velocity was measured using the anemometer. The opening slot of the wind tunnel was covered by a metal sheet to control the air flow and temperature. The air temperature was monitored until it reached a constant value, indicating that steady state had been attained. Normally 1 - 2 hours was required to achieve steady state, i.e. before the drying investigation commenced.

The material to be tested was pre-dried for at least one day before an experiment, by placing it inside a dessicator which contained molecular sieve and silica gel. The dried material was weighed and then well mixed with a weighed quantity of pure distilled water. The wet material was then placed into the sample tray and settled by vibration on a sieve shaker. When the sample tray was full, the surface was scraped level.

When the apparatus achieved a constant air temperature, the drying operation was commenced. The metal sheet which covered the slot, was removed and the sample tray, containing the wet material, was placed carefully on the suspended framework plate, allowing the hot air to pass over the surface of the bed. The initial readings of time, weight and temperatures were then registered immediately.

During an experiment, the weight loss and temperature distribution were measured at intervals of approximately every 10 minutes. The temperature at each depth was

measured by using the thermocouple selector and registered with an accuracy ± 0.5°C. Different air temperatures of 84°C, 74°C, 64°C and 54°C were used to dry the different materials.

CHAPTER 5

TEMPERATURE DISTRIBUTION IN CONVECTIVE DRYING

5.1 INTRODUCTION

The experimental apparatus described in the previous chapter was used to dry characteristic hygroscopic and non-hygroscopic materials under forced convection.

This chapter reports the temperature distribution profiles which were recorded to investigate the stages of drying and the phenomenon of the receding evaporation front. A plot of moisture content versus time and the drying rate curve were in each case matched with the temperature profile. The position of the receding evaporation front was determined as a function of time. The variation in the estimated velocity of the front was correlated with variation in the drying rate.

Glass beads of 100, 400 and 4000 μm diameter which act as a porous medium, and cylindrical polystyrene pellets of approximately 300 μm diameter and 400 μm length, were selected as non-hygroscopic materials. As discussed in Chapter 3, moisture normally moves through such non-hygroscopic materials under the action of capillary force. Activated alumina of 150 mesh and a wood powder comprising non-homogenous particles were selected as hygroscopic materials. In the case of such hygroscopic materials, moisture migration is normally controlled by diffusion.

All experiments in this chapter were carried out in an insulated glass tray, 8.3 cm in diameter and 3.2 cm deep, as shown in Fig. 5.1. Drying was carried out at a constant air temperature of 84°C and an air velocity of 0.5 m/s. The upstream wet bulb temperature was in the range of 38°C - 39°C in all experiments corresponding to a humidity of 0.02 kg H_2O/kg dry air.

The influence of varying air temperature on the temperature distribution profile was also investigated. Glass beads of 100 μm and 400 μm diameter were dried at air temperatures of 54°C, 64°C and 74°C. An experiment involving evaporation of pure distilled water was also performed for comparison and to check the wet bulb temperature. An experiment involving the heating of a bed of dry solid beads by a forced air flow at 84°C was also carried out to investigate the temperature distribution profile.

The variation in initial moisture content usually affects only the duration of the constant rate period and not the rate of drying. The greater the initial moisture content, the longer the constant rate period and vice versa. Therefore, for each material under such conditions, there is a specific value of moisture content, i.e. the critical moisture content, below which the constant rate period will not occur. According to this concept, and because of the lack of experimental data on initial moisture content in the drying literature, each experiment was repeated more than once, with a different initial moisture content. The results from repeated experiments which showed most clearly the stages of drying in a practical period, were selected for recording and analysis. These are shown in the following section. The total time for each experiment was approximately 12 - 13 hours, including approximately two hours at the beginning to allow the apparatus to reach steady state

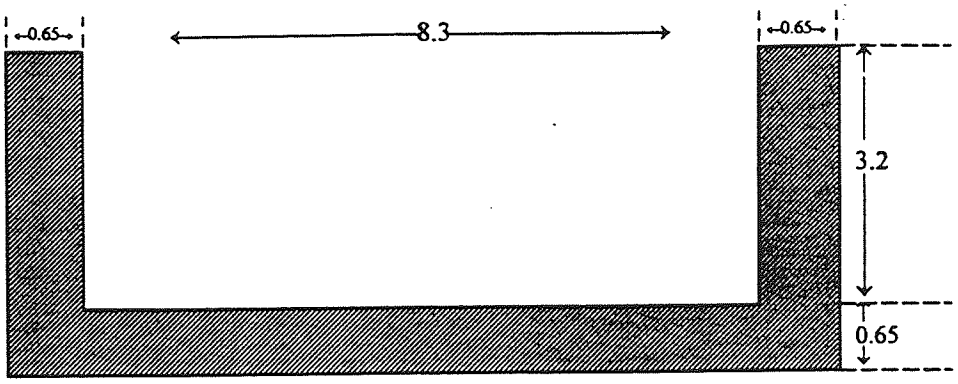

Figure 5.1 A glass sample tray, 8.3 cm internal diameter and 3.2 cm deep; insulated with neoprene rubber; dimensions in (cm).

conditions.

Data obtained from drying experiments was measured as total weight of wet material plus weight of sample tray and framework, W_t, at different times. These data were converted to rate of drying data as follows,

$$\text{Weight of the wet material only : } W^* = W_t - W_{(f+t)} \qquad (5.1\text{-}1)$$

where $W_{(f+t)}$ represents the weight of an empty sample tray plus weight of framework. If W_s is the weight of dry solid, then the moisture content at any time, X is,

$$X = \frac{W^* - Ws}{Ws} \qquad (\text{kg } H_2O/\text{kg dry solid}) \qquad (5.1\text{-}2)$$

From a plot of moisture content, X, versus time, t, the slope of the tangent dX/dt, can be calculated as:

$$\frac{dX}{dt} = \frac{X(i+1) - Xi}{t(i+1) - ti} \qquad (\text{kg } H_2O/\text{kg dry solid-h}) \qquad (5.1\text{-}3)$$

The drying rate per unit area can be defined as,

$$\mathbf{m} = -\frac{ms}{A}\frac{dX}{dt} \qquad (\text{kg } H_2O / m^2\text{-h}) \qquad (5.1\text{-}4)$$

5.2 BEDS OF NON-HYGROSCOPIC MATERIALS

5.2.1 Glass Beads, 100 μm

Beds of glass beads of 100 μm diameter, and initial moisture content of X_o = 0.2 were subjected to forced convective drying at 84°C. The total bed depth was 3.2 cm and the total dry weight of solid was 266.5 g . The resulting temperature distribution profiles, recorded in Fig. 5.2, demonstrate clearly the stages of drying, i.e. the pre-constant rate period, the constant rate period, the first falling rate period and the second falling rate period.

The temperature of the bed rose from ambient temperature (22°C) to a steady value at t=70 min., the start of the constant rate period. This initial period, termed the pre-constant rate period, is usually short. During the constant rate period, the surface temperature was 38°C which was close to the wet bulb temperature, whilst the temperature at the bottom remained at 32°C. Thus, there was a temperature difference of 6°C between the surface and the bottom. This remained constant throughout the whole of the constant rate period.

At a specific point, t=165 min., the surface temperature rose gradually, indicating the end of the constant rate period and the beginning of the first falling rate period. The moisture content corresponding to this point represents the critical moisture content of the material, i.e. the point at which there was insufficient water on the surface to maintain a continuous film of water. (The entire surface is no longer wetted and dry patches begin to

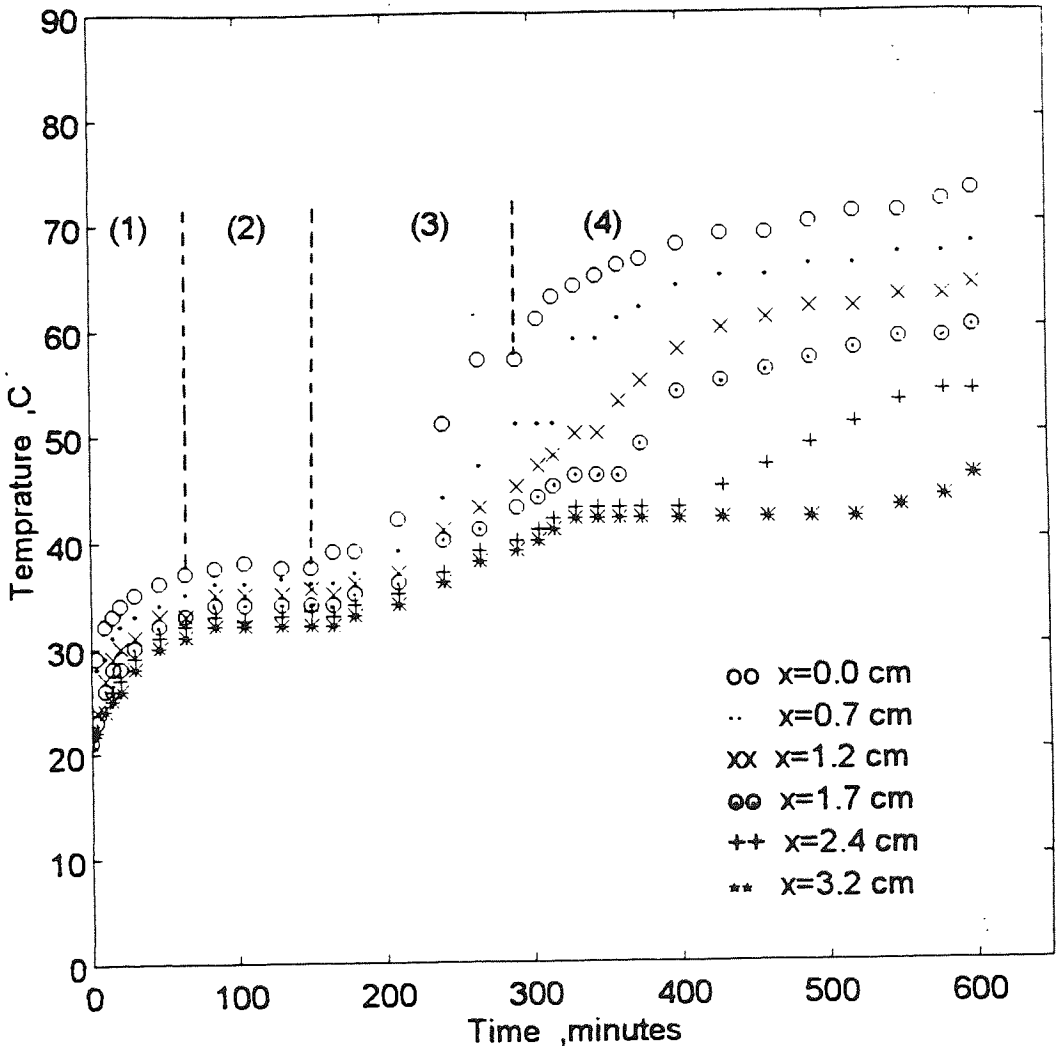

Figure 5.2 Temperature distribution profiles within a bed of glass beads (100 μm); air temperature 84°C. [x = distance of plane beneath surface]
(1) pre-constant rate period
(2) constant rate period
(3) first falling rate period
(4) second falling rate period.

form, although this was not observable here.)

During the first falling rate period the temperature at each depth increased slightly and another constant temperature period was approached. The duration of the second period of constant surface temperature was short, about 25 mins., and the temperature was 57°C. The surface temperature then rose sharply at t=290 min. and continued to rise for a longer time until it approximated to the air temperature. This point, at which the surface temperature increased, indicated the start of the second falling rate period with the surface 'dried-out' under the prevailing air conditions.

The experimental temperature profiles also showed that when the surface became dry, the subsurface layer remained at a constant temperature, 51°C. Evaporation occurred at this sublayer level, i.e. the evaporation plane receded from the surface to this layer. This plane divided the bed into a thin dried zone on the surface and a wet zone comprising the rest of the bed. Again, the duration of the second period of constant subsurface temperature was normally short; the temperature then rose rapidly once another dry layer had formed. The plane of evaporation slowly receded from the subsurface layer to another sublayer. Thus the receding evaporation front divided the system into a hotter dry zone near the surface and a wet zone towards the bottom of the sample.

Fig. 5.2 also demonstrates that during the second falling rate period, the bottom temperature remained constant at 42°C, for a longer time than other layers; it then rose quickly when the dry zone extended throughout the bed. The point at which the temperature at each depth increased, indicated the position of the receding evaporation

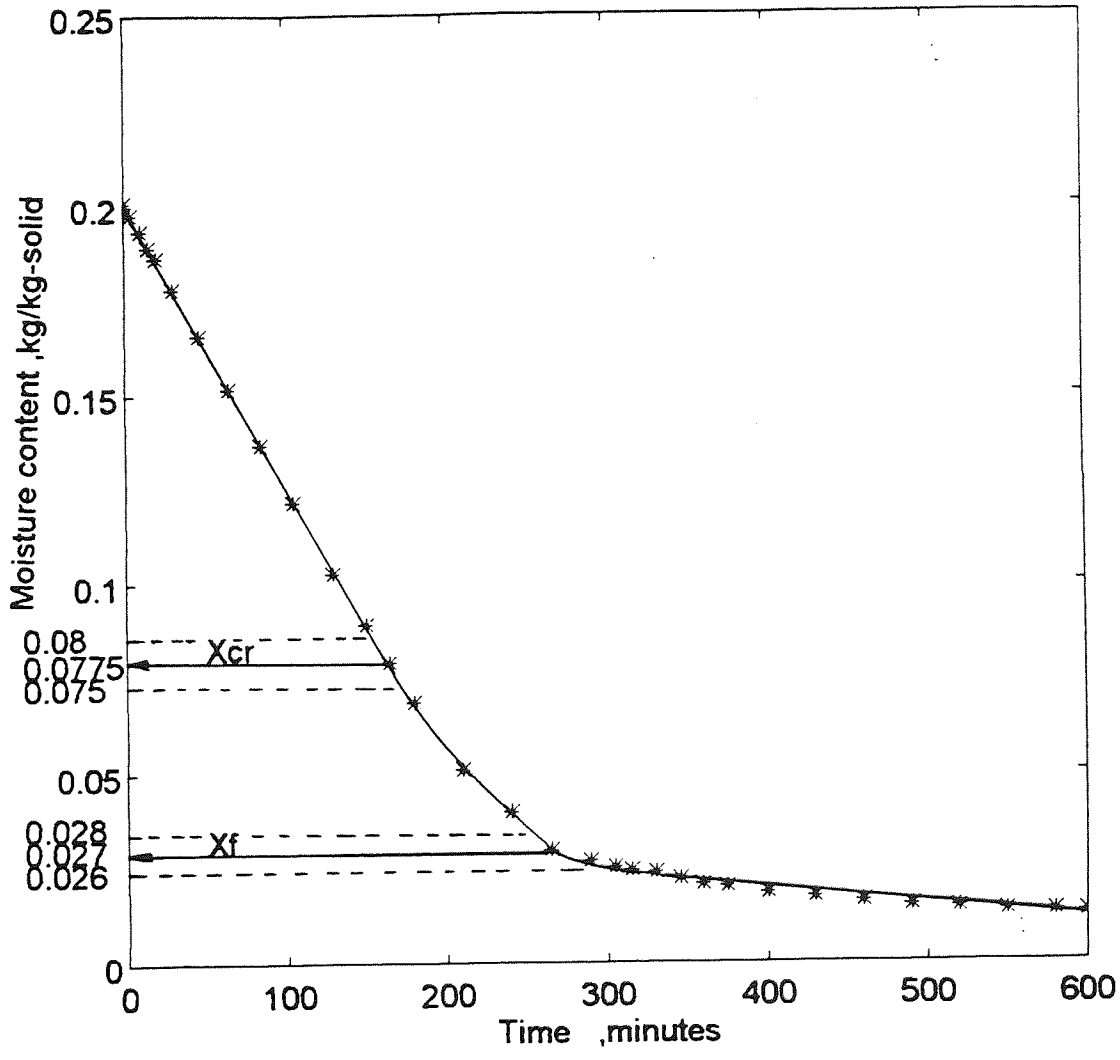

Figure 5.3 Moisture content versus time within a bed of glass beads (100 μm); air temperature 84 °C,
Xcr: critical moisture content
Xf : moisture content corresponding to the beginning of the second falling rate period.

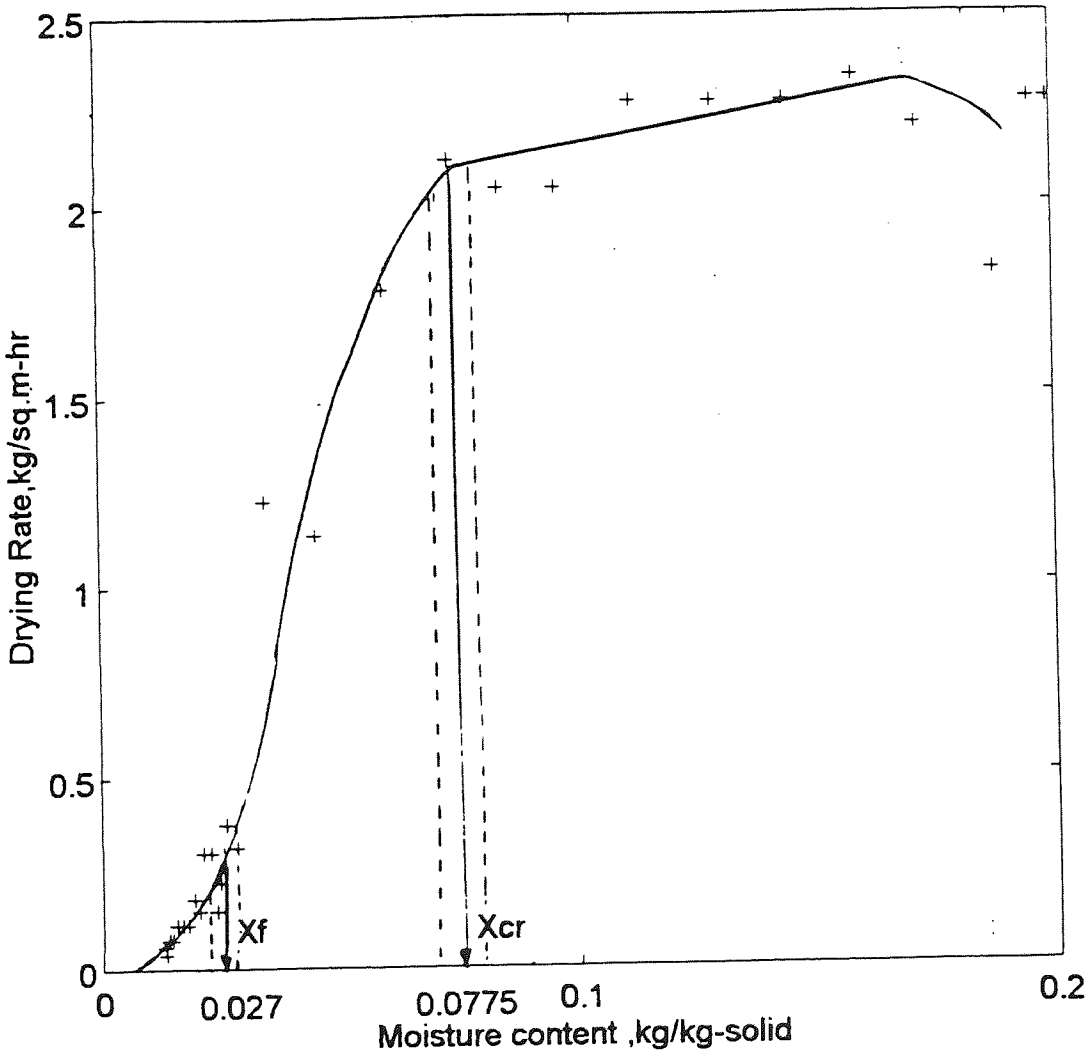

Figure 5.4 Drying rate curve for bed of glass beads (100 μm); air temperature 84 °C.

front at that time.

A plot of moisture content versus time is shown in Fig. 5.3. The critical moisture content can be determined, from a tangent to the curve, as approximately X_{cr}=0.075. The point at which the second falling rate period begins is usually determined at a point where the curve again changes slope abruptly, as in Fig. 2.1. This point is always difficult to determine, but by considering the drying rate curve as in Fig. 5.4, together with the plot of moisture content versus time, it can be approximated as a moisture content of X_f=0.028.

As mentioned previously the temperature distribution profile, Fig. 5.2 clearly showed the critical moisture content point at t=165 min. and the beginning of the second falling rate period at t=290 min. These points were matched with the plot of moisture content versus time. At t=165 min. the corresponding moisture content was X_{cr}=0.08 and at t=290 min. the corresponding value was X_f=0.026. Therefore the critical moisture content value varied between 0.075 and 0.08, with a mean value estimated as X_{cr} = (0.075 + 0.08)/2 = 0.0775. The mean moisture content value corresponding to the beginning of the second falling rate period was X_f=(0.026+0.028)/2 = 0.027. Thus, the addition of the temperature distribution profile to the plot of moisture content versus time and to the drying rate curve, facilitated more accurate prediction of these points.

The temperature distribution profile showed the position of the receding evaporation front at any time. As discussed previously, these positions were determined at the points at which temperature at each depth increased after the second constant temperature level. These points were plotted against time and provided a significant graph from which the

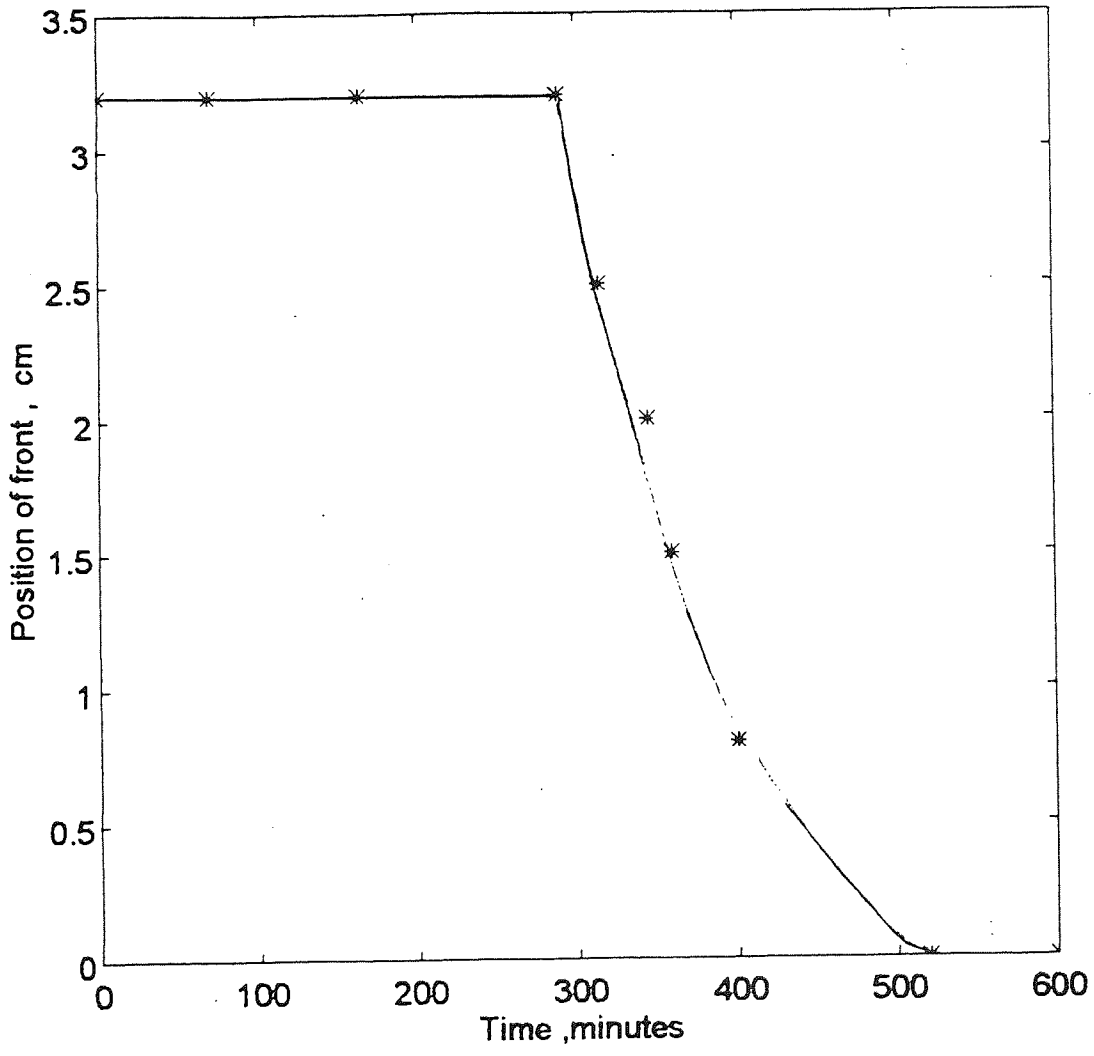

Figure 5.5 Position of receding evaporation front versus time within a bed of glass beads (100 μm); air temperature 84 °C.

position of the evaporation front could be determined accurately at any time. Figure 5.5 shows the position of the receding evaporation front, calculated from the bottom of the bed, as a function of time. This figure shows that the receding front, which always appears in the second falling rate period, remained at the surface until t=290 minutes; it then slowly receded inside the bed.

The velocity of the receding evaporation front can also be determined from Fig. 5.5, since time and position are known. Therefore, Fig. 5.5 represents a simple means of predicting the position and velocity of the front at any time.

The curve shown in Fig. 5.5 was similar in shape to the drying rate curve shown in Fig. 5.4. Thus, variations in velocity of the evaporation front are consistent with the changes in drying rate.

5.2.2 Glass Beads, 400 μm

Experiments were also conducted with beds of glass beads of 400 μm. The total bed depth was 3.2 cm and the total dry weight of solid was 267 g. The initial moisture content was $X_o = 0.23$; the air temperature, humidity and velocity were as before.

Figure 5.6 shows the temperature distribution profiles for this material. These profiles were similar to those with 100 μm glass beads [Fig. 5.2] and again clearly demonstrate the stages of drying. The constant rate period started at t=45 min. and terminated at t=155 min. During this stage, the surface temperature remained constant at

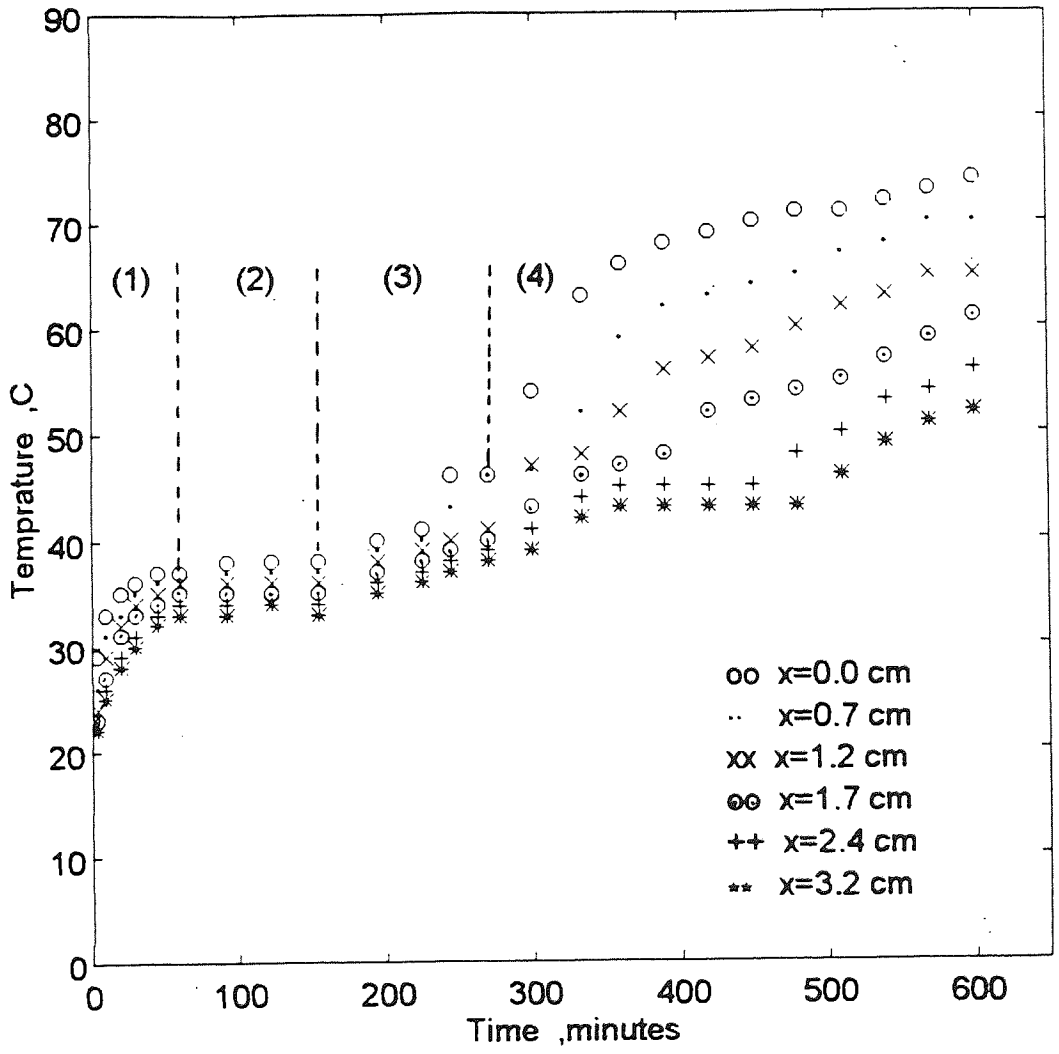

Figure 5.6 Temperature distribution profiles within a bed of glass beads (400 μm); air temperature 84 °C.

38°C, 5°C higher than the bottom temperature. At a specific point, t=155 min., the surface temperature rose gradually until it reached another constant temperature level. As with the 100 μm glass beads, this point represented the critical moisture content. The temperature at each depth also increased gradually to another constant temperature level. The duration of this constant level was longer for the bottom than for the surface.

The second falling rate period began when the temperature of the surface rose quickly after the second constant temperature level and a dry zone formed on the surface. The evaporation front again slowly receded from the surface and divided the system into a dry zone and a wet zone.

Figures 5.7 and 5.8 show a plot of moisture content versus time and a drying rate curve for glass beads of 400 μm diameter. From those two plots, the critical moisture content and the moisture content at the beginning of the second falling rate period can be determined approximately as $X_{cr} = 0.09$ and $X_f = 0.025$ respectively.

The temperature distribution profiles in Fig. 5.6, show that the critical point was reached at t=155 min. and the beginning of the second falling rate period at t=270 min. When these points were matched with the plot in Fig. 5.7, then the corresponding moisture contents were $X_{cr} = 0.11$ and $X_f = 0.035$ respectively. A more accurate average value of the critical moisture content would hence be $X_{cr} = 0.1$ and the moisture content at the beginning of the second falling rate period $X_f = 0.03$.

The temperature distribution profiles demonstrate that there were clear points at the

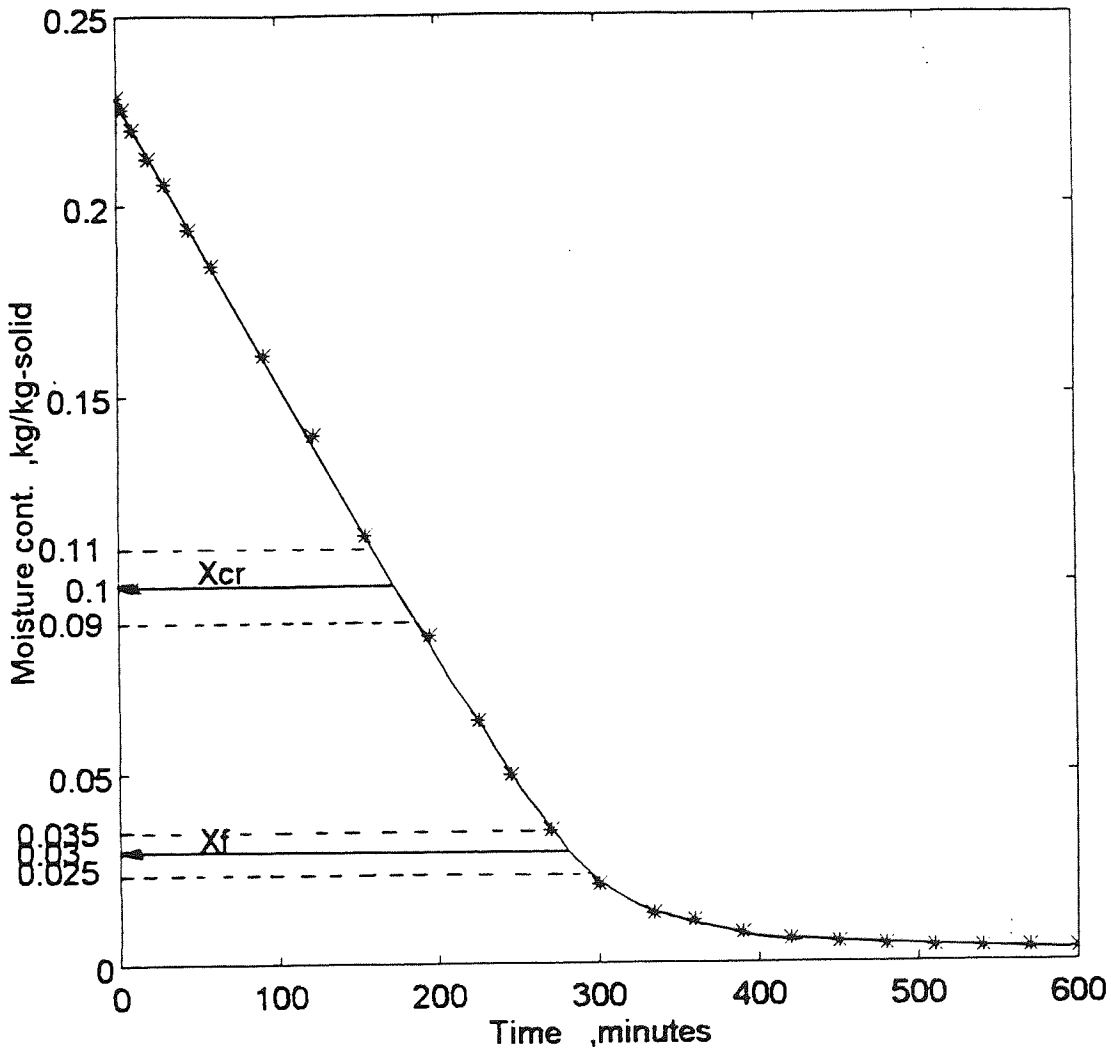

Figure 5.7 Moisture content versus time within a bed of glass beads (400 μm); air temperature 84 °C.

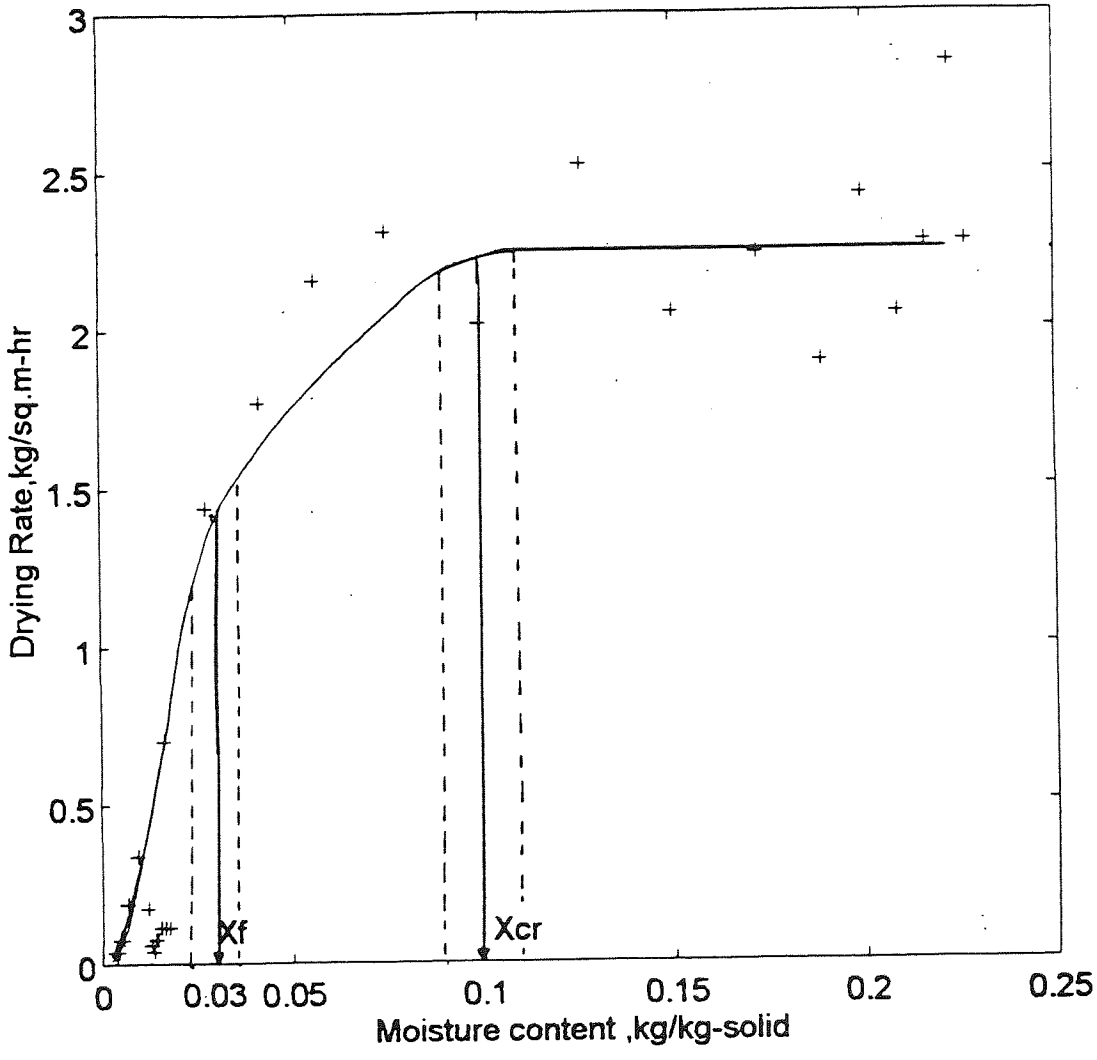

Figure 5.8 Drying rate curve for bed of glass beads (400 μm); air temperature 84 °C.

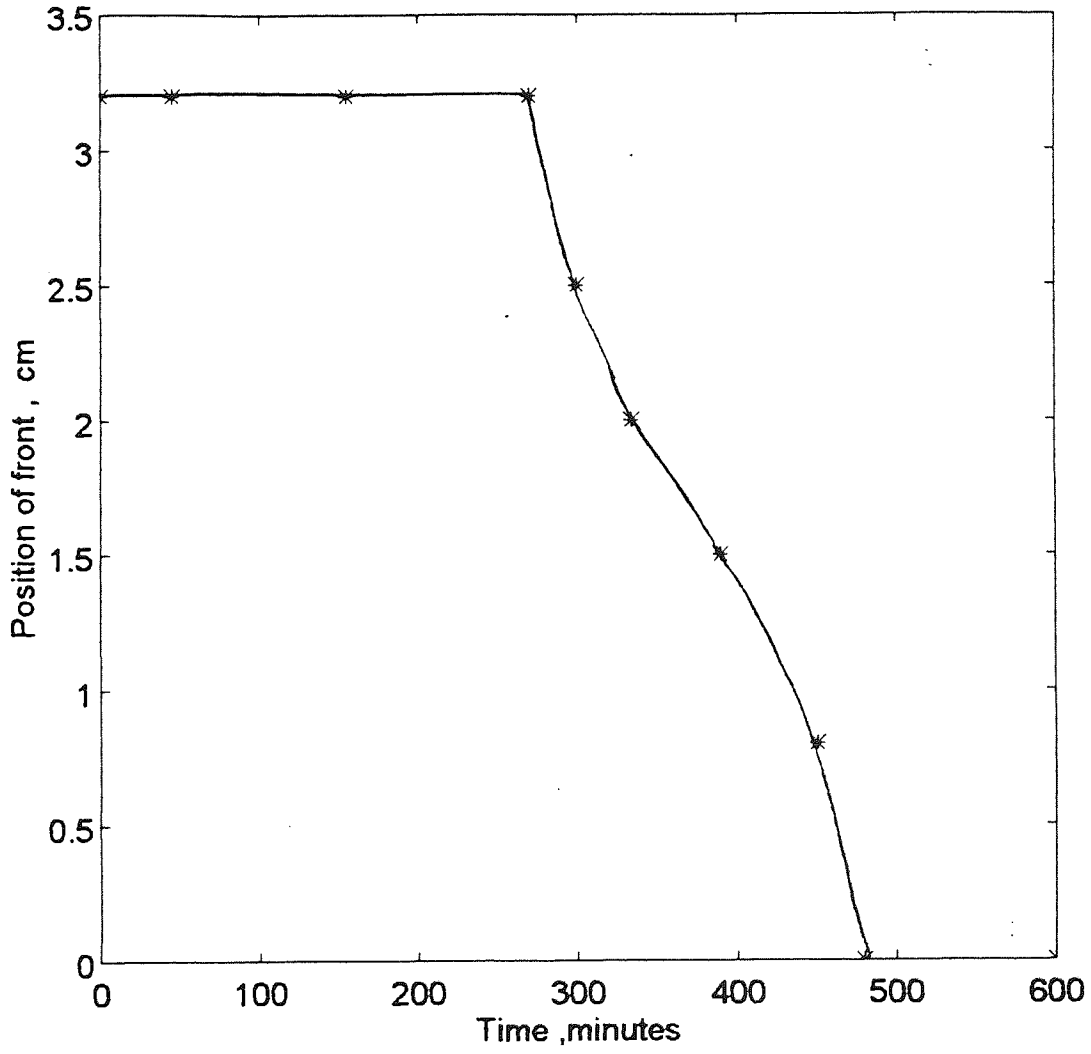

Figure 5.9 Position of the receding evaporation front versus time within a bed of glass beads (400 μm); air temperature 84 °C.

end of the second constant temperature level for each depth at which temperature increased suddenly. These points indicated the position of the receding evaporation front at the corresponding times. These are plotted in Fig. 5.9, providing a potential method for predicting the position and velocity of movement of the front at any time. This figure shows good agreement with the drying rate curve.

5.2.3 Glass Beads, 4000 μm

Beds of glass beads of 4000 μm diameter were also dried at an air temperature of 84°C. The initial moisture content was $X_o = 0.45$ and the total dry weight of solid was 210 g . The initial moisture content was increased deliberately in this experiment, because a constant rate period was not present when drying commenced at lower values.

The temperature distribution profiles, shown in Fig. 5.10, demonstrated only a short constant rate period despite the higher value of initial moisture content. This can be explained by the presence of large diameter pores within the bed of larger diameter beads. Hence the gravity force will be more significant than capillary force and have a considerable effect on the moisture distribution. Therefore, at the beginning of the experiment, moisture content will not be uniform throughout the body. The surface of the bed will tend to have a lower moisture content than the bottom, resulting in a short constant rate period.

The recorded surface temperature was 37°C throughout the constant rate period, i.e. close to the wet bulb temperature of 38°C. As with glass beads of 100 and 400 μm diameter, this temperature again increased at a critical point. In the second falling rate

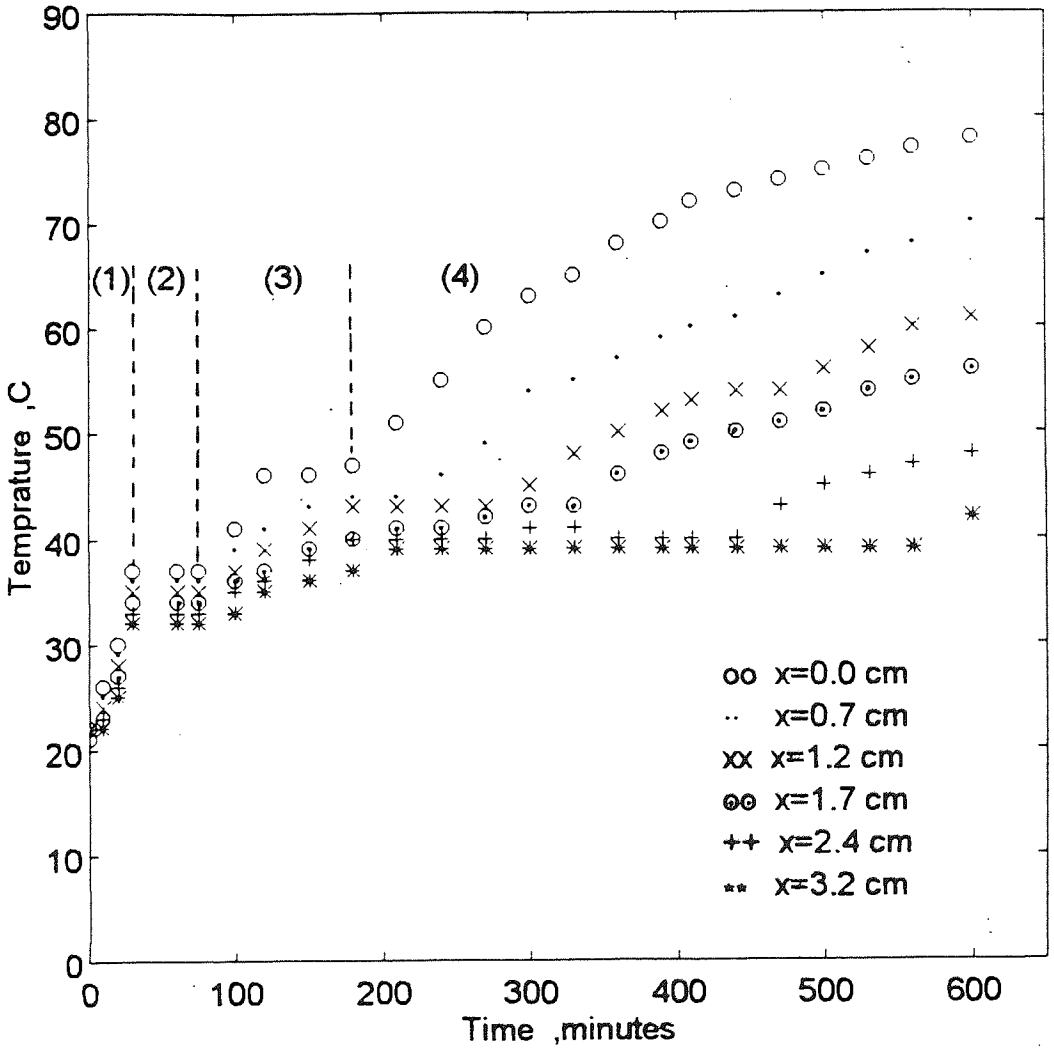

Figure 5.10 Temperature distribution profiles within a bed of glass beads (4000 μm); air temperature 84 °C.

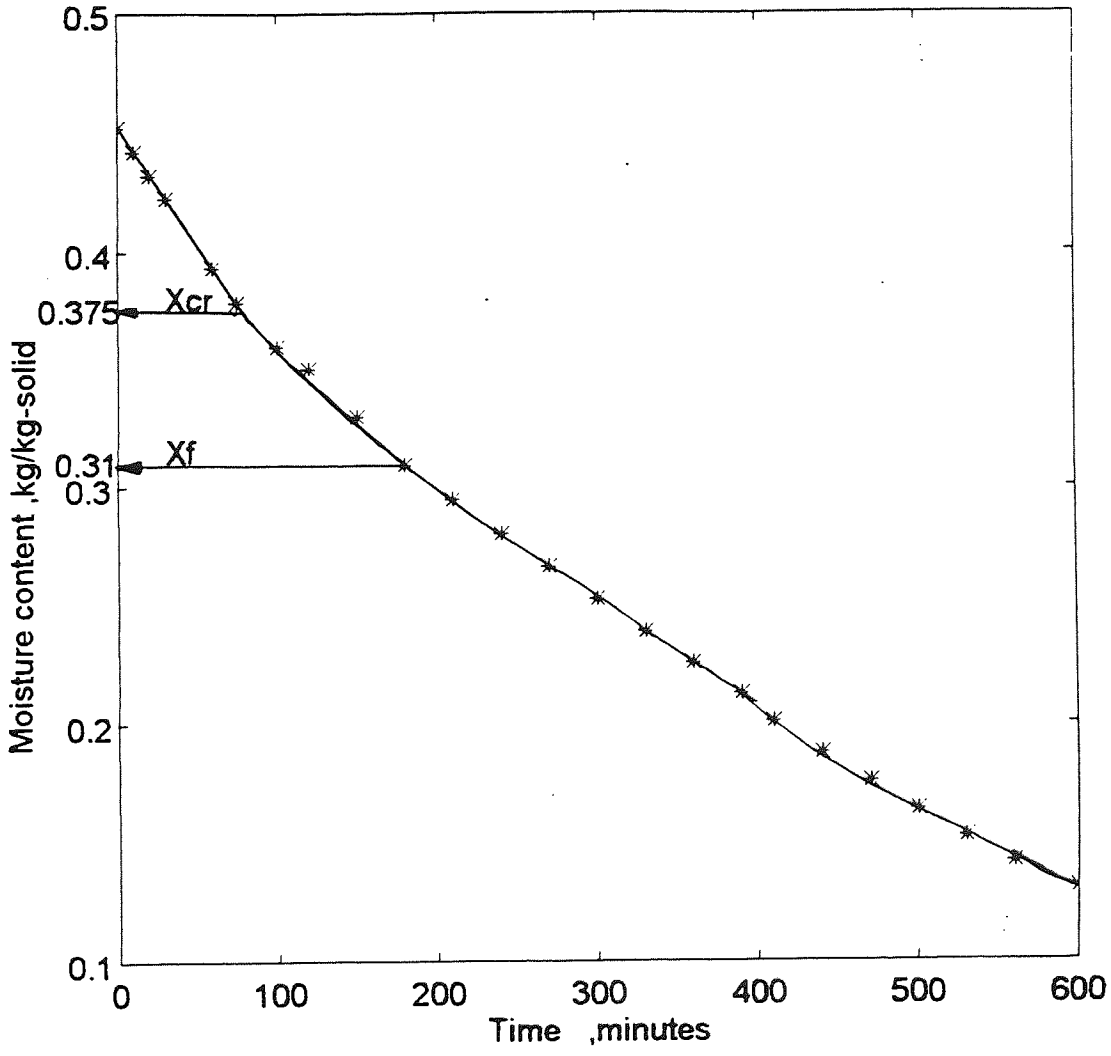

Figure 5.11 Moisture content versus time within a bed of glass beads (4000 μm); air temperature 84 °C.

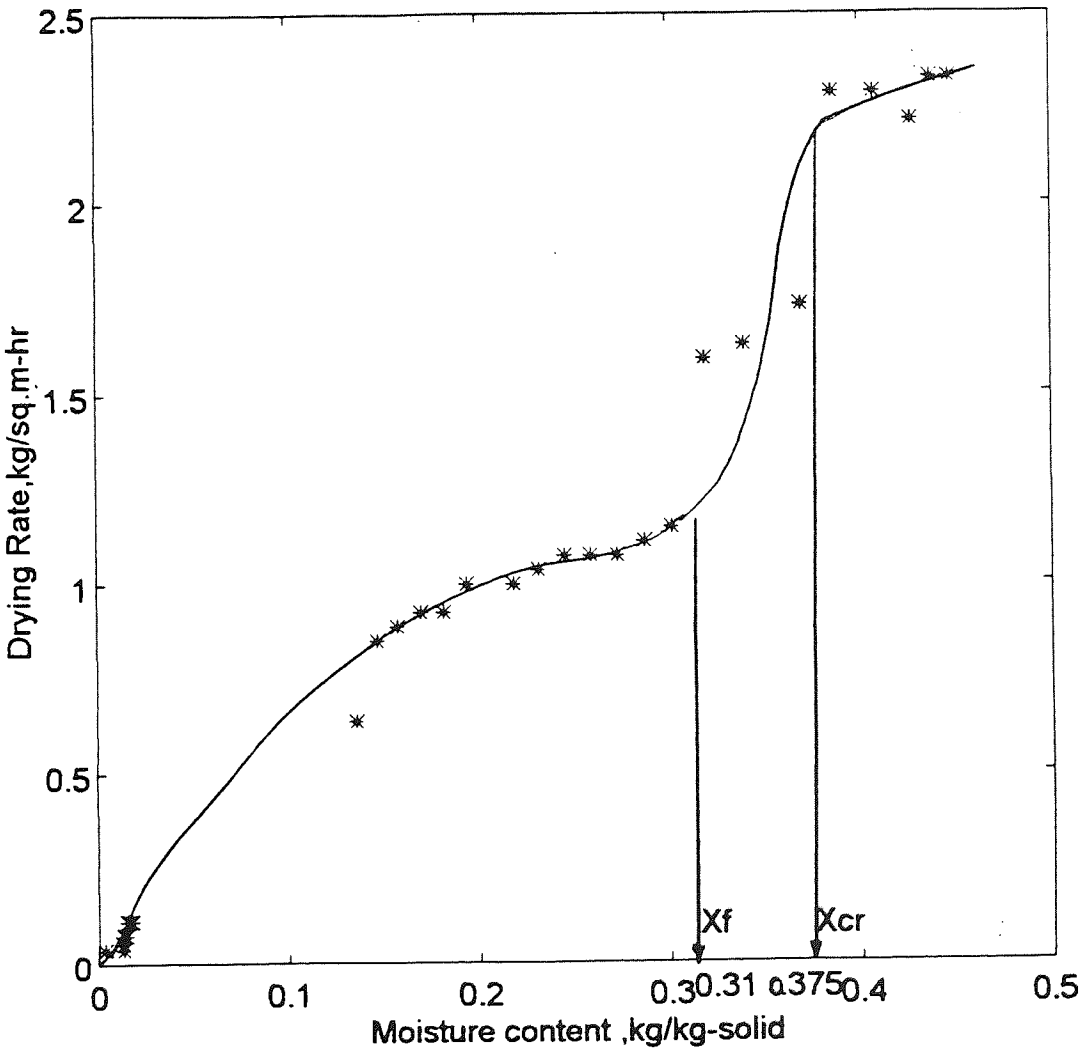

Figure 5.12 Drying rate curve for a bed of glass beads (4000 μm); air temperature 84 °C.

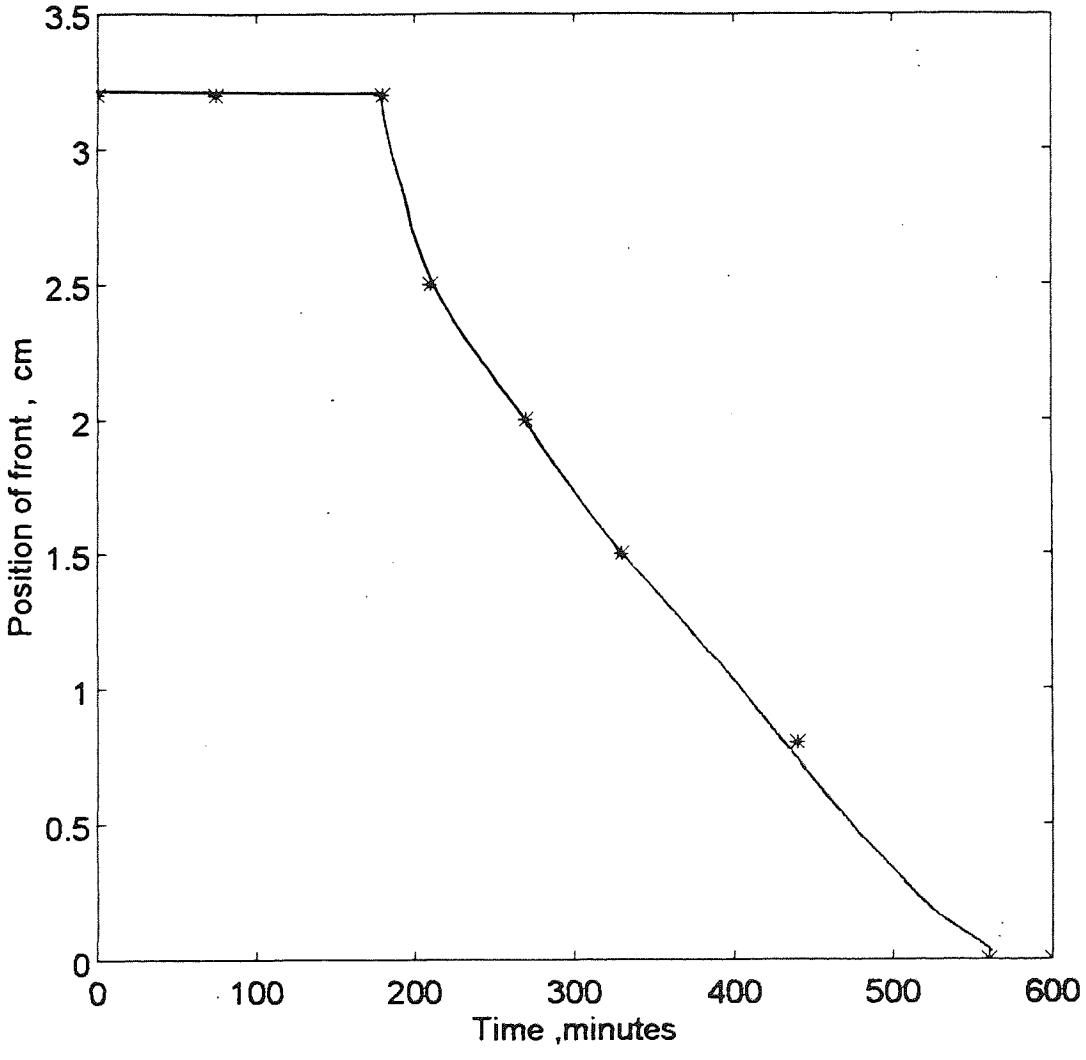

Figure 5.13 Position of receding evaporation front versus time within a bed of glass beads (4000 μm); air temperature 84 °C.

period, the system formed two regions, a hotter dry zone near the surface and a wet zone towards the bottom. After 500 min. the bottom of the bed was still wet, partly due to the large amount of moisture present there initially.

The plot of moisture content versus time and the drying rate curve are shown in Figures 5.11 and 5.12 respectively. Points in the temperature profile were matched with a plot of moisture content versus time. Accurate mean values of critical moisture content and that at the beginning of the second falling rate period were obtained by the matching method described earlier. These values were $X_{cr} = 0.375$ and $X_f = 0.31$ respectively.

Figure 5.13 shows a plot of the position of the receding front as a function of time. This graph again offered a simple means to predict the position of the evaporation front and its speed of movement at any time.

5.2.4 Polystyrene Pellets

A non-hygroscopic polymer in the form of cylindrical 300 μm diameter by 400 μm long polystyrene pellets was dried at an air temperature of 84°C. The total bed depth was 3.2 cm and the total dry weight of solid was 92.4 g . The initial moisture content was X_o = 0.77.

Figure 5.14 shows the temperature distribution profiles obtained. The constant rate period was short, i.e. extending only for a period of 50 minutes. The explanation for this was as for the glass beads of 4000 μm, i.e. the gravity force controlling liquid moisture

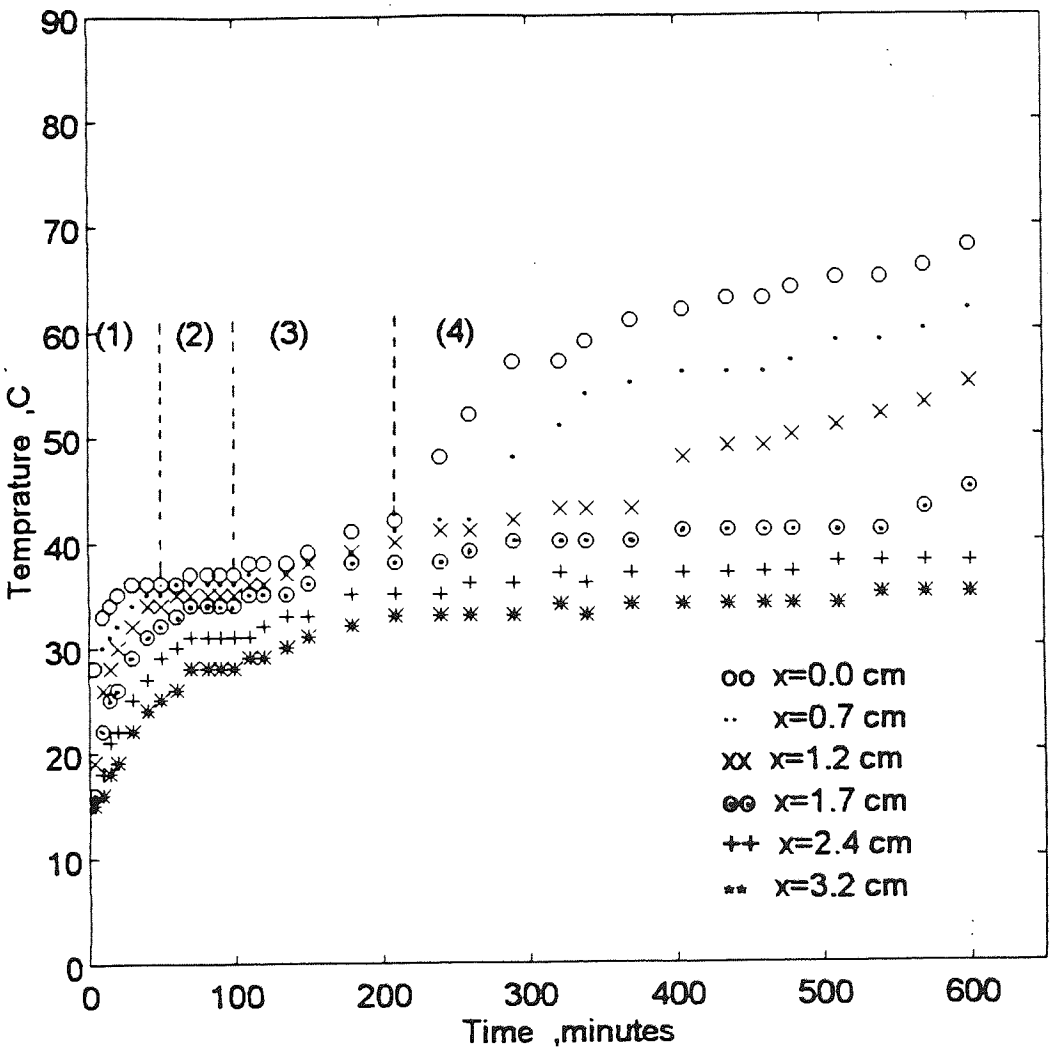

Figure 5.14 Temperature distribution profiles within a bed of polystyrene pellets; air temperature 84 °C.

movement in a medium containing large pores.

The profiles showed that after a time t = 100 min. the temperatures at various planes in the bed rose gradually until they reached short periods of constant temperature. At time t=210 min., the surface temperature increased rapidly because a dry zone formed on the surface.

The receding evaporation front present during the second falling rate period again divided the system into two zones; a hot dry zone near the surface and a wet zone towards the bottom. The profiles showed that after 10 hours drying time, the bottom temperature still indicated that the bottom of the bed was wet.

A plot of moisture content versus time is shown in Fig. 5.15. The exact moisture content corresponding to commencement of the second falling rate period appears difficult to determine. Therefore, consideration of the corresponding drying rate curve (Fig. 5.16) can assist to predict this moisture content with limited accuracy. To get a more accurate value of the critical moisture content and the moisture content at the beginning of the second falling rate period, these curves were correlated with the temperature distribution profiles. The critical moisture content was X_{cr} = 0.53, and the moisture content corresponding to the beginning of the second falling rate was X_f = 0.4.

The velocity and position of the receding evaporation front can be readily calculated from Fig. 5.17.

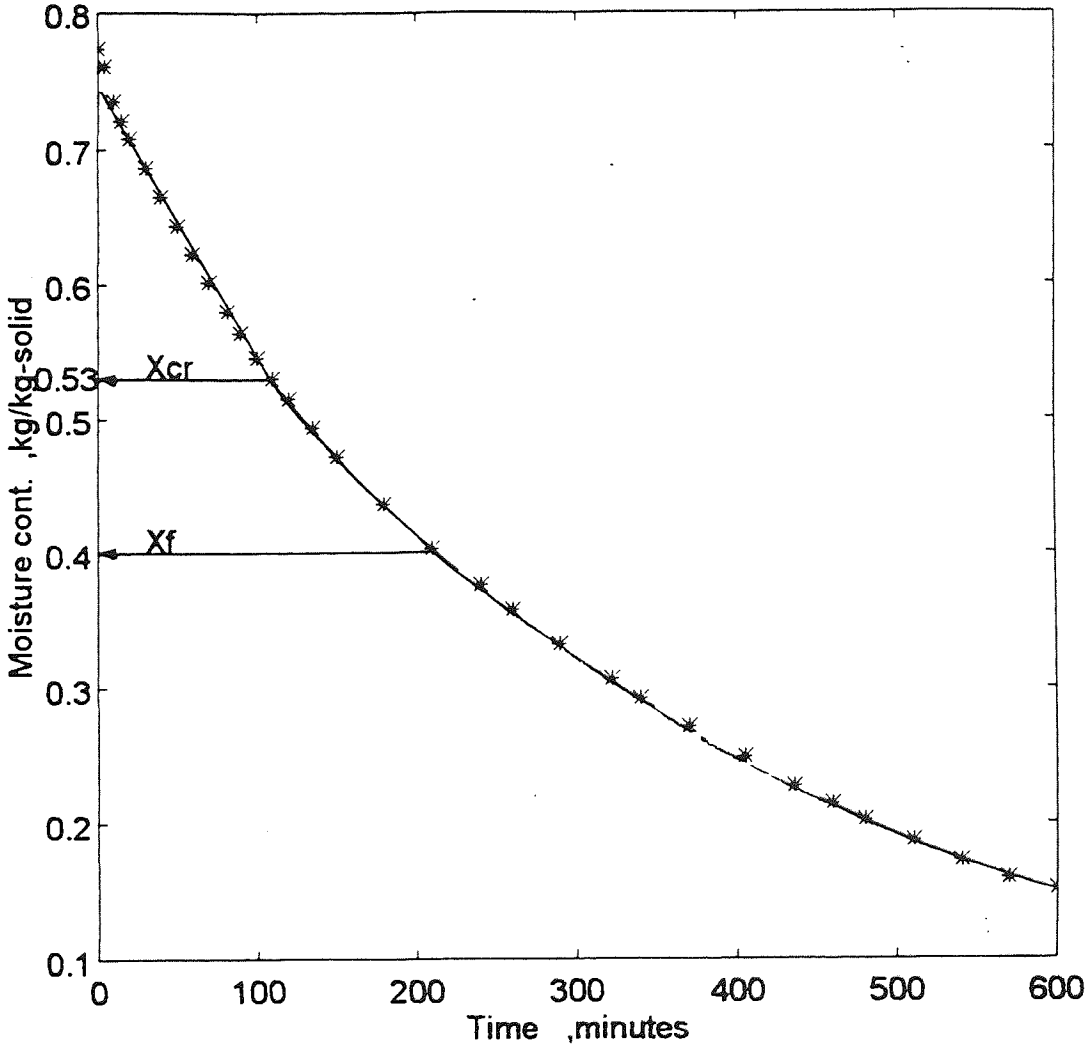

Figure 5.15 Moisture content versus time within a bed of polystyrene pellets; air temperature 84 °C.

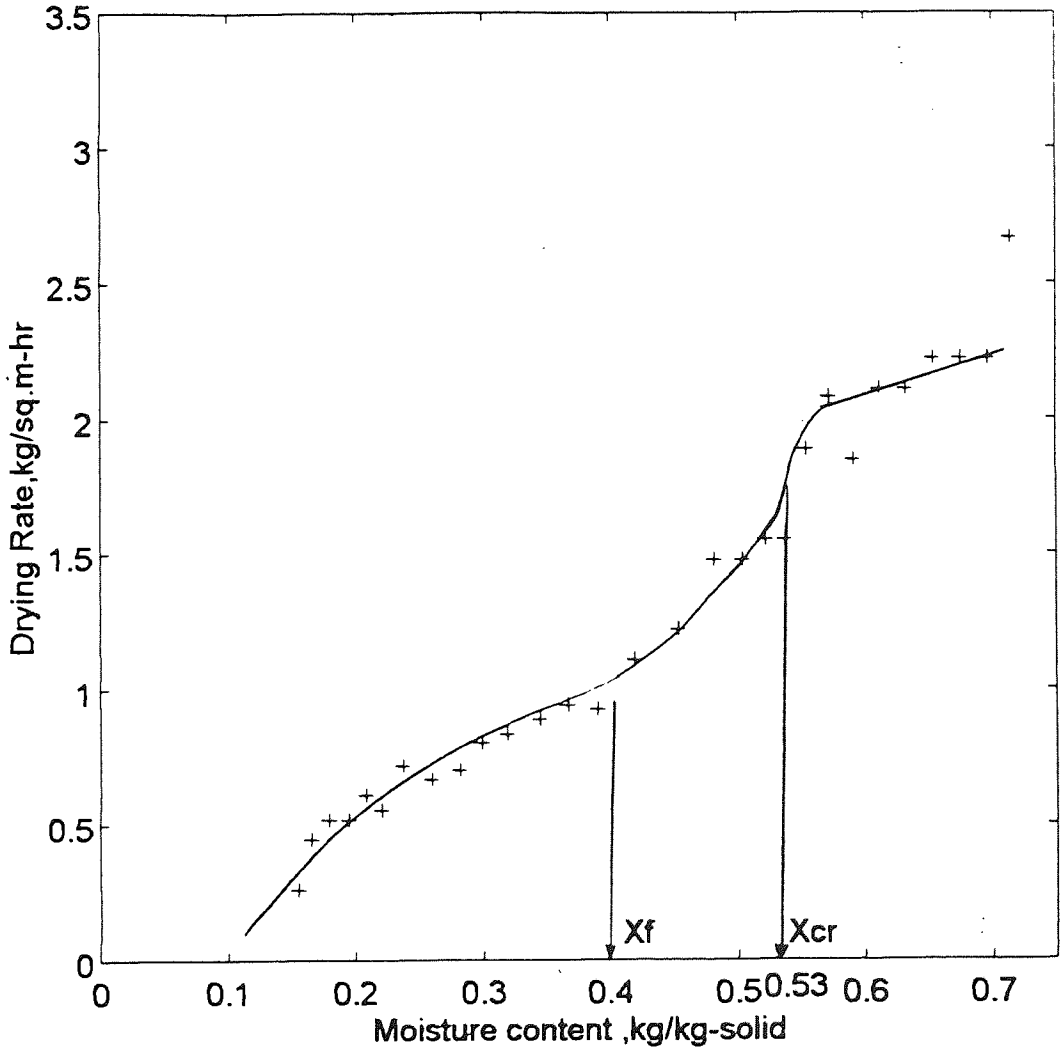

Figure 5.16 Drying rate curve for bed of polystyrene pellets; air temperature 84 °C.

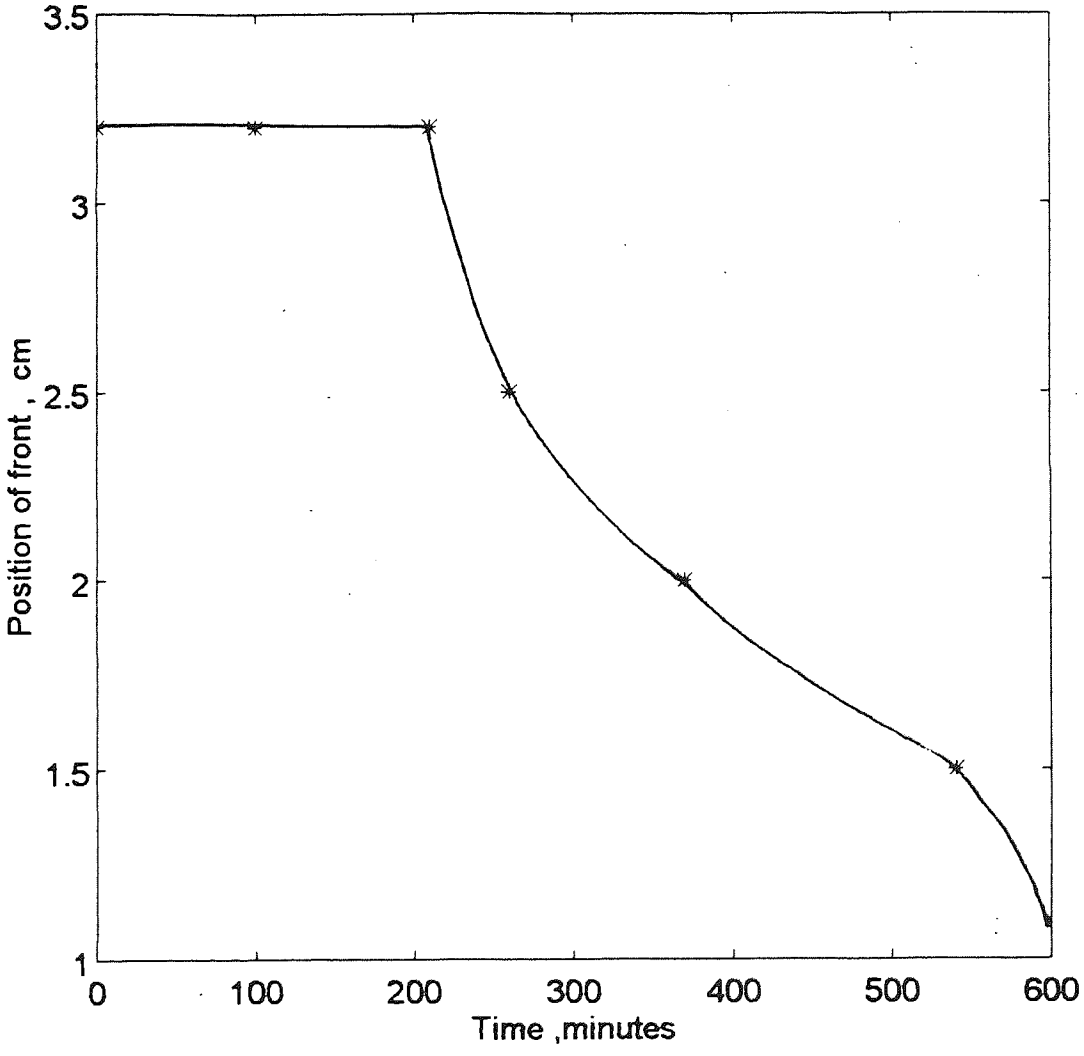

Figure 5.17 Position of receding evaporation front versus time within a bed of polystyrene pellets; air temperature 84 °C.

5.3 BEDS OF HYGROSCOPIC MATERIALS

5.3.1 Activated Alumina, 150 mesh

Beds of a hygroscopic material e.g. activated alumina 150 mesh, were also studied during forced convective drying. The initial moisture content was $X_o = 0.91$. The total bed depth was 3.2 cm and the total dry weight of the solid was 110 g .

The temperature distribution profiles are shown in Fig. 5.18. These profiles are similar to those for the non-hygroscopic materials. During the constant rate period, the surface temperature was 36.5°C and the bottom temperature was 34°C. There was a small difference in temperature from surface to the bottom of 2.5°C, which remained constant during the constant rate period. At time t=195 min. the surface temperature increased slightly indicating the end of the constant rate period. In a similar manner to the non-hygroscopic materials, the temperature of the bed increased gradually during the first falling rate period and another constant temperature period was approached.

The surface temperature rose sharply at t = 240, representing the beginning of the second falling rate period. The surface was dry whilst the rest of the bed remained wet. The subsurface layer 'dried out' at time t = 320 min. As a result, a small dry region formed at the top of the bed. The evaporation front slowly receded from the subsurface to another sublayer.

Figures 5.19 and 5.20 show the plot of moisture content versus time and the drying

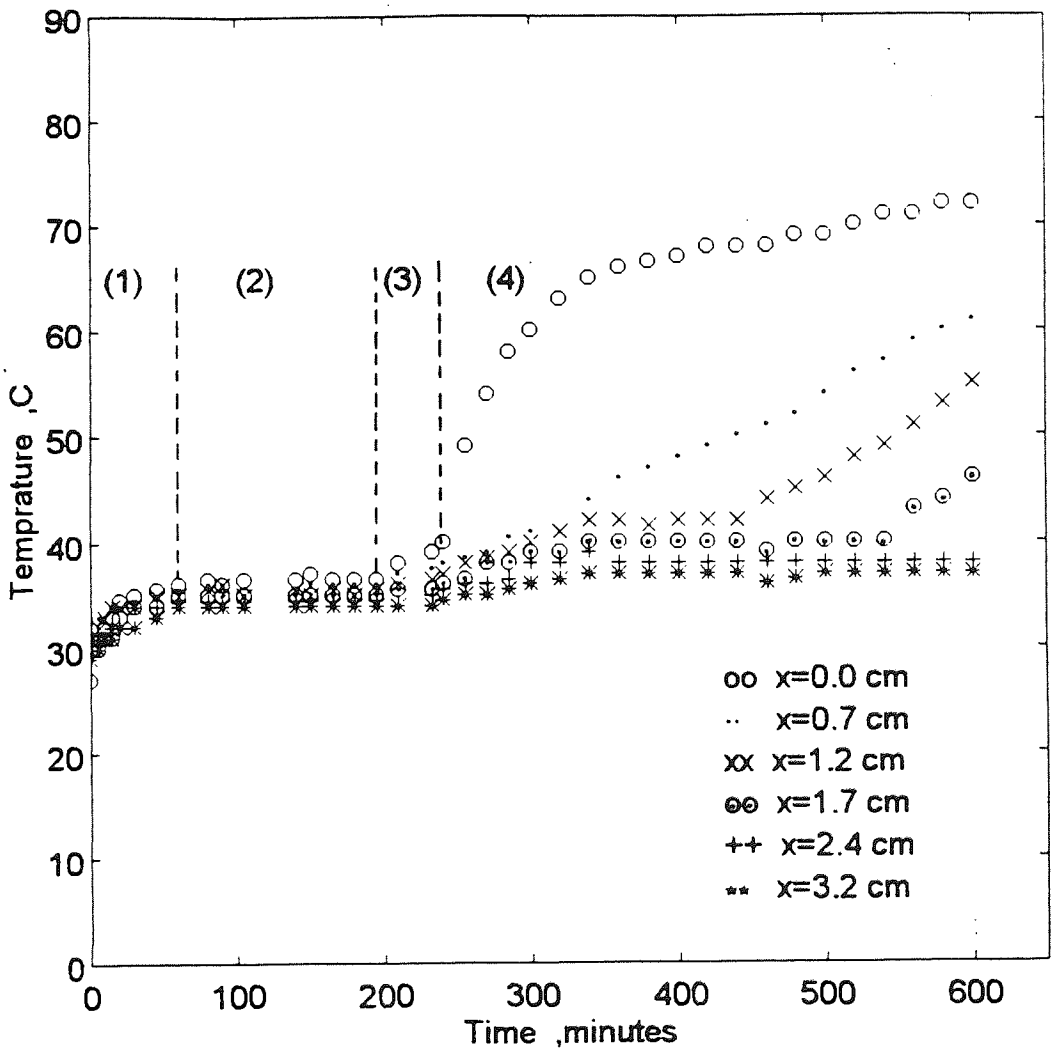

Figure 5.18 Temperature distribution profiles within a bed of activated alumina (150 mesh); air temperature 84 °C.

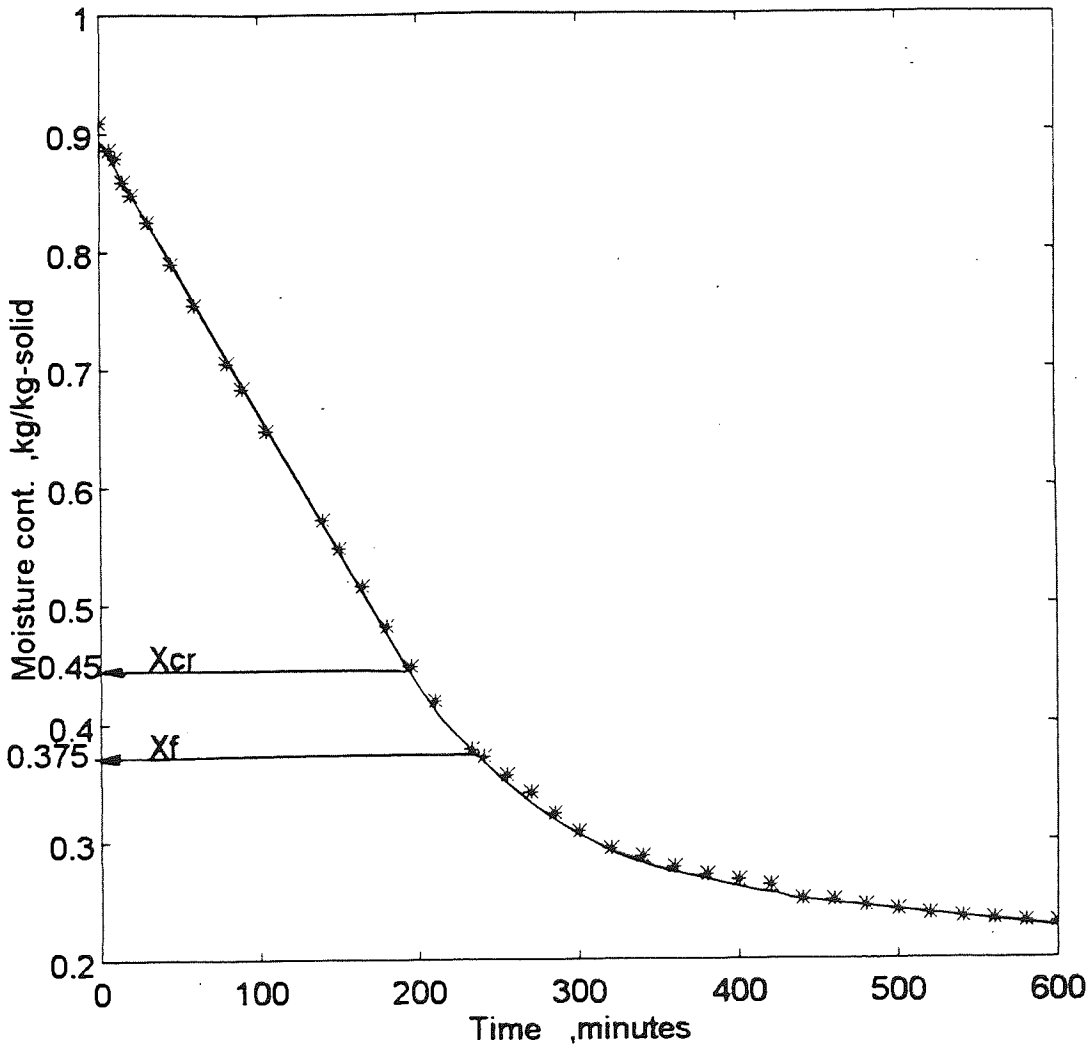

Figure 5.19 Moisture content versus time within a bed of activated alumina (150 mesh); air temperature 84 °C .

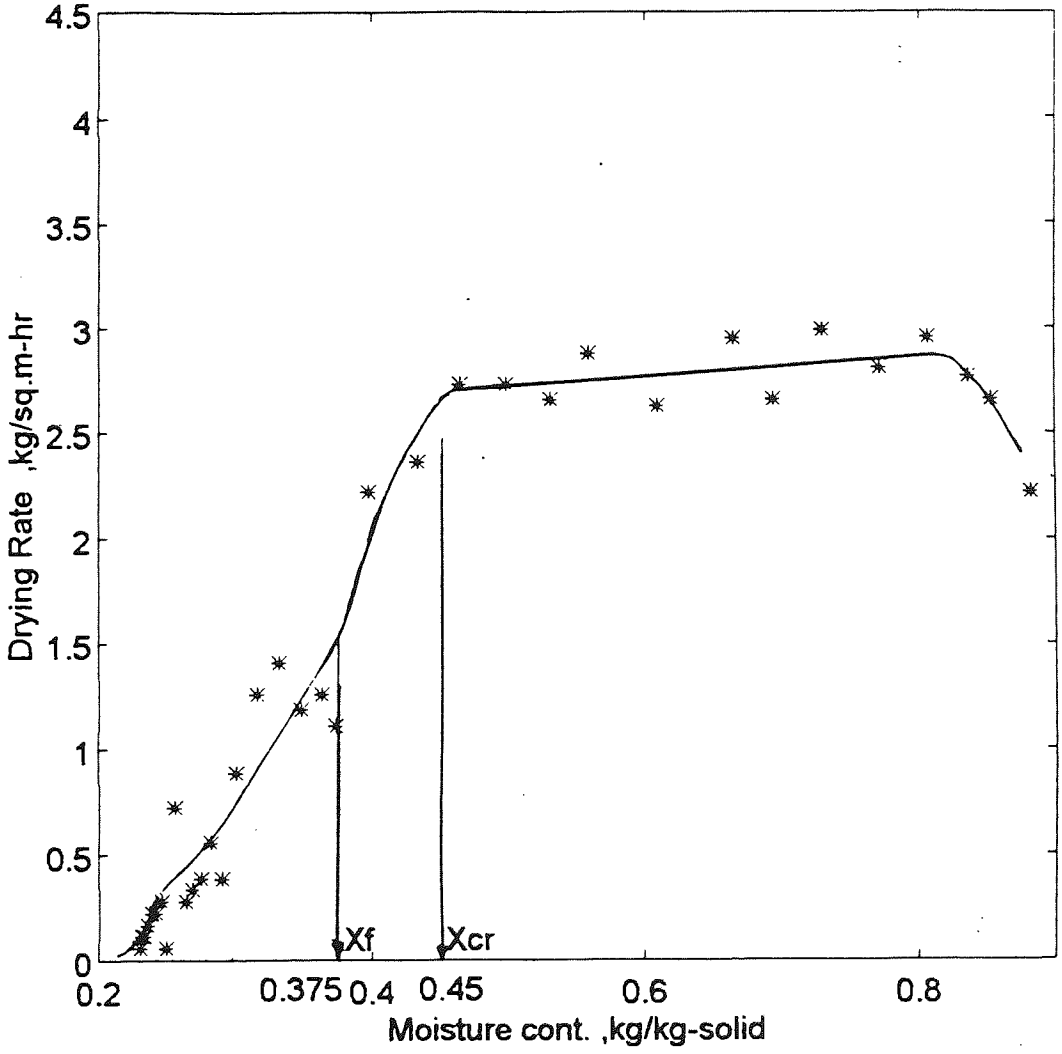

Figure 5.20 Drying rate curve for bed of activated alumina (150 mesh); air temperature 84 °C .

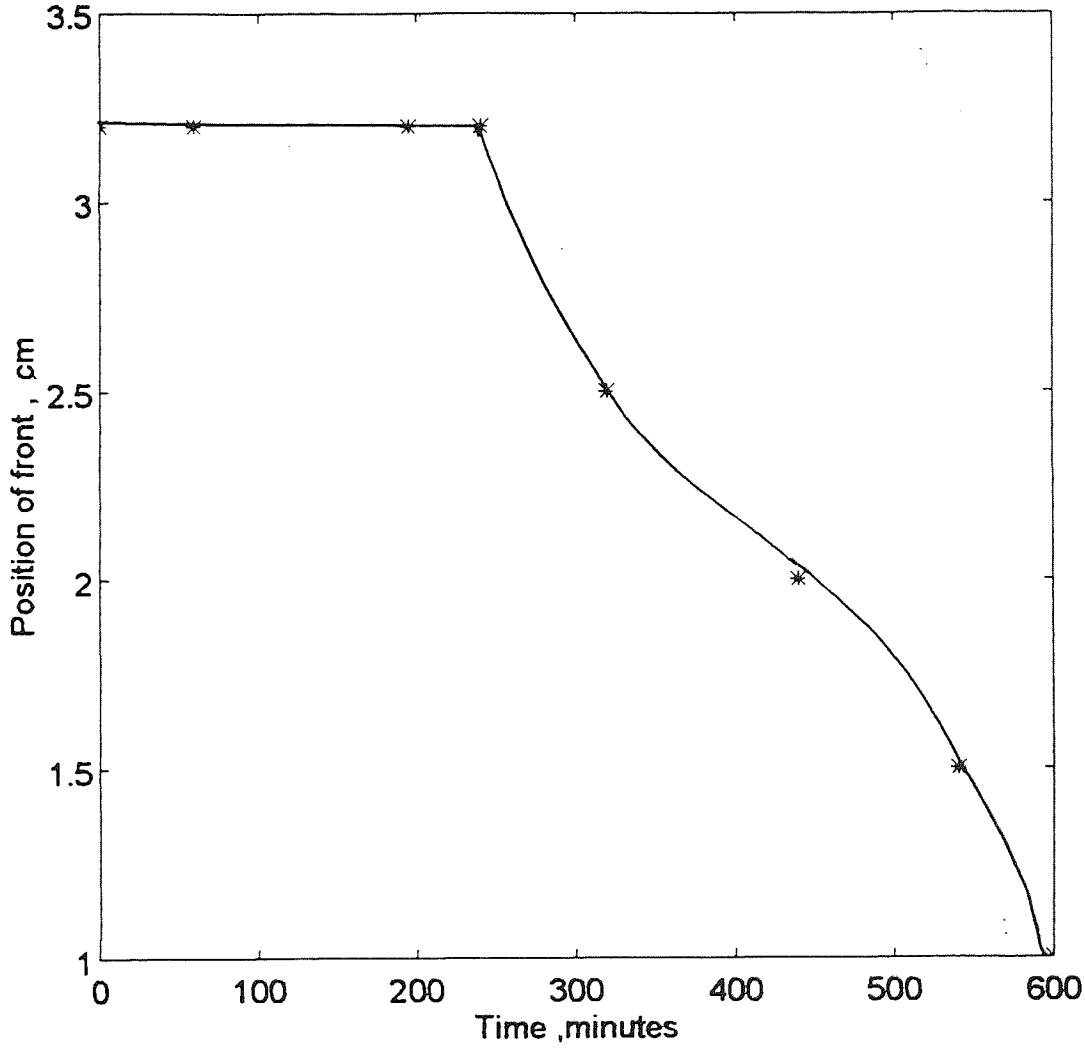

Figure 5.21 Position of receding evaporation front versus time within a bed of activated alumina (150 mesh); air temperature 84 °C.

rate curve respectively. These figures were matched with the temperature distribution profile. As a result, the critical moisture content was determined as $X_{cr} = 0.45$ and the moisture content corresponding to the beginning of the second falling rate was $X_f = 0.375$.

The temperature distribution profiles showed the positions of the receding evaporation front at any time. The positions were plotted against time and provided a significant graph, Fig. 5.21, from which the position of the receding front could be determined accurately at any time. This graph corresponds with the drying rate curve and the velocity of the evaporation plane could again be determined from it.

5.3.2 Wood Powder

A bed of non homogenous particles of wood with a total dry weight of 25.5 g was dried at an air temperature of 84°C. The initial moisture content was high, $X_o = 3.06$, since wood is highly hygroscopic and retains a large amount of bound water throughout its structure.

The resulting temperature distribution profiles, recorded in Fig. 5.22 demonstrate clearly the stages of drying. During the pre-constant rate period, the temperature within the bed increased from ambient temperature to steady values at time t = 50 min. The constant rate period extended from t = 50 min. to t = 180 min. The first falling rate period commenced with increasing surface temperature, as had occurred with the non-hygroscopic materials. As expected, the receding evaporation front appeared in the second falling rate period. This front divided the bed of wood powder into a dry zone at the top and a wet

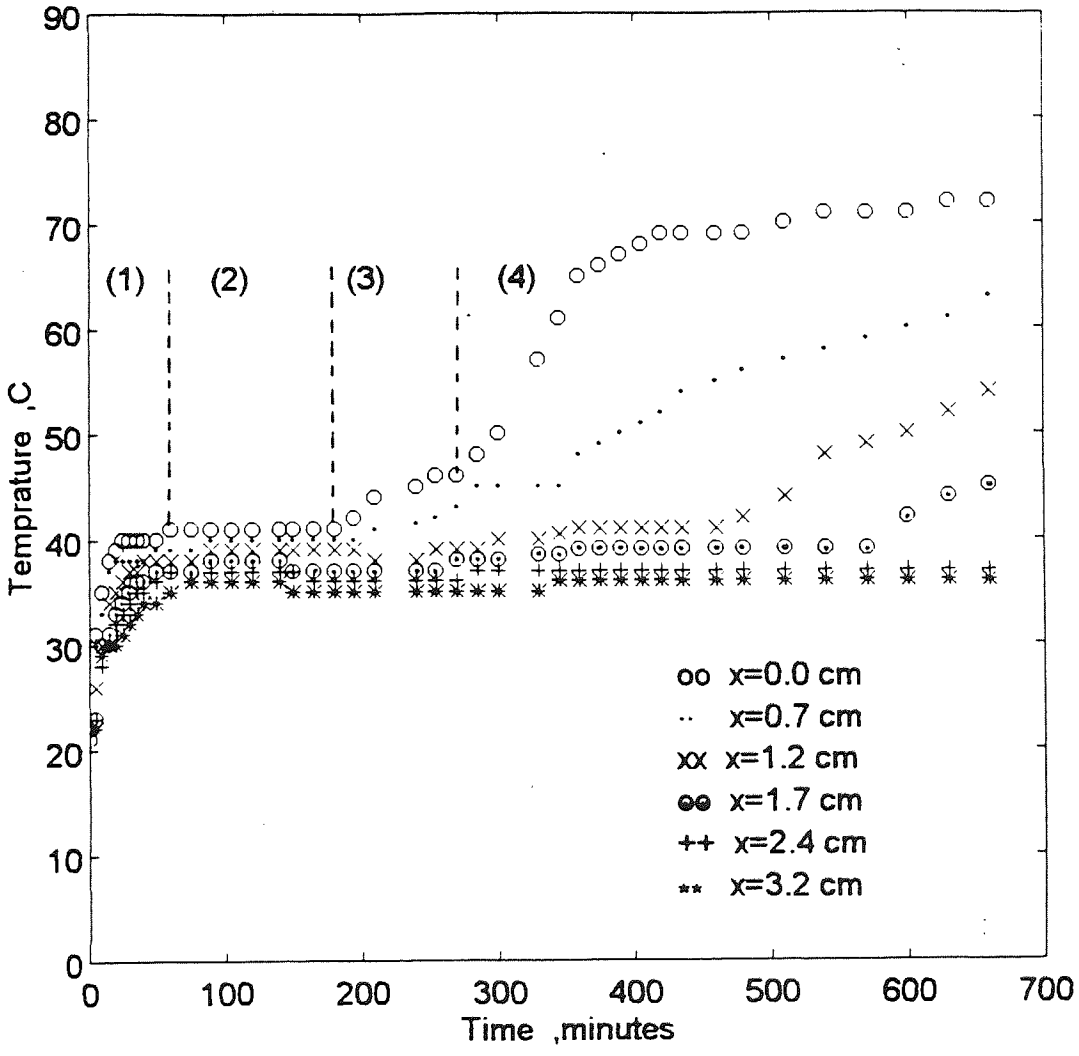

Figure 5.22 Temperature distribution profiles within a bed of wood powder; air temperature 84 °C.

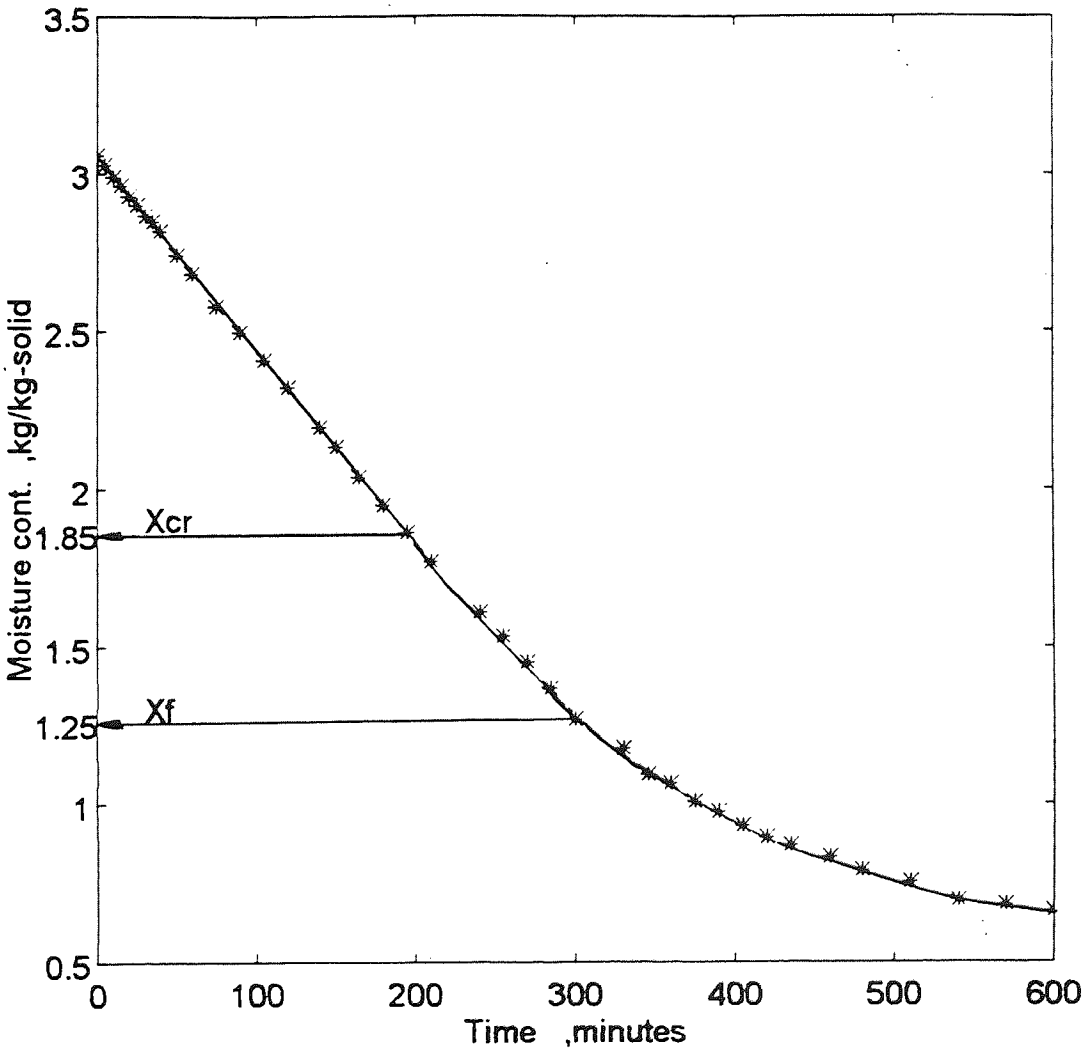

Figure 5.23 Moisture content versus time within a bed of wood powder; air temperature 84 °C.

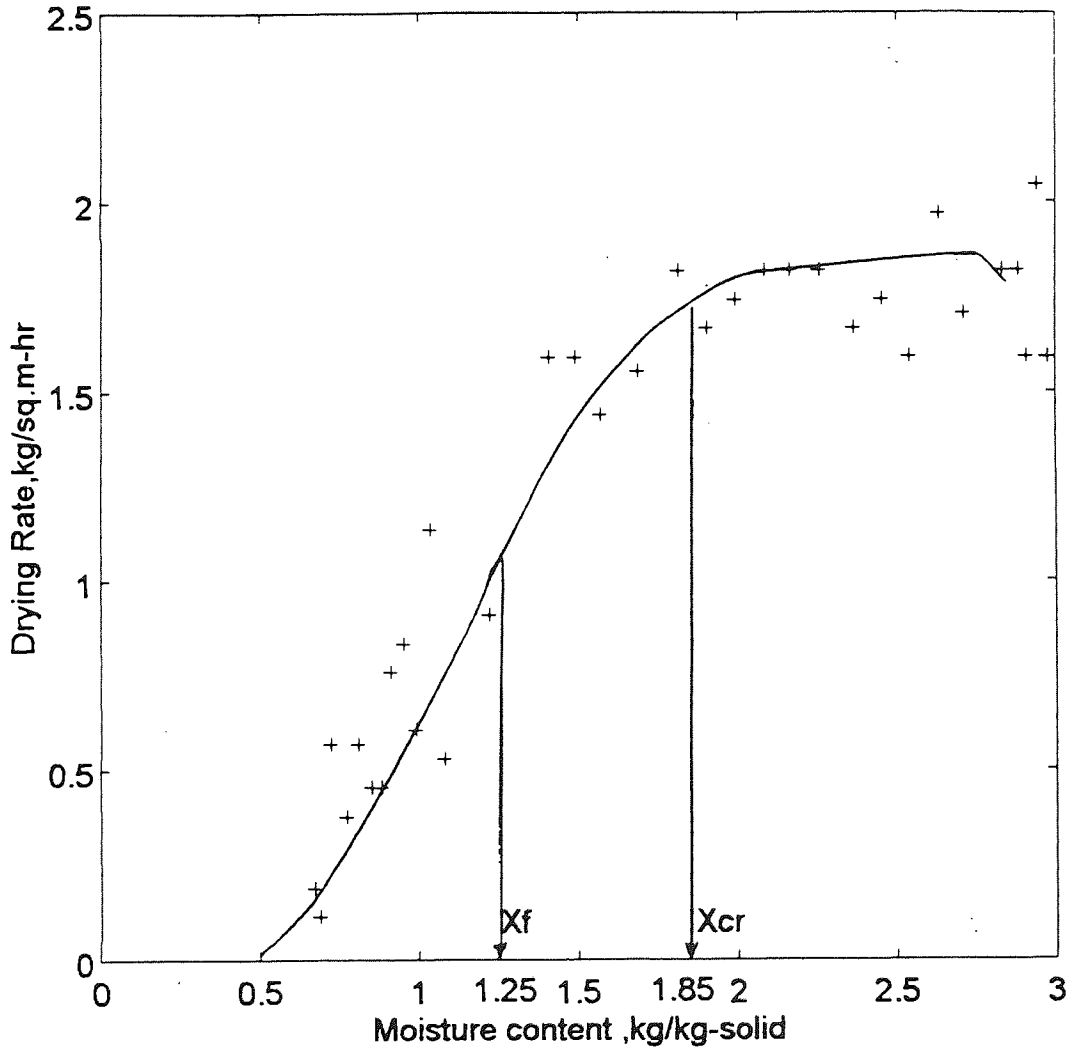

Figure 5.24 Drying rate curve for bed of wood powder; air temperature 84 °C.

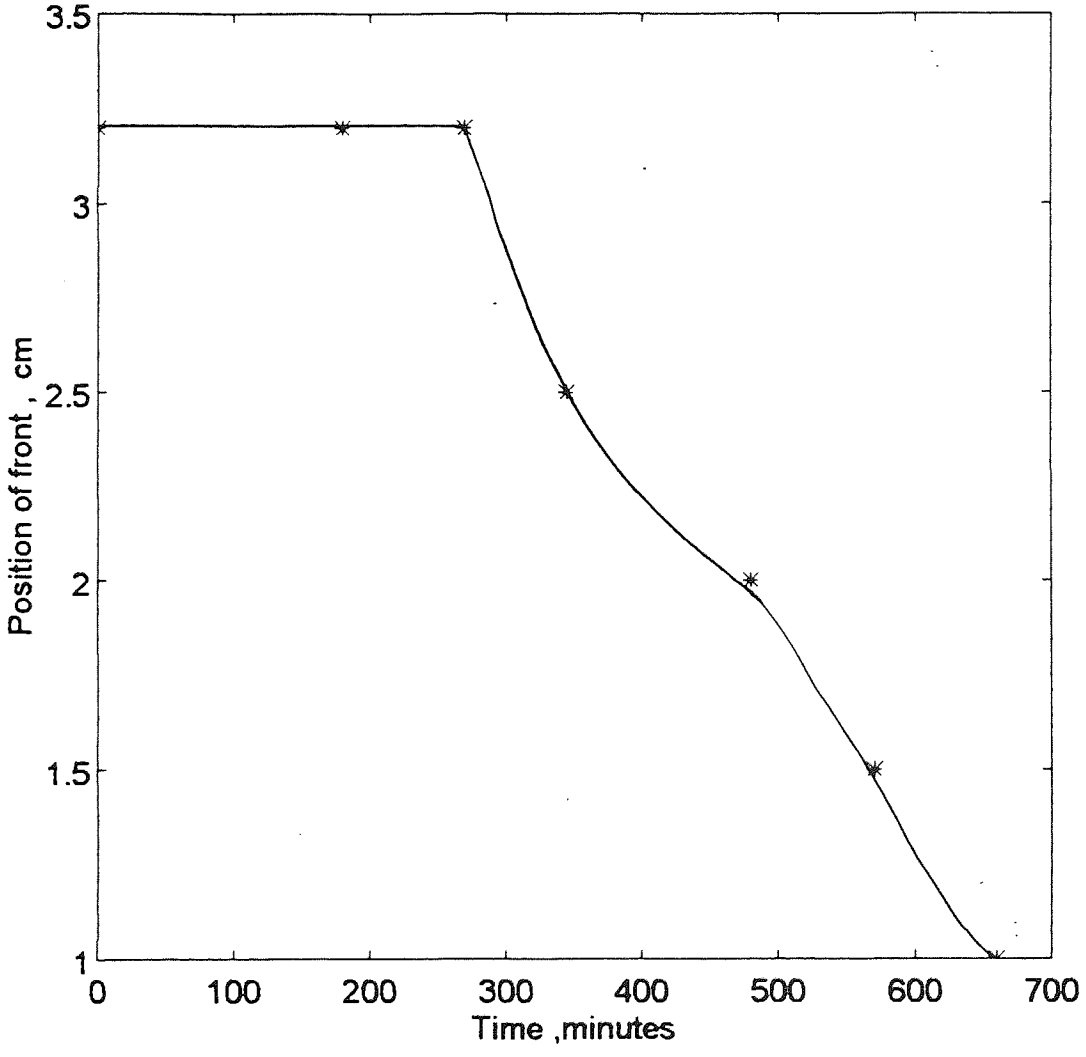

Figure 5.25 Position of receding evaporation front versus time within a bed of wood powder; air temperature 84 °C.

zone in the lower section.

Fig. 5.23 and Fig. 5.24 are plots of moisture content versus time and a drying rate curve respectively. These figures were correlated with the temperature profile to predict average values of the critical moisture content and the beginning of the second falling rate period. The average values were $X_{cr} = 1.85$ and $X_f = 1.25$ respectively. The position of the evaporation front is shown in Fig. 5.25, and as with the previous solids this was reasonably consistent with the drying rate curve.

5.4 EFFECT OF VARYING AIR TEMPERATURE

Temperature distribution profiles were determined at other air temperatures. Glass beads of 400 μm diameter were dried at an air temperature of 74°C. In other respects, the experimental conditions were the same as when the material was dried at 84°C; i.e. similar air velocity, humidity, dimensions of the sample tray and initial moisture content. Glass beads of 100 μm diameter were dried at air temperatures of 64°C and 54°C, with conditions again similar to those at 84°C.

5.4.1 Air Temperature of 74°C

Glass beads of 400 μm diameter were dried at an air temperature of 74°C. The total bed depth was 3.2 cm and the total dry weight of solid was 266 g . The initial moisture content was $X_o = 0.23$.

Figure 5.26 shows the temperature distribution profiles. The duration of the constant rate period was 150 min; as would be expected this was longer than with an air temperature of 84°C, when it was 110 min. The reduced drying rate at 74°C is shown in Fig. 5.28. During the constant rate period there was a small gradient of 2.5°C in temperature between the surface and the bottom. The surface temperature was 36.5°C, close to the measured wet bulb temperature of 36°C.

The first falling rate period started at t = 240 min. The surface temperature rose gradually to another constant temperature level of 46.5°C. As in the experiment at 84°C, the temperature at each depth increased slightly and another constant gradient was approached. The temperature of the surface then rose rapidly at t = 400 min., indicating the start of the second falling rate period. The subsurface layer remained at constant temperature for a short time then at time t=420 min., the temperature rose sharply once another dry layer had formed. The plane of evaporation slowly receded from the surface, dividing the system into two regions, a hot region and a colder region. After 11 hours drying, the bottom was still wet and a few hours more were needed to dry out the material completely, i.e. to the equilibrium moisture content of the solid.

A plot of moisture content versus time is shown in Fig. 5.27. The drying rate curve is shown in Fig. 5.28. During the constant rate period the average drying rate was approximately 1.75 kg/m^2-h . Clearly, this value is smaller than obtained at 84°C, (2.25 kg/m^2-h). Thus as would be expected, the greater the air temperature, the higher the drying rate. The same method was used to determine the mean values of the critical moisture content and the beginning of the second falling rate period as at 84°C. At 74°C the

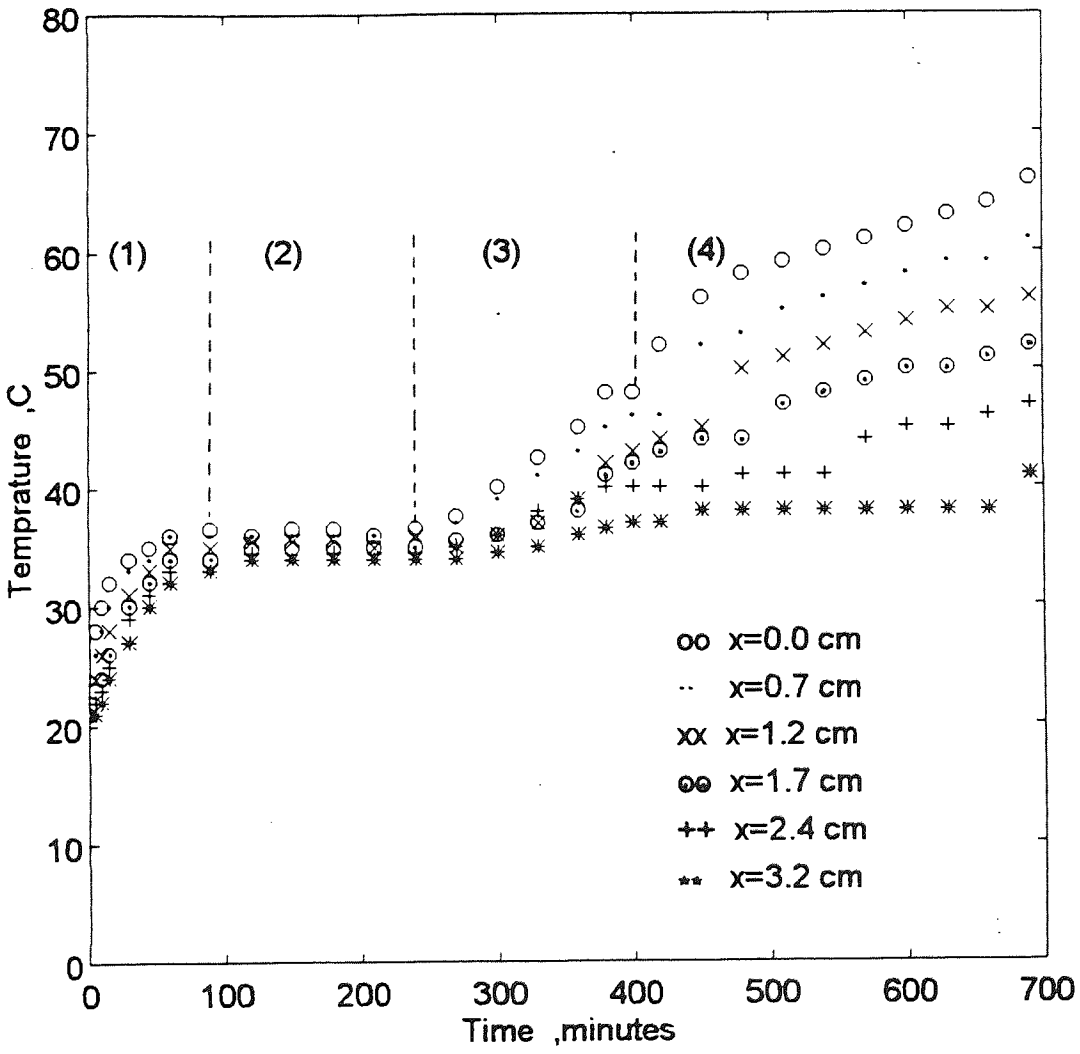

Figure 5.26 Temperature distribution profiles within a bed of glass beads (400 μm); air temperature 74 °C.

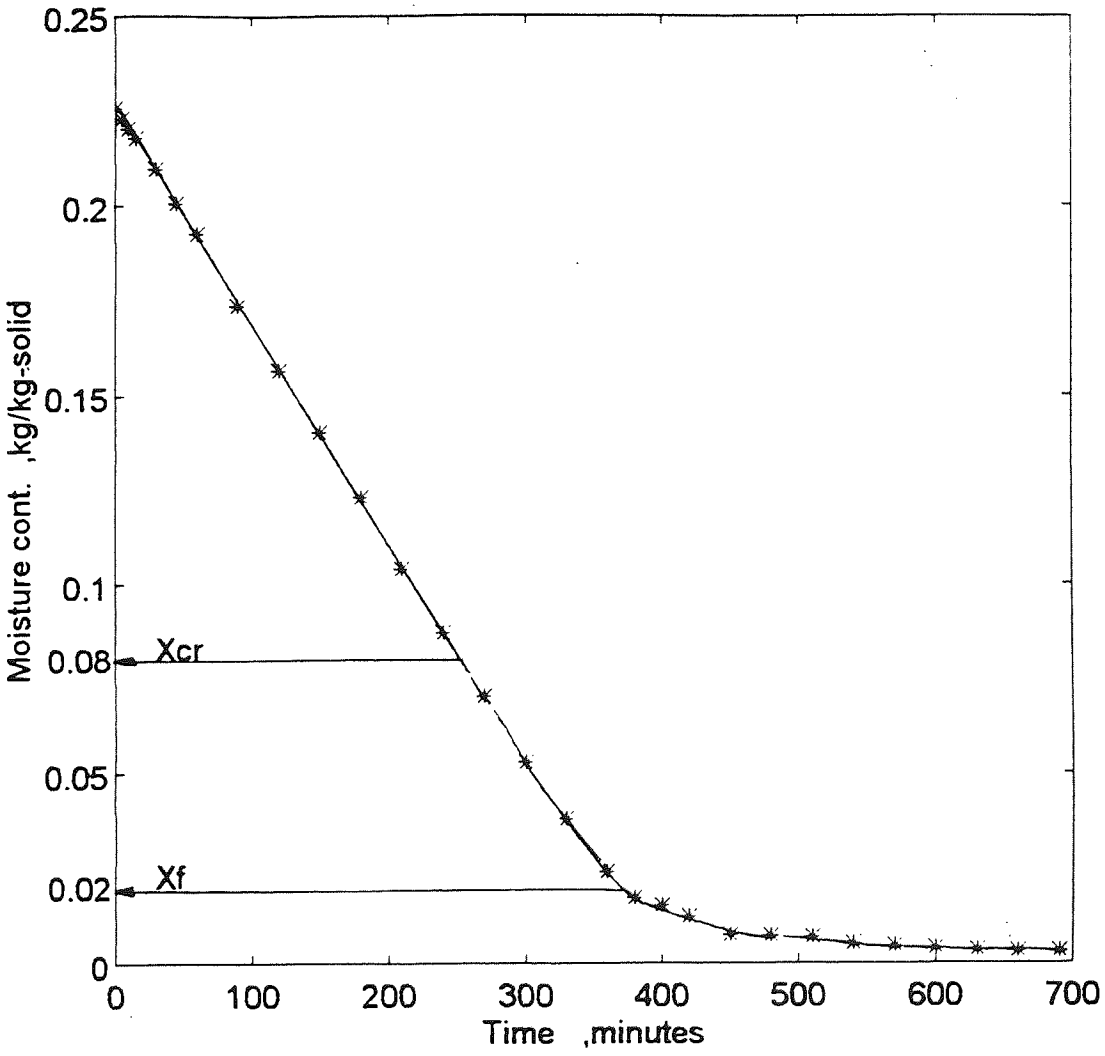

Figure 5.27 Moisture content versus time within a bed of glass beads (400 μm); air temperature 74 °C.

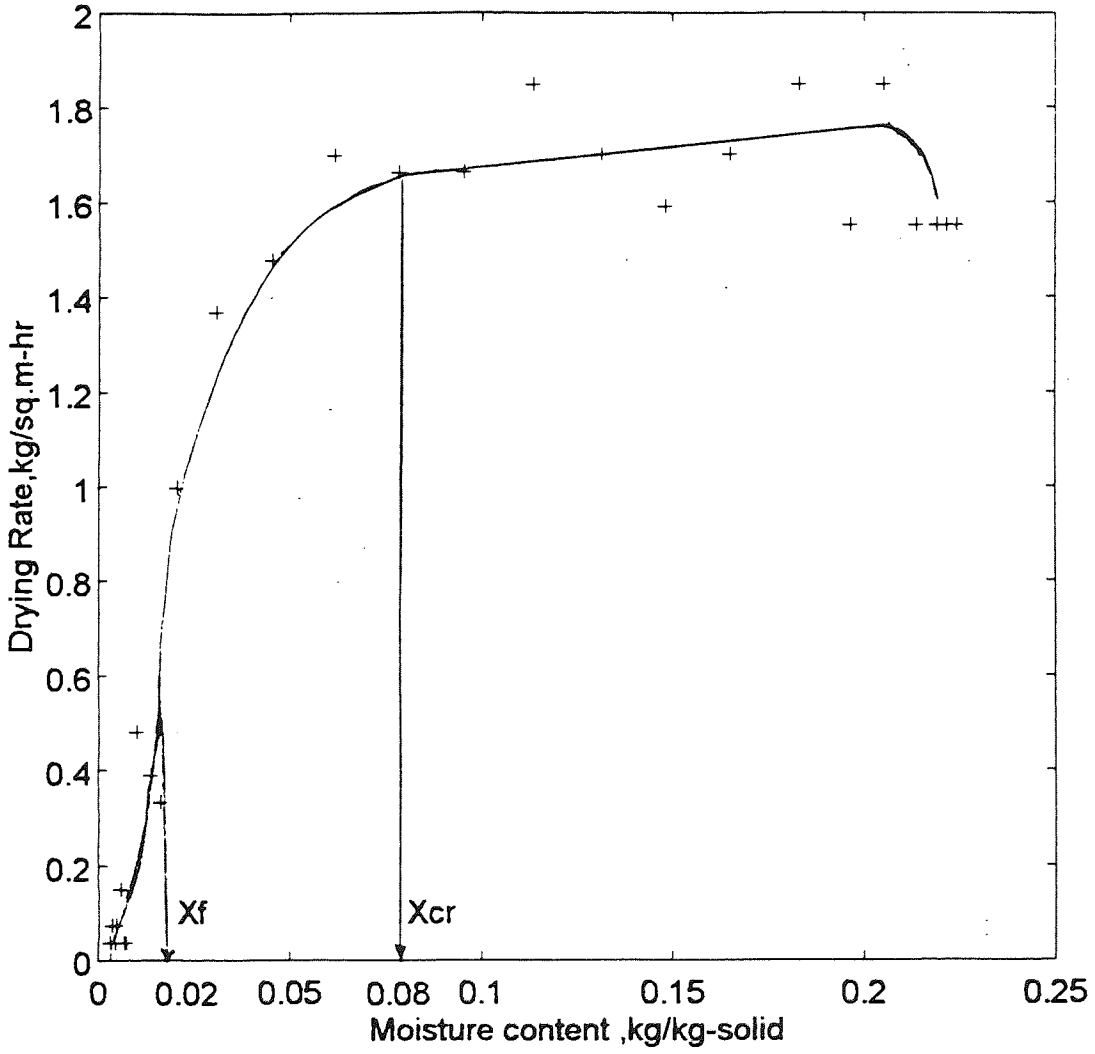

Figure 5.28 Drying rate curve for bed of glass beads (400 μm); air temperature 74 °C.

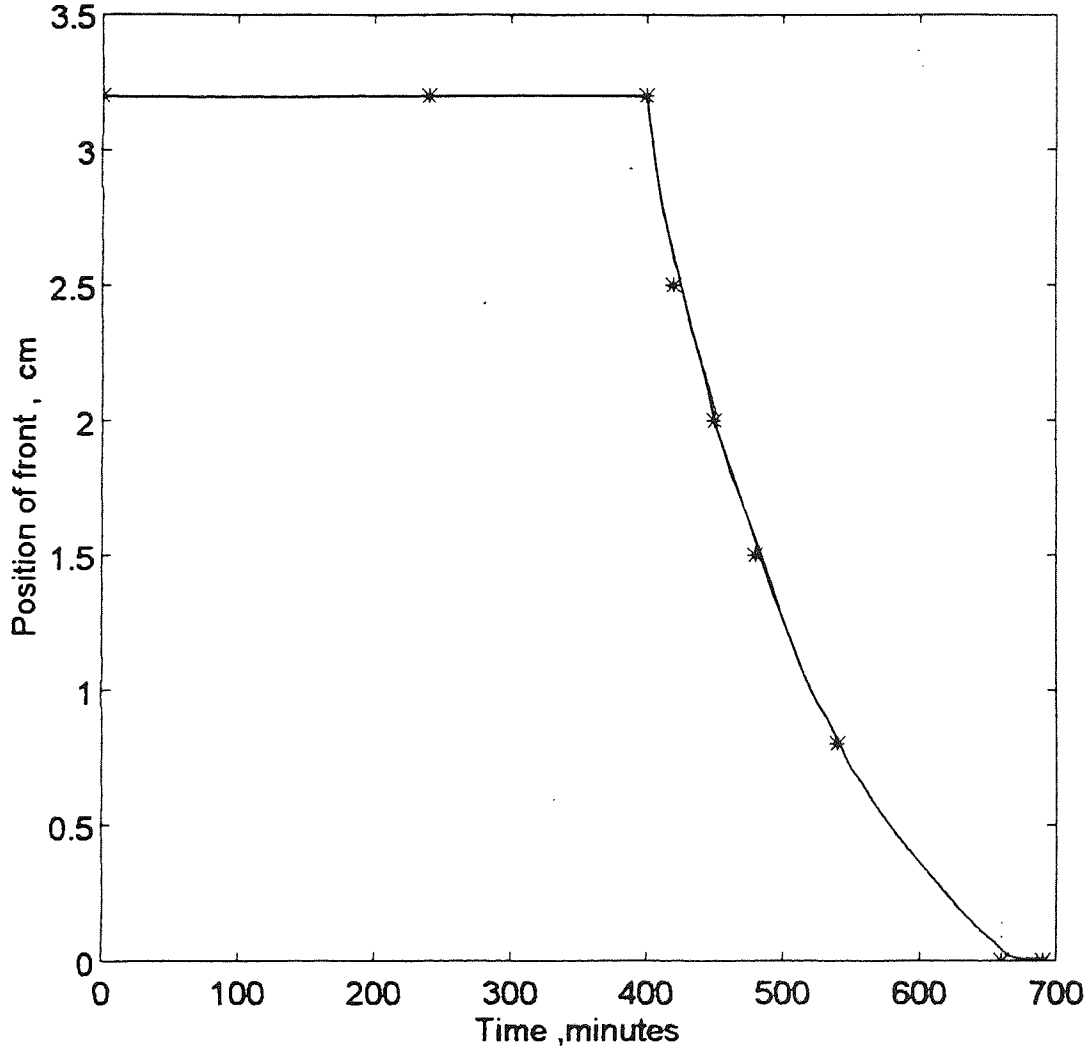

Figure 5.29 Position of receding evaporation front versus time within a bed of glass beads (400 μm); air temperature 74 °C.

correlated values for these points, were $X_{cr} = 0.08$ and $X_f = 0.02$ respectively.

Again, a significant graph, from which the position of the receding evaporation front at any time can be determined, was plotted in Fig. 5.29. The velocity of the evaporation plane at any time can also be predicted from this.

5.4.2 Air Temperature of 64°C

Glass beads of 100 μm diameter were dried at an air temperature of 64°C. The experiment started with an initial moisture content of $X_o = 0.2$. The total dry weight of the solid was 266.5 g .

The temperature distribution profiles, shown in Fig. 5.30, illustrated clearly the stages of drying. The constant rate period started at t = 75 min. and terminated at t = 210 min; naturally this was longer than for the similar experiment at 84°C. The surface temperature was 31.5°C, and the bottom temperature 29.5°C.

The temperature distribution profiles show that at a specific point t = 210 min., the temperature of the bed suddenly increased, identifying the critical point and the beginning of the first falling rate period. The temperature at each depth continued to rise until a constant temperature level was reached. Again, a dry zone formed on the surface at the beginning of the second falling rate period, and as expected a receding evaporation front was observed in this period, dividing the system into a hot dry zone near the surface and a cold wet zone towards the bottom.

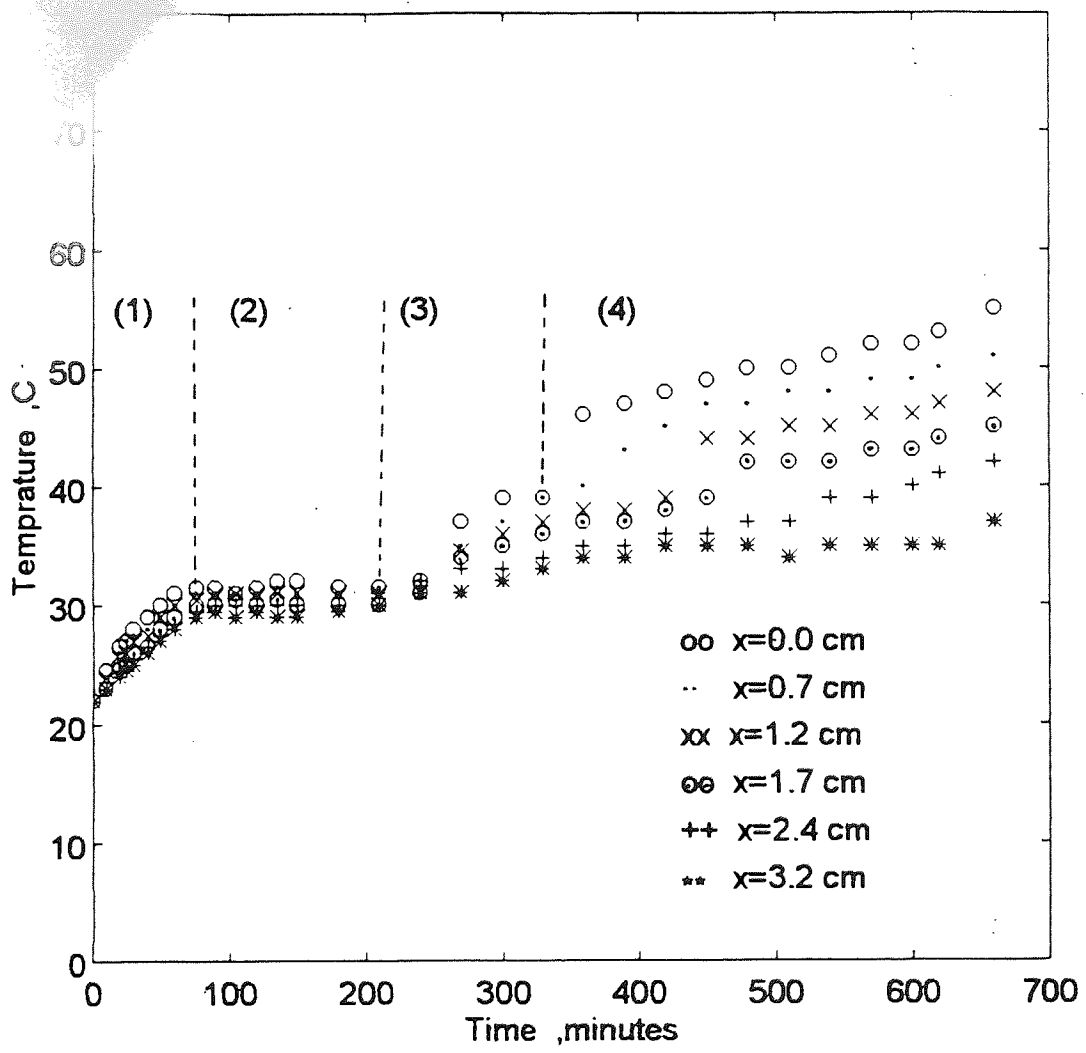

Figure 5.30 Temperature distribution profiles within a bed of glass beads (100 μm); air temperature 64 °C.

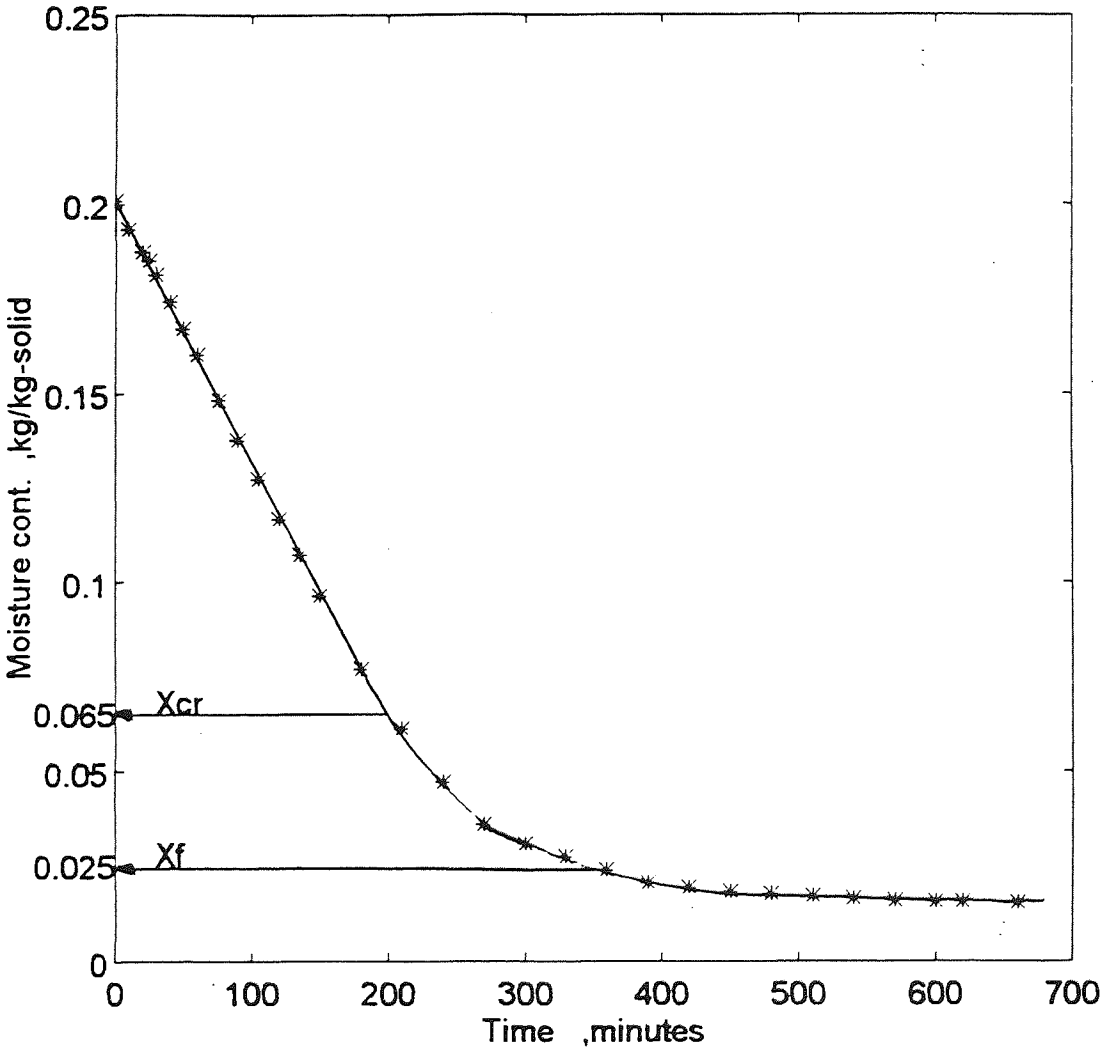

Figure 5.31 Moisture content versus time within a bed of glass beads (100 μm); air temperature 64 °C.

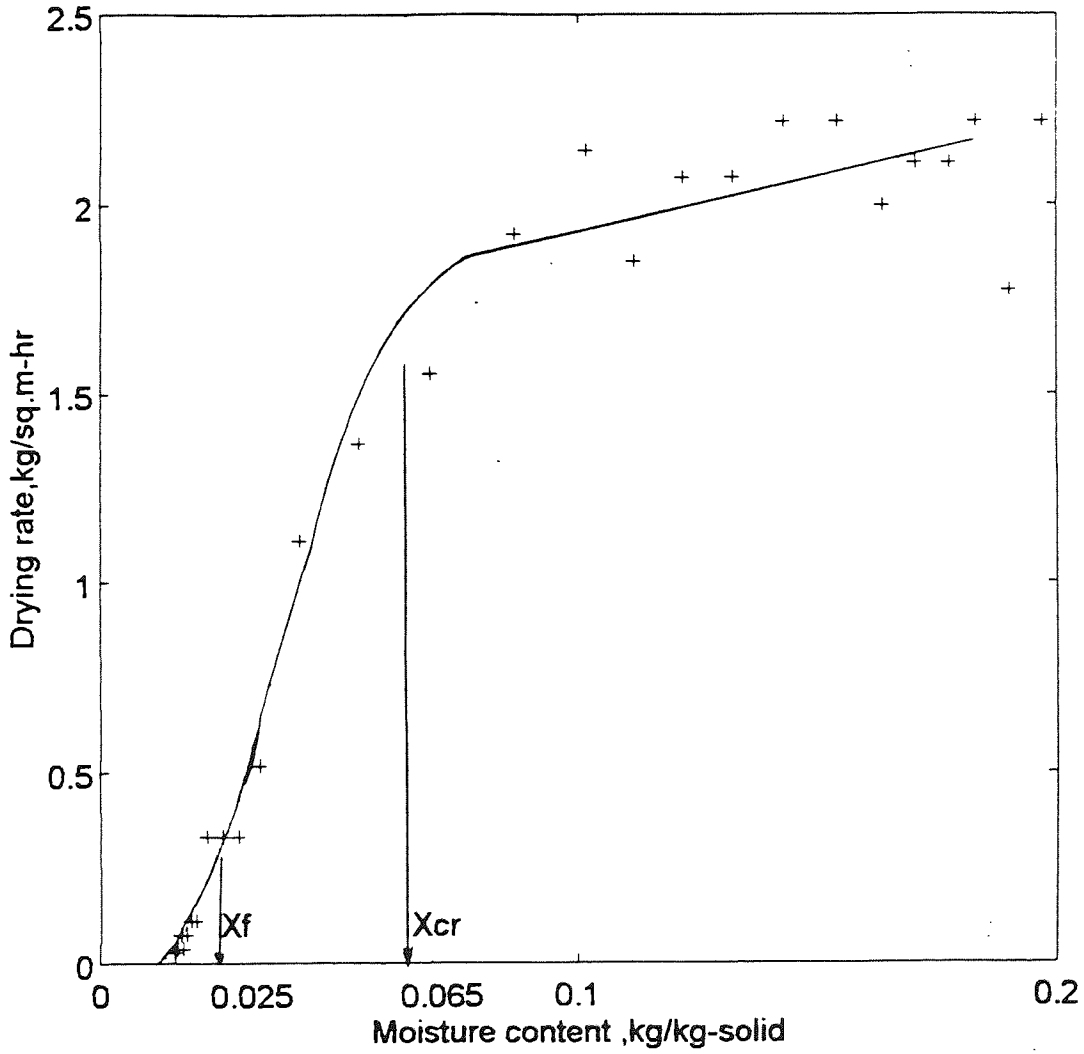

Figure 5.32 Drying rate curve for bed of glass beads (100 μm); air temperature 64 °C.

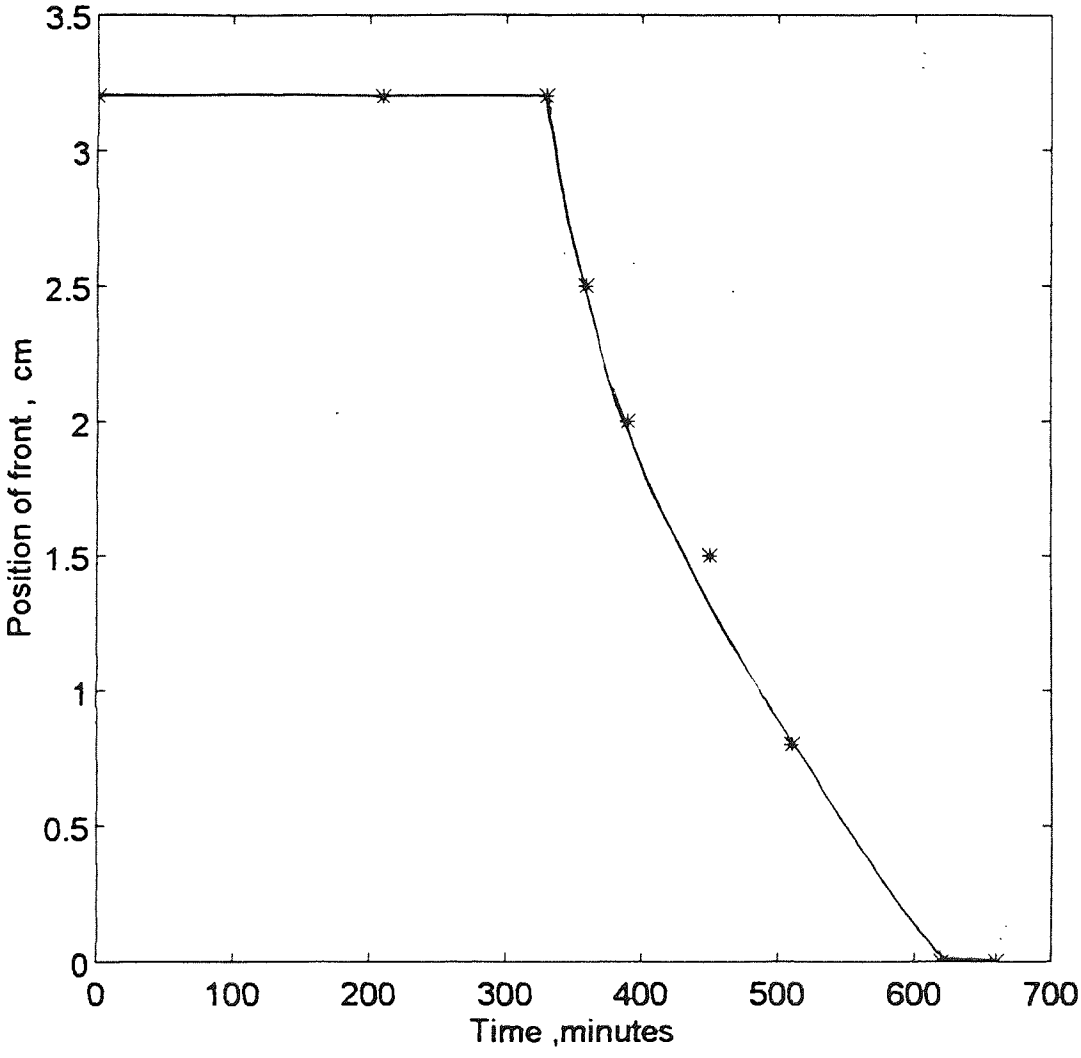

Figure 5.33 Position of receding evaporation front versus time within a bed of glass beads (100 μm); air temperature 64 °C.

Figures 5.31 and 5.32 show the plot of moisture content versus time and the drying rate curve respectively. These figures were matched with the temperature profile. The average value of the critical moisture content was $X_{cr} = 0.065$ and at the beginning of the second falling rate period $X_f = 0.025$. During the constant rate period, the drying rate of glass beads was somewhat lower at 64°C than at 84°C.

The position of the evaporation front at any time can be easily determined from Fig. 5.33, which shows that the velocity of the front is consistent with the drying rate.

5.4.3 Air Temperature of 54°C

Glass beads of 100 μm were dried at an air temperature of 54°C. The initial moisture content was $X_o = 0.2$. The total dry weight of solid was 268 g .

Figure 5.34 shows the temperature profiles in this experiment. The duration of the constant rate period was 180 min. Obviously, this duration was longer than that at 84°C and 64°C. The surface temperature was approximately equal to the bottom temperature, i.e. almost no gradient in temperature existed.

During the falling rate period, the general shape of the distribution profile was similar to some extent to the previous profiles. Again, the two zones and the receding evaporation plane appeared in this period.

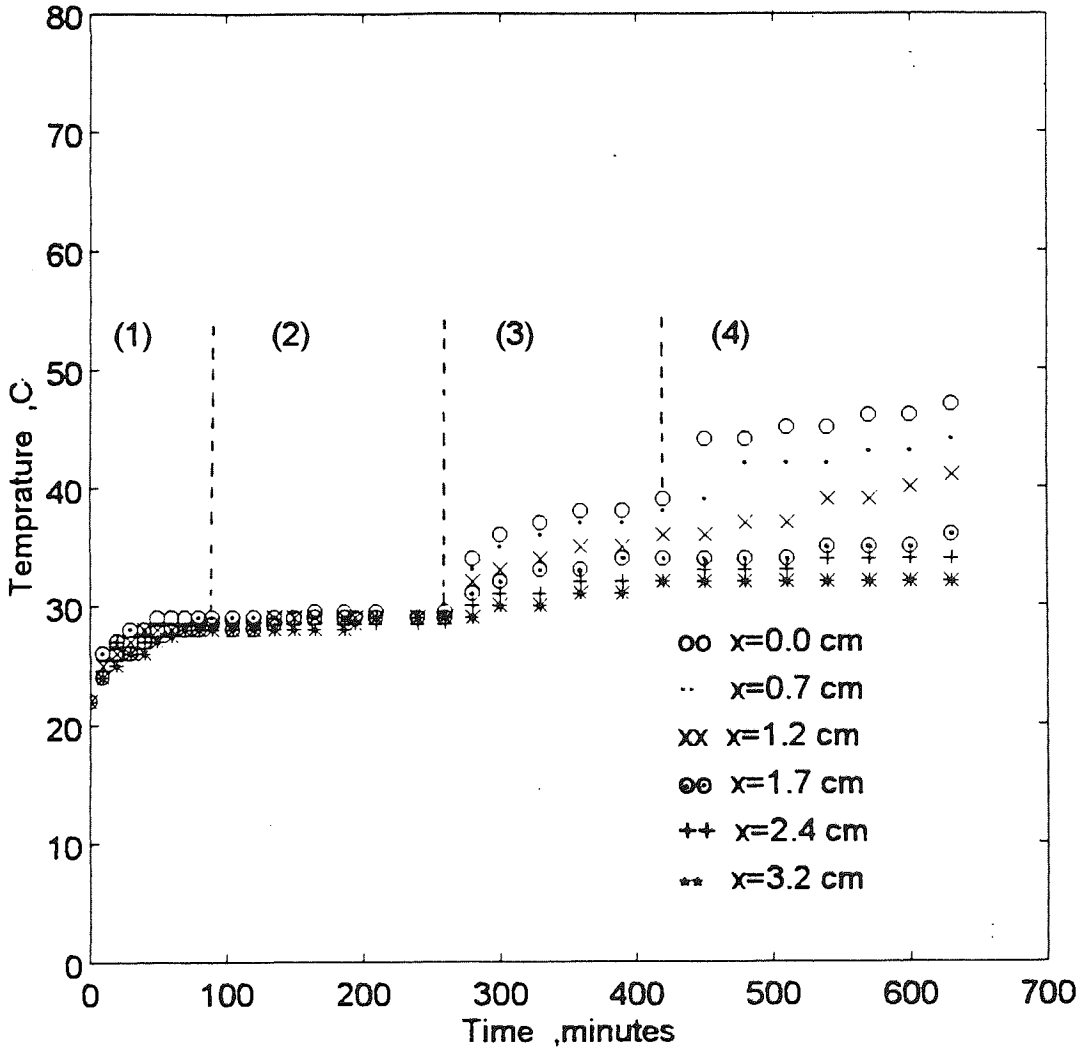

Figure 5.34 Temperature distribution profiles within a bed of glass beads (100 μm); air temperature 54 °C.

5.5 POOL OF DISTILLED WATER

During the constant rate period of drying with saturated solids, a continuous film of water is present at the surface and evaporates as if the solid were not present. The temperature of the saturated surface usually equals the wet bulb temperature. The evaporation from a pool of distilled water was therefore observed to check the wet bulb temperature and temperature distribution. The conditions were similar to those used for drying the hygroscopic and non-hygroscopic materials at an air temperature of 84°C and the initial pool depth was 3.2 cm. The measured wet bulb temperature was 38°C.

The resulting temperature distribution profiles are recorded in Fig. 5.35. The thermocouples and the level of water were observed through the window of the tunnel. At time t = 10 min., the top thermocouple was on the surface of water and the temperature indicated 36°C. The second thermocouple was observed on the surface at time t = 40 min. and the temperature indicated 37.5°C. After 43 min., the surface of the water receded beneath this thermocouple and the temperature increased quickly, since the thermocouple became directly contacted with the hot air. At time t = 140 min., the third thermocouple was observed on the surface and the temperature indicated 38°C. In the case of the fourth, fifth and sixth thermocouples also, when they were on the surface, the corresponding temperature was 38°C. Thus, the wet bulb temperature can be considered as 38°C.

In this experiment no gradient in temperature was recorded, because of heat transfer through the distilled water by natural convection compared with conduction in solids; the latter establishes a moisture gradient through its structure, leading to a temperature

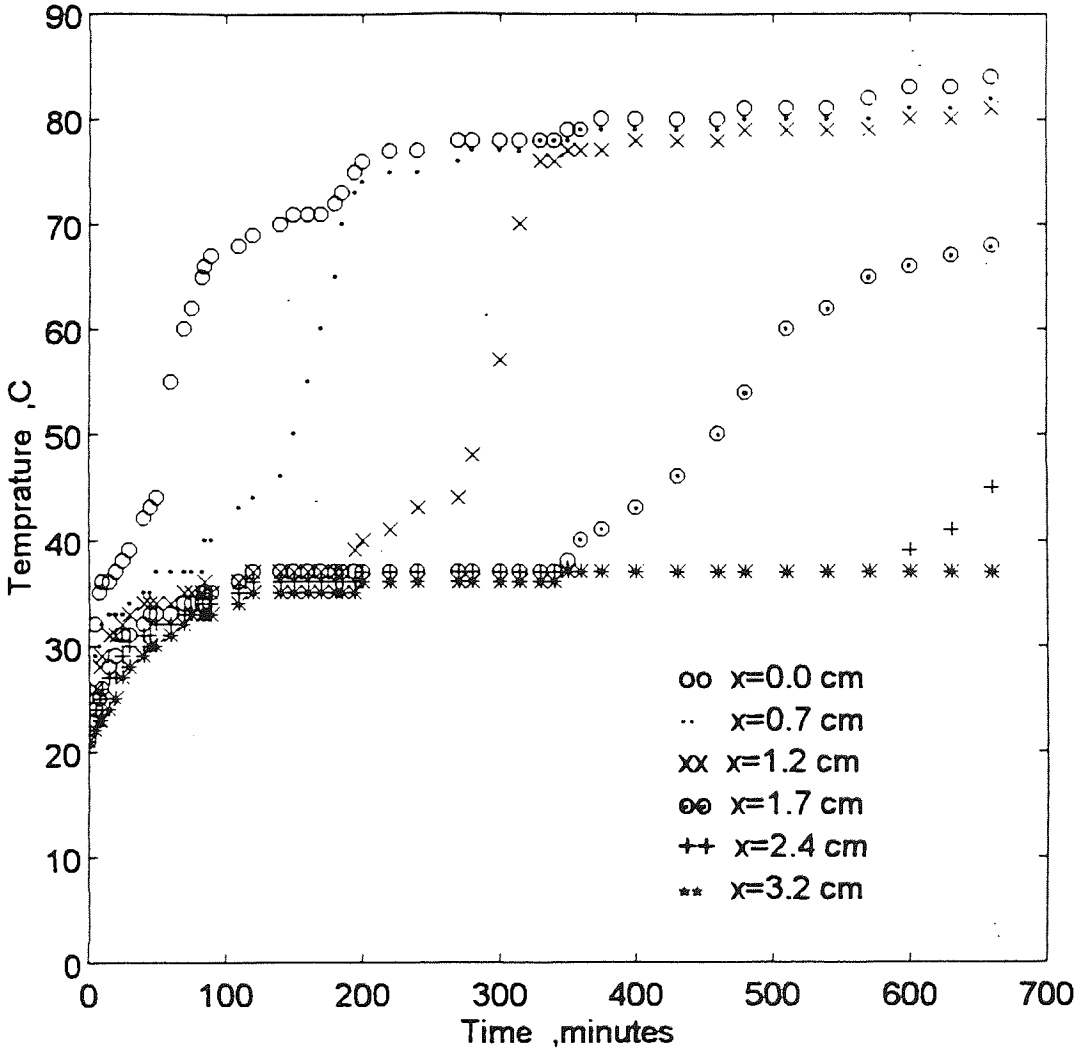

Figure 5.35 Temperature distribution profiles within a pool of pure distilled water; air temperature 84 °C.

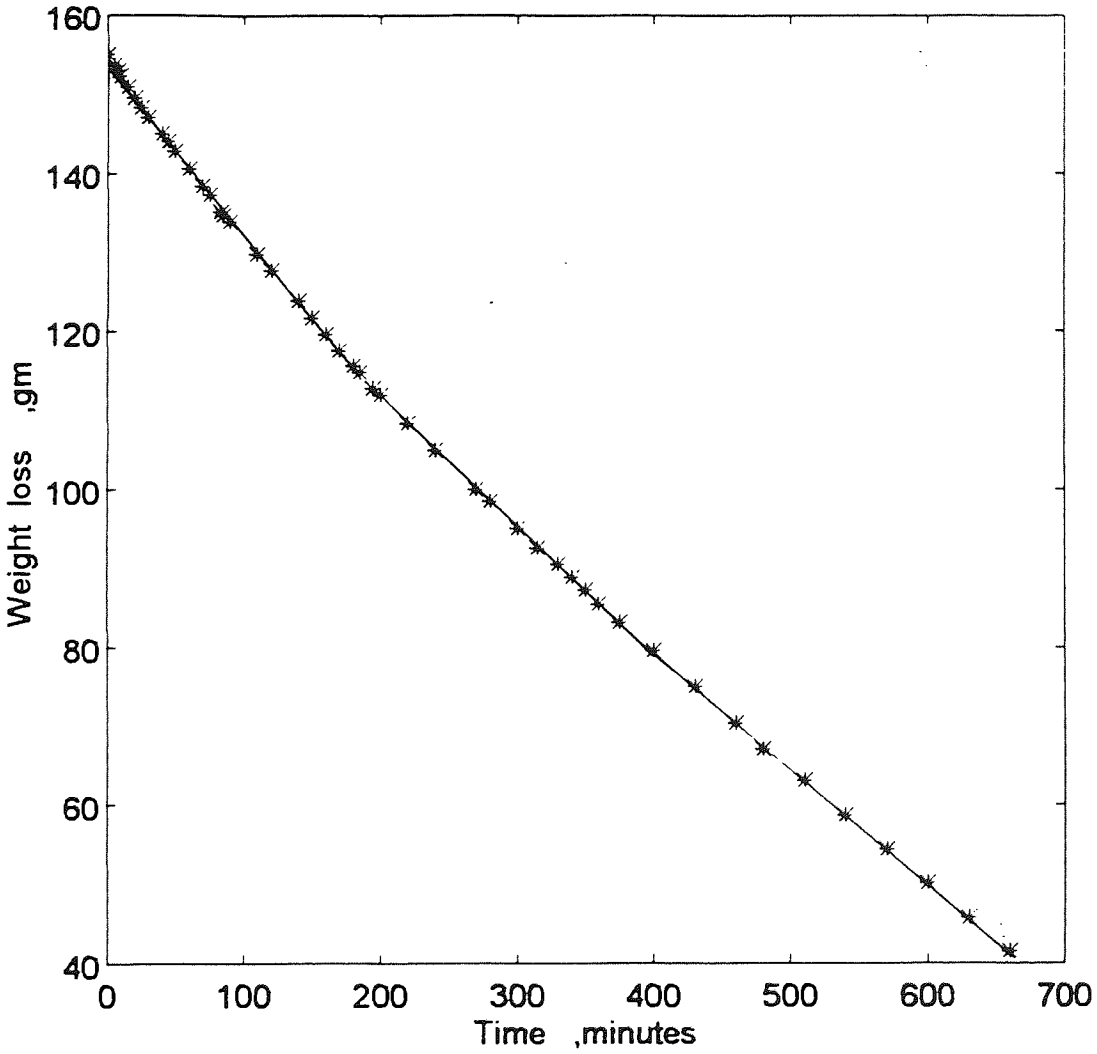

Figure 5.36 Weight loss of pool of pure distilled water versus time; air temperature 84 °C.

gradient.

A plot of weight loss versus time is shown in Fig. 5.36, demonstrating an almost linear relationship between the amount of water evaporated and the time. This was expected, since the distilled water did not contain any discrete or dissolved solids and the process was simply one of evaporation.

5.6 BED OF DRY SOLID

In the previous experiments, the temperature distribution profiles were recorded during a duration up to 700 min., where the moist solids became almost completely dried out. However, the solids may take a longer time to reach their equilibrium moisture content; because drying is very slow in the later stages. The temperature distribution profiles may continue with the same form. Therefore, it was desirable to carry out an experiment beginning with a pure dry solid, to investigate the temperature distribution profiles.

A dry bed of glass beads of 100 μm diameter was heated up in a flow of air at 84°C. The conditions of the experiment were similar to those applied for drying the wet bed. Figure 5.37 shows the temperature distribution profiles within the bed. The temperature rose quickly from ambient temperature to establish a constant temperature gradient between the various levels. The surface temperature approached the air temperature, whilst the bottom temperature was 53°C. The gradient in temperature remained constant for 10 hours. This confirmed that the drying experiments with hygroscopic and non-hygroscopic

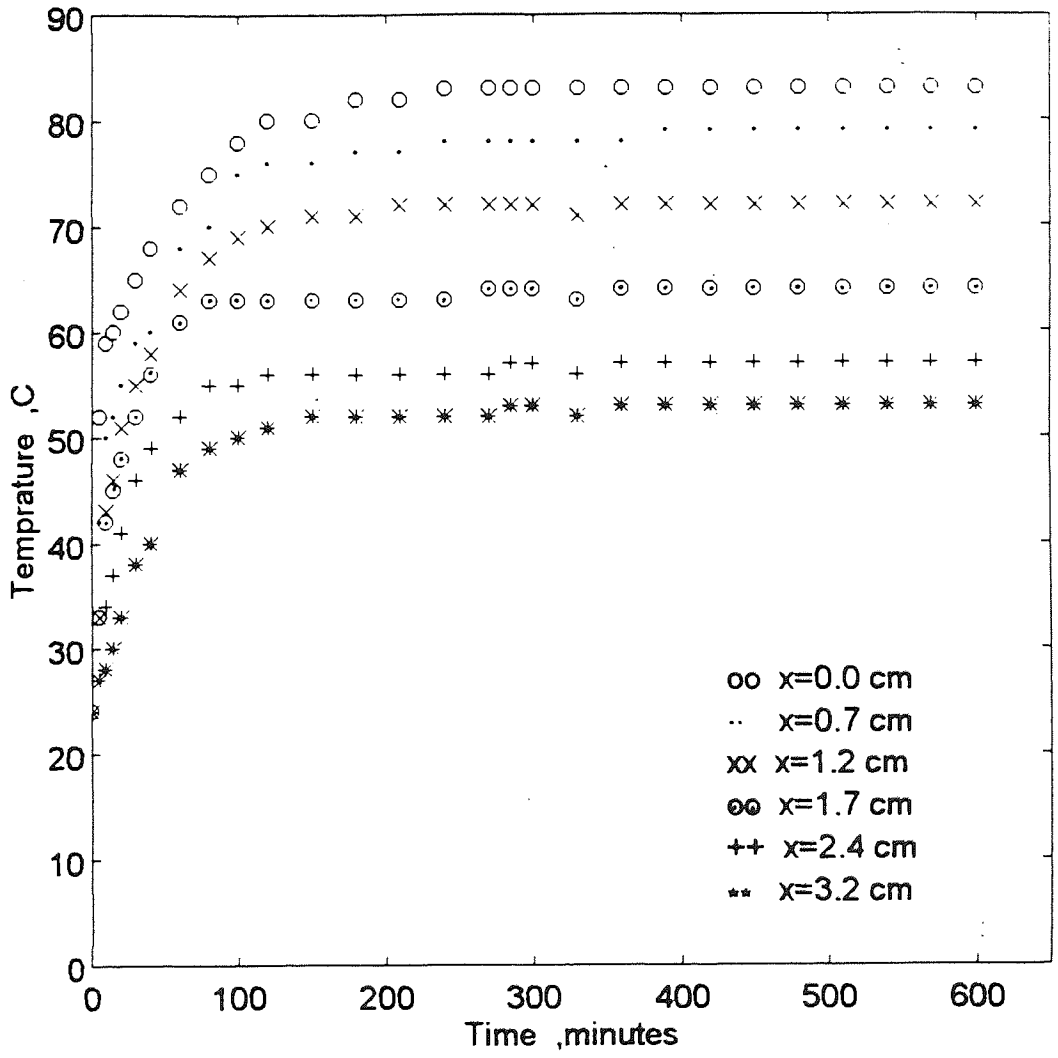

Figure 5.37 Temperature distribution profiles within a bed of dry glass beads (100 μm); air temperature 84 °C .

materials at air temperature of 84°C, the temperature profile will take the form of a constant gradient in temperature when the body approaches the equilibrium moisture content.

5.7 CONCLUSIONS

The temperature distribution profiles determined within flat beds of hygroscopic materials provided useful information on the mechanisms of convective drying. It identified clearly the stages of drying; i.e. the pre-constant rate period, the constant rate period, the first falling rate period and the second falling rate period.

With a fixed initial moisture content and a constant gas velocity, the duration of the constant rate period depended on the dry bulb temperature of the forced air stream. As expected the lower the air temperature, the longer the constant rate period. In this period, the temperature of the surface usually approximated to the wet bulb temperature. A significant result relative to this period was that during the constant rate period at the high air temperature, a temperature gradient was present throughout the body. This gradient stayed constant during the whole period. The gradient in temperature was reduced when the air temperature was decreased. At a low air temperature, 54°C, the gradient was not observed clearly; and the temperature of the surface approximated to the temperature at the bottom of the bed. Therefore, the temperature gradient may disappear completely at air temperatures less than 50°C.

It was concluded that the magnitude of the gradient in bed temperature during the constant rate period depends upon the convective air temperature. The gradient also

depends on the type of material, since different gradients were obtained with the different solids. The structure of the material may play an important role in the distribution of moisture content throughout the bed. As expected, no gradient in temperature was obtained with a pool of distilled water due to natural convective effects.

The temperature distribution profiles illustrated that at a specific time, the temperature of the bed at each depth increased slightly until it approached another constant temperature level. This time usually corresponded to the critical moisture content and the start of the first falling rate period. At the second level of constant temperature at each depth, an equilibrium state may occur. The second period of constant surface temperature was usually short. The temperature then rose sharply and continued to rise until it approximated to the air temperature. The point at which surface temperature increased indicated the start of the second falling rate period, with a thin dry zone formed on the surface. The subsurface layer remained at a constant temperature level whilst evaporation occurred, i.e the plane of evaporation receded from the surface to the subsurface layer. The temperature of this layer was observed to rise suddenly at a specific point, due to the formation of another dry layer. This point indicated the position of the receding evaporation front at that time (128). The evaporation plane slowly receded from the subsurface layer to another sublayer. Thus, the receding evaporation front divides the system into two regions : a hotter dry zone in the upper section of the system and a wet zone toward the bottom. A physical model can be constructed to describe this phenomenon. Figure 5.38 shows the physical model of the receding evaporation front and the two regions during the second falling rate period. The temperature profile takes the form of a constant gradient in temperature when the bed becomes 'dried out', since only

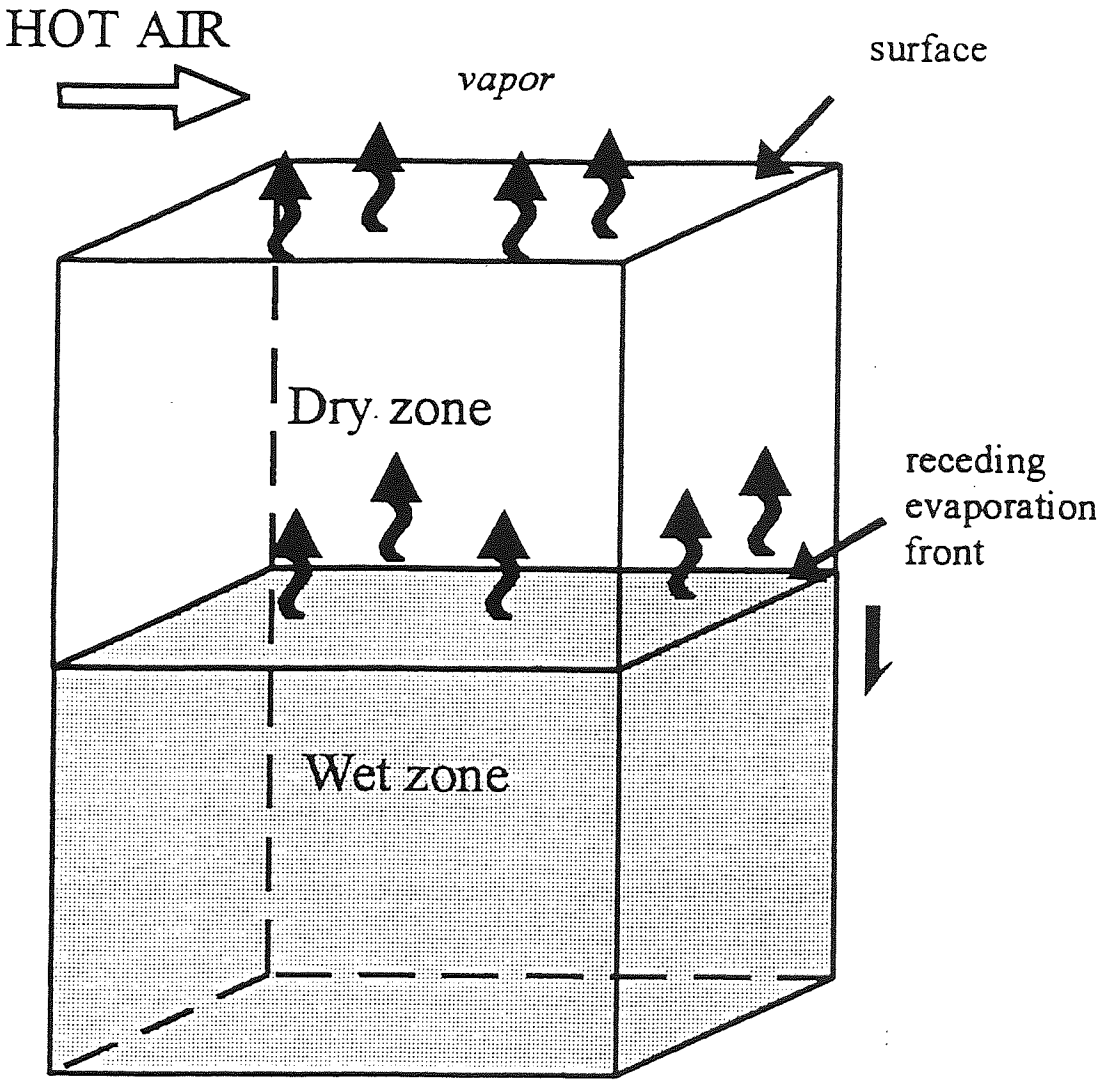

Figure 5.38 Physical model of the receding evaporation front and the two zones which appear during the 2nd falling rate period.

conductive heat transfer is then involved.

The temperature distribution profiles within the hygroscopic materials studied were in general similar to those within the non-hygroscopic materials. It was difficult to make a clear distinction between the temperature profiles of each type. However, the durations of the stages of drying were longer with the hygroscopic material because of the bound water in their structure.

Matching the temperature distribution profiles with the plot of moisture content versus time and with the drying rate curve, provided an effective method for predicting the extent of each drying stage. By this method, the critical moisture content and the moisture content corresponding to the beginning of the second falling rate period were determined accurately.

The temperature profiles exhibited points at which the temperature at each depth increased after the second constant temperature level. These points were plotted against time and provided a useful graph from which the position of the evaporation front at any time could be determined easily and accurately. It also provided a simple means to calculate the velocity of the front at any time. The graph was always similar to the drying rate curve; so the movement or velocity of the receding front was consistent with the drying rate.

CHAPTER 6

A NEW MATHEMATICAL MODEL FOR CONVECTIVE DRYING

6.1 INTRODUCTION

Mathematical models which deal with temperature distribution profiles during convective drying have been discussed in section (3.3) in Chapter 3. It was concluded that none of the models reported in the literature were successful in describing the drying behaviour and predicting the temperature distribution within various materials. As mentioned previously, Szentgyorgyi's model (114, 115) shows a satisfactory result and seems more acceptable than others. Moreover, it was applied to the results of experiments performed under similar conditions to those in the current research. Therefore, it was chosen to be evaluated for comparison.

Figures 6.1 and 6.2 show temperature distribution profiles within beds of glass beads of 100 μm diameter and of activated alumina compared with results predicted from Szentgyrgyi's model. These figures demonstrate the following features. The pre-constant and the constant rate periods are not clear and cannot be distinguished from each other. Moreover, there was no temperature gradient throughout the bed. During the falling-rate period, the difference between the predicted temperatures at the surface and bottom was very small compared with the experimental results. Also, no temperature difference was predicted for the wet region contrary to reality. In general, Szentgrorgyi's model is shown

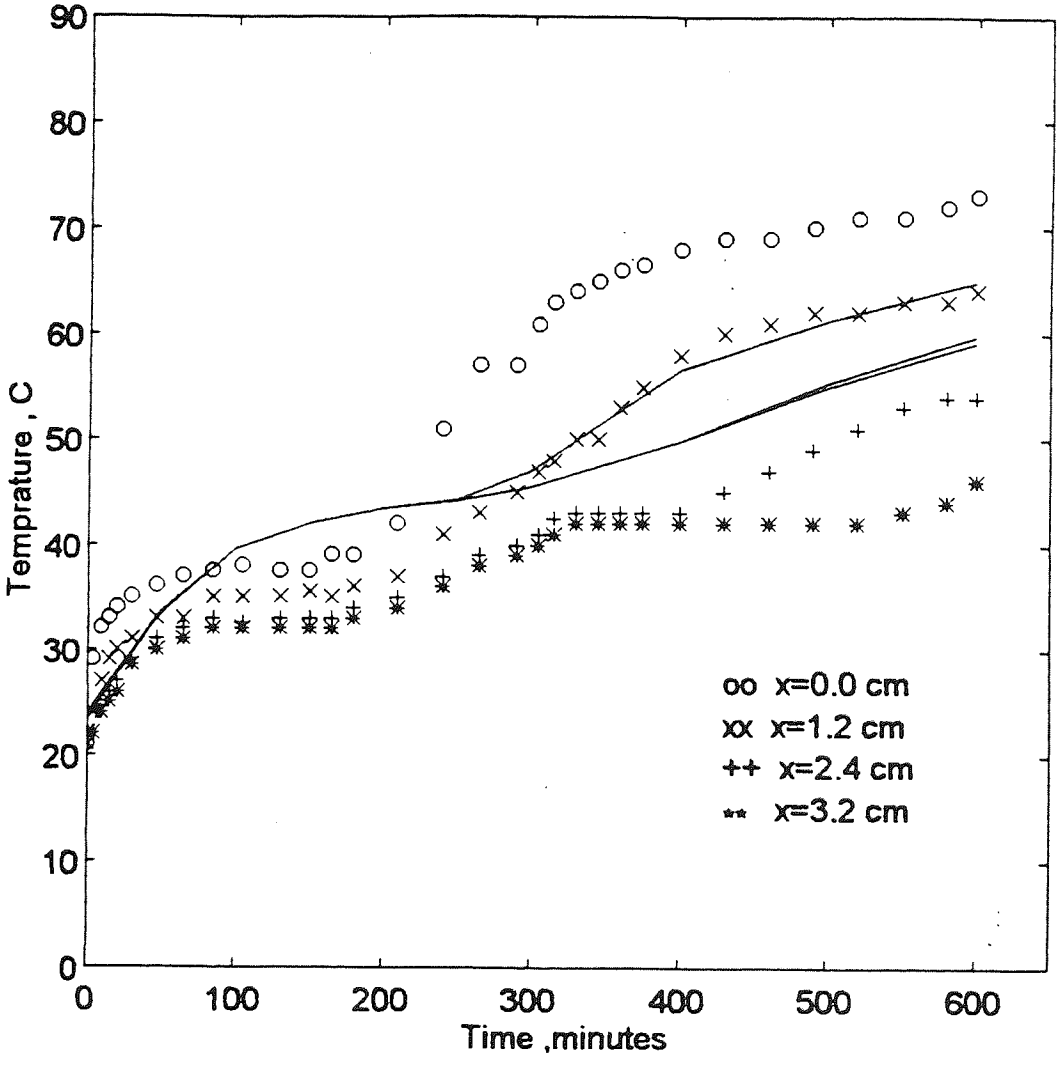

Figure 6.1 Predicted results from Szentgyorgyi's model compared with experimental results for a bed of glass beads (100 μm); air temperature 84 °C; [Predictions, complete curves relative to the same four depths as the experimental data].

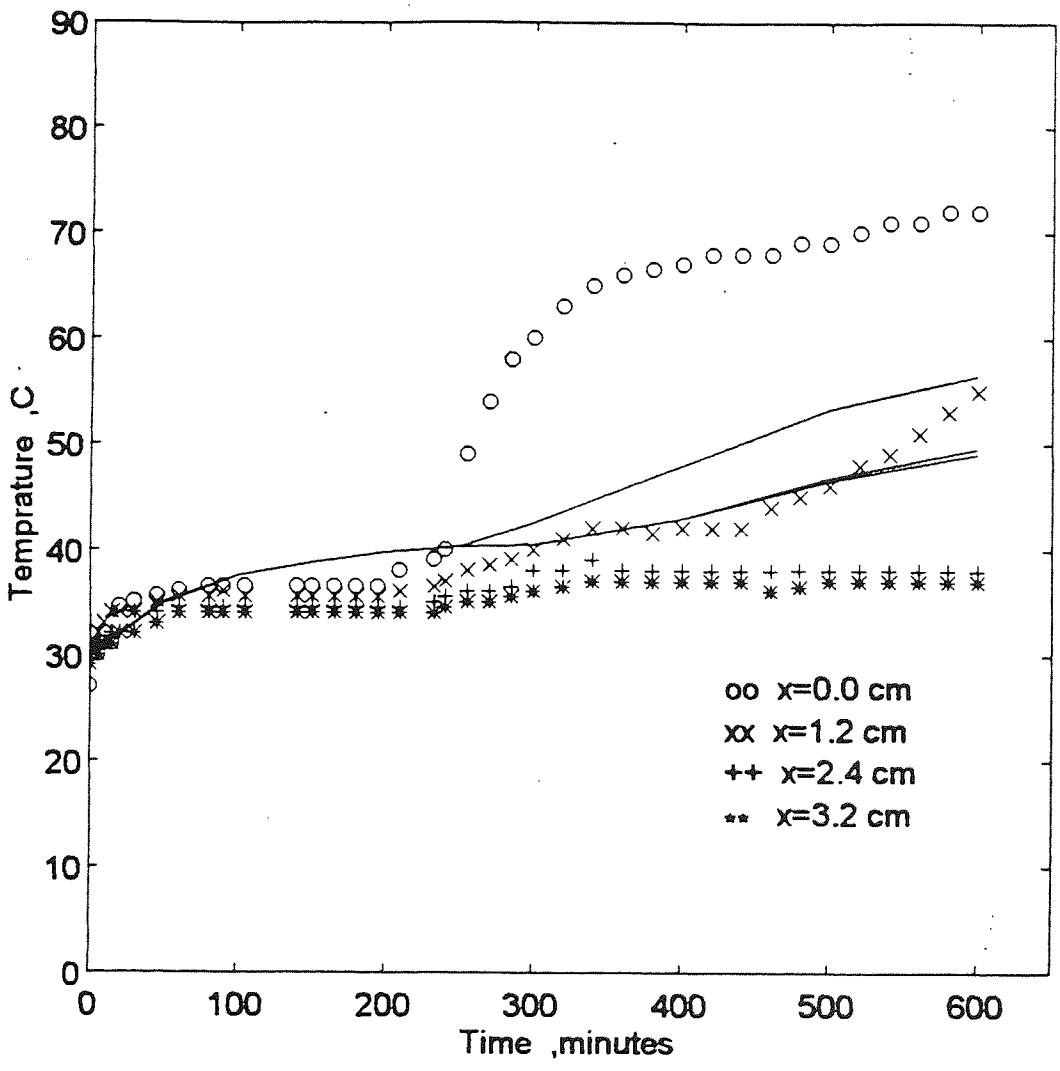

Figure 6.2 Predicted results from Szentgyorgyi's model compared with experimental results for a bed of activated alumina, 150 mesh; air temperature 84 °C;

to be insufficient to predict the temperature distribution within beds of such materials. Therefore, it was considered advantageous to study heat and moisture transfer mechanisms throughout the drying wet material and to develop an effective model.

In this chapter a new model is proposed to predict temperature distribution profiles within thick, flat beds or slabs of hygroscopic or non-hygroscopic materials drying under forced convection. The slab is assumed to be well insulated at the sides and base, and evaporation takes place only from the surface. The proposed model was divided into three stages : a pre-constant rate period, a constant rate period, and a falling-rate period. Since the correct values of the physical properties and coefficients of the tested materials play an important role in solving the model, these aspects are discussed in section (6.5).

6.2 PRE-CONSTANT RATE PERIOD

Many authors ignore the pre-constant rate period in spite of its importance, since it establishes the initial temperature gradient within a bed. During the pre-constant rate period the temperature within the bed of wet material increases rapidly with time and varies with the depth. Thus, unsteady state conditions of heat transfer occur during this period; a complicated solution is therefore required to solve the heat transfer equations. However, presumably because the duration of the pre-constant rate period is so short compared with other stages (approximately less than 10% of the total drying period), researchers have paid less attention to it.

In the pre-constant rate period the heat transferred to the body raises its initial

temperature to a certain value resulting in an unsteady state condition. Assuming that heat is transferred only by conduction through the solid skeleton, the heat flux, $q_m = -\lambda_m \frac{\partial T}{\partial x}$.

Therefore, the differential equation for heat transfer can be developed from the basic principles of the energy balance in one direction of the wet sample as,

$$\frac{\partial T}{\partial t} = \alpha_m \frac{\partial^2 T}{\partial x^2} \tag{6.2-1}$$

where α_m is the effective thermal diffusivity of the wet material,

$$\alpha_m = \frac{\lambda_m}{\rho_s Cp_m} \tag{6.2-2}$$

Assuming the whole body has a uniform initial temperature of T_o, the initial conditions are,

$$T_o = T|_{x=0} = T|_{x=L} \tag{6.2-3}$$

At the external surface, x = 0, the boundary conditions can be written on the basis of Fig. 6.3, as,

$$-\lambda_m \frac{\partial T}{\partial x} = h(T_a - T_s) - m_p \Delta hv \tag{6.2-4}$$

The drying rate in the pre-constant period, $\dot{m}_p$, is defined as

$$\dot{m}_p = Mw \frac{k'_c}{RT}(P_s - P_{va}) \tag{6.2-5}$$

The drying rate, $\dot{m}_p$, the surface temperature, T_s, and the vapour pressure at surface, P_s, in the above equations vary with time. However mean values for $\dot{m}_p$, T_s and P_s may be used, since the pre-constant period is short. The mean value of T_s can be determined as an average value of the initial and final temperature of the surface. However, the final surface temperature in the pre-constant period is the surface temperature in the constant rate period which is usually equal to the wet bulb temperature. The same procedure can also be used to calculate a mean value of P_s which may then be used to obtain an average value for the drying rate, $\dot{m}_p$.

The boundary condition at x = L is,

$$-\lambda_m \frac{\partial T}{\partial x} = 0 \tag{6.2-6}$$

The heat transfer equation (6.2-1) is non-linear. Thus, a mathematical solution such as an integral method described in references (129, 130) is required to solve it. In this method a penetrated depth, $\delta(t)$, is defined as a quantity which has a property such that for $x \geq \delta(t)$, the temperature remains at its equilibrium value and no heat is transferred beyond this point. In the present integral formulation, the temperature profile is assumed to be

parabolic in form.

$$T = C_o + C_1 x + C_2 x^2 \tag{6.2-7}$$

where C_o, C_1 and C_2 are coefficients depend on time, the initial conditions, at $x = \delta$, will be,

$$T\big|_{x=\delta} = C_o + C_1\delta + C_2\delta^2 = T_o \tag{6.2-8}$$

Differentiating Eq. (6.2-7) with respect to x, yields,

$$\frac{\partial T}{\partial x} = C_1 + 2C_2 x \tag{6.2-9}$$

Thus, the boundary conditions give,

$$-\lambda_m \frac{\partial T}{\partial x}\bigg|_{x=0} = -\lambda_m C_1 = h(T_a - T_s) - \mathbf{m}_p \Delta hv \tag{6.2-10}$$

and since no heat is transferred at $x \geq \delta$ then,

$$-\lambda_m \frac{\partial T}{\partial x}\bigg|_{x=\delta} = C_1 + 2C_2\delta = 0 \tag{6.2-11}$$

Solving C_o, C_1 and C_2 in Eqs. (6.2-8), (6.2-10) and (6.2-11); and substituting their values

into the polynomial expression for T, Eq. (6.2-7) yields,

$$T = T_o + \left(\frac{1}{2\lambda_m}\right) * \left[h(T_a - T_s) - \dot{m}_p \Delta hv\right] * \left[\delta - 2x + \frac{x^2}{\delta}\right] \qquad (6.2\text{-}12)$$

Equation (6.2-1) may now be solved by multiplying both sides by dx, and then integrating over the zone x = 0 to x = δ. Thus, the right hand side of Eq. (6.2-1) yields

$$\int_0^{\delta} \alpha_m \frac{\partial^2 T}{\partial x^2}.dx = \alpha_m . \left[\left.\frac{\partial T}{\partial x}\right|_{x=\delta} - \left.\frac{\partial T}{\partial x}\right|_{x=0}\right]$$

$$= \left(\frac{\alpha_m}{\lambda_m}\right) * \left[h(T_a - T_s) - \dot{m}_p \Delta hv\right] \qquad (6.2\text{-}13)$$

The left hand side of Eq. (6.2-1) will be

$$\int_0^{\delta} \frac{\partial T}{\partial t}.dx = \frac{\partial}{\partial t}\left[\int_0^{\delta} T.dx - T_o\,\delta\right]$$

$$= \frac{\partial}{\partial t}\left[\int_0^{\delta} \left(T_o + \frac{1}{2\lambda_m}[h(T_a - T_s) - \dot{m}_p \Delta hv] * [\delta - 2x + \frac{x^2}{\delta}]\right)dx - T_o\,\delta\right] \qquad (6.2\text{-}14)$$

Solving the internal integration of Eq. (6.2-14) and rearranging yields,

$$\int_0^{\delta} \frac{\partial T}{\partial t} \cdot dx = \frac{\partial}{\partial t}\left[\left(\frac{\delta^2}{6\lambda_m}\right)\left(h(T_a - T_s) - m_p\ \Delta hv\right)\right] \qquad (6.2\text{-}15)$$

Eq. (6.2-13) is equivalent to Eq. (6.2-15) from which the final solution for δ can be obtained:

$$\delta = \sqrt{(6\alpha_m t)} \qquad (6.2\text{-}16)$$

Finally, substituting values of δ into Eq. (6.2-12) yields:

$$T = T_o + \left(\frac{1}{2\lambda_m}\right) * \left[h(T_a - T_s) - m_p\ \Delta hv\right] * \left[\sqrt{(6\alpha_m t)} - 2x + \frac{x^2}{\left(\sqrt{6\alpha_m t}\right)}\right] \qquad (6.2\text{-}17)$$

At the end of the pre-constant rate period, the temperature at the surface equals the wet-bulb temperature. Hence solution of Eq. (6.2-17) for time t at x = 0, gives the total time of the pre-constant period, i.e. time at the end of pre-constant rate period, as,

$$t_p = \left(\frac{2}{3}\right) * \left(\frac{\lambda^2_m}{\alpha_m}\right) * \left[\frac{(T_{wb} - T_o)}{\left(h(T_a - T_{wb}) - m_p\ \Delta hv\right)}\right]^2 \qquad (6.2\text{-}18)$$

Equations (6.2-17) and (6.2-18) represent a complete solution to predict the temperature distribution profiles during the pre-constant rate period.

6.3 CONSTANT RATE PERIOD

During the constant rate period, conditions external to the wet material being dried may control the rate of drying. The internal mechanisms for water transport within the material are sufficient to supply liquid water to the surface of the solid to maintain saturation. The temperature gradient throughout the bed at the end of the pre-constant rate period, t_p , is obviously equal to that at the beginning of the constant rate period. Therefore, the temperature at each depth at the start of the constant rate period may be solved using equations (6.2-17) and (6.2-18). This gradient in temperature remains constant until the moisture has been reduced to a critical point, t_{cr}, which indicates the end of the constant rate period and the beginning of the first falling rate period. Thus, to obtain a complete distribution profile for the constant rate period, the appropriate value of t_{cr} is required.

In general, the drying rate is defined as

$$\mathbf{m} = -\frac{ms}{A}\cdot\frac{dX}{dt} \tag{6.3-1}$$

This can be rearranged and integrated over the duration of the constant rate period, i.e. from ($t = t_P$ at $X = X_P$) to ($t = t_{cr}$ at $X = X_{cr}$)

$$\int_{tp}^{tcr} dt = \int_{Xp}^{Xcr} -\frac{ms}{Am}\,dX \tag{6.3-2}$$

During the constant rate period, the drying rate actually changes slightly with time. This is demonstrated by the drying rate curves for various materials in Chapter 5. Keey, R. (131) supported this concept and stated that "a constant" drying rate is almost never found. However, in order to simplify the model, it may be assumed that the drying does remain constant and $\mathbf{m} = \mathbf{m}_c$. Thus, the constant drying rate, $\mathbf{m}_c$., can be obtained by applying the basic energy balance to the flat slab,

$$\mathbf{m}_c = Mw \cdot \frac{k'_c}{RT}\left(P_s - P_{va}\right) \tag{6.3-3}$$

where P_{va} is the partial pressure of vapour in the air stream, which can be estimated from the value corresponding to the dew point in steam tables. P_S is the vapour pressure of water at the surface and can be determined by Clausius - Clapeyron equation. The temperature of the surface during the constant period is usually equal to the wet-bulb temperature i.e. $T_s = T_{wb}$.

Integrating Eq. (6.3-2) for this period yields,

$$t_{cr} = \frac{ms}{A\mathbf{m}_c}\left(X_p - X_{cr}\right) + t_p \tag{6.3-4}$$

A general correlation for X_{cr} is defined as,

$$X_{cr} = X^* + \frac{\varepsilon \rho_{WL}}{\rho_s} \tag{6.3-5}$$

where X* is the equilibrium moisture content. ε is the porosity defined as the ratio of the volume of voids in the wet material being filled with liquid to the volume of the wet material itself.

X_p in Eq. (6.3-2) is the moisture content at t_p; and can be obtained by integrating Eq. (6.3-1) over the duration of the pre-constant rate period.

$$\int_{to}^{tp} dt = \int_{Xo}^{Xp} -\frac{ms}{A\,\mathbf{m}_p} dX \tag{6.3-6}$$

which yields

$$X_p = X_o - \frac{\mathbf{m}_p\, t_p A}{ms} \tag{6.3-7}$$

6.4 FALLING-RATE PERIOD

During the falling-rate period, the drying rate decreases with time and the rate of internal moisture transfer to the material surface typically controls the drying process. The rate of transfer is therefore controlled 'by material-type, physical form and condition-specific'. 'Dry patches' which form on the surface, indicate the beginning of the first falling

rate period, associated with an increase in the temperature of the surface. This period is of relatively short duration. A thin dry layer then forms on the surface indicative of the beginning of the second falling rate period and the development of the so-called, receding evaporation front. Thus the system separates into a hotter dry zone in the upper section and an inner wet zone of higher moisture content. Moisture in the wet region, which is usually in a liquid phase, moves mainly by a capillary force within non-hygroscopic materials and by liquid diffusion within hygroscopic materials. The vapour pressure of the moisture at the interface is always equal to that at saturation. Thus, evaporation occurs at the interfacial plane. Moisture then transfers throughout the dry region as a vapour by diffusion.

Examination of the experimental results (Chapter 5), showed that during the first falling rate period, the temperature of the surface increased gradually followed by a short period of constant temperature. The surface temperature then increased again at the beginning of the second falling rate period. Thus, the temperature distribution profile within the first and the second falling rate periods appeared almost as a profile of one stage. In addition, during the first falling rate period, dry spots form on the surface indicating that a dry zone commenced. Therefore, the two periods can be assumed approximately to comprise one falling rate period, commencing at t_{cr}.

Heat and mass transfer during the unsteady state conditions in the falling rate period of the flat slab is shown in Fig. 6.4. Therefore, the energy balance can be written as follows:

In the wet region $f(t)<x<L$

$$\frac{\partial T_w}{\partial t} = \alpha_w \frac{\partial^2 T_w}{\partial x^2} \tag{6.4-1}$$

where subscript, w, denotes the wet zone. α_w is the effective thermal diffusivity of the wet zone,

$$\alpha_w = \frac{\lambda_w}{\rho_s Cp_w} \tag{6.4-2}$$

where λ_m is the effective thermal conductivity in the wet zone, and Cp_w its heat capacity.

In the dry region $0 < x < f(t)$

$$\frac{\partial T_d}{\partial t} = \alpha_d \frac{\partial^2 T_d}{\partial x^2} \tag{6.4-3}$$

where subscript, d, denotes the dry zone. α_d , is the effective thermal diffusivity of the dry zone,

$$\alpha_d = \frac{\lambda_d}{\rho_s Cp_d} \tag{6.4-4}$$

λ_d and Cp_d are the effective thermal conductivity and the heat capacity of the dry zone respectively.

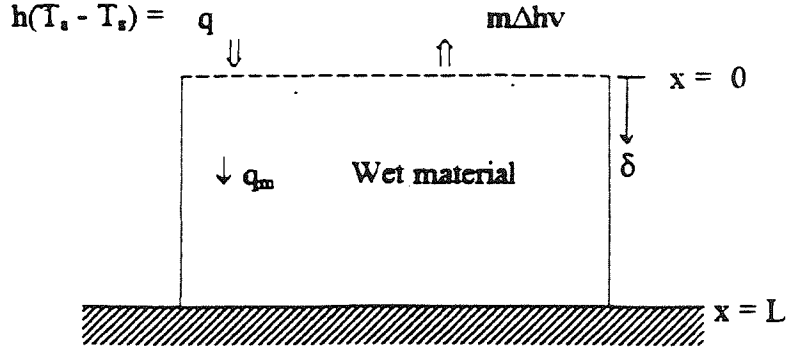

Figure 6.3 Heat and mass transfer during the pre-constant and the constant rate periods.

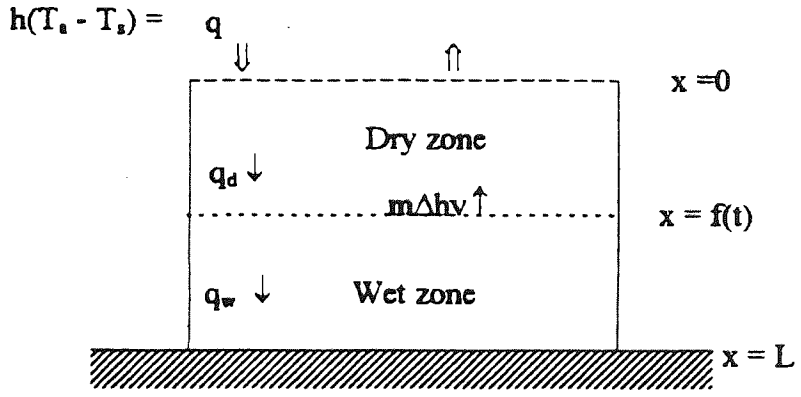

Figure 6.4 Heat and mass transfer during the falling rate period.

The initial temperature at the commencement of the falling rate period is equal to the temperature at t_{cr}. Thus the temperature at each depth at the start of the falling rate period corresponds with that at time t_{cr}.

The boundary conditions at the surface, x = 0, are

$$-\lambda_d \frac{dT_d}{dx} = h(T_a - T_s) \tag{6.4-5}$$

The energy flux to the interface required to bring about the phase change is $\mathbf{m}\Delta hv$. The position of the receding evaporation front, f(t), varies with time and the moving boundary conditions at the evaporation front are

$$-\lambda_d \frac{\partial T_d}{\partial x} + \lambda_w \frac{\partial T_w}{\partial x} = \mathbf{m}\Delta hv \tag{6.4-6}$$

and

$$T_d = T_w = T_f \tag{6.4-7}$$

The boundary conditions at the bottom of the sample, x = L,

$$-\lambda_w \frac{\partial T_w}{\partial x} = 0 \tag{6.4-8}$$

$\mathbf{m}$ in Eq. (6.4-6) is the drying rate during the falling period. This rate varies with time and can be defined as

$$\mathbf{m} = \frac{MwK'_G}{RT}\left(P_f - P_{va}\right) \tag{6.4-9}$$

where K'_G is an overall mass transfer coefficient, previously defined by Waananen (132) as a combined coefficient accounting for both external and internal resistances. A general correlation for K'_G has been written as follows

$$\frac{1}{K'_G} = \frac{1}{k'_c} + \frac{z}{D_{eff}} \tag{6.4-10}$$

where k'_c = external mass transfer coefficient; D_{eff} = effective internal moisture diffusivity and z = characteristic sample dimension. In the two zone model, z, can be represented as the distance from the surface to the receding evaporation front, f(t).

P_f in Eq. (6.4-9) is the vapour pressure of water at the evaporation front and varies with time. The vapour pressure, P_f, is a saturated pressure and can be plotted on the saturated curve of water as in Fig. 6.5. The slope of the saturated curve between P_f and P_{va} can be written as

$$s = \frac{P_f - P_{va}}{T_f - T_{dew}} \tag{6.4-11}$$

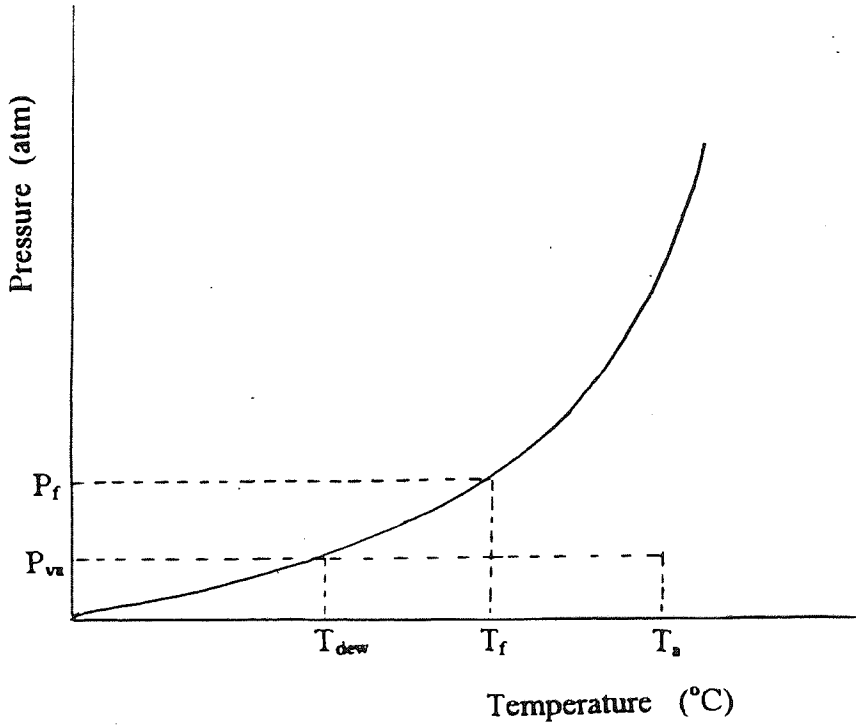

Figure 6.5 Saturation curve of water.

Rearranging and substituting Eq. (6.4-10) and Eq. (6.4-11) into Eq. (6.4-9) yields

$$\mathbf{m} = \frac{Mw}{RT}\frac{s(T_f - T_{dew})}{\left(\frac{1}{k'_c} + \frac{f(t)}{D_{eff}}\right)} \tag{6.4-12}$$

Therefore, the above equation represents a useful correlation to estimate the drying rate during the falling rate period.

During the falling rate period, the moisture content concentrates in the wet zone, i.e. the moisture content of the dry zone approximates to zero. Thus, the ratio of volume of the instantaneous water content, *mw*, to the volume of the initial water content, mw_o equals the ratio of volume of wet zone to the total volume of the system, which yields

$$\frac{(mw / \rho_{WL})}{(mw_o / \rho_{WL})} = \frac{(L - f(t))A}{LA} \tag{6.4-13}$$

Solving Eq. (6.4-13) in terms of moisture content (X = *mw/ms*) gives,

$$\frac{X}{X_o} = \frac{L - f(t)}{L} \tag{6.4-14}$$

Rearranging Eq. (6.4-14), the instantaneous moisture content can be written as

$$X = X_o - X_o \frac{f(t)}{L} \tag{6.4-15}$$

Differentiating Eq. (6.4-15) with respect to time, t

$$\frac{dX}{dt} = -\frac{X_o}{L}\frac{df(t)}{dt} \tag{6.4-16}$$

Substitution of Eq. (6.4-16) into Eq. (6.3-1) yields

$$\mathbf{m} = \frac{msX_o}{LA}\frac{df(t)}{dt} \tag{6.4-17}$$

Introduction of the term for the porosity, ε, as

$$\varepsilon = \frac{mw_o}{\rho_{WL}}\frac{1}{LA} = \frac{msX_o}{\rho_{WL}}\frac{1}{LA} \tag{6.4-18}$$

followed by substitution into Eq. (6.4-17) yields

$$\mathbf{m} = \rho_{WL}\,\varepsilon\frac{df(t)}{dt} \tag{6.4-19}$$

The term $\frac{df(t)}{dt}$ represents the velocity of the front. Because equation (6.4-12) equals Eq. (6.4-19), the velocity of the front can be written as

$$v = \frac{df(t)}{dt} = \frac{1}{\rho_{WL}\varepsilon}\frac{Mw}{RT}\frac{s(T_f - T_{dew})}{\left(\frac{1}{k'_c} + \frac{f(t)}{D_{eff}}\right)} \qquad (6.4\text{-}20)$$

During the falling rate period, the temperature of the evaporation plane varied with time and with position. This was described by the heat transfer equations (6.4-1) and (6.4-3); and with the boundary conditions equations (6.4-5 - 6.4-8). These equations are non-linear, and are difficult to solve, for such boundary conditions, by common numerical methods. Therefore, a method of solution was developed based on the method of finite difference (133-136), a modified form of the so-called explicit method.

The final solution of the temperature distribution in the falling rate period at each depth can be obtained by solving these equations using the correlation for the front velocity Eq. (6.4-20). A complete solution of the finite difference method of the differential equations is shown in Appendix A.

6.5 THE PHYSICAL PROPERTIES OF THE MATERIALS AND THE DRYING CONDITIONS

6.5.1 Heat And Mass Transfer Coefficients

Many empirical or semi-empirical formulae are available in the drying literature (137-144) to determine the heat transfer coefficient, h, and the mass transfer coefficient, k'_c. The heat transfer coefficient, h, is described as:

$$h = h_c + h_r \tag{6.5-1}$$

where h_c and h_r are convective and radiant heat transfer coefficients respectively.

The convective heat transfer coefficient, h_c, can be determined for the case of an air stream flowing parallel to a flat plate using the equation of Nusselt,

$$Nu = \frac{h_c \ell}{\lambda_a} = 0.664 (Re, \ell)^{0.5} Pr^{0.33} \tag{6.5-2}$$

where ℓ is the distance traversed by the air flow. In this work ℓ represents the diameter of the sample tray. Re, ℓ is the Reynolds number with respect to the effective length or diameter of tray and can be defined as:

$$Re, \ell = \frac{\ell \upsilon \rho}{\mu} \tag{6.5-3}$$

Pr is the Prandtl number and can be represented as:

$$Pr = \frac{Cp\mu}{\lambda_a} \tag{6.5-4}$$

The properties υ, ρ, Cp, μ and λ_a are the velocity, density, specific heat, viscosity and thermal conductivity of air respectively. These properties are calculated at the film

temperature $T_f = \frac{(T_s + T_a)}{2}$ where T_s is the surface temperature of the wet material which can be assumed to be the wet bulb temperature.

The radiant heat transfer coefficient in Equation (6.5-1) can be determined as:

$$h_r = \varepsilon(5.676)\frac{\left(\frac{T_r}{100}\right)^4 - \left(\frac{T_s}{100}\right)^4}{T_r - T_s} \qquad (6.5\text{-}5)$$

where T_r is the temperature of the inside surface of the tunnel (K), approximately close to hot air temperature. The emissivity factor, ε, for the polished stainless steel is 0.074. The units of h_r will be $W/m^2 K$.

The mass transfer coefficient, k'_c, can be determined from the equation of Sherwood as:

$$Sh = \frac{k'_c \ell}{D_{AB}} = 0.664\,(Re, \ell)^{0.5}\, Sc^{0.33} \qquad (6.5\text{-}6)$$

where D_{AB} is the diffusivity of moisture vapour in the air. Sc is the Schmidt number defined as:

$$Sc = \frac{\mu}{\rho D_{AB}} \qquad (6.5\text{-}7)$$

6.5.2 Thermal Conductivity and Specific Heat

The effective thermal conductivity of a wet material has been studied by many authors (145-151). However it was difficult to obtain a correct value for this coefficient, since it is a function of moisture content. Moyne (146) has presented a correlation from which to calculate the effective thermal conductivity,

$$\lambda_{eff} = \lambda_s + \lambda_{diff} f_{exp} \tag{6.5-8}$$

where λ_{diff} is thermal conductivity due to vapour diffusion defined as,

$$\lambda_{diff} = \frac{D_{AB} Mw}{RT} \frac{dP_{va}}{dT} \cdot \Delta hv \tag{6.5-9}$$

The term $\frac{dP_{va}}{dT}$, represents the slope of the saturation curve between the dew point and wet bulb temperatures. f_{exp} is an experimental factor dependent on the moisture content. According to Moyne's explanation f_{exp} can in general be assumed as unity for the wet material and zero for the dried solid.

The thermal conductivity of the solid, λ_s, in Equation (6.5-8) is always represented as: $\lambda_s = A + B\overline{X}$, where A and B are constants and $\overline{X}$ is the average moisture content in each region. The average moisture content for the dry zone can be assumed as zero,

whereas for the wet zone, it can be assumed equal to $\frac{X_{cr}}{2}$.

The specific heat of wet material, Cp, is a function of moisture content. It is defined as:

$$Cp = Cp_s + Cp_{WL}\,\overline{X} \qquad (6.5\text{-}10)$$

where Cp_s and Cp_{wl} are the specific heats of solid and liquid water respectively. $\overline{X}$ is the average moisture content in each region. Again, $\overline{X} = 0$ for the dry zone, and $\overline{X} = \frac{X_{cr}}{2}$ for the wet zone.

6.5.3 Diffusivity

An accurate prediction of the diffusivity of moisture within a solid is generally not possible because of lack of knowledge of the theory of the solid state. However some semi-empirical equations have been proposed (152-162). During the falling rate period the effective diffusivity within the wet material is a combination of liquid and vapour diffusivities:

$$D_{eff} = D_{eff,liq} + D_{eff,vap} \qquad (6.5\text{-}11)$$

The effective liquid diffusivity, $D_{eff,liq}$ can be determined as follows:

$$D_{eff,liq} = \left(\frac{\varepsilon}{\tau}\right) \cdot D_{AB} \qquad (6.5\text{-}12)$$

where D_{AB} is diffusivity of vapour in air, ε is the porosity and τ is the tortuosity factor. Approximate values of τ for some materials can be found in (160).

The diffusion of a vapour in a solid depends on the ratio $\frac{dc}{\lambda^*}$, where dc, denotes the pore or capillary diameter. It can be estimated from the pore distribution curve given by Vyas (81). The pore diameter, dc, of each of the materials being tested are listed in Table (6.2). λ^* is a mean free path defined as

$$\lambda^* = \frac{3.2\mu}{P}\sqrt{\frac{RT}{2\pi Mw}} \qquad (6.5\text{-}13)$$

The calculated value of the ratio $\frac{dc}{\lambda^*}$ for the materials being dried were found to lie within the range $20 \langle \frac{dc}{\lambda^*} \langle 0.2$. This range has been given by Treybal (140), as one in which the effective vapour diffusivity might be determined by the equation,

$$\frac{1}{D_{eff,vap}} = \left(\frac{1}{D_k} + \frac{1}{D_{AB}}\right)\frac{\tau}{\varepsilon} \qquad (6.5\text{-}14)$$

where D_k is the Knudsen diffusivity of water vapour,

$$D_k = 48.5dc\left(\frac{T}{Mw}\right)^{0.5} \qquad (6.5\text{-}15)$$

6.6 THE MODEL RESULTS

Correlations to calculate the physical properties of the materials being dried and the drying conditions were described in the previous sections. The experimental conditions employed were similar for all experiments. The samples of wet material were placed in an insulated sample tray of 8.3 cm diameter and 3.2 cm deep, and a stream of air was passed over their surfaces. Table 6.1 summarises the experimental drying conditions.

TABLE 6.1 The experimental drying conditions :

T_a	84	(°C)
T_{wb}	38	(°C)
H	0.02	(kgH_2O/kg dry air)
υ	0.5	(m / s)
ρ_{WL}	968	(kg/m^3)
Cp_{WL}	4200	(J/kg.K)
Δhv	2217.5	(kJ/kg)
h	10.19	(W/m^2 K)
k'_c	0.01	(m/s)
D_{AB}	3.45×10^{-5}	(m^2/s)

The calculated physical properties of the glass beads 100 μm, polystyrene pellets,

activated alumina and wood powder are listed in Table 6.2.

The proposed equations for the pre-constant rate period, the constant rate period and the falling rate period have been computed in a program using Turbo-Pascal, V.6. The complete program is included in Appendix B.

The data given in Table 6.1 and Table 6.2 were loaded in the program to test the validity of the proposed model. Four levels of temperature were selected from each set of experimental results for glass beads of 100μm, polystyrene pellets, activated alumina and wood powder to compare with the numerical results obtained by the program. These temperatures corresponded to depths of x = 0, x = 1.2 cm, x = 2.4 cm and x = 3.2 cm.

The experimental temperature distribution profiles and the predicted profiles for glass beads of 100 μm are shown in Fig. 6.6. During the stages of drying, the predicted temperature distribution throughout the bed agreed well with the experimental results. The model predicted the temperatures in the pre-constant and the constant rate periods with excellent accuracy. The predicted temperatures were only 1°C less than the experimental values. The model also predicted the duration of the constant rate period with accuracy. During the falling rate period the calculated temperature distribution was satisfactory and agreed to some extent with the experimental one.

The experimental and calculated results for polystyrene pellets are shown in Fig. 6.7. The model predicted the temperature distribution profiles over the entire drying period with a satisfactory accuracy. The predicted duration of the constant rate period was however 91

min. longer than the experimental one. The first falling rate period was not demonstrated clearly by the model. However, during the falling rate period, the predicted surface temperature agreed well with the experimental data. The predicted temperatures of the wet zone were approximately 5°C greater than the actual temperatures.

TABLE 6.2: The physical properties of the materials being dried:

Property		Glass beads 100μm	Polystyrene pellets	Activated alumina	Wood powder
ρ_s	(kg/m^3)	2000	690	770	368
Cp_s	(J/kg K)	836	1500	1005	2385
ε	(-)	0.32	0.43	0.6	0.47
$d_c \times 10^6$	(m)	1	2.5	3.3	2.6
X*(kgH_2O/kg dry solid)		0.005	0.1	0.1	0.55
m_p	(kg/m^2h)	0.39	0.29	0.51	0.39
m_c	(kg/m^2h)	0.65	0.65	0.65	0.65
λ_s	(W/m.K)	$0.35+2.24\overline{X}$	$0.13+0.4\overline{X}$	$0.19+0.51\overline{X}$	$0.1+0.002\overline{X}$
λ_w	(W/m.K)	0.891	0.74	0.75	0.713
λ_d	(W/m.K)	0.35	0.13	0.19	0.1
α_w	(m^2/h)	0.00138	0.00139	0.00135	0.0014
α_d	(m^2/h)	0.00076	0.00045	0.00088	0.00041
$D_{eff} \times 10^5$	(m^2/s)	0.79	1.24	1.88	1.42

The predicted temperature distribution within beds of activated alumina are plotted

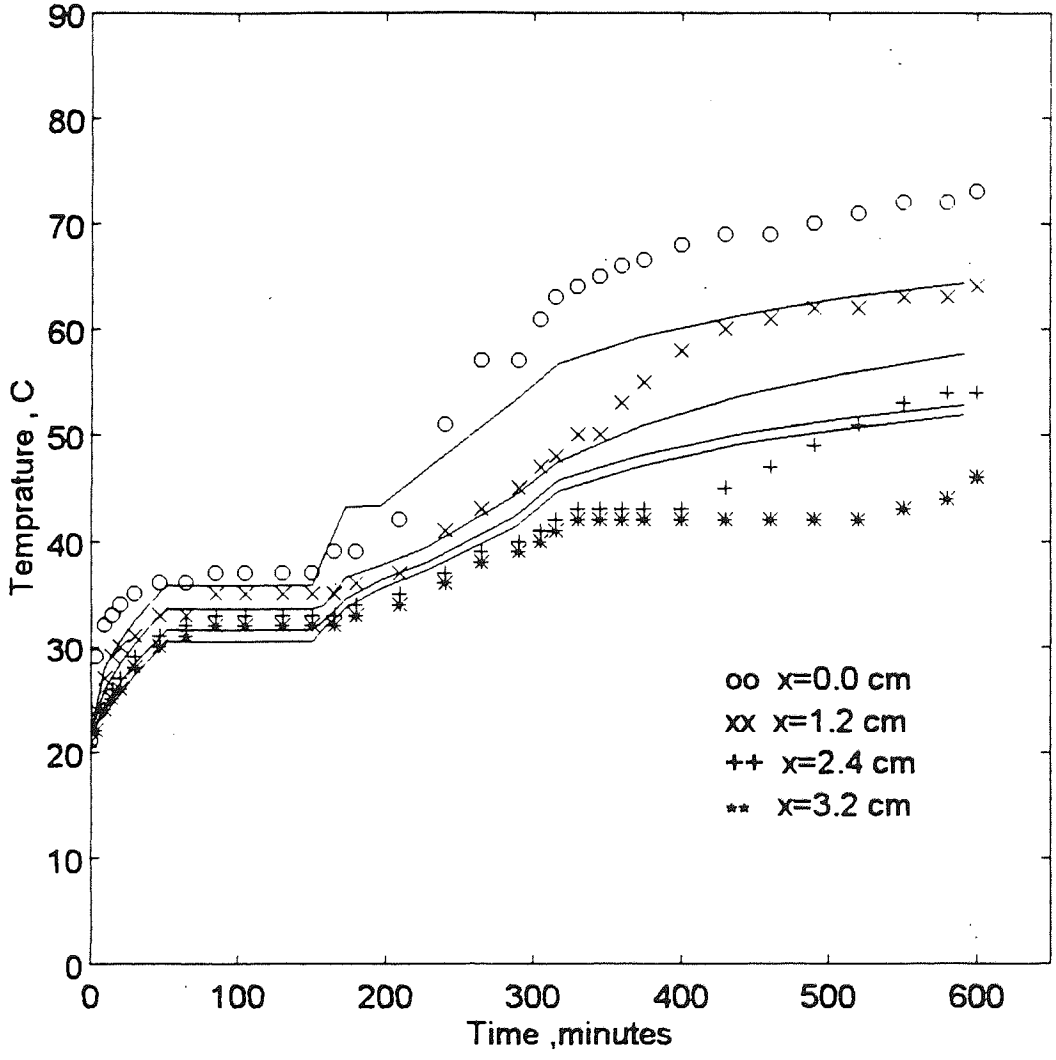

Figure 6.6 Predicted and experimental temperature distribution profiles within a bed of glass beads (100 μm); air temperature 84 °C; [Predictions, complete curves relative to the same four depths as the experimental data].

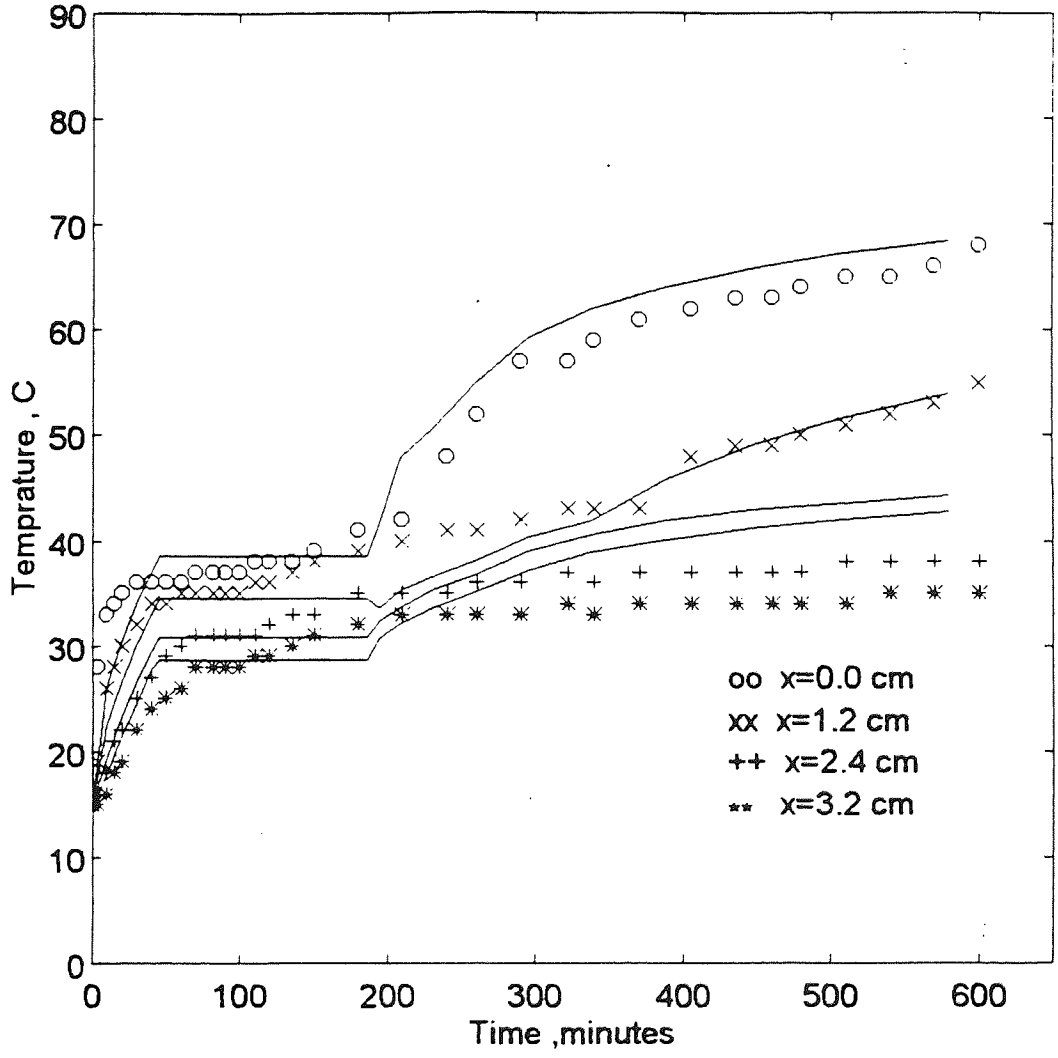

Figure 6.7 Predicted and experimental temperature distribution profiles within a bed of polystyrene; air temperature 84 °C.

in Fig. 6.8 and compared with experimental data. During the pre-constant and the constant rate period, an excellent prediction for the temperature distribution was obtained. The predicted duration of the constant rate period also agreed well with the experimental duration. The temperature distribution in the falling rate period showed a satisfactory agreement, i.e. within ±5°C. Again, the predicted temperatures in the wet zone were slightly greater than the experimental results.

The numerical solution for the temperature distribution profiles within the bed of wood powder is shown in Fig. 6.9. During the pre-constant rate period a good agreement was obtained between the predictions and experimental results. However, less agreement was obtained in the constant rate period. The first falling rate period was not clearly demonstrated by the model. The predicted temperatures in the second falling rate period were reasonable, i.e. within ±4°C of the experimental results

To test the validity of the proposed model for other air temperatures, the results of two experiments with air temperatures of 64°C and 54°C were chosen for comparison. The calculated effective thermal conductives of the wet zone, λ_w , at the two air temperatures were 0.8 W/m.K and 0.768 W/m.K respectively. Those for the dry zone, λ_d , were 0.35 W/m.K at both air temperatures. The drying rates during the pre-constant period, m_p , and the constant period, m_c, at an air temperature of 64°C were 0.352 kg/m².h and 0.5 kg/m².h respectively. The corresponding drying rates at an air temperature of 54°C were 0.295 and 0.4 kg/m².h respectively.

The predicted and experimental results for the temperature distributions in a bed of

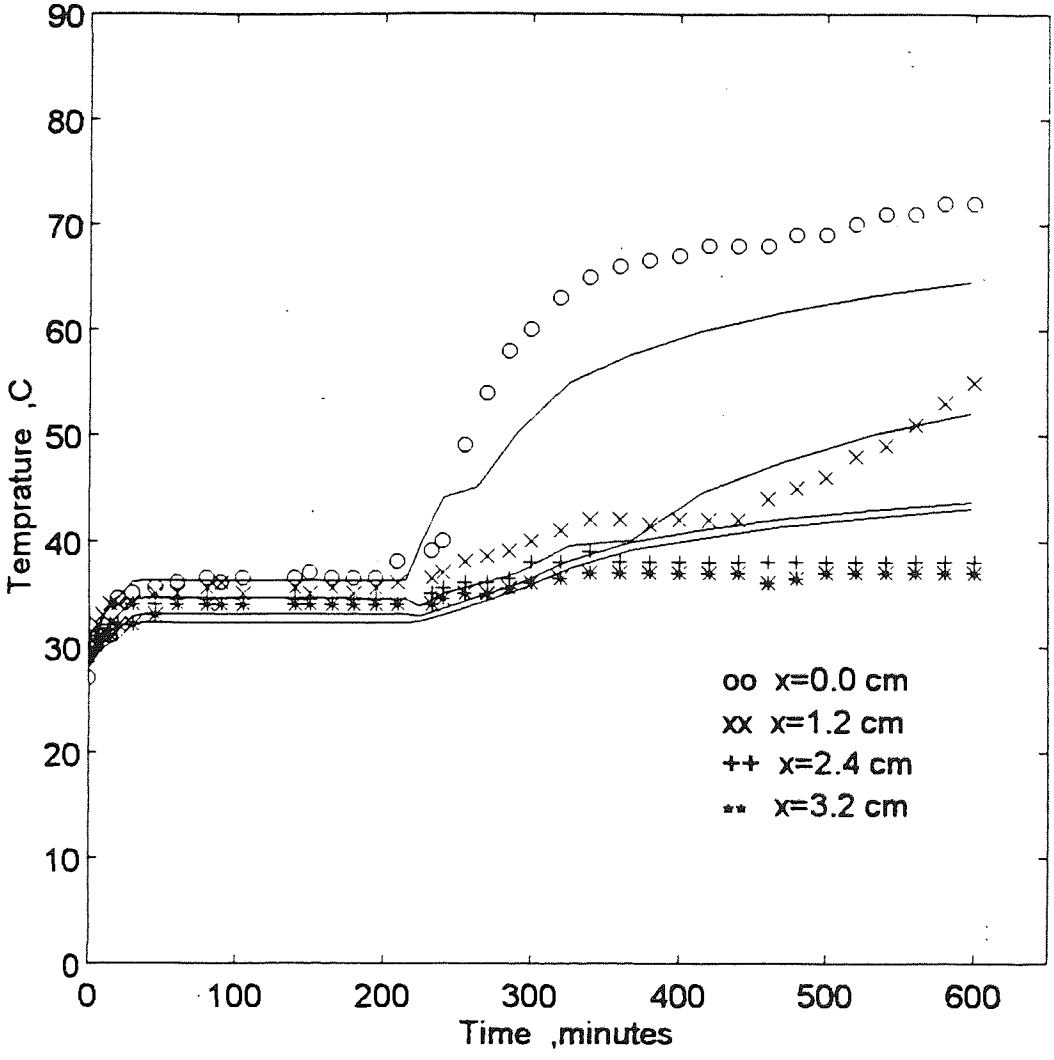

Figure 6.8 Predicted and experimental temperature distribution profiles within a bed of activated alumina, 150 mesh; air temperature 84 °C.

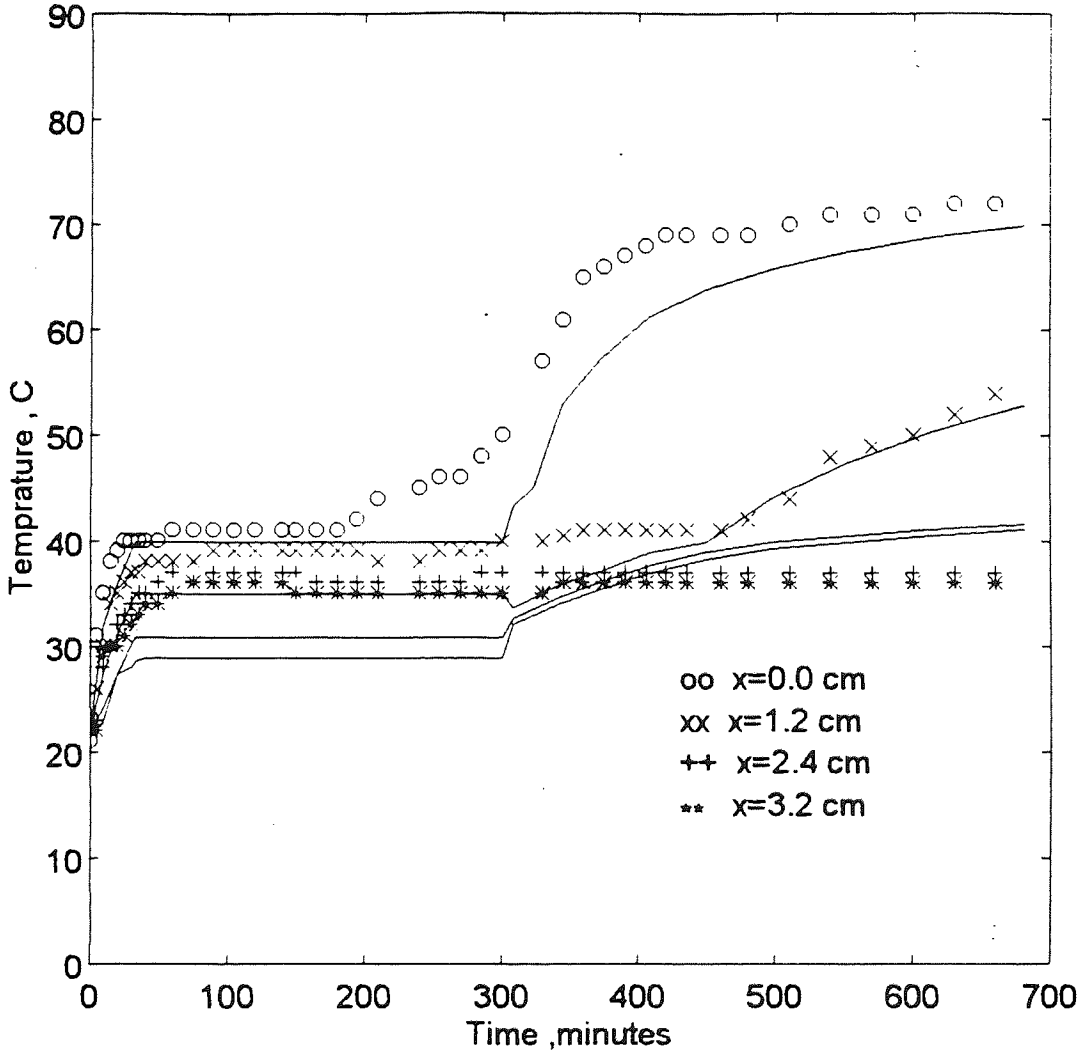

Figure 6.9 Predicted and experimental temperature distribution profiles within a bed of wood powder; air temperature 84 °C.

glass beads of 100 μm at an air temperature of 64°C are shown in Fig. 6.10. Good agreement was obtained between the predicted values and the experimental values over the entire drying period. The model provided an excellent prediction of the duration and the temperature distribution profile in both the pre-constant and the constant rate periods. A reasonable fit, within ±4°C, was obtained for the temperature distribution in the falling rate period.

Figure 6.11 shows the predicted and experimental results for a bed of 100 μm glass beads at an air temperature of 54°C. Satisfactory agreement is demonstrated in the pre-constant rate and the constant rate periods. An excellent prediction was obtained for the duration of the constant rate period. The profiles also show good accuracy in the falling rate period, i.e. temperature predictions correlated within ±2°C in all positions.

The proposed model predicted the total time required to complete the drying process, i.e. for the solid to reach its equilibrium moisture content. Table 6.3 shows the predicted total time for completion of the drying operation for the tested materials. However, there was no experimental data for comparison, since the experimental data were only recorded up to 700 min.

The complete predicted data for the temperature distributions within the bed over the entire period of drying are shown in Appendix C.

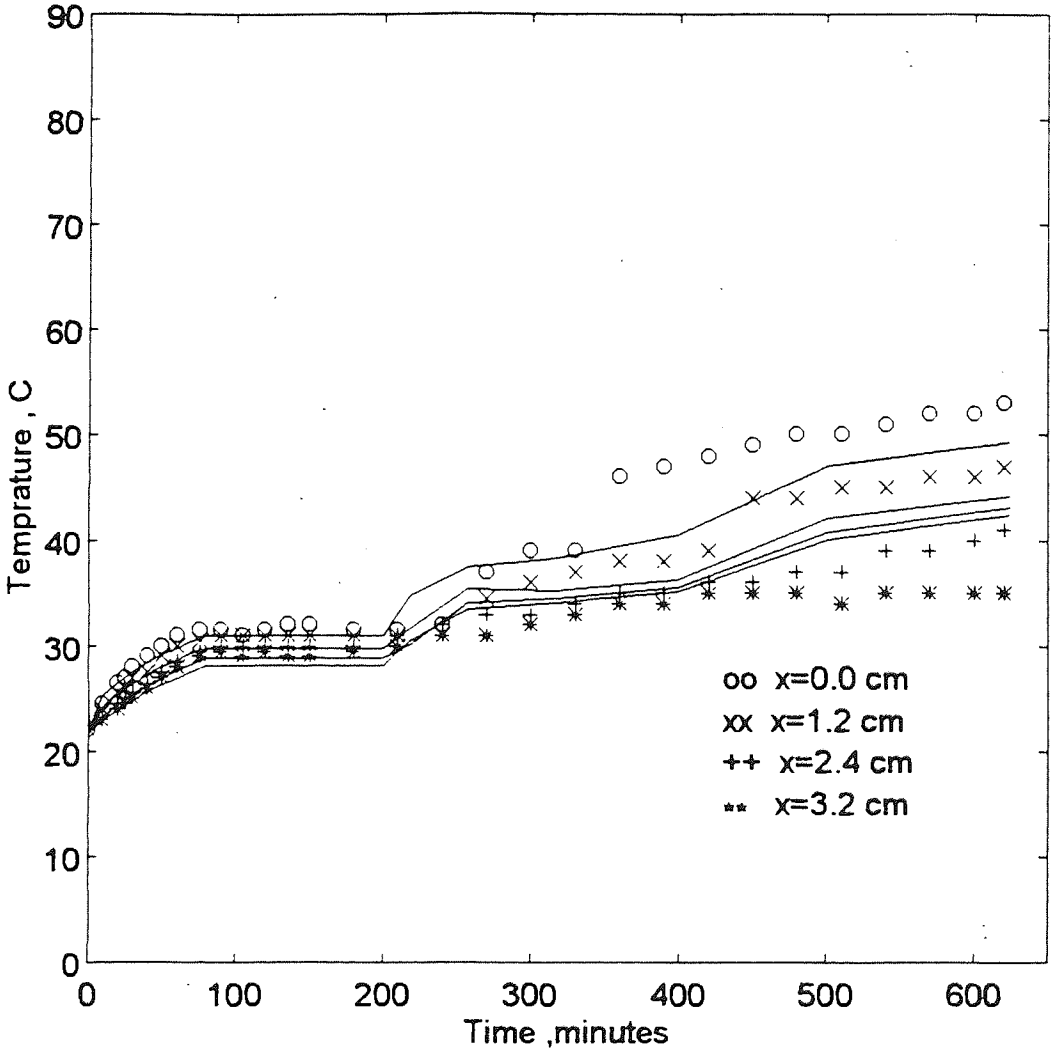

Figure 6.10 Predicted and experimental temperature distribution profiles within a bed of glass beads (100 μm); air temperature 64 °C.

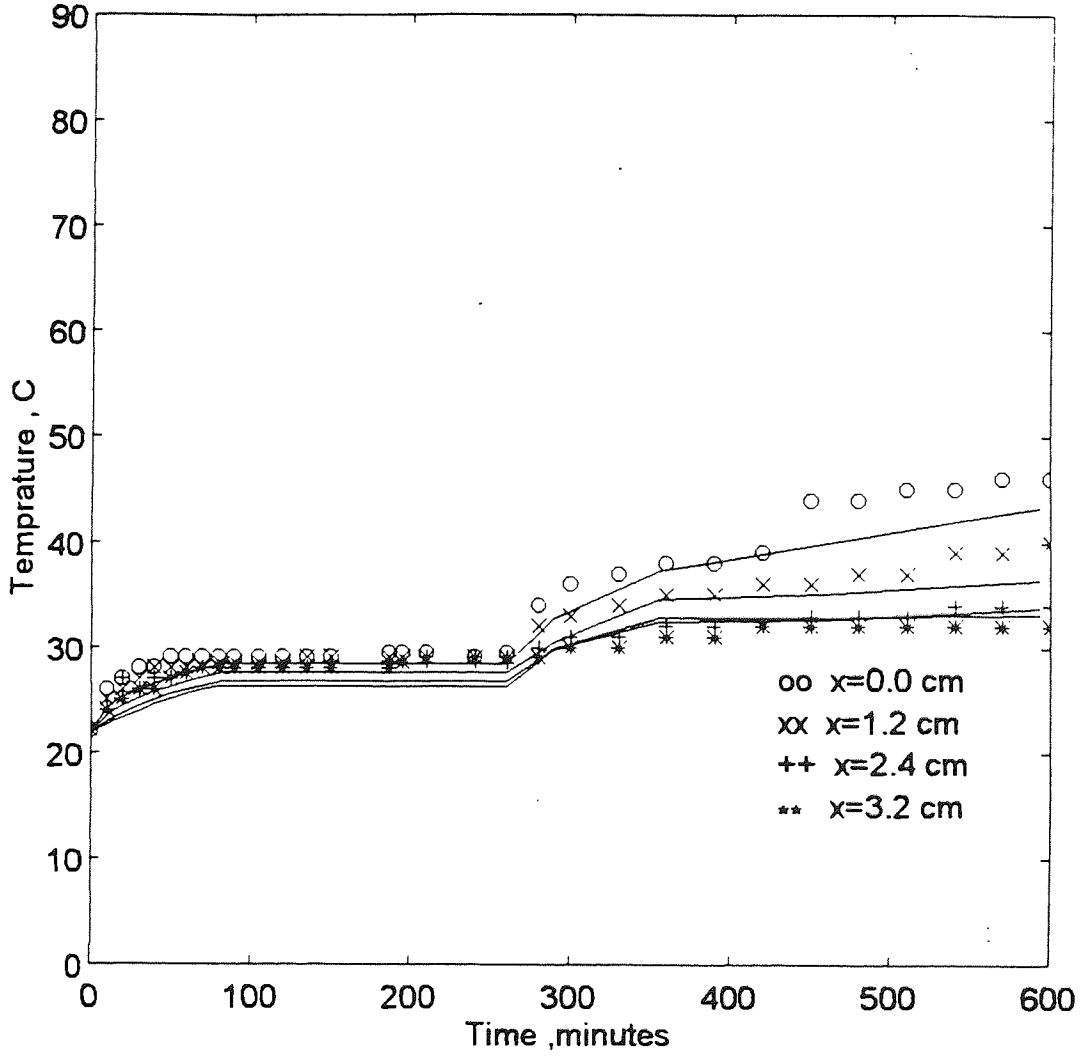

Figure 6.11 Predicted and experimental temperature distribution profiles within a bed of glass beads (100 μm); air temperature 54 °C.

TABLE 6.3: The predicted total time

Tested Material	Predicted time (min)
Glass beads 100 μm, 84°C	1250.26
Polystyrene pellets, 84°C	1153.21
Activated alumina, 84°C	1138.25
Wood powder, 84°C	1232.82
Glass beads 100 μm, 64°C	3021.13
Glass beads 100 μm, 54°C	3925.62

6.7 DISCUSSION AND CONCLUSIONS

The new model predicted temperature distributions throughout the beds of hygroscopic and non-hygroscopic materials which were in good agreement with the experimental data. The mathematical model also showed good accuracy when it was validated at different air temperatures. During the pre-constant and the constant rate periods, the predicted temperatures provided a good fit with the experimental results. The least satisfactory fit was obtained for the case of wood powder. This was partly because an average value of the vapour pressure at the surface was used in the calculation of the drying rate in the pre-constant rate period, $\mathbf{m}_p$, whereas the vapour pressure at the surface varies with time.

The estimated duration of the constant rate period was generally in good agreement with the experimental data. The accuracy in the case of polystyrene pellets and wood powder was not as good as in the rest of the experiments. The assumption that the drying rate had a constant value during the constant rate period, made little difference to the prediction of the drying rate, $\mathbf{m}_c$, but will affect the prediction of the value of t_{cr}, leading to some differences in the estimated duration. The model was also able to predict the total time to complete the drying operation.

The model of the falling rate period was based on the assumption that the first and second falling rate periods were as one stage. Hence the first falling rate period did not appear clearly in the numerical solution. However, the temperature distributions were in good agreement with the experimental results.

The predicted temperature distributions in the wet zone were always higher than the experimental data. This arose because an average value of moisture content, $\overline{X}$, was assumed to be equal $\frac{X_{cr}}{2}$ in the calculation of the effective thermal conductivity of the wet zone. However, the moisture content varies with time and depth during the falling rate period. Thus, finding a relationship between the distribution of moisture content throughout the body with time would facilitate more accurate predictions.

Although the model was only validated for beds 3.2 cm deep, it should be acceptable for predicting the temperature distribution within deep beds of both hygroscopic and non-hygroscopic solids. It may also be applicable to other types, e.g. colloidal materials, food

stuffs and fibrous materials.

In general, the proposed model allows rapid prediction of the temperature distribution profiles throughout the entire drying period. It therefore provides a tool to predict the temperature distribution within thick beds of hygroscopic and non-hygroscopic materials. The results can be used to predict drying behaviour under other conditions as an aid in optimising design and operation of drying equipment; the avoidance of thermal degradation due to overheated zones is an obvious example.

CHAPTER 7

VARIATION OF TEMPERATURE DISTRIBUTION ACCORDING TO MATERIAL LENGTH

7.1 INTRODUCTION

In a separate series of experiments, temperature distribution profiles were recorded during the drying of hygroscopic and non-hygroscopic materials in smaller diameter trays (d = 5.3 cm) than in the work described in Chapter 5, but with similar initial and external experimental conditions.

Glass beads of 100 μm diameter were dried in trays of 8.3 cm, 6.2 cm, 5.3 cm and 2.6 cm diameter; the depths were 6.5 cm, 4.7 cm and 3.2 cm. Each tray was insulated with either neoprene rubber of latex foam, which have very low thermal conductivities of 0.0025 W/m.K and 0.0009 W/m.K respectively.

Measurements were made of the temperatures at different depths of each bed. The relationships between the drying rate and effective length, and air temperature were investigated, using air temperatures of 84°C, 64°C and 54°C.

Beds of glass beads of 100 μm diameter were also dried in rectangular trays of different lengths at an air temperature of 84°C. The temperature profiles during

evaporation from a pool of pure distilled water and within a bed of dry solid were also recorded.

The variations in diameter and depth of trays, and in air temperature made it possible to study the influence of these variables upon temperature gradients within various beds and upon the drying rate. In this chapter, the results of these experiments are reported and discussed, and conclusions drawn.

7.2 TEMPERATURE PROFILES IN A SMALLER DIAMETER TRAY (d = 5.3 cm)

Temperature distribution profiles were investigated for beds of glass beads of 100 μm and 400 μm diameter, polystyrene pellets, activated alumina of 150 mesh, and wood powder. These materials were dried in a sample tray of similar depth to that used in Chapter 5, i.e. L = 3.2 cm, but with a smaller diameter, 5.3 cm as shown in Fig. 7.14. Since the tray diameter represents the distance traversed by the airflow over the surface of the bed, the object was to evaluate the influence of this effective distance upon the temperature profiles and upon the drying rate.

The inner wall and the bottom of the sample tray were lined with 0.55 cm of neoprene rubber sheet of very low thermal conductivity, λ = 0.0025 W/m.K to eliminate conductive heat transfer to the sample via the wall or bottom of the tray.

In order to observe the effect of variation of tray diameter, i.e. the 'effective length', on the temperature distribution profiles, the materials were dried under external conditions similar to those used in the experiments described in Chapter 5, with a sample tray of larger diameter, d = 8.3 cm, i.e. an air velocity of 0.5m/s, an inlet air humidity of 0.02 kgH_2O/kg dry air and an air temperature of 84°C. The initial temperature and the initial moisture content of each material were also as described as in Chapter 5. Hence, the only variable was the tray diameter.

Figures 7.1 - 7.5 show the experimentally-determined temperature distribution profiles for beds of glass beads of 100 μm and 400 μm diameter, polystyrene pellets, activated alumina and wood powder respectively. These demonstrate an unexpected trend during the constant rate period in that a temperature gradient was established with the temperature at the bottom always exceeding that at the surface. This was in direct contrast to the situation with the larger diameter tray, 8.3 cm, where the surface temperatures always exceeded those within the bed, as described in Chapter 5.

The temperature distribution profiles within the bed of glass beads of 100 μm diameter demonstrated that the bottom temperature was approximately 57°C, which exceeded the surface temperature of 42°C. The latter was slightly higher than the wet-bulb temperature of 38°C. The gradient in temperature between the surface and bottom remained constant during the constant rate period. At time t = 120 min., the surface temperature increased slightly, indicating the beginning of the first falling rate period, and at time t = 195 min., it became greater than the bottom temperature. This may indicate the beginning of the second falling rate period, when the surface became 'dried out'. During

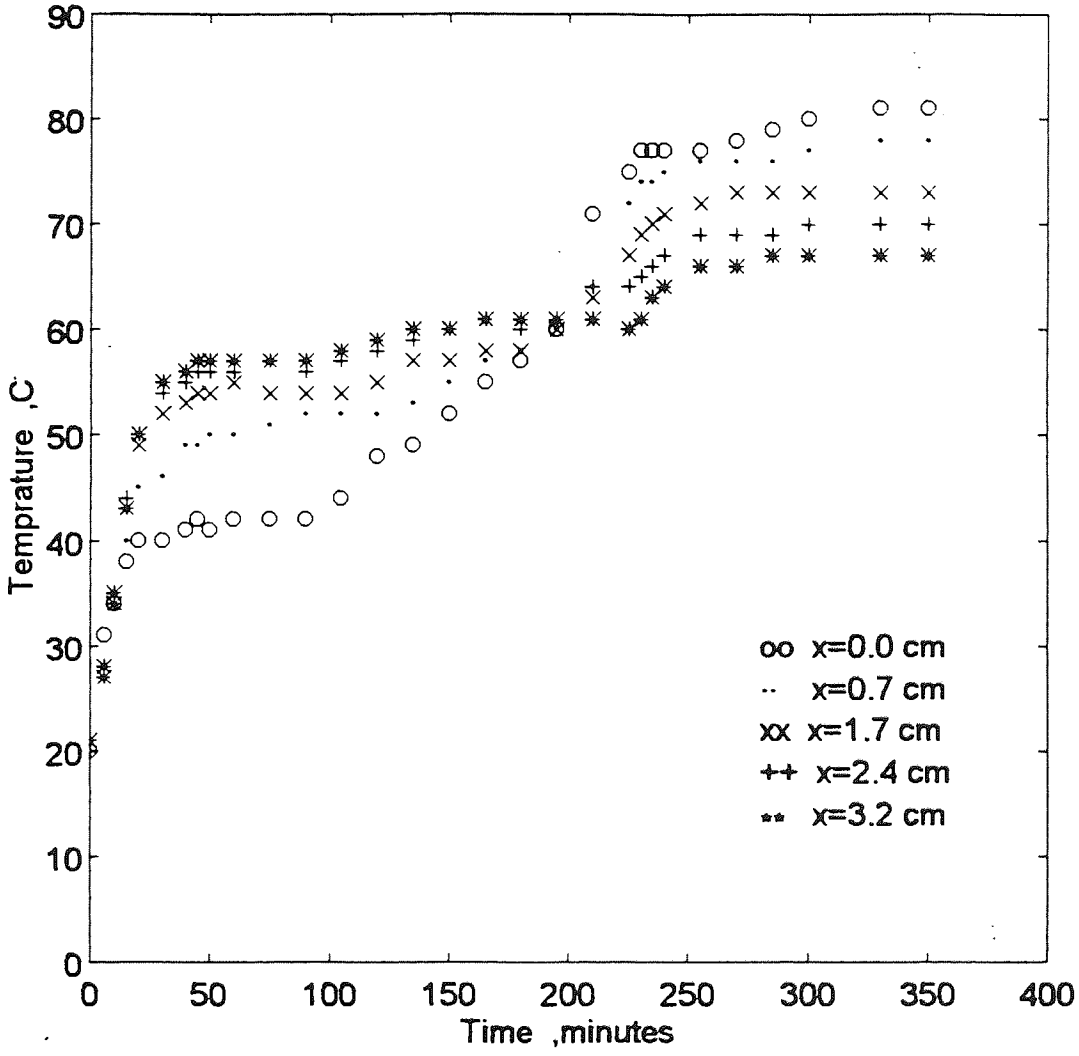

Figure 7.1 Temperature distribution profiles within a bed of glass beads (100 μm); tray d = 5.3 cm, L = 3.2 cm; air temperature 84°C, [x = distance of plane beneath surface].

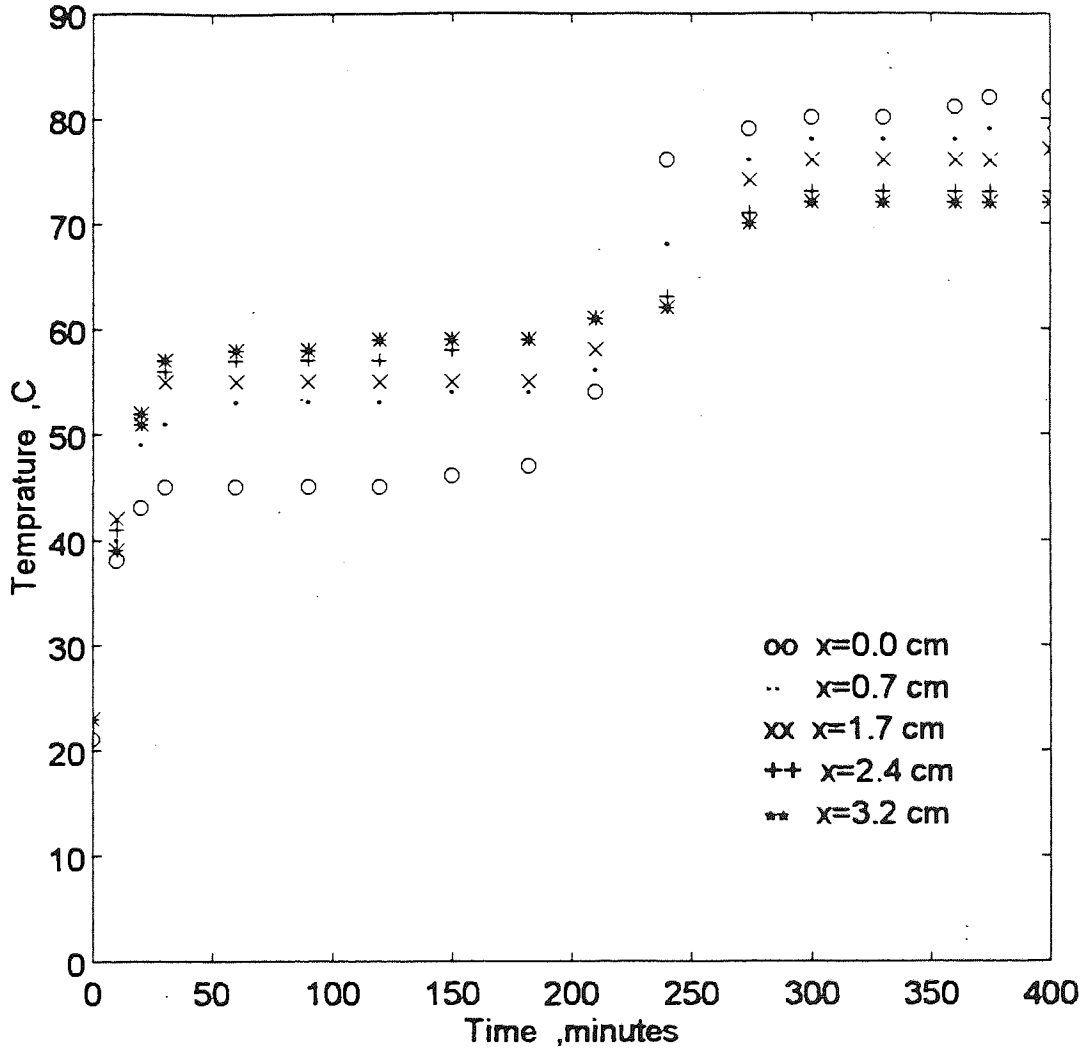

Figure 7.2 Temperature distribution profiles within a bed of glass beads (400 μm); tray d = 5.3 cm, L = 3.2 cm; air temperature 84°C.

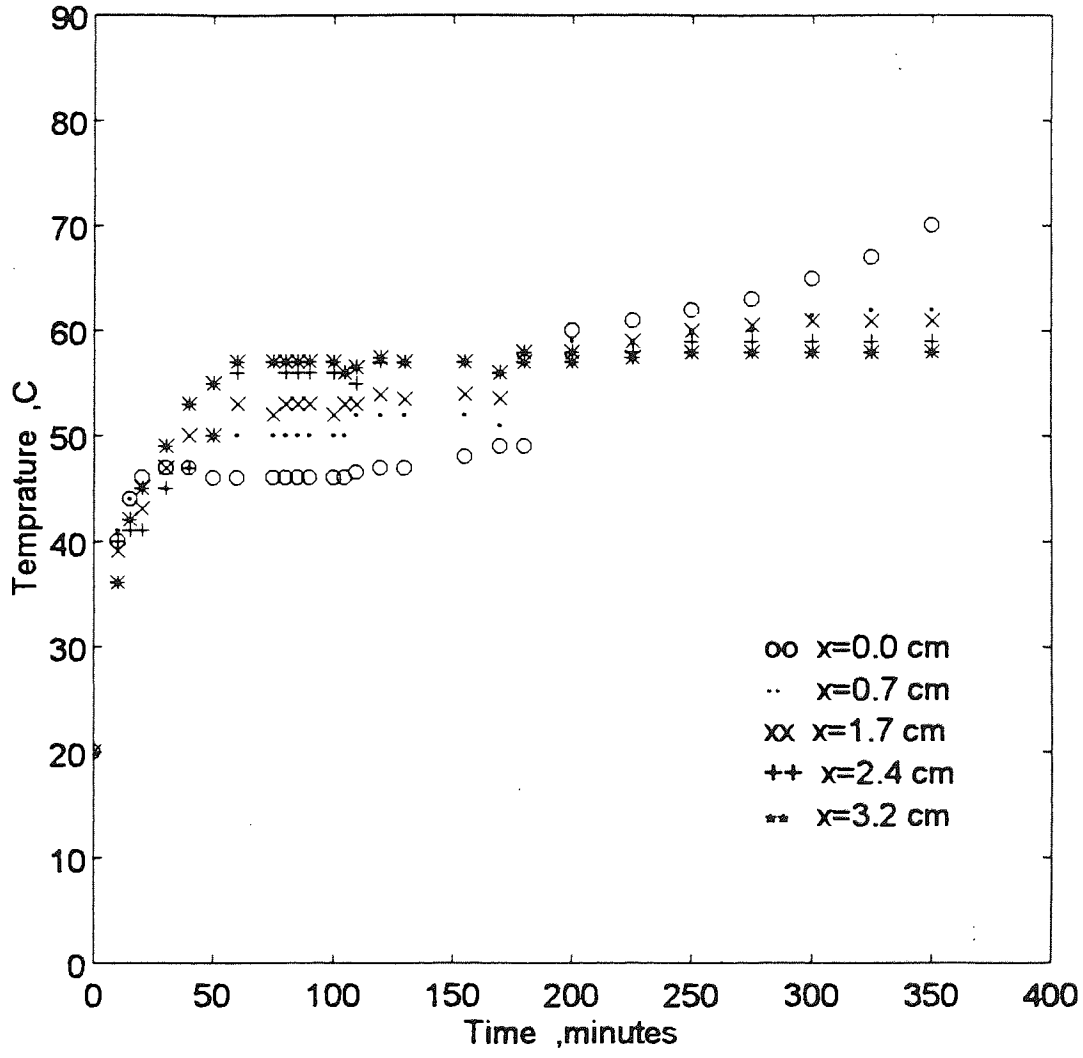

Figure 7.3 Temperature distribution profiles within a bed of polystyrene pellets; tray d = 5.3 cm, L = 3.2 cm, air temperature 84°C.

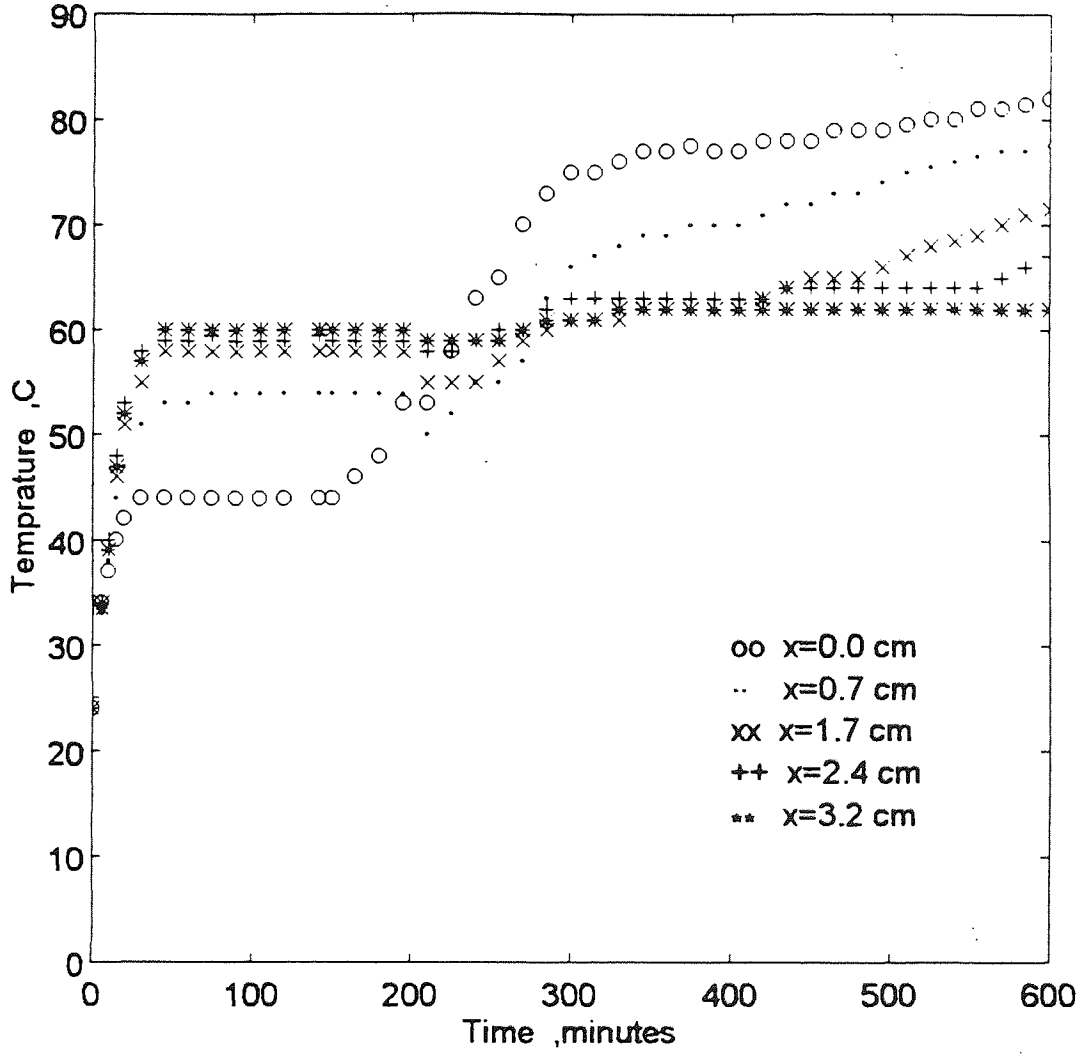

Figure 7.4 Temperature distribution profiles within a bed of activated alumina;150 mesh tray d = 5.3 cm, L = 3.2 cm; air temperature 84°C.

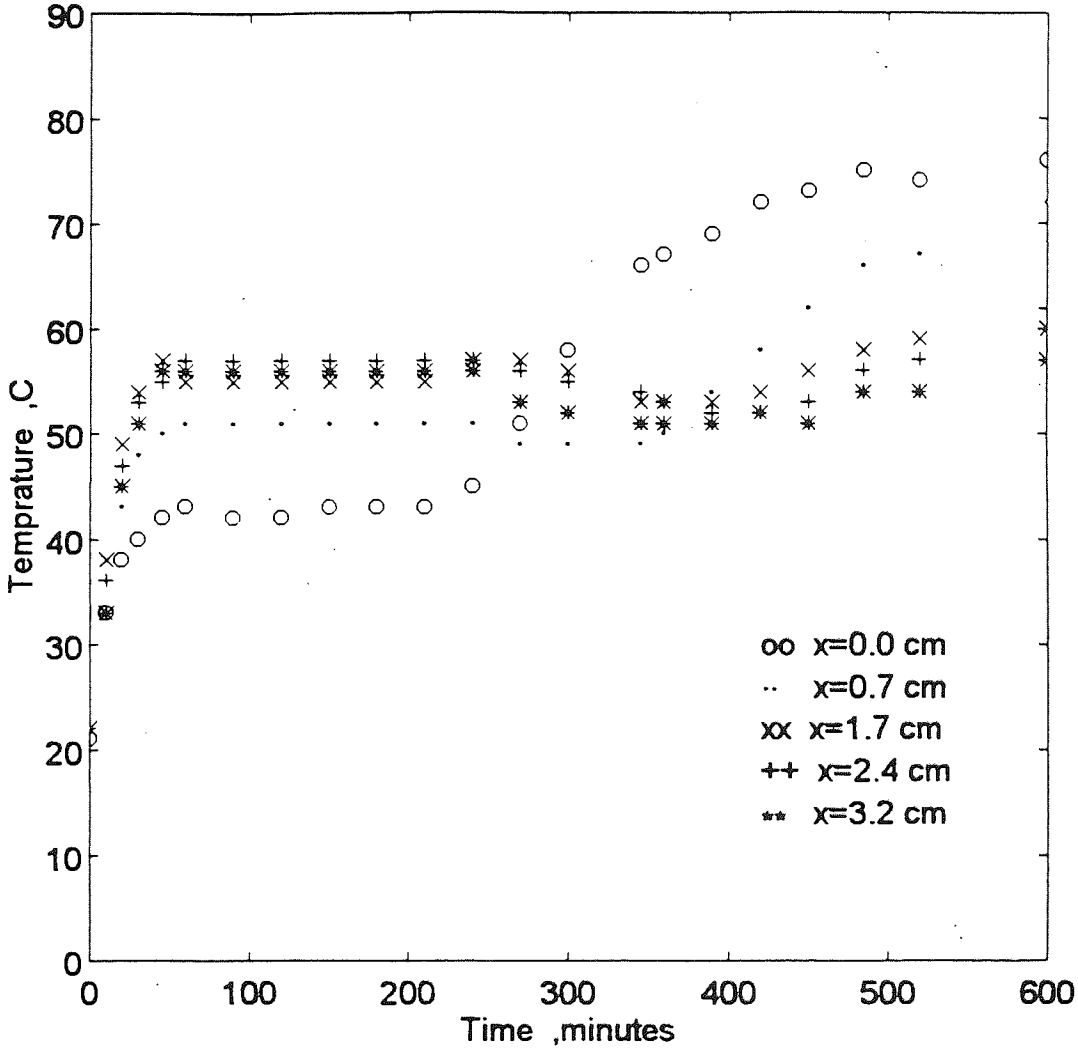

Figure 7.5 Temperature distribution profiles within a bed of wood powder; tray d = 5.3 cm, L = 3.2 cm; air temperature 84°C.

the second falling rate period, the temperature profile continued to resemble that obtained with the larger diameter tray. However, the surface temperature reached 81°C, close to air temperature, in a shorter time. Thus, it can be concluded that the total drying time was reduced when the smaller tray diameter was used.

Figure 7.2 shows the temperature distribution profile within a bed of glass beads of 400 μm diameter. These profiles are similar to those for glass beads of 100 μm diameter. Again, a temperature gradient was established with the temperature at the bottom always exceeding that at the surface during the constant rate period, which validates the earlier observations.

The temperature distribution profiles within a bed of polystyrene pellets are shown in Fig. 7.3. The temperature levels were slightly erratic at the beginning of the constant rate period but the bottom temperature later became higher than the surface temperature. The form of the temperature profiles was presumably affected by gravitational effects on the moisture within the relatively large pores between the larger polystyrene pellets.

Figure 7.4 shows the temperature profiles within a bed of activated alumina of 150 mesh. A clear inversion in the temperature gradient was obtained during the constant rate period, i.e. the surface temperature was 44°C, whilst the bottom temperature attained 60°C. At time t = 220 mins., the surface temperature became the greater, and the second falling rate period started.

The temperature profiles within a bed of wood powder are shown in Fig. 7.5. The surface temperature was 40°C, identical with the surface temperature in the larger diameter tray. This temperature was a little higher than the wet-bulb temperature of 39°C; the bottom temperature was 56°C. Again, the total time required to complete the drying operation was shorter than with the larger tray diameter.

It can be concluded that with an air temperature of 84°C an inversion in temperature profiles was always observed during the constant rate period with the smaller tray diameter (d = 5.3 cm). The temperature of the surface was a little above, or equal to, the wet-bulb temperature. The total drying time was reduced when a small diameter tray was used.

Plots of average moisture content versus time for beds of glass beads of 100 μm and 400 μm diameter, activated alumina and wood powder, are shown in Figures 7.6 to 7.9. Figures 7.10 to 7.13 show the drying rate curves for each material. The average constant drying rates were estimated and compared with those reported in Chapter 5, as shown in Table 7.1.

The data indicate that drying rate for each material in a tray of 5.3 cm was always higher than in a tray of 8.3 cm diameter.

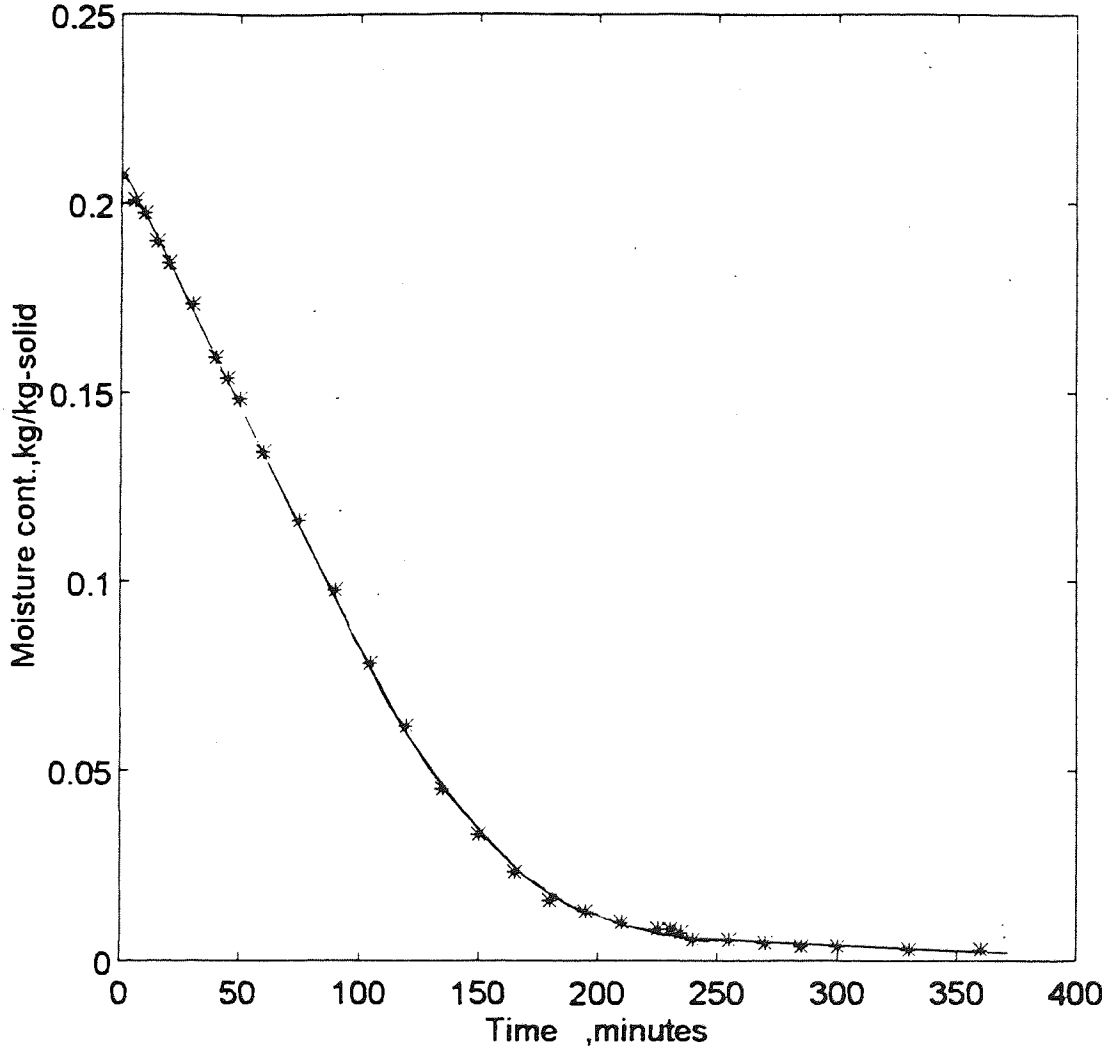

Figure 7.6 Average moisture content versus time for a bed of glass beads (100 μm); tray d = 5.3 cm, L = 3.2 cm; air temperature 84°C.

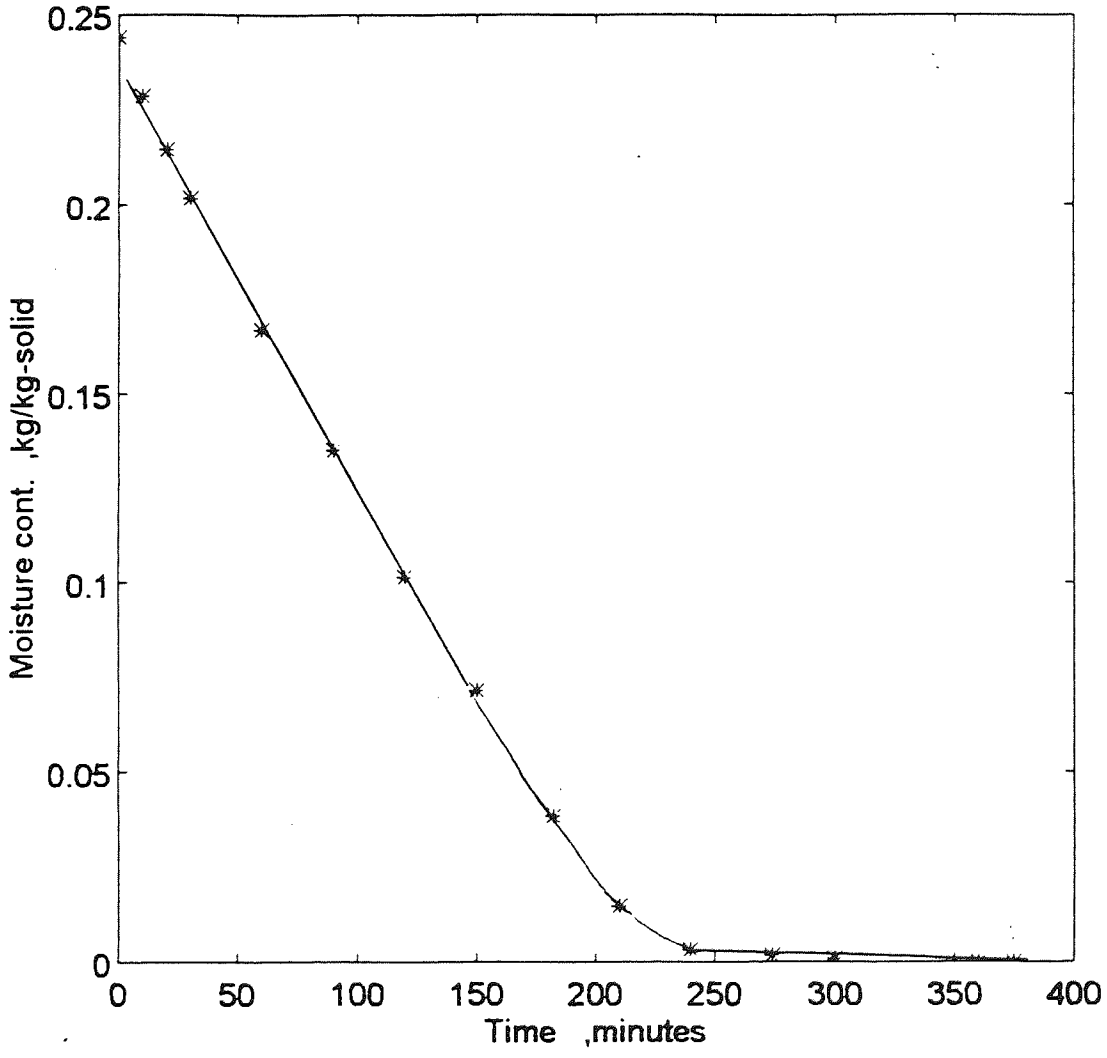

Figure 7.7 Average moisture content versus time for a bed of glass beads (400 μm); tray d = 5.3 cm, L = 3.2 cm; air temperature 84°C.

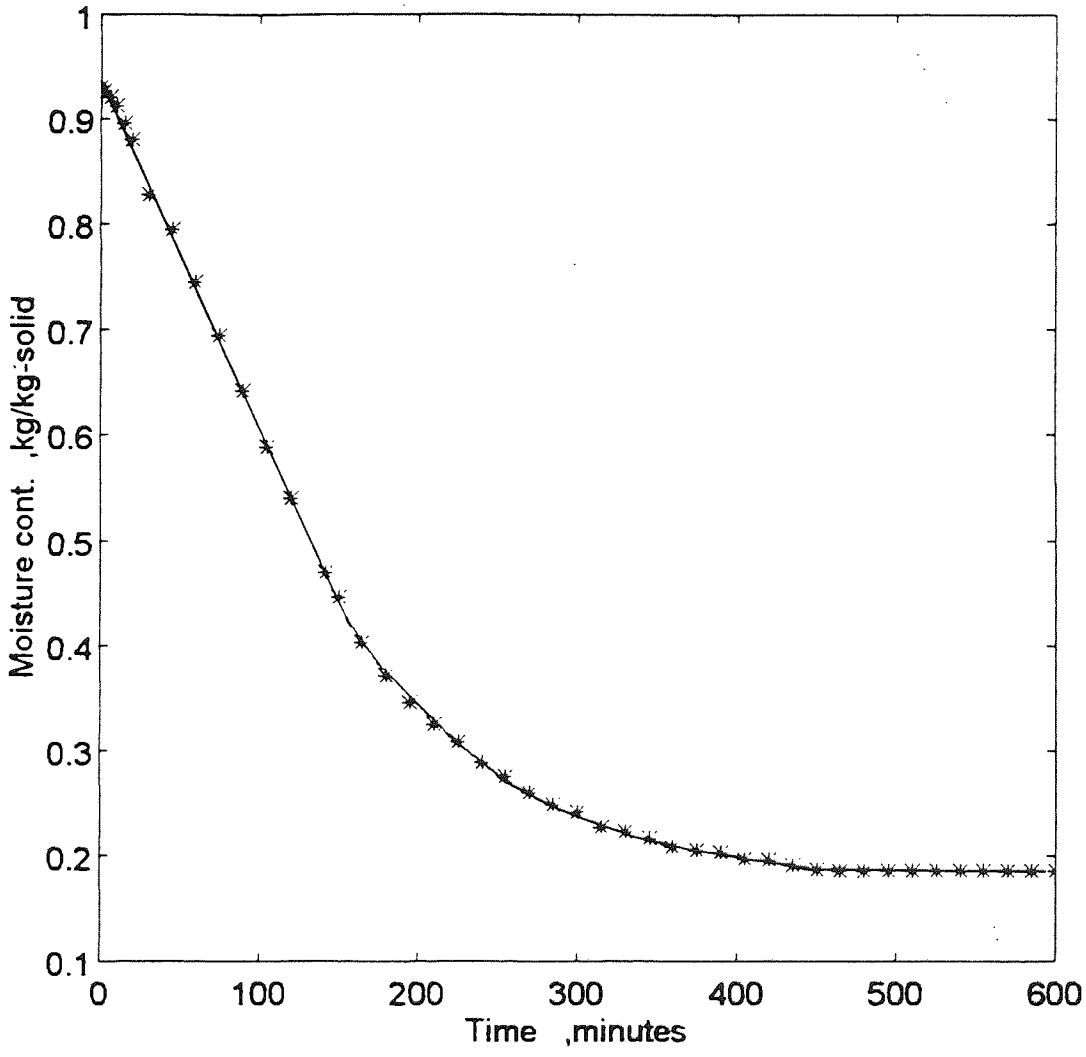

Figure 7.8 Average moisture content versus time for a bed of activated alumina, 150 mesh; tray d = 5.3 cm, L = 3.2 cm; air temperature 84°C.

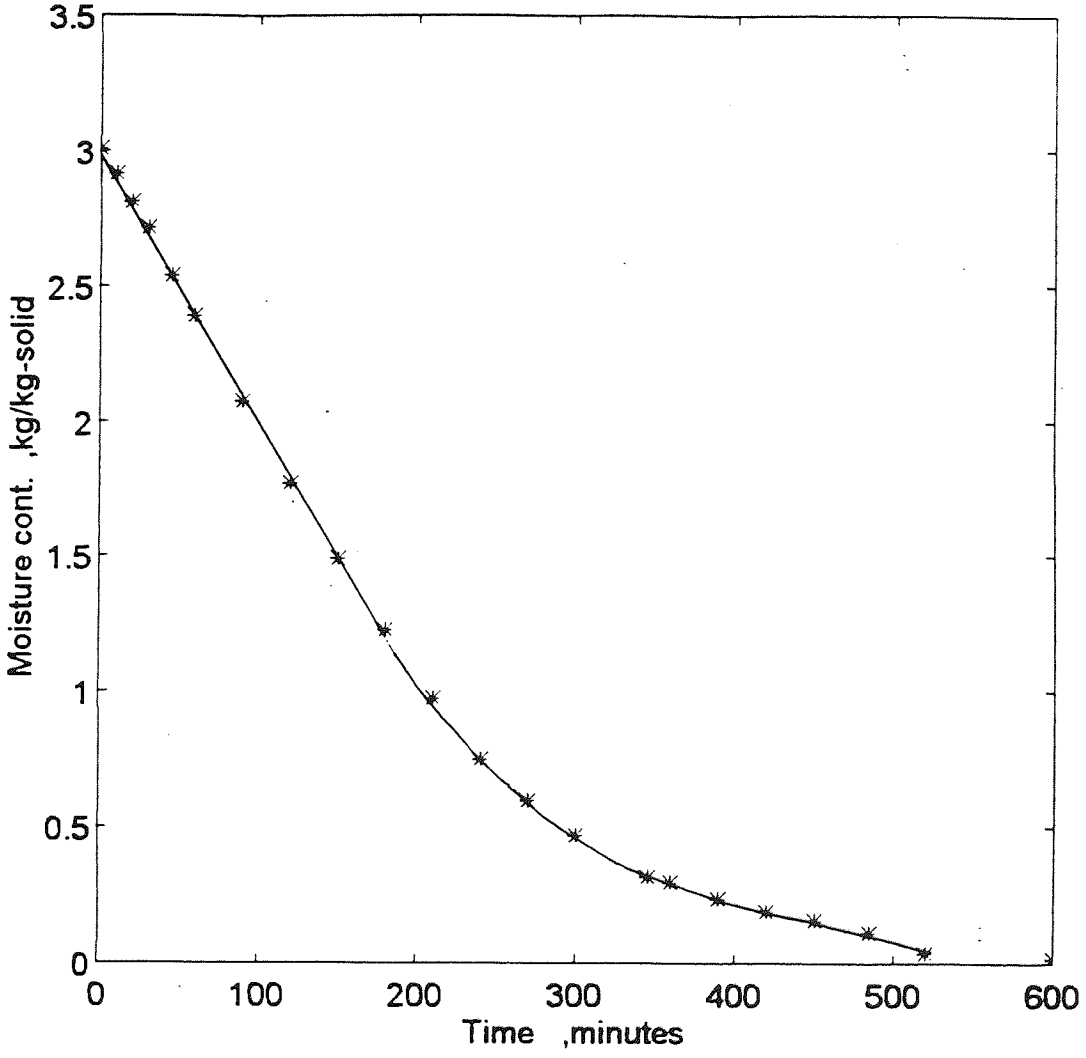

Figure 7.9 Average moisture content versus time for a bed of wood powder; tray d = 5.3 cm, L = 3.2 cm; air temperature 84°C.

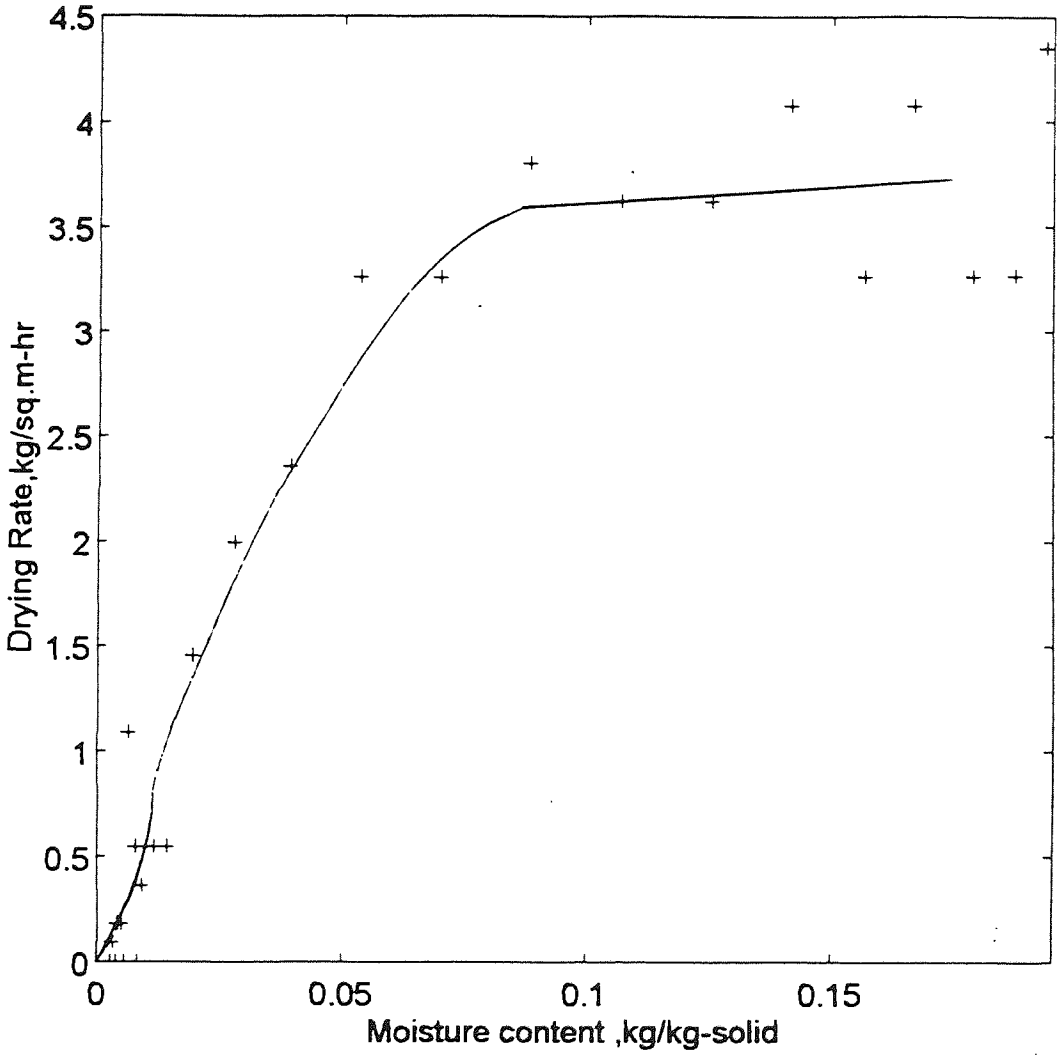

Figure 7.10 Drying rate curve for a bed of glass beads (100 μm); tray d = 5.3 cm, L = 3.2 cm; air temperature 84°C.

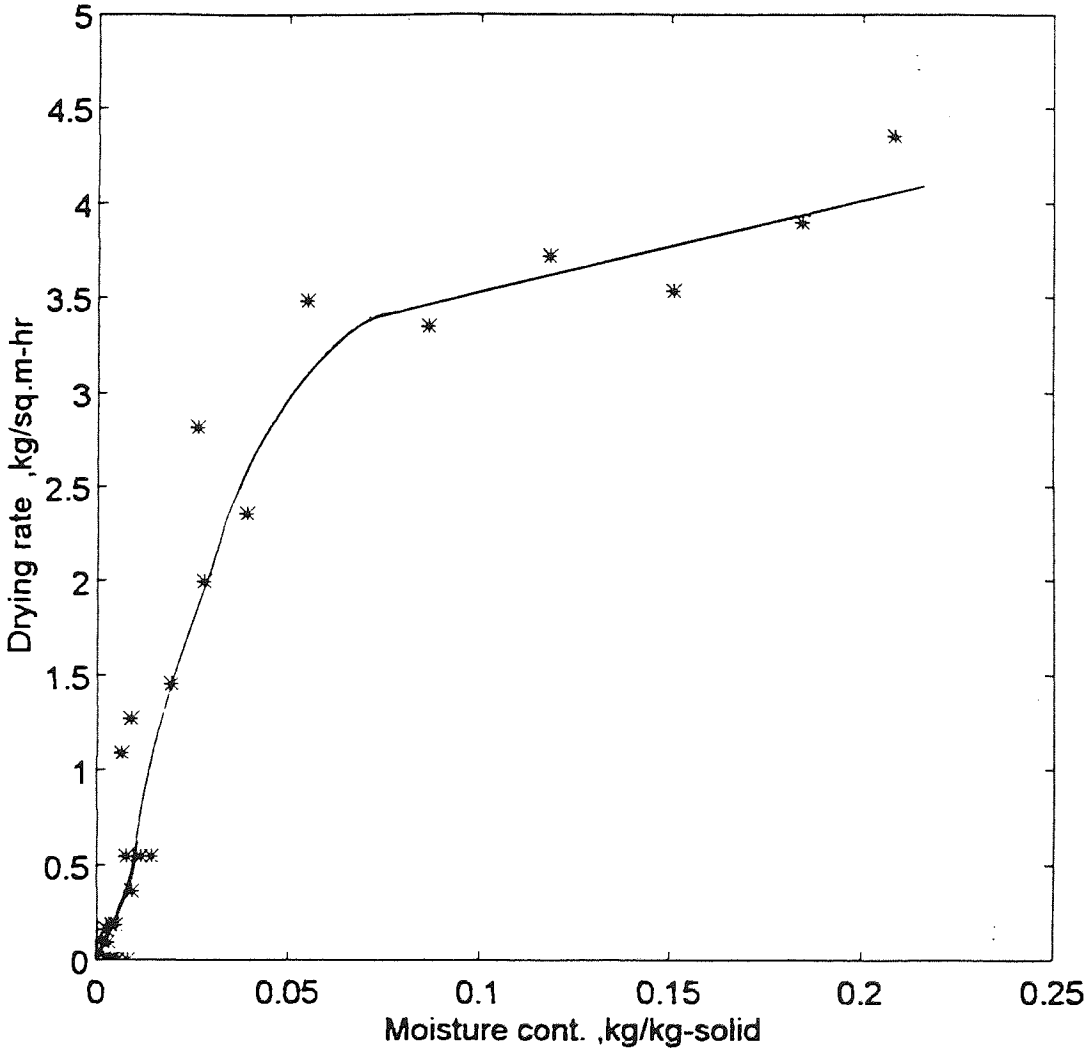

Figure 7.11 Drying rate curve for a bed of glass beads (400 μm); tray d = 5.3 cm, L = 3.2 cm; air temperature 84°C.

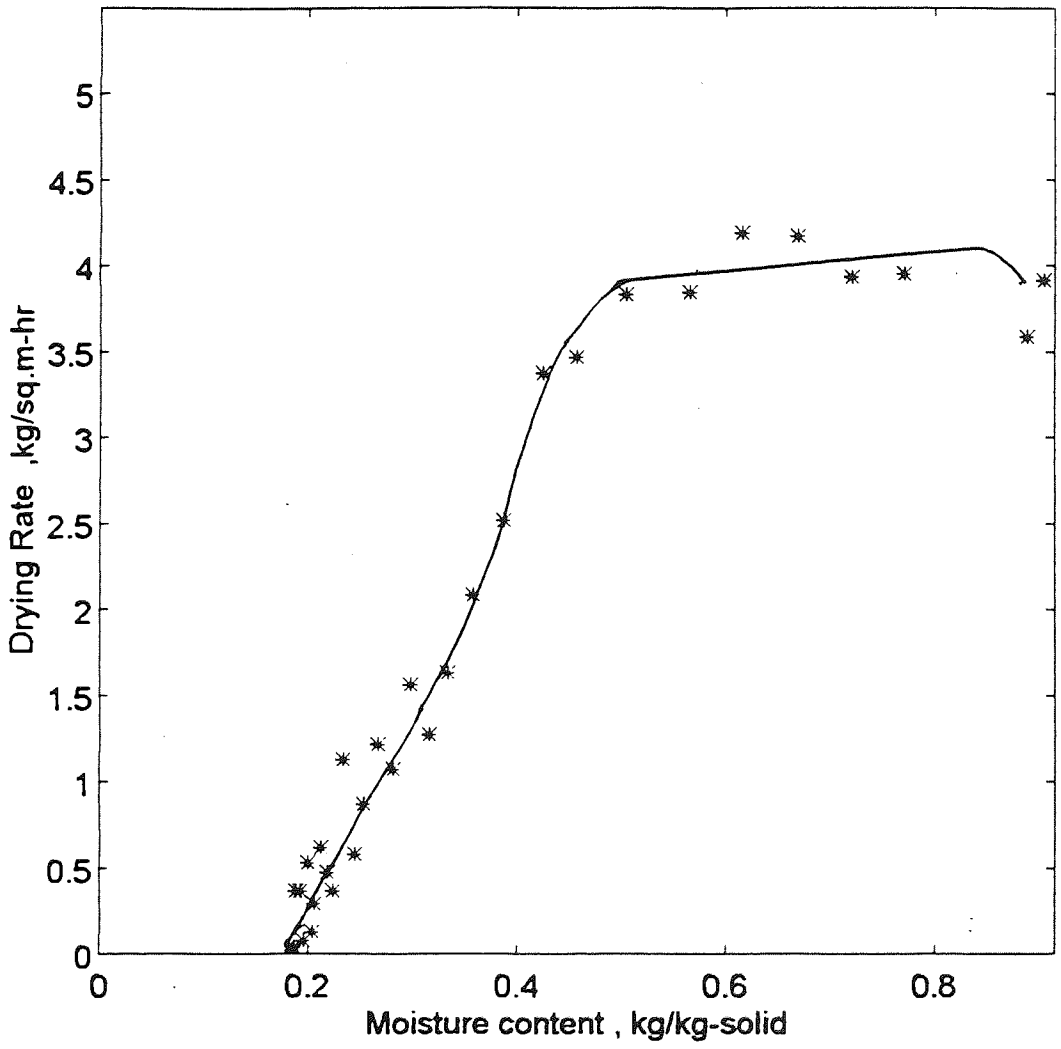

Figure 7.12 Drying rate curve for a bed of activated alumina, 150 mesh; tray d = 5.3 cm, L = 3.2 cm; air temperature 84°C.

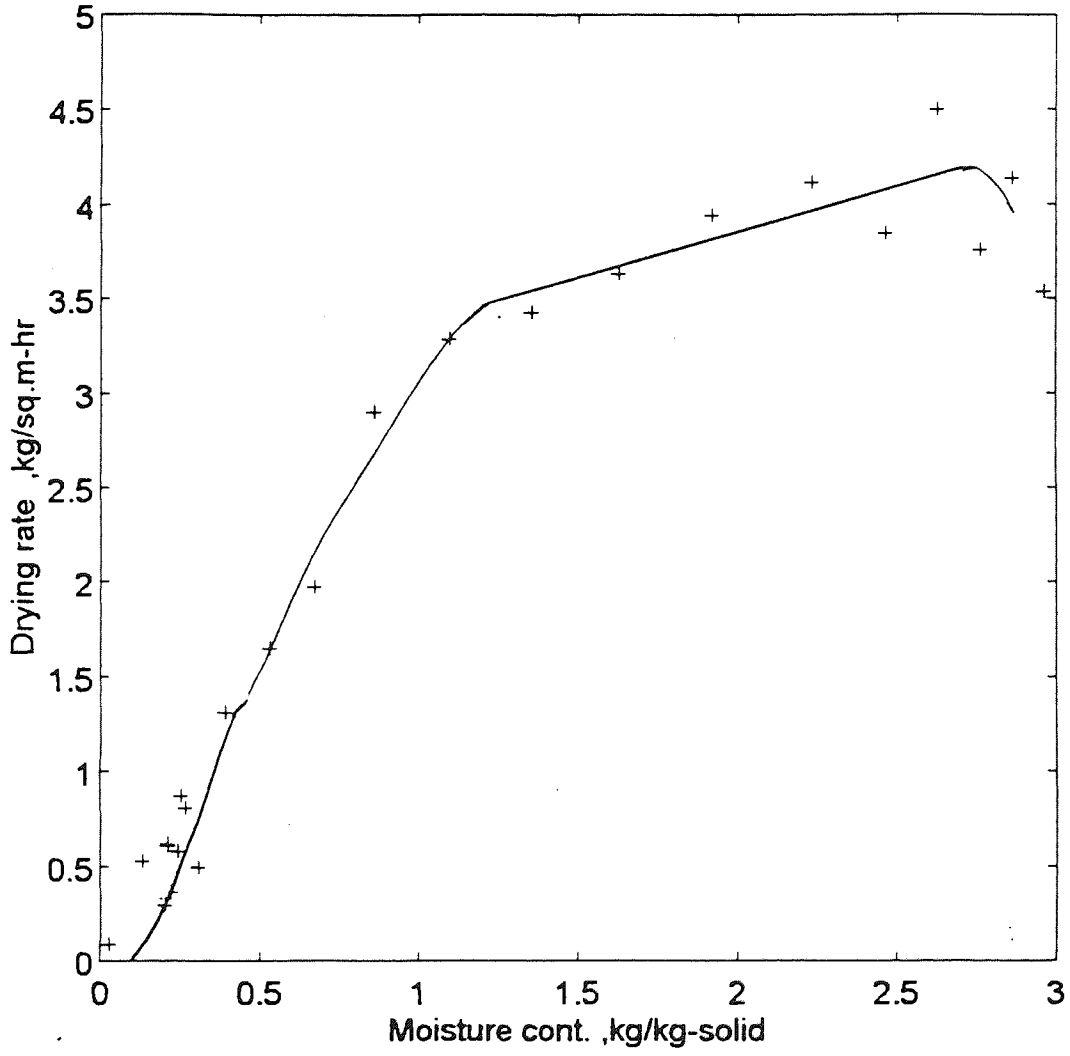

Figure 7.13 Drying rate curve for a bed of wood powder; tray d = 5.3 cm, L = 3.2 cm; air temperature 84°C.

Table 7.1 The average constant drying rates

Material	Drying rate of tray diameter 8.3 cm (kg/m^2-h)	Drying rate of tray diameter 5.3 cm (kg/m^2-h)
G.B 100 μm	2.25	3.5
G.B 400 μm	2.25	3.5
Polystyrene	2.2	–
Act. Alumina	2.8	4
Wood Powder	1.85	3.8

7.3 OTHER DIMENSIONS

In the previous section, an inversion in the temperature profile was observed during the constant rate period when using the smaller diameter tray. The drying rates were also increased. This section reports the results of other experiments conducted to obtain more information about the inversion phenomenon and the variation of the drying rate with variation of tray diameter.

Glass beads of 100 μm diameter were dried in sample trays having a similar depth but of different diameters. Initial and external conditions were similar to those applied in the work described in the previous section. The temperatures in the constant rate period were of particular interest, since the inversion in temperature gradient usually occurs in this period.

The glass beads were dried in a tray of diameter 2.6 cm and depth 3.2 cm. Thicker insulation, namely a 1.9 cm layer of latex foam, was used in this experiment, to further eliminate any conductive heat transfer through the bottom and walls of the glass tray as shown in Fig. 7.15. This type of insulation has a very low thermal conductivity, $\lambda = 0.0009$

W/m.K. The temperature distribution profiles obtained are shown in Fig. 7.20. Clearly during the constant period, the bottom temperature was greater than that of the surface; i.e 59°C, compared with 43°C. Both bottom and surface temperatures were higher than when a tray of 5.3 cm diameter was used. At time, t = 115 min., the temperature of the surface exceeded that of the bottom; this would seem to indicate the start of the second falling rate period. This time was less than that obtained with a tray of 5.3 cm diameter, which implies that the total time required to complete the drying operation would also be less.

Another experiment was carried out under the same conditions, but using a sample tray with a greater diameter, d = 6.2 cm, whilst the depth was kept at 3.2 cm, as shown in Fig. 7.16. The temperature profiles observed are shown in Fig. 7.21. An inversion in the temperature profile was observed during the constant rate period, but the difference in temperature between the bottom and the surface was less than those obtained with trays of 2.6 cm and 5.3 cm diameter. The bottom temperature was 50°C, and the surface temperature 40°C. Fig. 7.22 shows the drying rate curve. The drying rate during the constant rate period was 3 kg/m^2-h , which was less than that for a tray of 5.3 cm. Clearly, the total time required to complete drying would also be longer.

The experimental data resulting from the drying of beds of glass beads of 100 μm in trays of similar depth (3.2 cm) but of different diameters (2.6 cm, 5.3 cm, 6.2 cm and 8.3 cm) at 84°C are shown in Table 7.2.

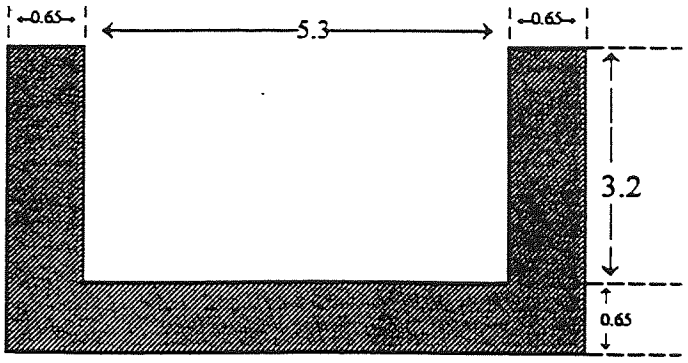

Figure 7.14 A glass sample tray, 5.3 cm internal diameter and 3.2 cm deep, insulated with neoprene rubber; dimensions in (cm).

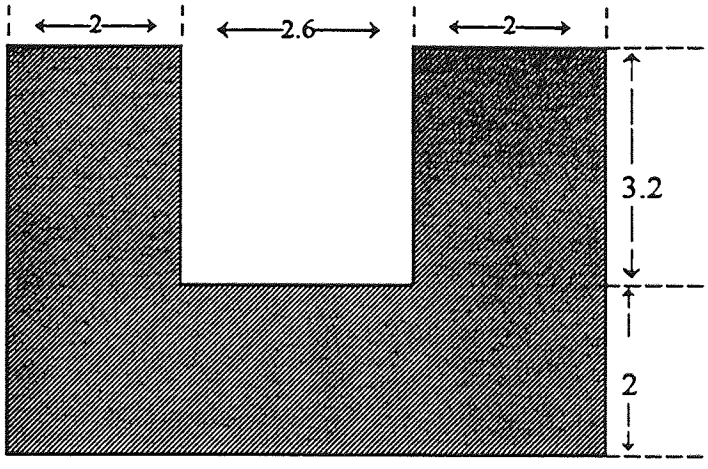

Figure 7.15 A glass sample tray, 2.6 cm internal diameter and 3.2 cm deep; insulated with latex foam; dimensions in (cm).

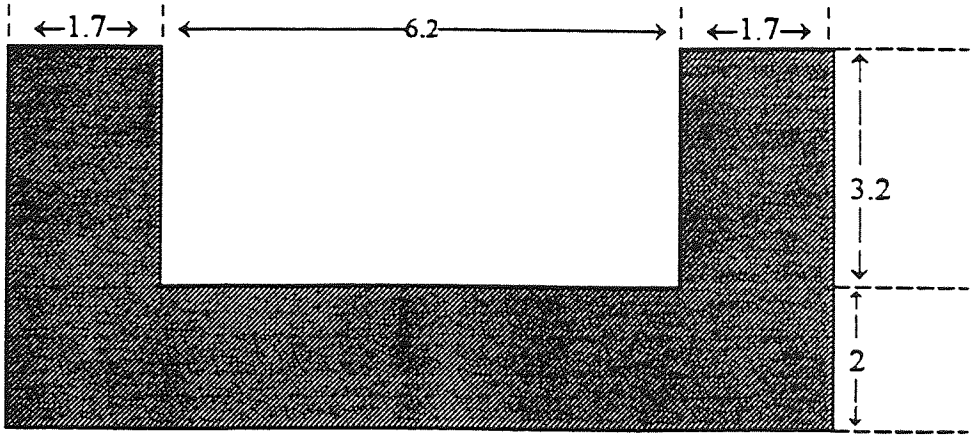

Figure 7.16 A glass sample tray, 6.2 cm internal diameter and 3.2 cm deep insulated with latex foam; dimensions in (cm).

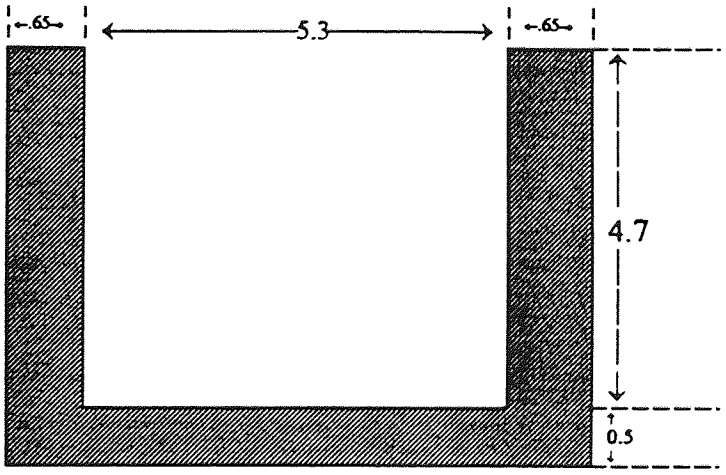

Figure 7.17 A glass sample tray, 5.3 cm internal diameter and 4.7 cm deep; insulated with neoprene rubber; dimensions in (cm).

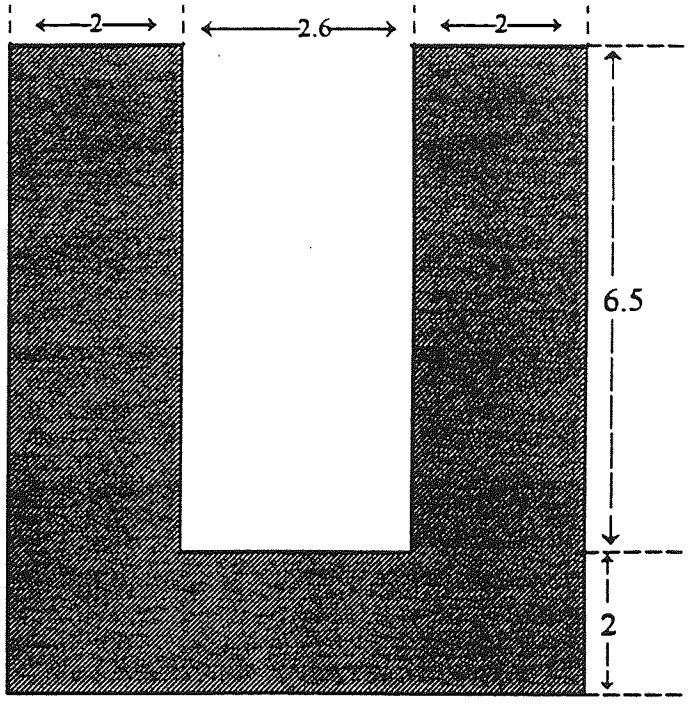

Figure 7.18 A glass sample tray, 2.6 cm internal diameter and 6.5 deep; insulated with latex foam; dimensions in (cm).

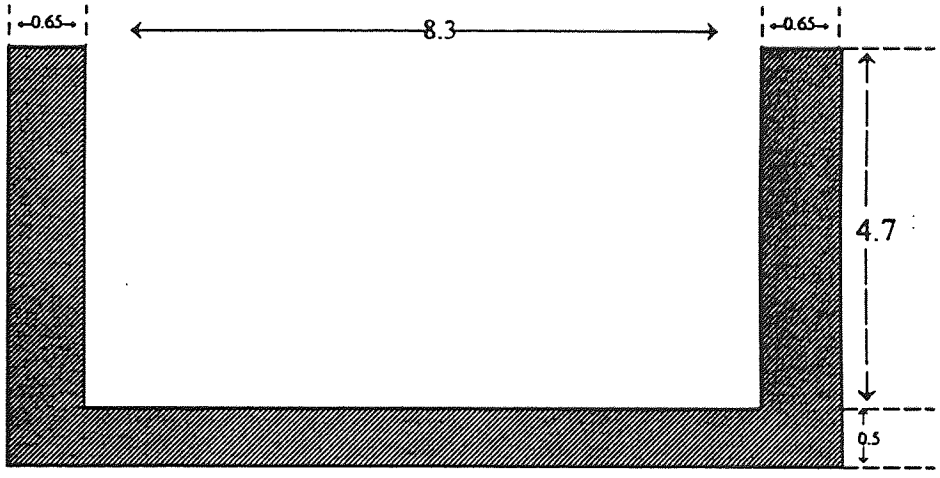

Figure 7.19 A glass sample tray, 8.3 cm internal diameter and 4.7 cm deep; insulated with neoprene rubber; dimension in (cm).

Table 7.2 Results of drying beds of glass beads (100 μm) at an air temperature of 84°C in trays of 3.2 cm depth and different diameters.

	Diameter of Tray			
	2.6 cm	5.3 cm	6.2 cm	8.3 cm
Temperature of bottom, T_b (°C)	59	57	50	32
Temperature of surface, T_s (°C)	43	42	40	38
Difference of temperature, ΔT (°C)	16	15	10	-6
Time to beginning of the 2nd falling period, t (min.)	115	195	215	290
Average values of constant drying rate, m_c (kg/m²-h)	--	3.5	3.0	2.25

Table 7.2 demonstrates that the bottom temperature varied significantly with the variation in the tray diameter; the smaller the tray diameter, the higher the bottom temperature. With tray diameters of 2.6 cm, 5.3 cm and 6.2 cm, the temperature of the bottom, T_b, exceeded that of the surface. That is, a temperature inversion occurred in trays of smaller diameter, as discussed in Section 7.9.

With the tray of 8.3 cm diameter, the bottom temperature was less than that of the surface. This result can be considered 'normal', and would also be expected with larger tray diameters.

The surface temperature, T_s, did not vary significantly with the tray diameter. It was always close to the wet-bulb temperature (38°C - 39°C). Therefore, the difference in temperature, ΔT, between the bottom and the surface reduced as the diameter was increased. For a tray of diameter 8.3 cm, the difference in temperature, ΔT, had a negative value. Thus, it can be concluded that an 'inversion point' at which the temperature of the

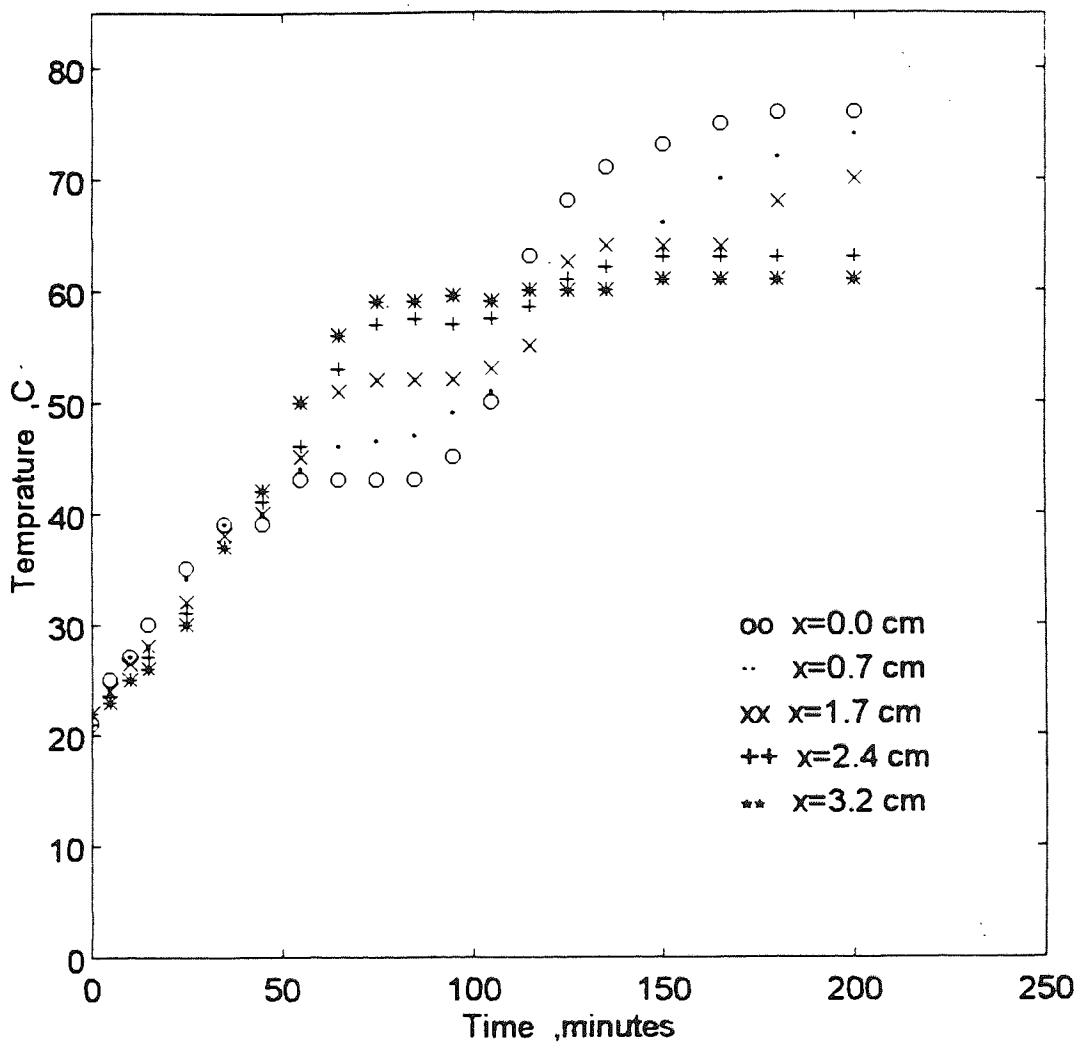

Figure 7.20 Temperature distribution profiles within a bed of glass beads (100 μm); tray d = 2.6 cm, L = 3.2 cm; air temperature 84°C.

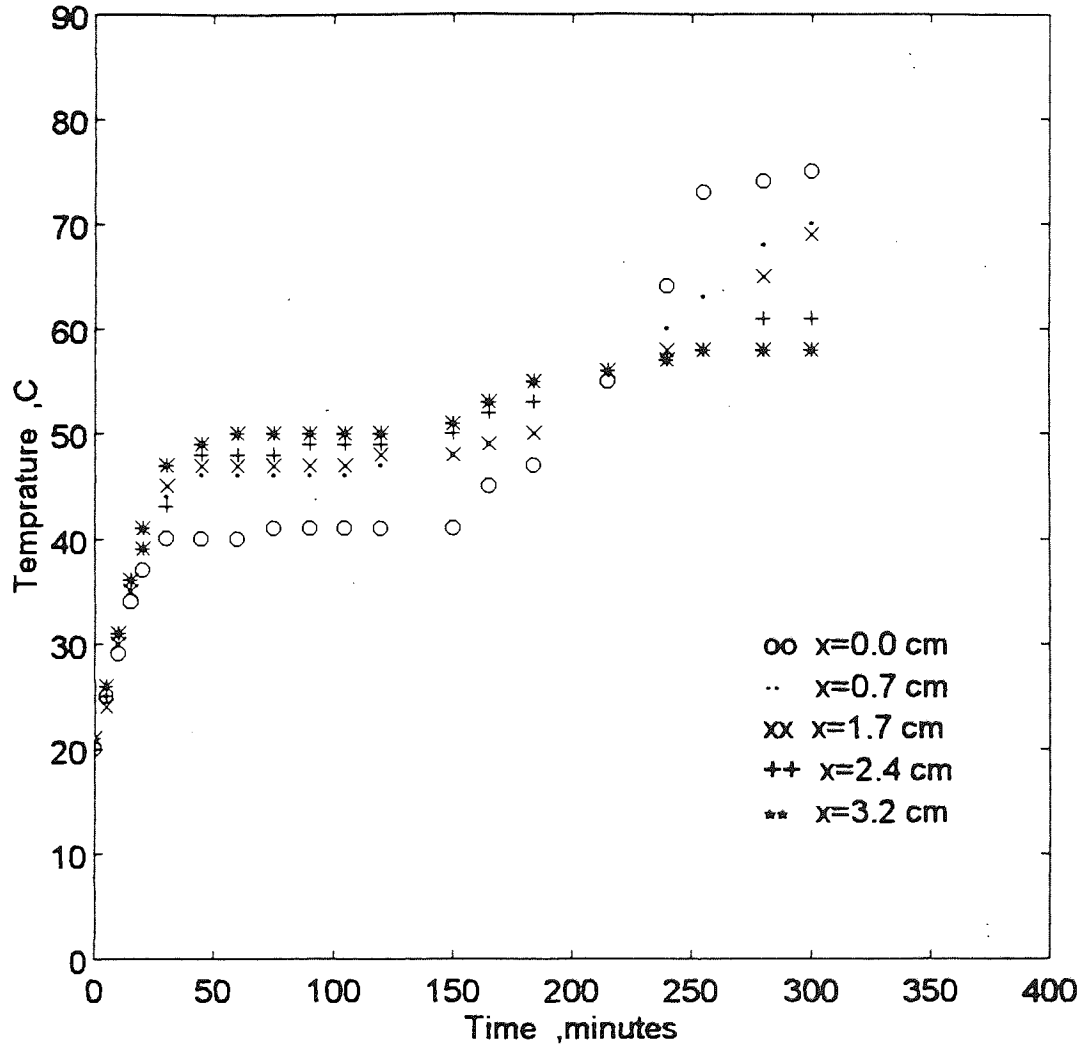

Figure 7.21 Temperature distribution profiles within a bed of glass beads (100 μm); tray d = 6.2 cm, L = 3.2 cm; air temperature 84°C.

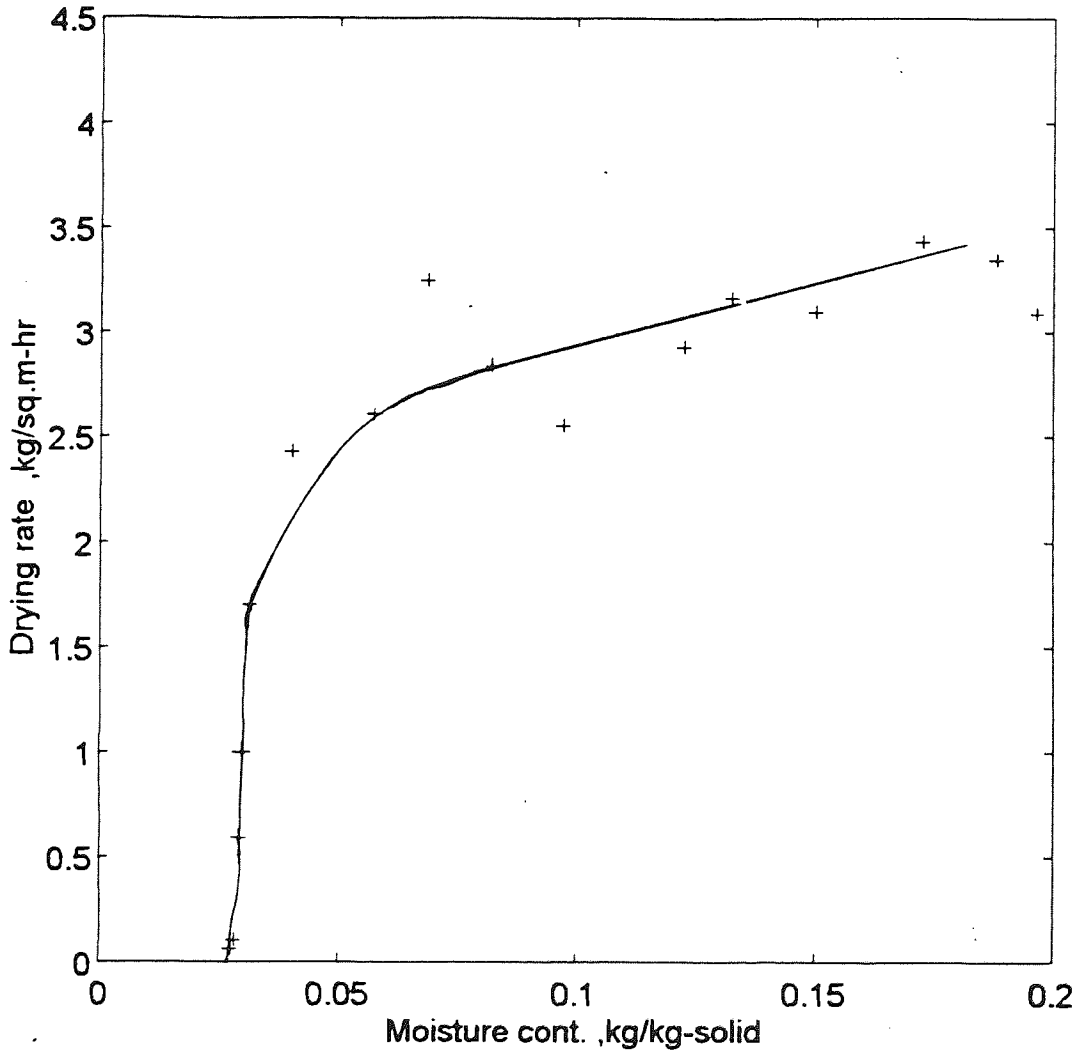

Figure 7.22 Drying rate curve for a bed of glass beads (100 μm); tray d = 6.2 cm, L = 3.2 cm; air temperature 84°C.

bottom would be equal to the surface temperature may be expected to arise at a critical diameter between 6.2 cm and 8.3 cm.

Table 7.2 also showed that the average drying rate also increased when the tray diameter was decreased. For this reason, the time to the beginning of the second falling rate period decreased when the tray diameter was reduced. Thus, the total time required to complete the drying operation would have decreased with a reduction in tray diameter.

With glass beads of 400 μm, polystyrene pellets, activated alumina and wood powder an inversion in temperature occurred in the sample tray of 5.3 cm diameter. Thus, the inversion point for these at an air temperature of 84°C will be within the range 5.3 cm - 8.3 cm.

7.4 THE EFFECT OF BED DEPTH

Experiments were next conducted to investigate the effect of bed depth on the temperature distribution profiles. Beds of glass beads of 100 μm of different depth were dried in sample trays of similar diameter. The experimental conditions were similar to those used previously. The temperatures of both the bottom and surface of bed were recorded.

Seven thermocouples were inserted at different depths in a tray of 5.3 cm diameter and 4.7 cm deep. The dimensions of the tray are shown in Fig. 7.17. The temperature profiles observed for this case are shown in Fig. 7.23 for comparison with those shown in Fig. 7.1, for the tray of 5.3 cm diameter and 3.2 cm depth. Fig. 7.23 shows that the bottom

temperature was greater than the surface temperature; this result was similar to the case of the tray of 3.2 cm depth. However, both the bottom and the surface temperatures were lower than in the first case. At time t = 260 min., the surface temperature became higher than the bottom temperature, indicating the beginning of the second falling rate period. This duration was longer than in the previous case.

To investigate further the effect of depth, an experiment was carried out using a sample tray of 2.6 cm diameter and 6.5 cm deep as shown in Fig. 7.18. Only three thermocouples were inserted at different depths, but these were adequate to observe the inversion in temperature. The temperature profiles are shown in Fig. 7.24. The results of this experiment were compared with the results of the tray of 2.6 cm diameter and 3.2 cm depth, shown in Fig. 7.20. Again, an inversion in the temperature was observed during the constant rate period. The bottom temperature was 49°C, and the surface temperature was 37°C. These temperatures were slightly lower than with a 3.2 cm depth. The time to the beginning of the second falling period was t = 340 min., i.e. longer than the time recorded with the smaller depth.

Another experiment was performed with a tray of 8.3 cm diameter and 4.7 cm deep, as shown in Fig. 7.19. The temperature distribution profiles are shown in Fig. 7.25 for comparison with the results with the tray of diameter 8.3 cm and depth 3.2 cm reported in Chapter 5. The results showed that the form of the temperature distribution was similar to that with the smaller depth tray. T_b was less than T_s, i.e. inversion in temperature did not occur. The bottom temperature was 28°C and the surface temperature was 34°C. These temperatures were a little less than in the former case and the time to the beginning of the

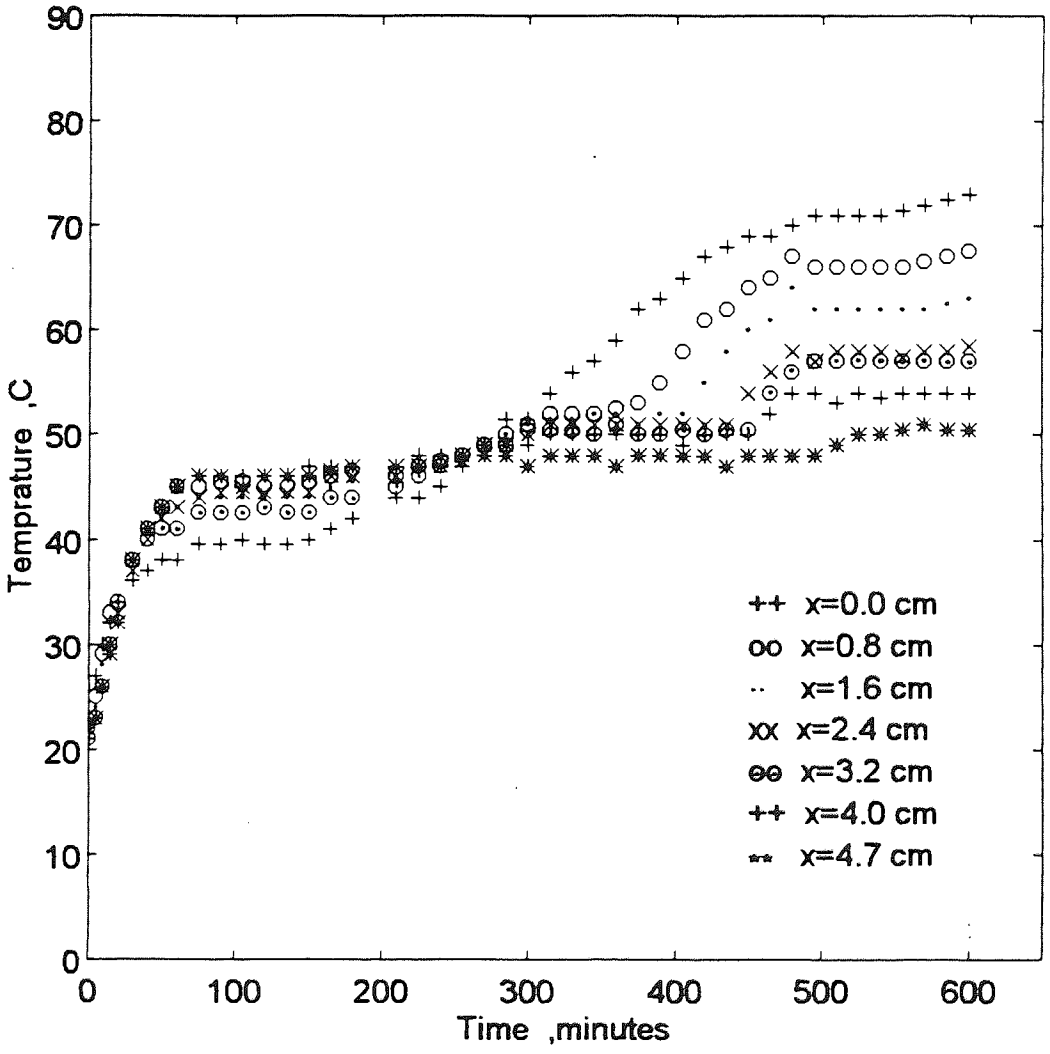

Figure 7.23 Temperature distribution profiles within a bed of glass beads (100 μm); tray d = 5.3 cm, L = 4.7 cm; air temperature 84°C.

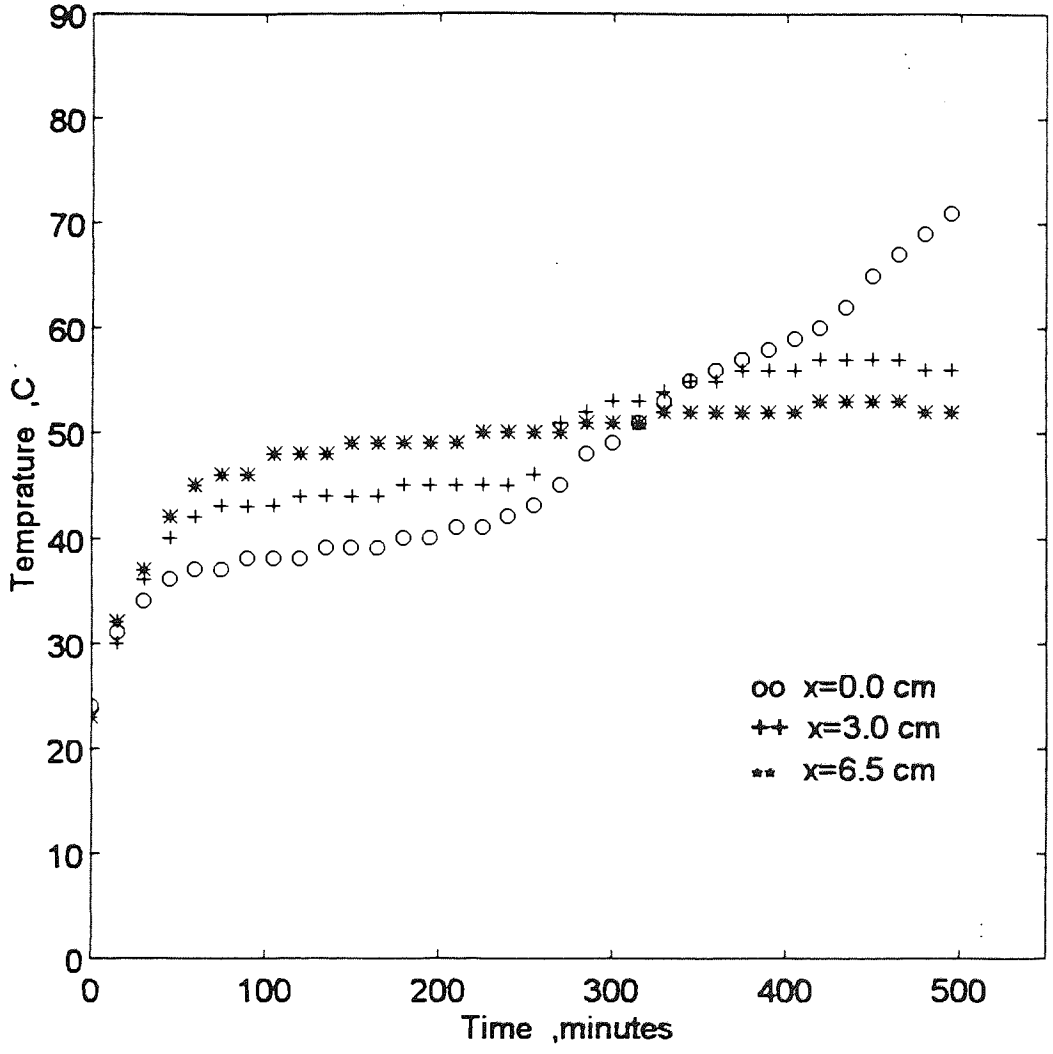

Figure 7.24 Temperature distribution profiles within a bed of glass beads (100 μm); tray d = 2.6 cm, L = 6.5 cm; air temperature 84°C.

second falling period was longer, (t = 360 min. for a tray 4.7 cm deep and t = 290 min. for a tray 3.2 cm deep).

It can be concluded that an inversion in the temperature difference occurred with the small tray diameter at various depths. Both the surface and the bottom temperatures reduced with an increase in bed depth. For the case of the large diameter (d > 8 cm), T_s was always greater than T_b. This difference may be expected to exist for any greater length, i.e. an inversion in temperature will not occur.

It can also be concluded that the time to reach the beginning of the second falling rate period increases with an increase in bed depth. Thus, the total time required to complete the drying operation increases as depth of the bed increases. This result can be expected, because when the depth increases, the volume of the bed increase, and hence the moisture hold-up.

A comparison can be made between the temperature profiles in Fig. 7.23 and 7.25, since only the tray diameters differ, i.e. 5.3 and 8.2 cm diameter. In Fig. 7.23, T_b was greater than T_s, in contrast Fig. 7.25, T_s was greater than T_b. This observation adds support to the conclusion that inversion in temperature occurs at a small diameter, d < 8 cm. The time to beginning of the second falling period is also reduced with a reduction in the tray diameter.

In general, the variation of tray diameter (effective length) has a significant effect on the temperature profile and an inversion in the temperature profile was always apparent in

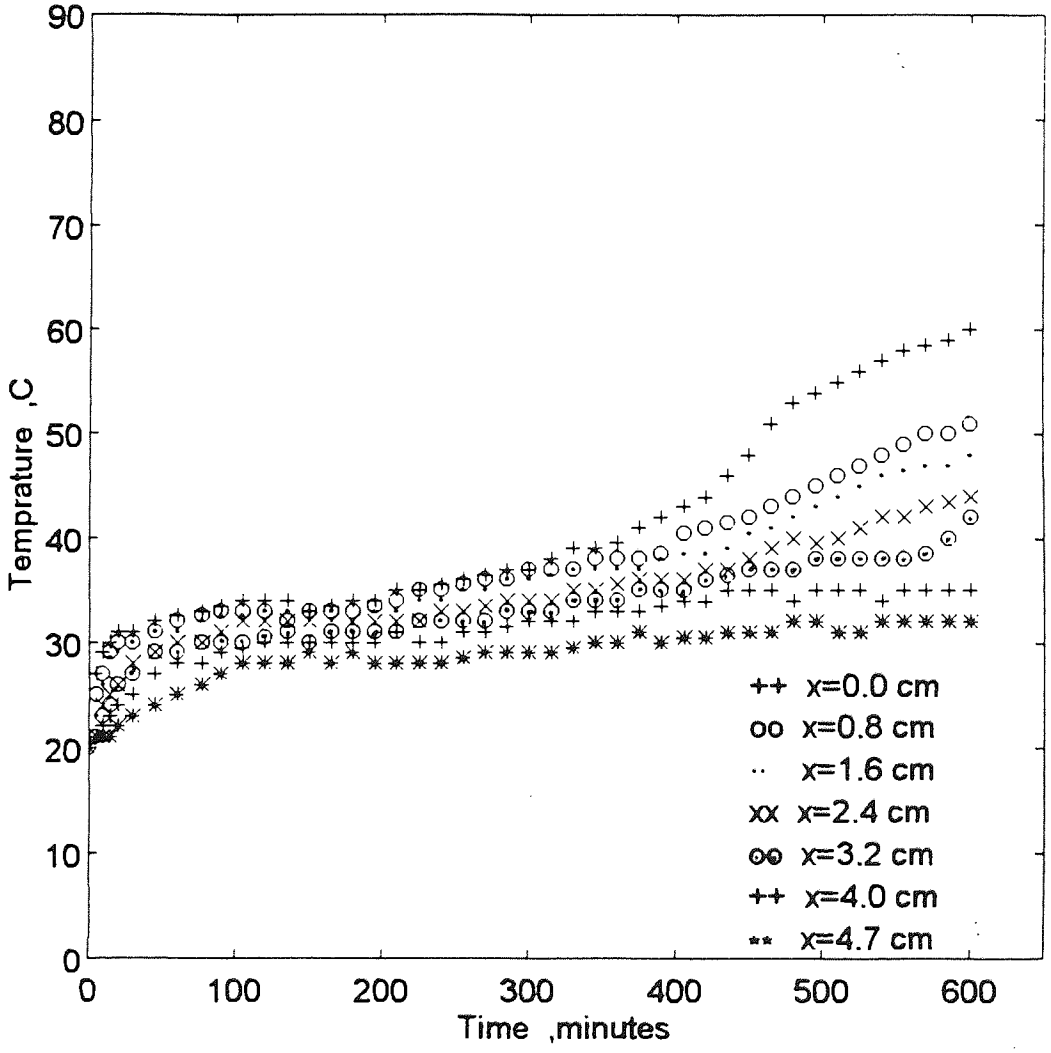

Figure 7.25 Temperature distribution profiles within a bed of glass beads (100 μm); tray d = 8.3 cm, L = 4.7 cm; air temperature 84°C.

trays <8 cm diameter. By comparison, variation in depth had little effect on the temperature distribution. During the constant rate period, the drying rate did not change with variation of depth, a result predictable from theory, but it did increase with a decrease in diameter.

7.5 RECTANGULAR TRAYS

In the previous experiments, the drying rate and the temperature distribution profiles were investigated using circular sample trays. Three experiments were subsequently performed using rectangular sample trays. Beds of glass beads of 100 μm were dried at an air temperature of 84°C ; the other experimental conditions were similar to those used previously.

The first tray was 8.3 cm long, 3.7 cm wide and 3.2 cm deep, positioned such that the direction of air flow was parallel to the length of the tray, as shown in Fig. 7.26. The temperature distribution profiles obtained are shown in Fig. 7.29. In a second experiment the direction of air flow was at right angles to the length of the tray as shown in Fig. 7.27. The temperature distribution profiles observed are shown in Fig. 7.30. The two profiles show that during the constant rate period, the surface temperature was in a range 38°C - 39°C, whilst the bottom temperature was in a range 32°C - 35°C.

As a check on the inversion in temperature distribution observed when using the small diameter circular sample tray, an experiment was performed with a bed of glass beads in a rectangular tray 5.3 cm long, 3.7 cm wide and 3.2 cm deep. The dimensions of the tray and the direction of air flow are shown in Fig. 7.28. The experimental temperature

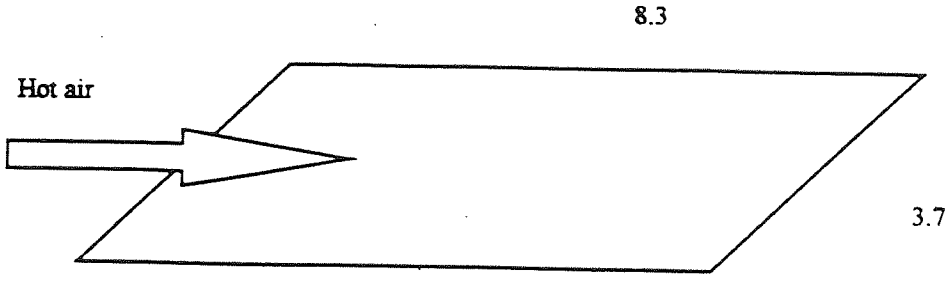

Figure 7.26 Air flow parallel to the length of a rectangular tray;
ℓ = 8.3 cm, w = 3.7 cm, L = 3.2 cm

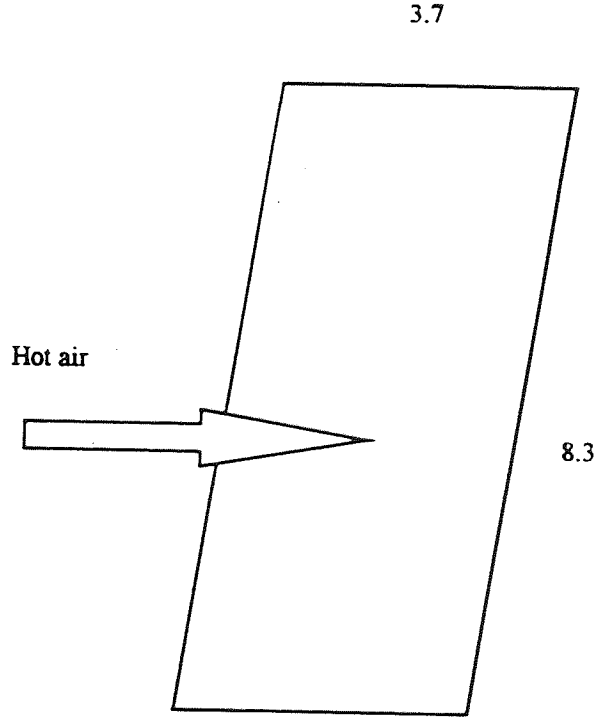

Figure 7.27 Air flow at right angle to the length of a rectangular tray;
ℓ = 8.3 cm, w = 3.7 cm, L = 3.2 cm

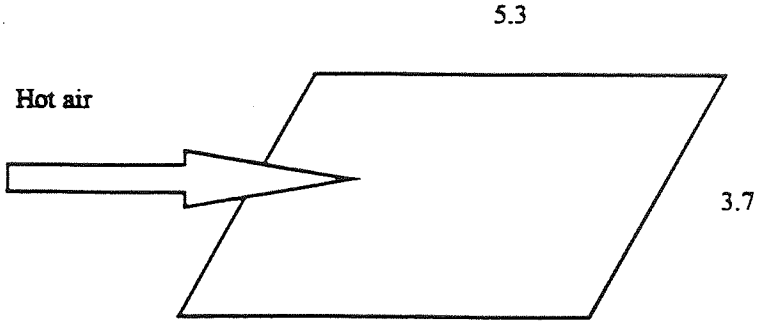

Figure 7.28 Air flow parallel to the length of a rectangular tray;
$\ell = 5.3$ cm, w = 3.7 cm, L = 3.2 cm

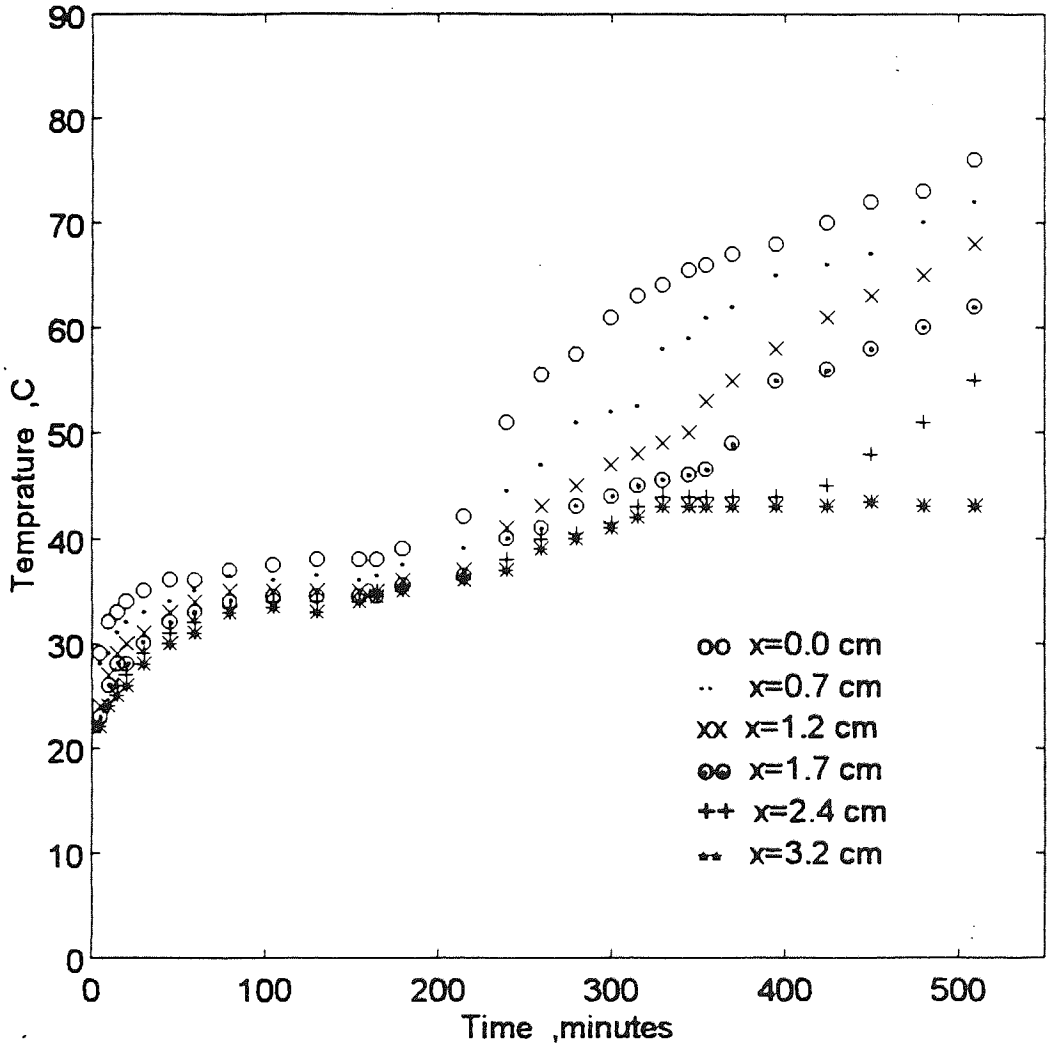

Figure 7.29 Temperature distribution profiles within a bed of glass beads (100 μm); rectangular tray ℓ = 8.3 cm, w = 3.7 cm, L = 3.2 cm; air temperature 84°C; Direction of air flow parallel to the length.

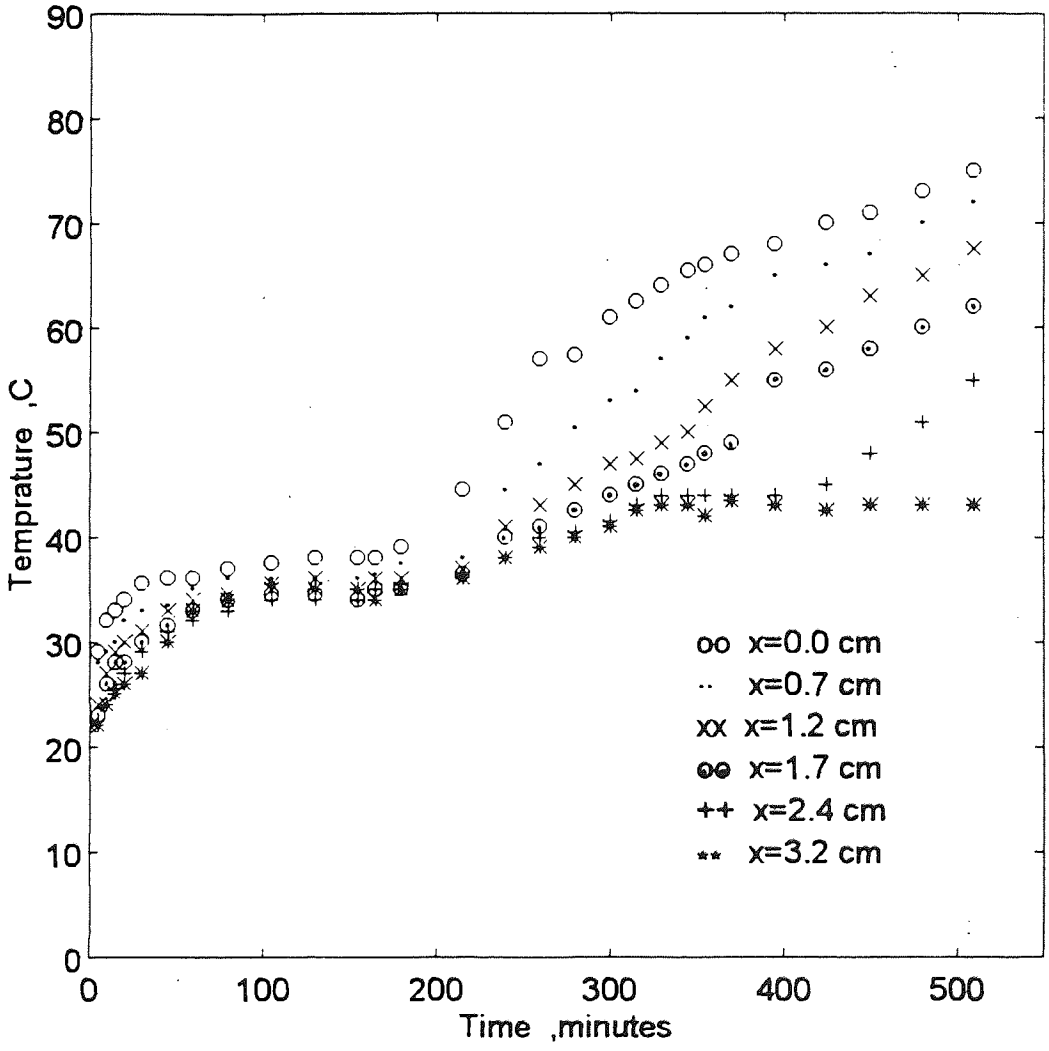

Figure 7.30 Temperature distribution profiles within a bed of glass beads (100 μm); rectangular tray ℓ = 8.3 cm, w =3.7 cm,L = 3.2 cm; air temperature 84°C; Direction of air at right angle to the length.

distribution profiles are shown in Fig. 7.31 and again demonstrate an inversion in the temperature difference. This confirmed the conclusion that with a small effective length (less than 8 cm) an inversion in the temperature gradient occurs. Comparison of these profiles with those obtained with the circular tray of 5.3 cm diameter (Fig. 7.1) showed good agreement.

No measurements of weight loss were made during the above experiments. Hence, the drying rate curve could not be plotted. However, the drying rate can reasonably be expected to vary with the effective length as with the circular trays.

7.6 EFFECT OF AIR TEMPERATURE

Beds of glass beads of 100 μm diameter were dried at air temperatures of 64°C and 54°C, in a sample tray of 5.3 cm in diameter with a bed depth of 3.2 cm. The temperature distribution profiles obtained are shown in Fig. 7.32 and Fig. 7.33. An inversion in temperature gradient again was observed. The effect of air temperature on the temperature gradient can be deduced from these profiles and those shown in Fig. 7.1 (air temperature 84°C). Both the bottom and surface temperatures decreased when the air temperature was decreased; the difference between them also decreased. Therefore, at low air temperature, below approximately 50°C, it may be expected that the surface and bottom temperature will be close, as concluded in Chapter 5.

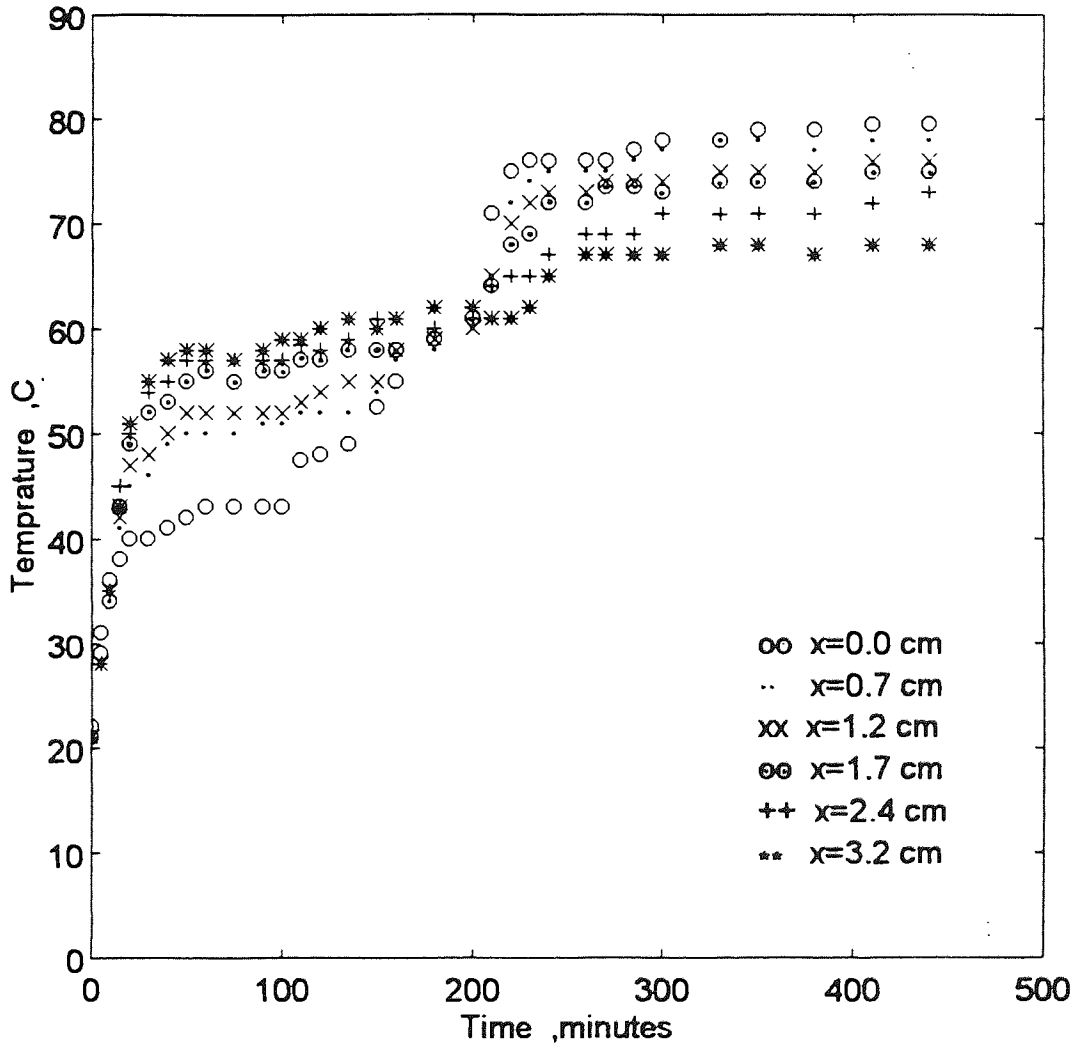

Figure 7.31 Temperature distribution profiles within a bed of glass beads (100 μm); rectangular tray ℓ = 5.3 cm, w = 3.7 cm, L = 3.2 cm, air temperature 84°C.

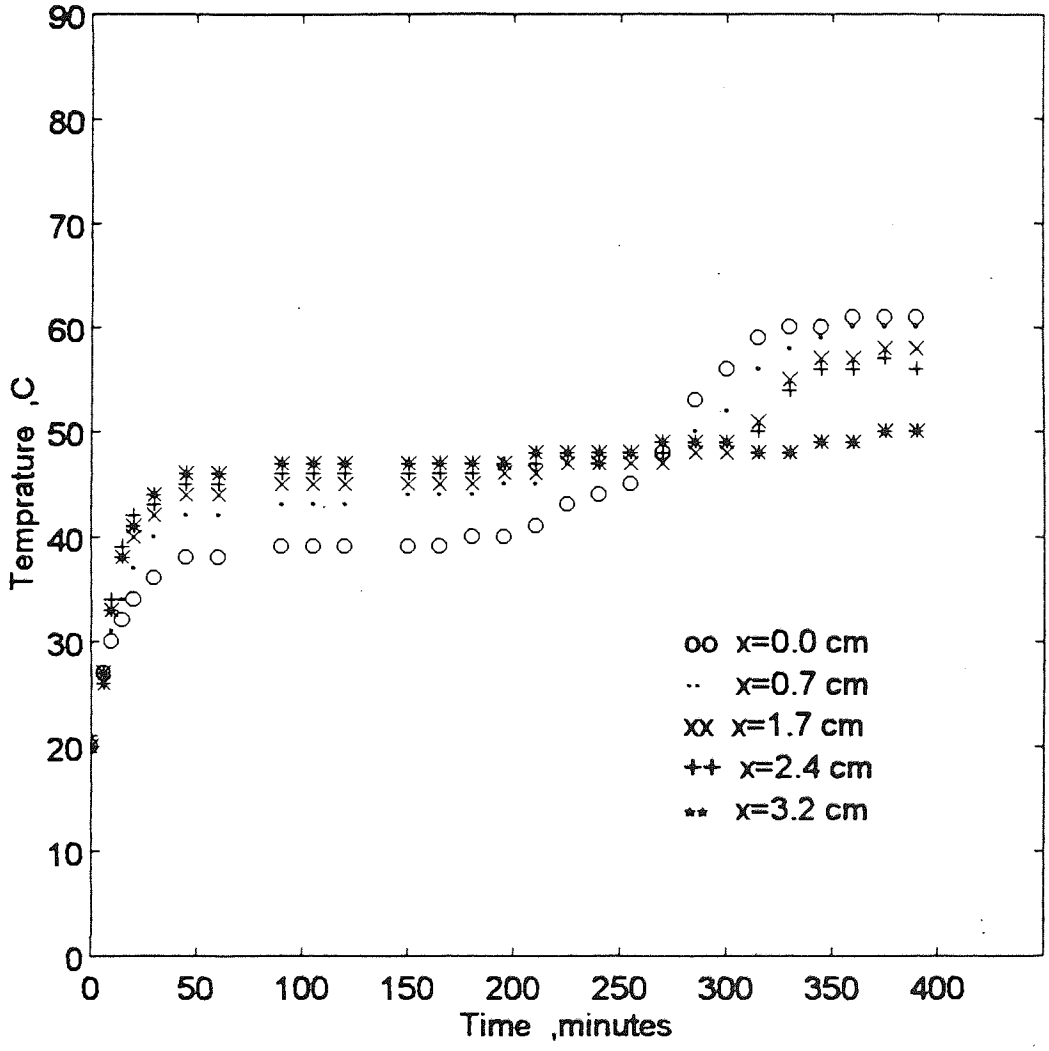

Figure 7.32 Temperature distribution profile for glass beads (100 μm); tray d = 5.3 cm, L = 3.2 cm; air temperature 64°C.

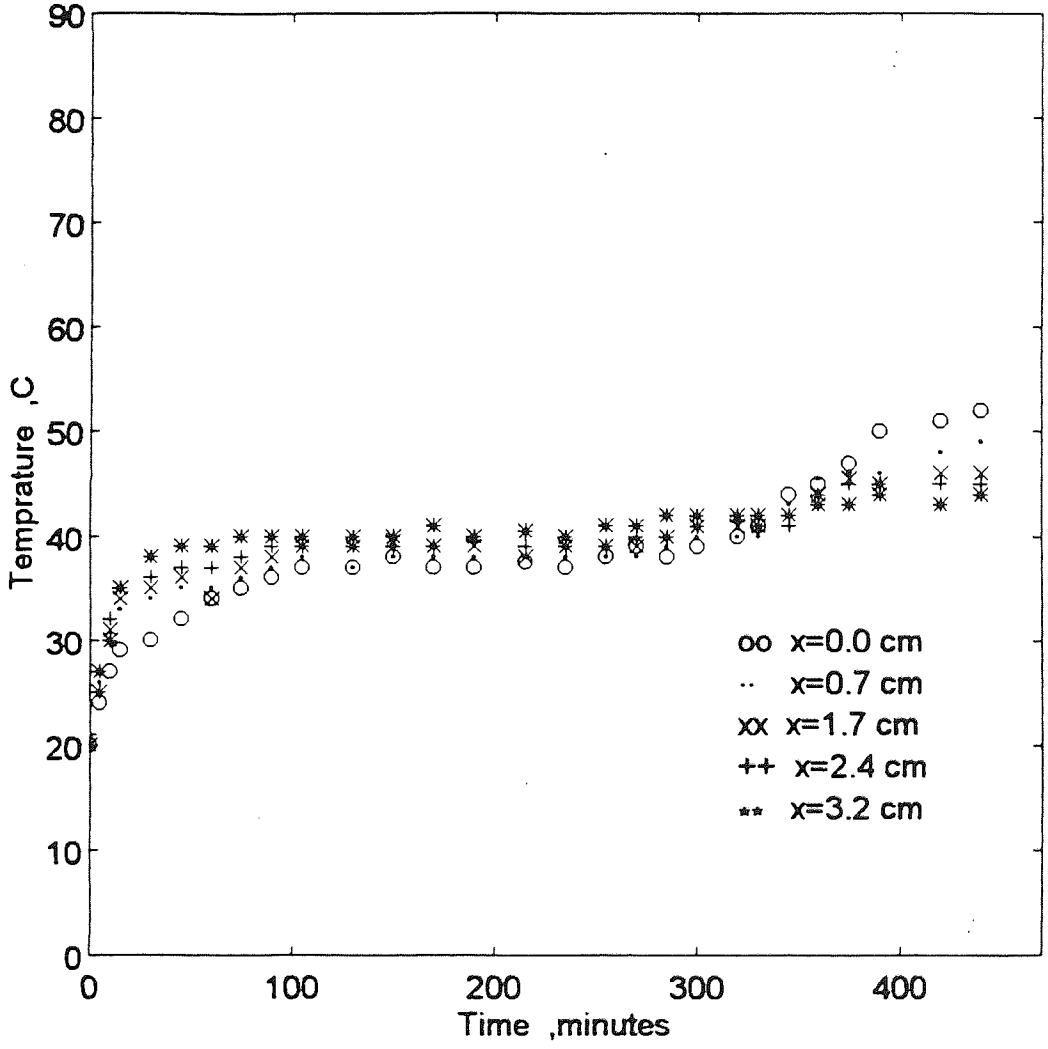

Figure 7.33 Temperature distribution profile for glass beads (100 μm); tray d = 5.3 cm, L = 3.2 cm; air temperature 54°C.

The second falling rate period commenced after times of 335 min., 280 min. and 195 min. at air temperatures of 54°C, 64°C and 84°C respectively. Hence as expected, the extent of the falling period decreased with increasing air temperature.

Figure 7.34 shows the drying rate curve for the bed of glass beads at air temperature of 64°C. The average drying rate was 2.5 kg $H_2O/m^2.h$ greater than that obtained with the sample tray of 8.3 cm (2 kg $H_2O/m^2.h$) shown in Fig. 5.32; i.e. the drying rate increased with a decrease in tray diameter.

Figures 5.2, 5.30 and 5.34 in Chapter 5, show the experimental temperature profiles for glass beads of 100 μm diameter dried in a tray 8.3 cm in diameter and 3.2 cm deep at different air temperatures. By comparison with Figures 7.1, 7.32 and 7.33, which show the profiles for the same material in a tray 5.3 cm in diameter and 3.2 cm deep, it can be concluded that, (a) an inversion in temperature gradient appeared in the tray of smaller diameter; (b) both T_s and T_b decreased when the larger diameter tray was used; and (c) the difference in temperature, ΔT, also decreased with the tray of larger diameter. These results are similar to those reported in the previous sections.

7.7 POOL OF DISTILLED WATER

Two experiments involving simply the evaporation of pure distilled water were carried out, using two trays of 2.6 cm and 5.3 cm diameter and 3.2 cm depth. Fig. 7.35 and Fig. 7.36 show the temperature profiles obtained. The surface level of water in both the

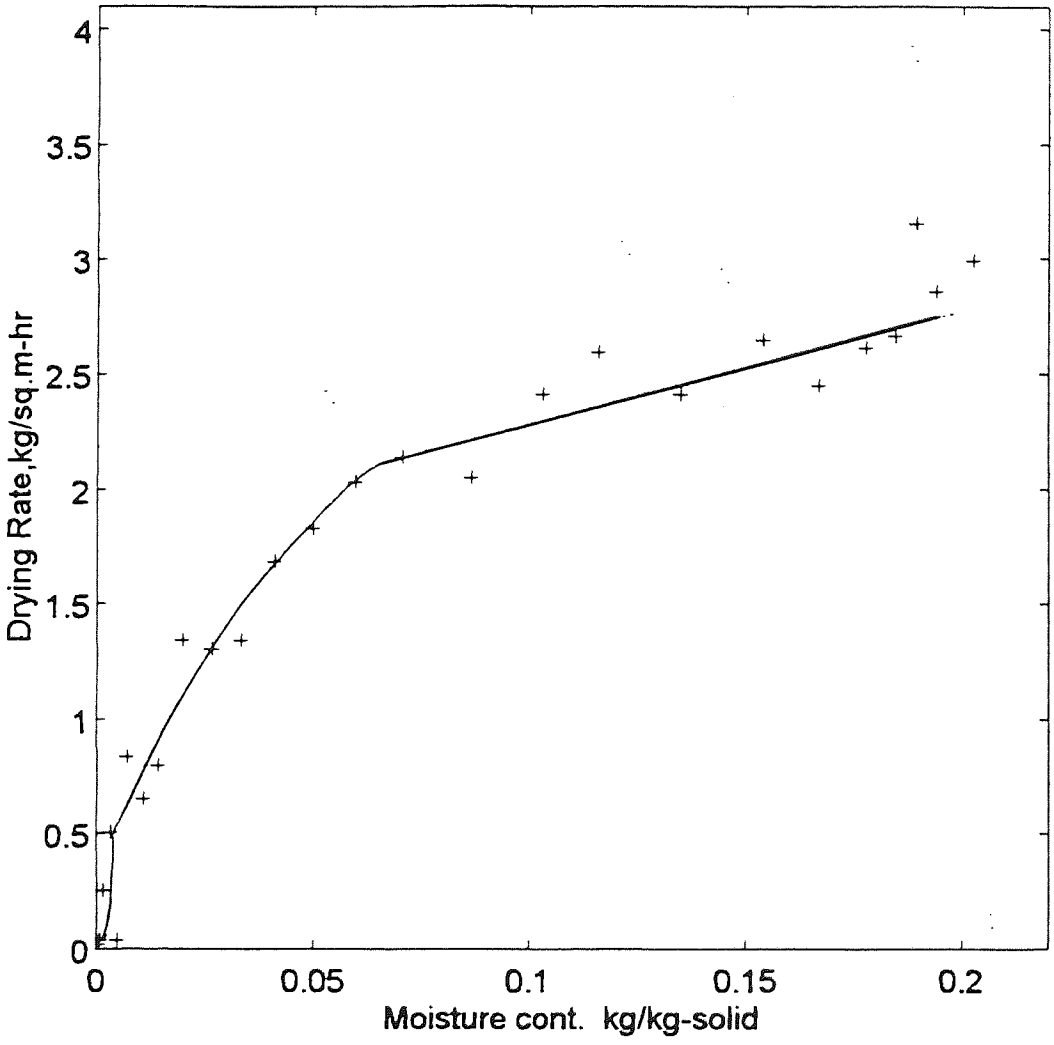

Figure 7.34 Drying rate curve for a bed of glass beads (100 μm); tray d = 5.3 cm, L = 3.2 cm; air temperature 64°C.

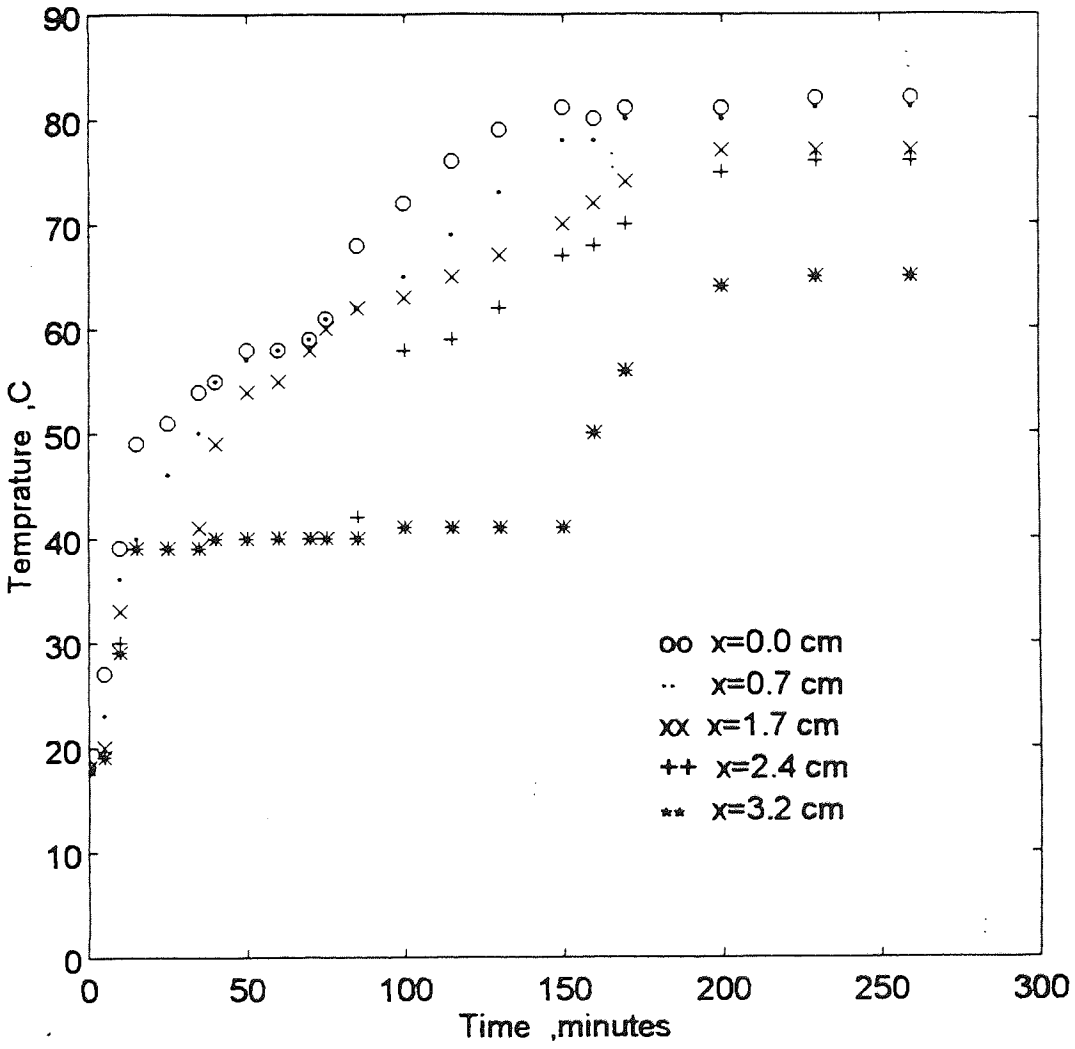

Figure 7.35 Temperature distribution profiles within a pool of distilled water; tray d = 2.6 cm, L = 3.2 cm; air temperature 84°C.

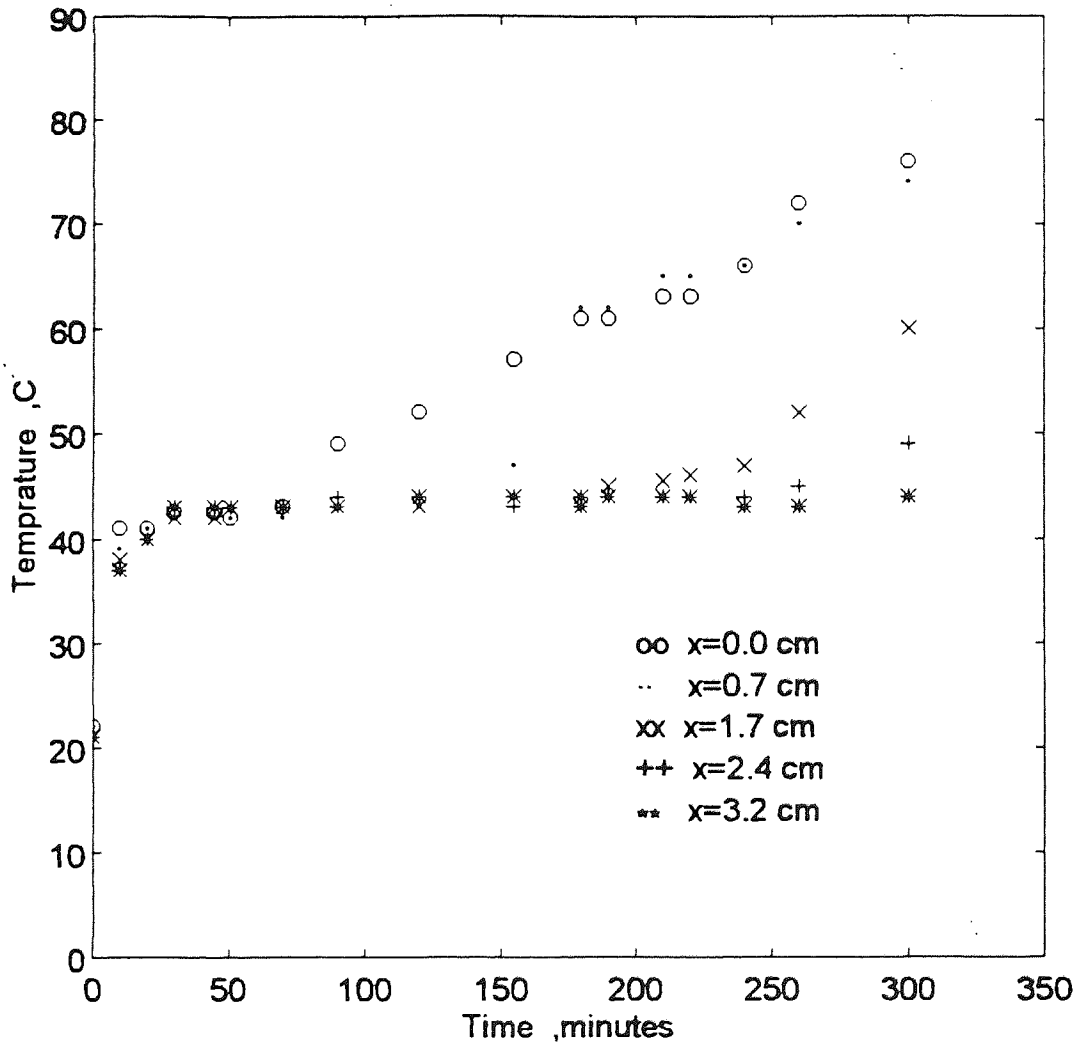

Figure 7.36 Temperature distribution profiles within a pool of distilled water; tray d = 5.3 cm, L = 3.2 cm; air temperature 84°C.

experiments obviously dropped with time. The thermocouple at the top then appeared above the surface of water, whereupon the temperature it indicated increased rapidly. After a short time, the second thermocouple from the top appeared above the level of water; the temperature it indicated then also increased rapidly. This was repeated for all of the thermocouples. However, T_b was always equal to T_s, and there was no gradient in the temperature. The surface temperature was 40°C in the case of the results shown in Fig. 7.35 and 43°C for Fig. 7.36. These temperatures were a little above the wet-bulb temperature of 39°C.

It is worth noting that T_b in Fig. 5.35 in Chapter 5 was also equal to T_s and no gradient occurred. Therefore, obviously since actual convection comes into play, an inversion in temperature profile cannot be observed in the case of a pure liquid, regardless of variation in tray diameter.

7.8 BED OF DRY SOLID

Dry glass beads of 100 μm diameter were heated in a tray of 5.3 cm diameter and 3.2 cm depth, at air temperature of 84°C. Figure 7.37 shows the temperature profiles in this experiment. Despite using a tray with a smaller diameter, no inversion was observed, obviously because only conductive heat transfer is involved. The temperatures of the surface and bottom were 81°C and 60°C respectively.

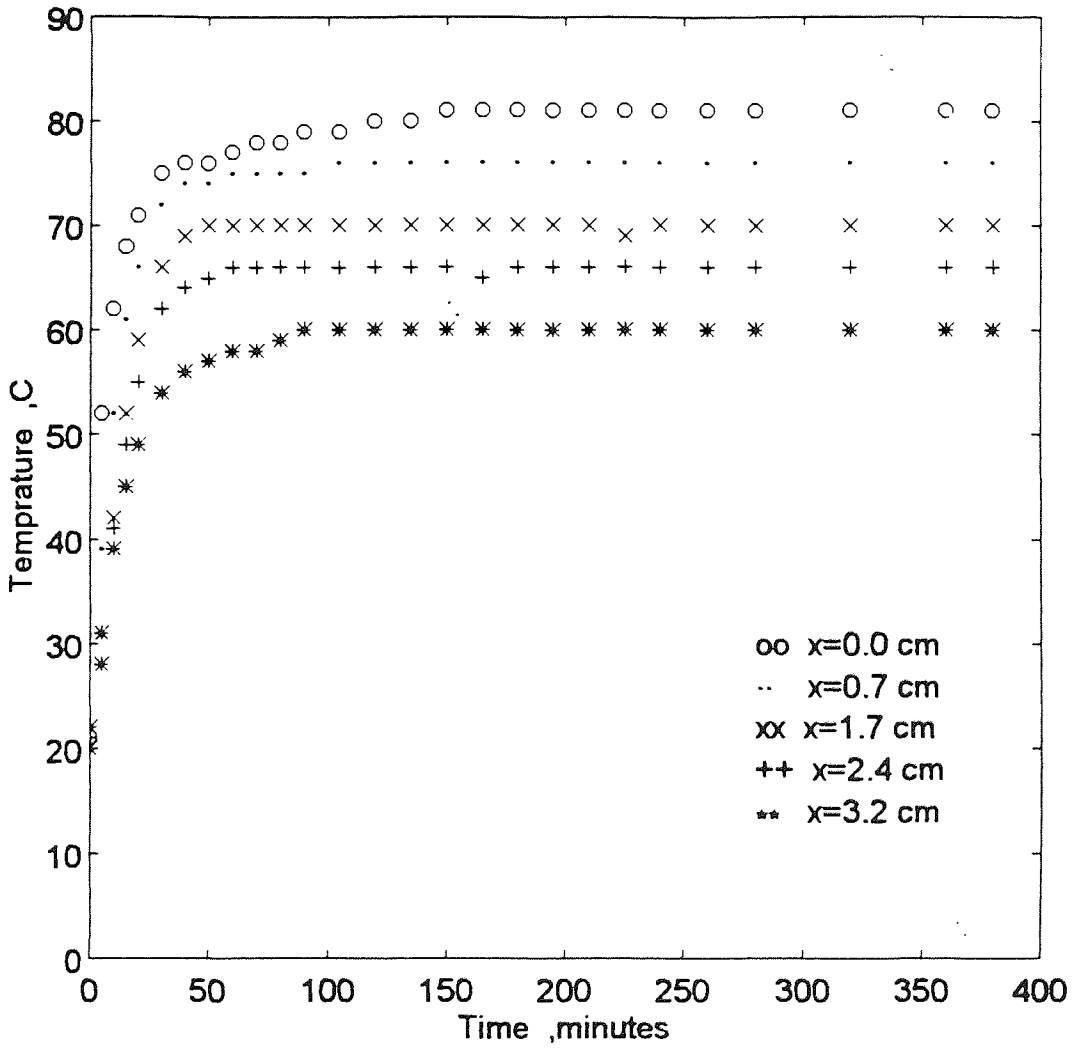

Figure 7.37 Temperature distribution profiles for a bed of dryglass beads (100 μm); tray d = 5.3 cm, L = 3.2 cm; air temperature 84°C.

7.9 DISCUSSION

In the experiments described earlier, drying hygroscopic and non-hygroscopic materials in trays of different dimensions, with different air temperatures, it was found that the bottom temperature and the drying rate increased significantly with variation in the effective length of the bed's surface. An inversion in temperature gradient was observed with all beds of effective length <8 cm. These conclusions will be discussed on the basis of the mechanisms of drying.

7.9.1 Heat and Mass Transfer Coefficients

During the constant rate period, external conditions play the predominant role in the drying process. The heat transfer coefficient, h, and mass transfer coefficient, k'_c, are functions of the fluid properties, the system geometry and the flow velocity. Most of the resistance to heat and mass transfer is considered to reside in a thin film adjacent to the surface. This effective film, or 'boundary layer', is affected by the geometry of the system and the roughness of the surface.

Methods for the prediction of magnitudes of convective heat and mass transfer coefficients for the case of wet materials dried by an air flow parallel to a flat plate in a wind tunnel are not fully developed. However, empirical and semi-empirical correlations have been proposed to determine h_c and k'_c for such cases. For the case of a wind tunnel, these coefficients are generally estimated by using the correlations for Nusselt number and Sherwood number in the following forms;

$$Nu = \frac{h_c \ell}{\lambda_a} = A(Re,\ell)^n \ Pr^{0.33} \qquad (7.9\text{-}1)$$

and

$$Sh = \frac{k_c' \ell}{D_{AB}} = B(Re,\ell)^m \ Sc^{0.33} \qquad (7.9\text{-}2)$$

Where,

λ_a : is the thermal conductivity of air

D_{AB} : is the diffusivity of vapour in air

A, B, n and m : are constants determined experimentally and depend upon both the fluid properties and the range of Reynolds number

ℓ : is the distance from the leading edge of the plate, i.e. it represents the effective length of the bed surface directly exposed to the air flow.

Re,ℓ : is the Reynolds number based on the effective length and can be defined as,

$$Re,\ell = \frac{\ell \rho \upsilon}{\mu} \qquad (7.9\text{-}3)$$

For values of the Reynolds number with respect to the swept length, Re,ℓ, greater than $3x10^6$ represents turbulent conditions (123). All physical properties are evaluated at the mean film conditions between the surface and the average bulk fluid states.

On the basis of Nusselt number, a correlation for the convective heat transfer film coefficient, h_c, has been proposed by Luikov (163, 164) for laminar flow, and $Pr \approx 0.7$ as:

$$Nu = \frac{h_c \ell}{\lambda_a} = 0.6(Re, \ell)^{0.5} \qquad (7.9\text{-}4)$$

Vyas (81) proposed a correlation to determine the heat transfer film coefficient for the case of a flat plate subjected to an air flow in a duct as,

$$Nu = \frac{h_c \ell}{\lambda_a} = 0.592\,(Re, \ell)^{0.5} \qquad (7.9\text{-}5)$$

Geankoplis also provided a correlation of heat transfer coefficient for this case (138), for $Re, \ell < 3x10^5$ and $Pr > 0.7$ as,

$$Nu = \frac{h_c \ell}{\lambda_a} = 0.664\,(Re, \ell)^{0.5}\, Pr^{0.33} \qquad (7.9\text{-}6)$$

Similar correlations for various ranges of Reynolds number are to be found in (89, 165).

The Prandtl number for air has a magnitude close to 0.7 within the range of air temperature 30 - 150°C. Thus, substituting the value of $Pr = 0.7$ into the term $(0.664\ Pr^{0.33})$ yields a value of 0.59. This explains the similarity between Eq. (7.9-4) and (7.9-6). However, Eq. (7.9-6) is more accurate and was taken as a working equation. Similar

correlations have been proposed (89, 138, 140) for the mass transfer coefficient, k'_c, and written as

$$Sh = \frac{k'_c \ell}{D_{AB}} = 0.664 \left(Re, \ell\right)^{0.5} Sc^{0.33} \qquad (7.9\text{-}7)$$

In all experiments mentioned previously, Re, ℓ had values between 628 - 1932, i.e. flow was laminar. Thus, equations (7.9-6) and (7.9-7) can be applied to determine the heat and mass transfer coefficients respectively. Noting that the diameter of the sample of tray, d, represents the characteristic dimension, ℓ, rearranging Eq. (7.9-6) and Eq. (7.9-7) and substituting Re, ℓ from Eq. (7.9-3) gives

$$h_c = 0.664 \, \lambda_a \left(\frac{\rho \upsilon}{\mu}\right)^{0.5} \frac{Pr^{0.33}}{\ell^{0.5}} \qquad (7.9\text{-}8)$$

and

$$k'_c = 0.664 \, D_{AB} \left(\frac{\rho \upsilon}{\mu}\right)^{0.5} \frac{Sc^{0.33}}{\ell^{0.5}} \qquad (7.9\text{-}9)$$

By substitution of the properties of air at average temperature of 61°C into Eq. (7.9-8), a plot of the variation in the convective heat transfer coefficient, h_c, versus the effective length, ℓ, can be obtained. This plot is shown in Fig. 7.38. It indicates that h_c increases

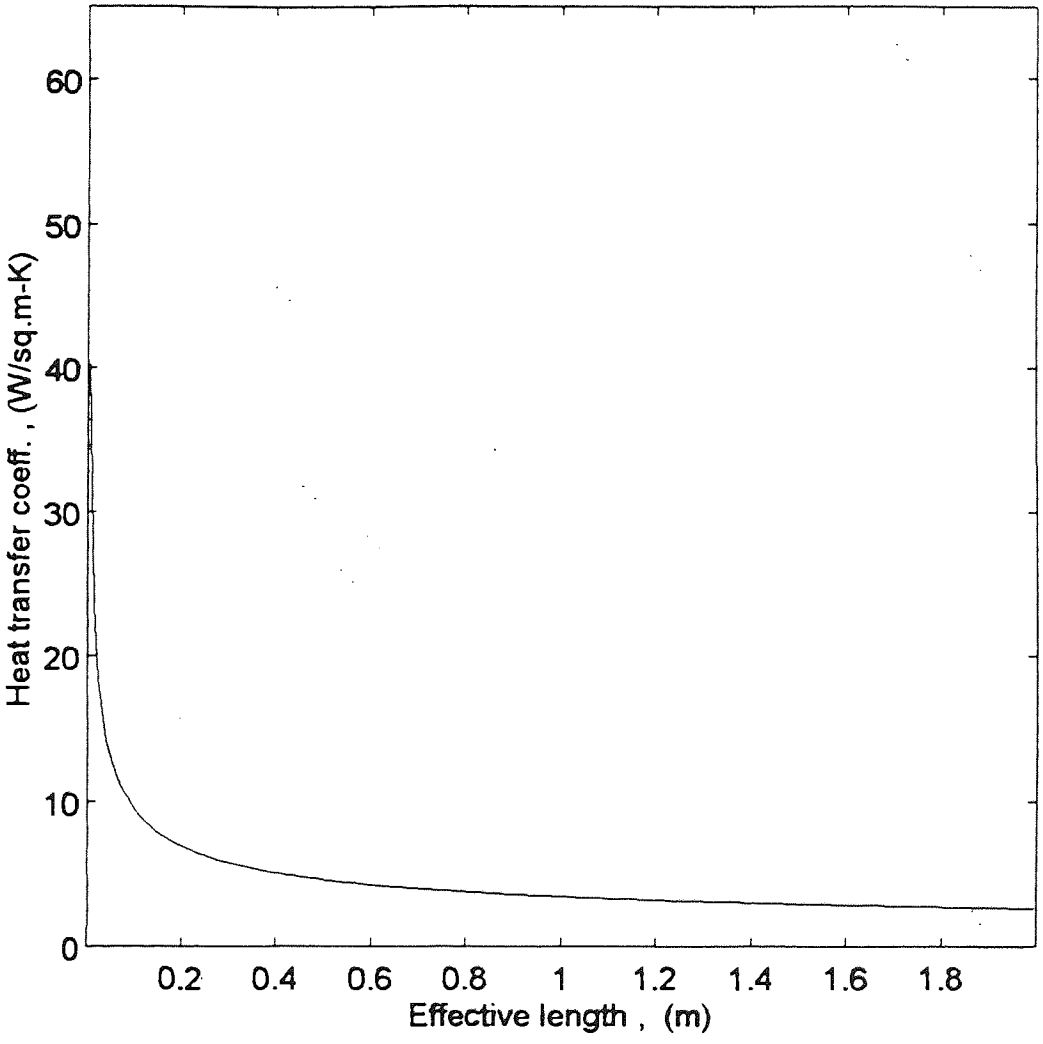

Figure 7.38 Calculated variation of heat transfer coefficient with effective length.

significantly when, ℓ, is decreased below approximately less than 20 cm, but remains virtually constant for large ℓ values.

A similar curve was obtained for mass transfer coefficient, k'_c, versus effective length, ℓ, as shown in Fig. 7.39.

The plots shown in Figures 7.38 and 7.39 demonstrate that the effective length, ℓ, parallel to the direction of air flow has a considerable effect on values of heat and mass transfer coefficients, with significant increases occurring at $\ell < 20$ cm.

7.9.2 Drying Rate

During the constant rate period, the drying rate was defined in Chapter 6 as,

$$\mathbf{m}_c = \mathrm{Mw}\frac{k'_c}{RT}(P_s - P_{va}) \qquad (7.9\text{-}10)$$

Clearly, by definition, the mass transfer coefficient is one factor controlling the drying rate and Equation (7.9-10) merely quantifies this. However, since the mass transfer coefficient is affected by the effective length, ℓ, as demonstrated in Fig. 7.39, the drying rate is also affected by the variation in length, ℓ, of any sample tray. As discussed in Chapter 4, the thickness of the thermal boundary layer adjacent to the surface increases as the distance from the leading edge increases. Hence the resistance to heat and mass transfer to, or from,the surface will also increase. Therefore, the rate of evaporation is reduced at

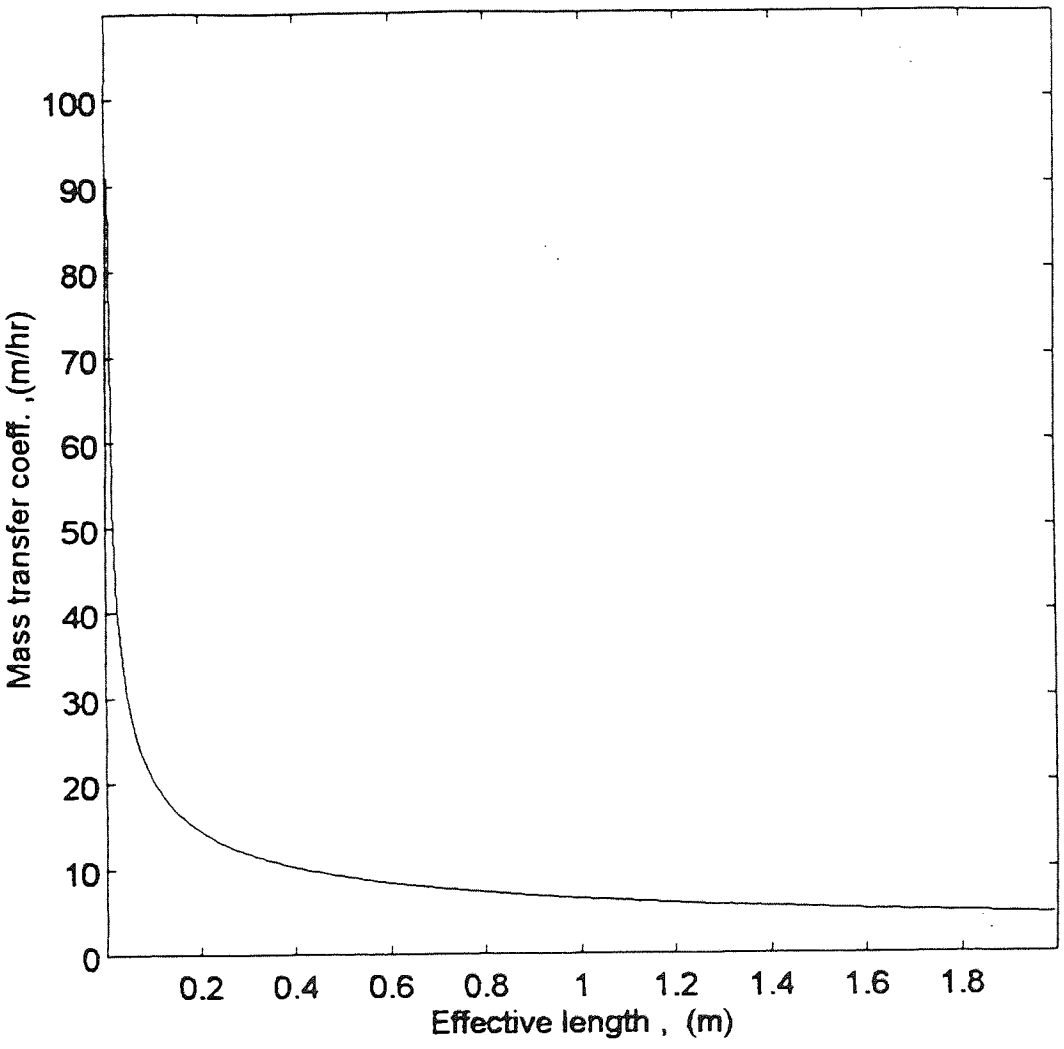

Figure 7.39 Calculated variation of mass transfer coefficient with effective length.

larger effective lengths. Based on Eq. (7.9-10) by substituting values of k'_c from Eq. (7.9-9), a plot of predicted, $\mathbf{m}_c$, against, ℓ, was obtained as shown in Fig. 7.40. This shows that the shorter the length, ℓ, of the tray's surface, the greater the drying rate, whereas, a longer length leads to a smaller almost constant drying rate. At even greater lengths, the drying rate will attain for all practical purposes, a constant value. This analysis explains why the drying rates obtained for materials dried in the small diameter tray were greater than those obtained in trays of large diameter.

The above theoretical analysis supported by the experimental results, gives a clear explanation for the phenomenon observed during the industrial drying of veneers and textiles, that drying rate decreases as a longer distance is exposed to the air flow (69). Timber veneers are usually dried in a long continuous conveyor type dryer, where a hot air flow moves parallel to the surface of the veneer. The length of the dryer is over 30 m which would be expected to give a low drying rate. For this reason, the drying is always enhanced by air jets through slots, holes or nozzles plenum chambers directly above the veneer, which reduces drying time by 25 - 50%. In the open drying process of fabrics such as textile sheets, the drying rate is usually increased by blowing air through the sheet, although this technique also, of course, increases the exposed surface area.

7.9.3 The Bottom Temperature

As discussed in Chapter 6, the temperature distribution throughout the bed at the end of the pre-constant rate period is equal to that at the beginning of the constant rate

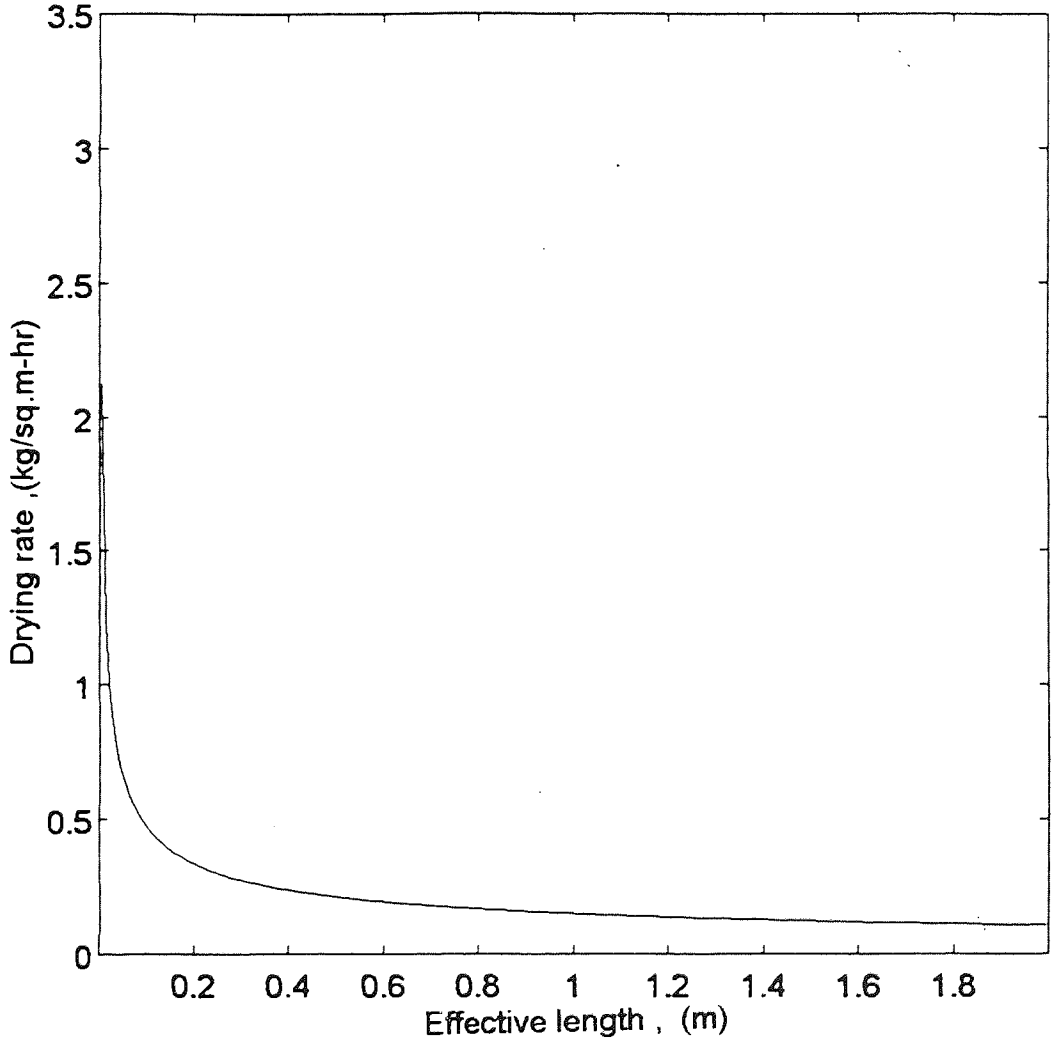

Figure 7.40 Predicted variation of drying rate with effective length.

period; it then remains constant during this period. Therefore, the temperature of the bottom, T_b, at x = L may be solved using Eq. (6.2-17) and expressed as

$$T_b = T_o + \left(\frac{1}{2\lambda_m}\right) * \left[h(T_a - T_s) - \mathbf{m}_p \, \Delta hv\right] * \left[\sqrt{(6\alpha_m t_p)} - 2L + \frac{L^2}{\left(\sqrt{6\alpha_m t_p}\right)}\right] \quad (7.9\text{-}11)$$

The heat transfer coefficient was defined in Eq. (6.5-1) as, $h = h_c + h_r$. The radiant heat transfer coefficient h_r, can be calculated from Eq. (6.5-5). The convective heat transfer coefficient, h_c, can be obtained by using Eq. (7.9-8) which accounts for the variation with effective length, ℓ; $\mathbf{m}_p$ can be obtained by using equation (6.2-5) at t_p, where the appropriate value of k'_c is used in Eq. (7.9-9).

The physical data for beds of glass beads of 100 μm in a tray of 0.032 cm deep at 84°C (mentioned in Chapter 6) were applied to Eq. (7.9-11). The surface temperature always varies very slightly with the tray diameter, as was found experimentally, but it was close to to the wet-bulb temperature. A plot of predicted bottom temperature, T_b, versus effective length, ℓ, was obtained as shown in Fig. 7.41. Provided the effective length of the tray is greater than 5.5 cm (the inversion point), the predicted bottom temperature is always less than the surface temperature. When the tray diameter is less than 5.5 cm, the predicted bottom temperature exceeds the surface temperature. This conclusion is in general agreement with the experimental result, although the inversion point for beds of glass beads of 100 μm at 84°C was determined to be between 6.2 cm and 8.3 cm diameter.

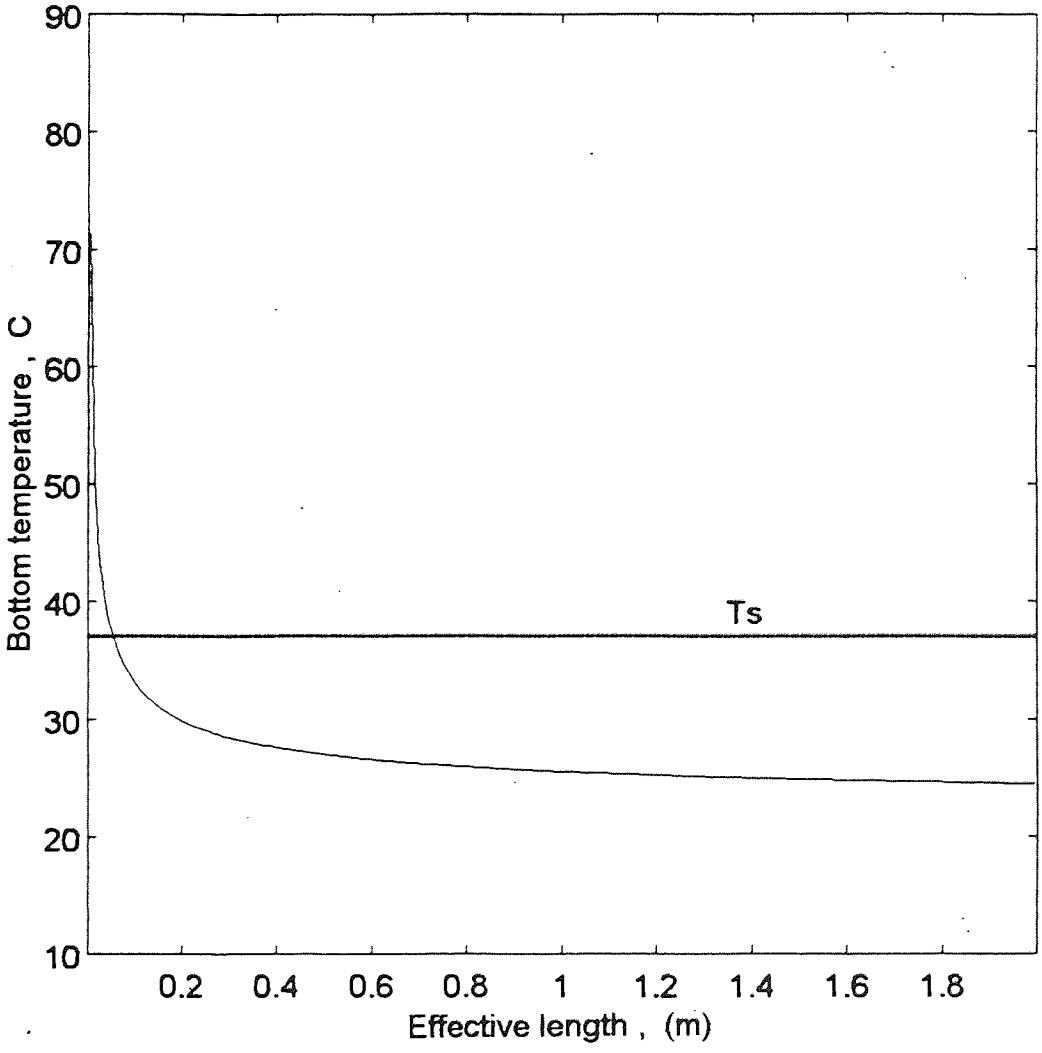

Figure 7.41 Calculated variation of bottom temperature with effective length for a bed of glass beads (100 μm); air temperature 84°C, [Ts: Surface temperature].

The physical data for glass beads of 400 μm at an air temperature of 84°C were also applied to Eq. (7.9-11). Fig. 7.42 shows that the predicted variation of the bottom temperature with effective length, was similar to that with beds of glass beads of 100 μm.

The physical data for beds of polystyrene pellets at an air temperature of 84°C were also applied to equation (7.9-11). The plot of T_b versus ℓ, in Fig. 7.43 again shows a predicted variation of bottom temperature with diameter similar to that with glass beads; i.e. the bottom temperature always decreases as the diameter is increased. The predicted inversion point was at ℓ = 4.5 cm, which is a little smaller than the experimental result, possibly due to the assumption that surface temperature equals the wet-bulb temperature.

Figures 7.44 and 7.45 show the calculated variation of T_b with ℓ for beds of activated alumina and wood powder respectively. The predicted inversion points, at lengths of 7.4 cm and 7.0 cm for the activated alumina and the wood powder respectively, are in good agreement with the experimental results.

As stated previously, the thickness of the thermal boundary layer adjacent to the surface increases with an increase in the effective distance from the leading edge; the resistance to heat transfer to the body will also increase. In the case of a small effective length, the resistance to heat transfer diminishes, since the thickness of the boundary layer in the vicinity of the surface thins. Thus, the rate of heat transfer to the body increases and more heat is available for transfer by conduction across the solid particles, increasing the temperature of the bed. At the surface, where evaporation occurs, the surface temperature is controlled by the external convective conditions, i.e. the humidity, velocity and the

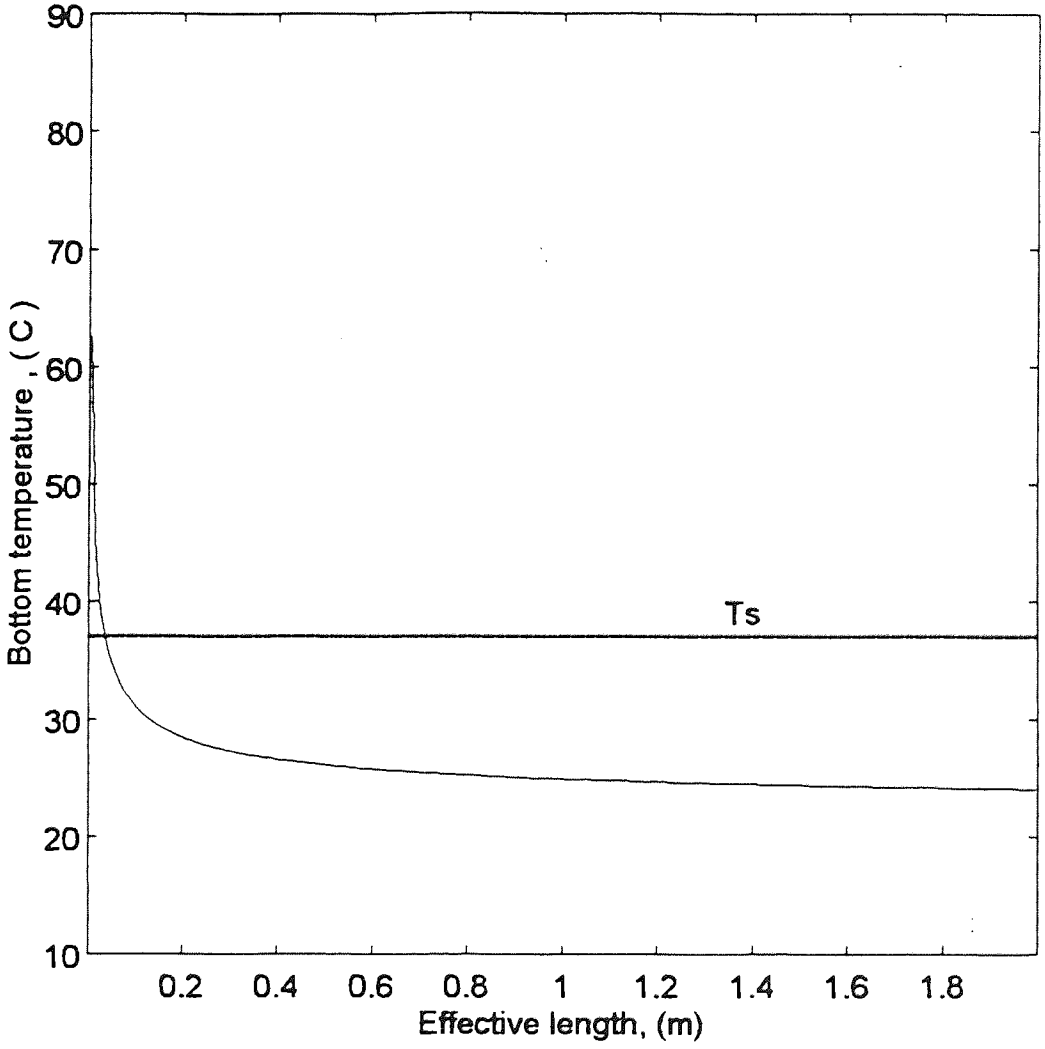

Figure 7.42 Calculated variation of bottom temperature with effective length for a bed of glass beads (400 μm); air temperature 84°C.

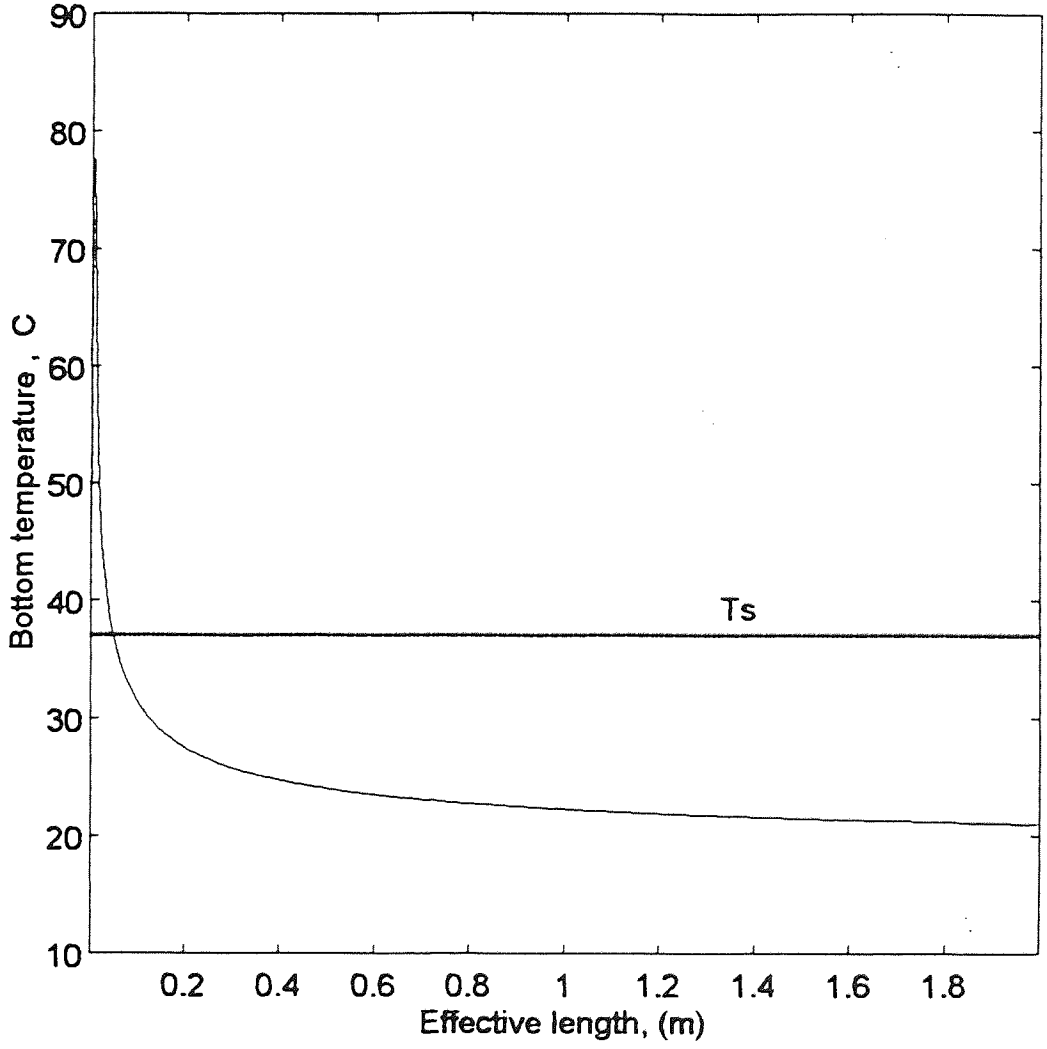

Figure 7.43 Calculated variation of bottom temperature with effective length for a bed of polystyrene pellets; air temperature 84°C.

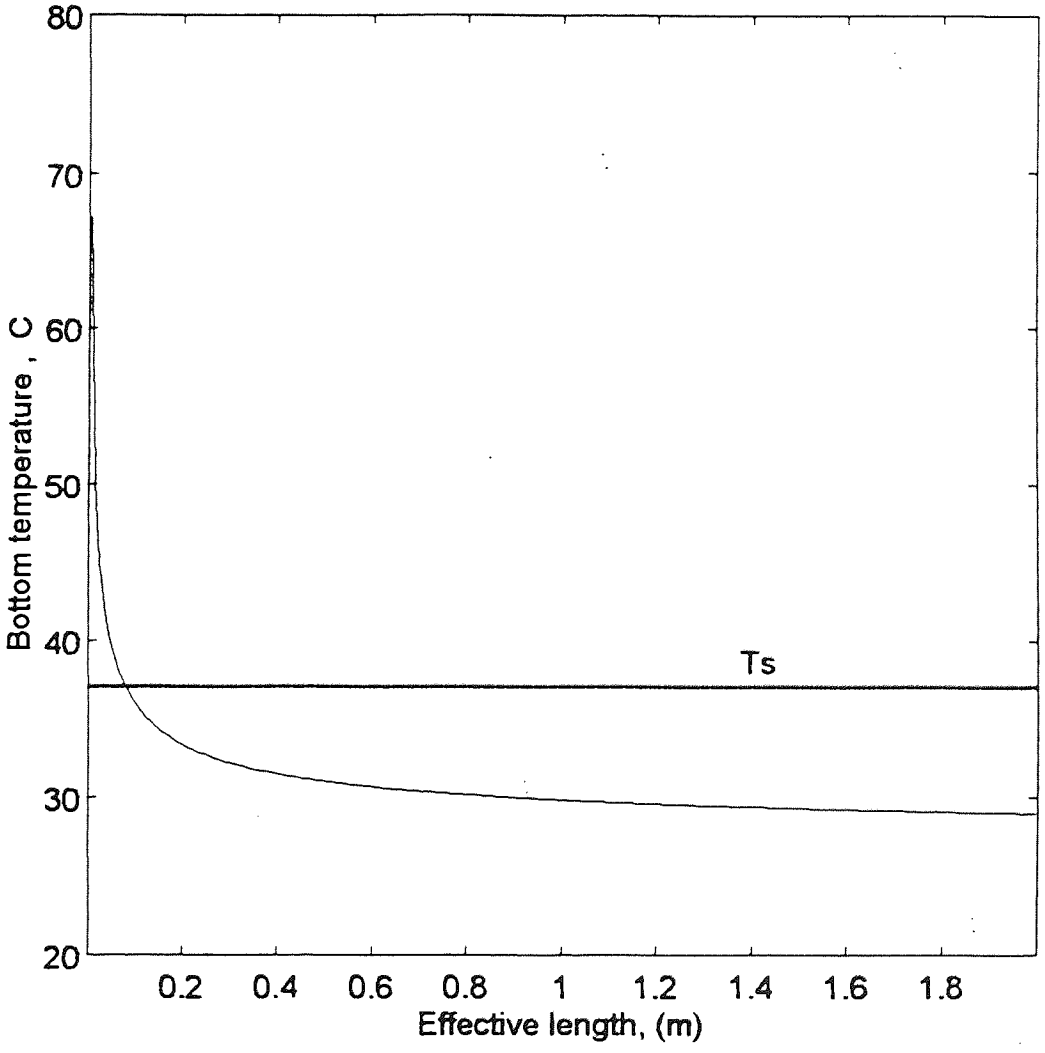

Figure 7.44 Calculated variation of bottom temperature with effective length for a bed of activated alumina, 150 mesh; air temperature 84°C.

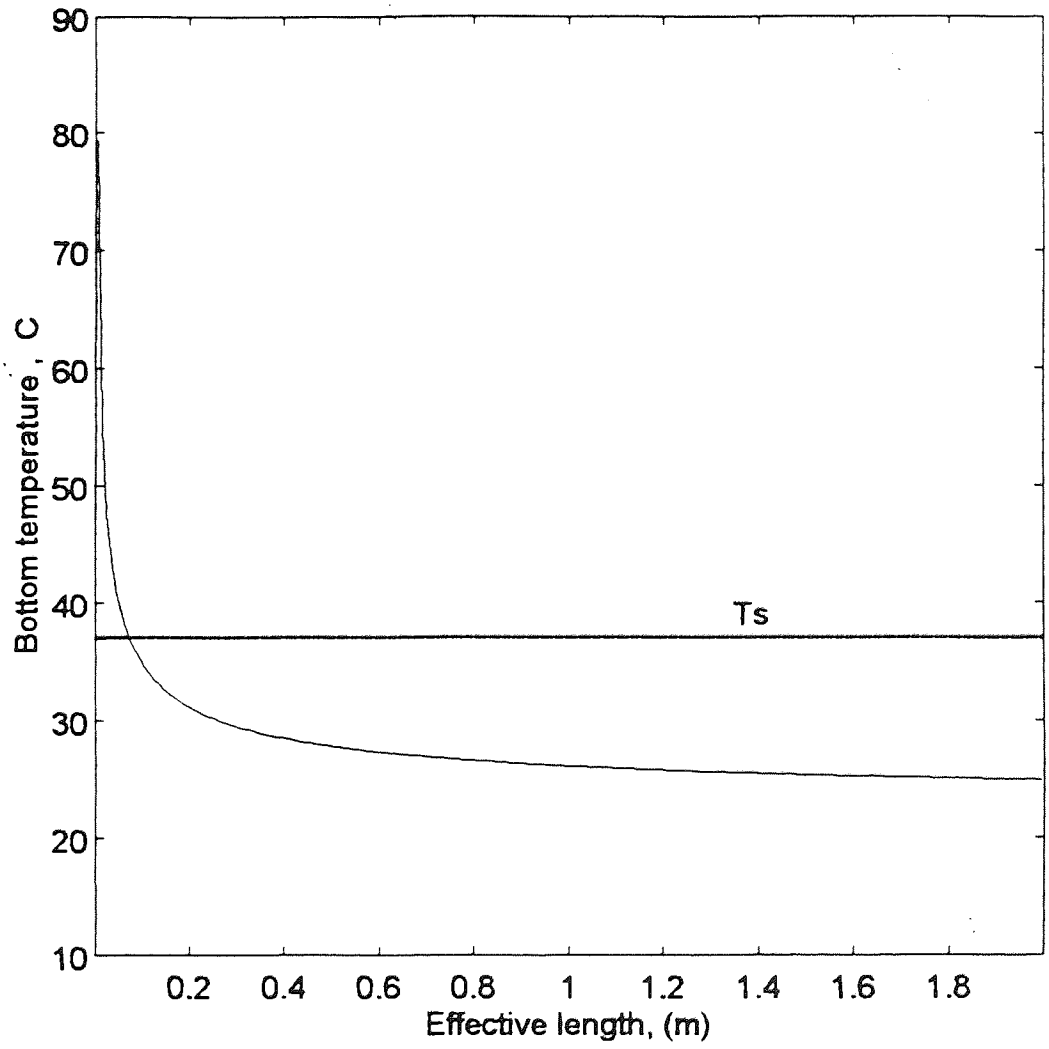

Figure 7.45 Calculated variation of bottom temperature with effective length for a bed of wood powder; air temperature 84°C.

temperature of the air stream. During the constant rate period, the temperature of the surface always fluctuates around the wet-bulb temperature. Therefore, the bottom temperature becomes greater than that of the surface. Thus the inversion phenomenon can be clearly observed in smaller diameter trays (128, 166).

In the case of a large effective length, the rate of heat transfer to the body is decreased, since the boundary layer is thicker. Surface temperature will again remain close to the wet-bulb temperature and hence, become greater than the bottom temperature, i.e. no inversion in temperature will occur.

7.10 CONCLUSIONS

The effective length is the most important criterion affecting the temperature distribution and the drying rate for a specific bed under set drying conditions. As stated previously, the heat and mass transfer coefficients are affected by the velocity of airflow, the geometry of the system and the type of flow. In the case of a flat tray, the geometry of the system is characterised by the effective length (diameter) of the tray, i.e. the distance that the gas flows over. The whole of the resistance to the heat and mass transfer can be regarded as residing within the boundary layer in the vicinity of the surface. The thickness of the thermal boundary layer adjacent to the surface increases as the distance from the leading edge increases. Hence the resistance to heat and mass transfer to, or from, the surface will also increase. Therefore, the rate of evaporation is reduced at larger effective lengths. Heat and mass transfer coefficients have been predicted to have very large values close to the leading edge, i.e. at a small effective length, where the thickness of the

boundary layer approaches zero. In contrast, the values of the coefficients decrease progressively with increased distance from the leading edge, i.e. with large effective length, as the boundary layer thickens. These variations in heat and mass transfer coefficients have a considerable effect on the drying rate and the temperature distribution through the bed.

During the constant rate period, it was concluded that at a certain effective length (usually less than 8 cm) the bottom temperature increases and becomes greater than that of the surface, termed an 'inversion phenomenon'. The temperature distribution measurements were verified in several ways to ensure this phenomenon was real, i.e. various materials were dried under different conditions using different sizes of sample trays with differing thicknesses of insulation. The experimentally determined surface temperature was always near the wet-bulb temperature.

The bottom temperature was calculated and plotted against effective length. The plots predicted the critical length (or tray diameter) at which inversion can occur (the inversion point). The predictions agreed well with the experimental data.

The inversion point will depend upon the type of material and the external conditions being applied. Therefore, for collection of drying data for scale-up purposes, specimen calculations may first be necessary to obtain suitable experimental results and to avoid their misinterpretation. In laboratory drying tests, for a flat slab of hygroscopic or non-hygroscopic material at high temperature, greater than 50°C, a minimum length (or tray diameter) of 20 cm may be preferable. The concept of a minimum tray size is recognised in some industrial drying laboratories, e.g. researching volatiles/flavour loss from slabs (167).

Interestingly, one commercial test rig to obtain data and drying curves for band or conveyor driers and through air circulation stoves provides for material to be spread on a 0.3 m square perforated tray with provision for upward or downward air flow (168). Obviously a larger size test tray is less prone to the introduction of significant errors due to 'edge effects' with any sample which shrinks during drying.

Attention also has to be paid to this phenomenon in the design of the dryers. The effective length of trays or plates must be considered, since this has a great effect on the temperature distribution and on the drying rate. It has been concluded that the drying rate increases with decreasing the effective length exposed to the drying medium; the total time required to complete drying will hence decrease. Minimising the total period of drying is always desirable in drying processes; therefore, designing trays of a smaller length or having cross-flow or multi-point gas injection may be helpful with large tray dryers.

CHAPTER 8

GENERAL CONCLUSIONS AND RECOMMENDATIONS

8.1 GENERAL CONCLUSIONS

The current work presents a generalised theoretical and experimental approach to convective drying of flat thick beds of hygroscopic and non-hygroscopic materials. The study adds a new concept to the mechanism of convective drying which may contribute to the theory of drying.

Temperature distribution profiles provide useful information on the mechanism of heat transfer and drying behaviour throughout thick beds of solids. Stages of drying, i.e. the pre-constant and constant rate period and the first and second falling rate periods, are clearly identifiable from the temperature profiles at any time.

The critical moisture content is important in the investigation of specific drying curves and in many cases, such data are necessary for solving mathematical models. It is, however, difficult to determine experimentally with accuracy. Moreover, it is difficult to obtain theoretically. Matching the temperature distribution profiles with the plot of moisture content versus time and with the drying rate curve, has been shown to provide an effective method of predicting the critical moisture content accurately. This method also helps in predicting the moisture content corresponding to the start of the second falling rate

period.

The receding evaporation front phenomenon is a relatively new theory in drying science and the literature review revealed that little work has been done in applying this theory. Thus, a need was identified to verify this theory. The results of the current experimental work have provided more explanations and supported this theory. The temperature distribution profiles for both hygroscopic and non-hygroscopic materials showed the existence of a receding evaporation plane during the falling rate period. This plane divided the system into two regions, a hotter dry zone in the upper section of the system and a wet zone near the bottom. A useful graph was established from which the position of the receding evaporation front at any time can be determined easily and accurately. It also provides a simple tool to calculate the velocity of the front at any time.

A new model was proposed which was able to successfully predict temperature distributions throughout the bed, taking into account the receding interface, and the two regions which appear in the falling rate period. This model showed good agreement when validated for various materials under different air temperatures. It was also able to predict the duration of each drying stage. The results can be used to predict drying behaviour under other conditions, to provide reliable information, create new techniques and improve the process design and operation.

Drying experiments, were also carried out in sample trays of different diameters under similar drying conditions. A new phenomenon, the 'inversion phenomenon' was found during the constant rate period. It appears that at a small effective length or tray

diameter (less than 8 cm), the bottom temperature increases and becomes greater than that of the surface. The experimental measurements were verified in several ways to ensure this phenomenon was real; various materials were dried under different conditions, using different sizes of sample trays, with different thickness of insulation. The inversion phenomenon was explained due to the formation of boundary layers in the vicinity of the surface and to the consequent variation in the heat and mass transfer coefficients with distance from the leading edge. The bottom temperature was calculated and plotted against the effective length. The plot predicted the critical effective length of tray at which inversion in temperature can occur (the inversion point). This plot will be helpful in the collection of data for scale-up purposes, both to predict such results and to avoid misinterpretation.

The drying rate increases with a decrease in tray diameter. This result, supported by the theoretical analysis, gives a clear explanation for the phenomenon observed during the industrial drying of veneers and textiles, that drying rate decreases as a longer length is exposed to the air stream. Thus, designing trays or tunnels of a smaller length or utilizing cross-flow could be useful to optimize large-scale operations.

It is commonly stated in the drying literature that no temperature gradient appears during the constant rate period, i.e. the temperature of the surface equals that of the bottom. However, this may be true only for drying solids at low air temperatures. In all the experiments carried out at air temperature >54°C, a clear difference in temperature distribution was observed throughout the bed. This is attributable to the moisture distribution throughout the bed being non-uniform so that thermal conductivities varied with

bed depth. Therefore, a temperature distribution is set up within the solid.

8.2 RECOMMENDATIONS FOR FURTHER WORK

Some recommendations are listed here for further studies on drying:

1. The temperature distribution profiles investigated for hygroscopic and non-hygroscopic materials provided useful information on the mechanisms of drying. This work should be further extended to investigate other materials such as colloidal materials, fibrous materials and food-stuffs, applying a wide range of drying conditions.

2. The receding evaporation front theory is worth further study, since it gives an acceptable explanation of the drying mechanism. This theory was investigated by recording temperature distribution, moisture distribution or both, throughout the bed. However, another useful technique would be to use coloured liquid, or to add inert vaporisable dye to distilled water, for use as the moisture. Thus, it would be possible to observe two distinguishable regions through a glass sample tray during the drying operation.

3. The present model was proposed to predict temperature distribution profiles for a flat slab where evaporation takes place only from the surface. This model should be further modified to include prediction of moisture content distribution. Moreover, the model can be extended for cases where evaporation occurs from all sides, such as granules on a conveyor belt dryer and droplets in spray dryers, taking into account the difference in boundary conditions.

4. The phenomenon of inversion in temperatures was observed in this research when small tray diameters, i.e. <0.08 m, were used. This phenomenon was explained on the basis of the characteristics of the boundary layer and its effect on local heat and mass transfer coefficients. More detailed study is desirable to obtain further understanding of this phenomenon. More experimental work, using various effective lengths, area shapes and depths under different drying conditions could be useful to obtain accurate values for the critical diameter at which inversion in temperature occurs.

5. At an early stage of this research, drying experiments by conduction were carried out for thick beds of various materials (169). As would be expected since the directions of heat and mass transfer are co-current, the temperature distribution profiles obtained differed considerably from those obtained by convective drying. It would be desirable to develop a mathematical model for this case, considering the basis used for the present model.

NOMENCLATURE

a	----	Width of wind tunnel	m
A	----	Exposed surface area of solid	m^2
A_c	----	Cross-sectional area of capillary	m^2
b	----	Length of wind tunnel	m
B	----	Permeability	l/s
B_a	----	Permeability of air	l/s
B_L	----	Permeability of liquid	l/s
B_{eff}	----	Effective permeability	l/s
C	----	Concentration	kg/m^3
C_0, C_1, C_2	----	Coefficients depend on time	
Cp	----	Specific heat capacity	J/kg K
Cp_m	----	Specific mass capacity	J/kg K
Cp_s	----	Specific heat capacity of solid	J/kg K
Cp_{WL}	----	Specific heat capacity of liquid water	J/kg K
d	----	Sample tray diameter or pipe diameter	m
dc	----	Capillary diameter	m
d_h	----	Hydraulic mean diameter	m
D	----	Diffusivity	m^2/s
D_{AB}	----	Diffusivity of vapour in air	m^2/s
D_{eff}	----	Effective diffusivity	m^2/s
$D_{eff, liq}$	----	Effective diffusivity of liquid	m^2/s
$D_{eff, vap}$	----	Effective diffusivity of vapour	m^2/s
D_k	----	Knudsen diffusivity	m^2/s
D_T	----	Non-isothermal mass diffusivity	m^2/s
D_w	----	Isothermal mass diffusivity	m^2/s
D*	----	Normalized effective transfer coefficient	
g	----	Acceleration due to gravity	m^2/s

f	----	Parameter dependent on structure of porous material	
f_{exp}	----	Experimental factor dependent on moisture content	
f(t)	----	Distance from the surface to the receding evaporation front	m
h	----	Heat transfer coefficient	$W/m^2 K$
h_c	----	Convective heat transfer coefficient	$W/m^2 K$
h_f	----	Energy head loss	m
h_r	----	Radiant heat transfer coefficient	$W/m^2 K$
Δhv	----	Latent heat of vaporization	J/kg
H	----	Absolute humidity	kg H_2O/kg dry air
H*	----	Single heaviside function (Eq. 3.3-6)	
k	----	Number of portions in the network of grid points ($k = L/n\Delta x$)	
$\bar{k}$	----	Unit factor on vertical axis of the coordinates system	
k'_c	----	Mass transfer coefficient	m/s
K'_G	----	Overall mass transfer coefficient	m/s
l	----	Length of pipe or characteristic length of system	m
ℓ	----	Effective length of the bed surface	m
L	----	Depth of the bed	m
m	----	Drying rate	kg H_2O/m^2 s
m_c	----	Drying rate in constant rate period	kg H_2O/m^2 s
m_p	----	Drying rate in pre-constant rate period	kg H_2O/m^2 s
ms	----	Mass of solid	kg
mw	----	Mass of water	kg
m(t)	----	Mass flux density	kg/m^2 s
Mw	----	Molecular weight of water	

n	——	Number of moles, or number of small distances in network of grid points	
P	——	Pressure	atm
P_f	——	Vapour pressure of water at the evaporation front	atm
P_{fc}	——	Pressure drop due to friction in capillary	atm
P_s	——	Vapour pressure at the surface	atm
P_{va}	——	Partial pressure of vapour in air	atm
P_w	——	Vapour pressure of water	atm
q	——	Heat flux	W/m^2
Q_L	——	Rate of liquid flow in capillary	m^3/s
r	——	Capillary radius, or radius of a granule	m
R	----	Universal gas constant	m^3 atm/k mol K
s	----	Slope of the saturated curve of water	atm/K
S	----	Entropy	J/K
t	----	Time	s
Δt	----	Time interval in network of grid points	s
t_{cr}	----	Elapsed time to critical moisture content	s
t_p	----	Elapsed time to the end of pre-constant rate period	s
t^*	----	Elapsed Time to attainment of equilibrium moisture content	s
T	----	Temperature	K
ΔT	----	Temperature difference	K
T_a	----	Air temperature	K
T_b	----	Temperature at the bottom of bed	K
T_{dew}	----	Dew point temperature	K
T_f	----	Temperature of the receding evaporation front	K
T_g	----	Gas temperature	K
T_s	——	Surface temperature	K

T_{wb}	——	Wet-bulb temperature	K
T'	——	Temperature after subsequent instant of time Δt	K
U	——	Internal energy	J
v	——	Velocity of the receding evaporation front	m/s
υ	——	Velocity of air stream	m/s
V	——	Volume	m^3
W	——	Water concentration	kg/ m^3
W_c	——	Critical water concentration	kg/ m^3
$W_{(f+t)}$	——	Weight of an empty sample tray plus weight of framework	kg
W_s	——	Weight of solid	kg
W_t	——	Total weight	kg
W*	——	Weight of wet material	kg
x	——	Distance of plane beneath bed surface	m
Δx	——	Small distance change in network of grid point	m
X	——	Moisture content	kg H_2O/kg dry solid
$\overline{X}$	——	Average moisture content	kg H_2O/kg dry solid
X_{cr}	——	Critical moisture content	kg H_2O/kg dry solid
X_f	——	Moisture content corresponding to the beginning of the second falling rate period	kg H_2O/kg dry solid
X_p	——	Moisture content at t_p	kg H_2O/kg dry solid
X*	——	Equilibrium moisture content	kg H_2O/kg dry solid
Y	——	Moisture content of air	kg H_2O/kg dry air
z	——	Characteristic sample dimension	m

GREEK LETTERS

α	——	Thermal diffusivity	m^2/s
α^*	——	Moisture diffusivity	m^2/s

δ	——	Boundary layer thickness, or penetrated depth	m
ε	——	Porosity or emissivity factor	
ε^*	——	Phase conversion factor of liquid into vapour	
θ	——	Angle of a conical diffuser	degrees
θ_i	——	Mass transfer potential	
θ_o	——	Initial mass transfer potential	
θ_s	——	Mass transfer potential of solid	
λ	——	Thermal conductivity	W/m K
λ_a	——	Thermal conductivity of air	W/m K
λ_{diff}	——	Thermal conductivity due to vapour diffusion	W/m K
λ_{eff}	——	Effective thermal conductivity	W/m K
λ_s	——	Thermal conductivity of solid	W/m K
λ^*	——	Mean free path	m
μ	——	Viscosity of the drying air	kg/m s
μ	——	Chemical potential	J/kg
μ_L	——	Viscosity of liquid	kg/m s
ρ	——	Density of air	kg/m^3
ρ_s	——	Density of solid	kg/m^3
ρ_L	——	Density of liquid	kg/m^3
ρ_{WL}	——	Density of liquid water	kg/m^3
σ	——	Vapour flux	$kg/m^2 s$
τ	——	Tortuosity factor	
φ	——	Source-sink of electromagnetic energy	W/m^3
Ψ	——	Percentage relative humidity	%

General Subscripts

d	——	Dry zone
i	——	Location step in network of grid points
j	——	Time level in network of grid points
m	——	Wet material
o	——	Initial
w	——	Wet zone

DIMENSIONLESS GROUPS

F	——	Fourier number	$\alpha t/l^2$
F_x	——	Fourier number based on x	$\alpha t/x^2$
KO	——	Kossovithich number	$\Delta hv\ (Cp/Cp_m)\ (\theta_o-\theta_s)/(T_s-T_o)$
Lu	——	Luikov number	α^*/α
Nu	——	Nusselt number	$h_c\ \ell/\lambda_a$
Pr	——	Prandtl number	$Cp\ \mu/\lambda_a$
Re	——	Reynolds number	$\upsilon\rho d/\mu$
Re,ℓ	——	Reynolds number based on effective length	$\upsilon\rho\ell/\mu$
Sc	——	Schmidt number	$\mu/\rho\ D_{AB}$
Sh	——	Sherwood number	$k'_c\ \ell/D_{AB}$
θ^*	——	Non-dimensional mass transfer potential	$(\theta_o-\theta_i)/(\theta_o-\theta_s)$

REFERENCES

1. Lewis, W.K. "The Rate of Drying of Solid Materials". J. Ind. Eng. Chem. Vol. 13, 1921, pp 427-432
2. Sherwood, T.K. "The Drying of Solids, Pt I", Ind. Eng. Chem. Vol. 21, 1929, pp 12-16
3. Sherwood, T.K. "The Drying of Solids, Pt II", Ind. Eng. Chem. Vol. 21, 1929, pp 976-980
4. Sherwood T.K. "The Drying of Solids, Pt III: Mechanism of the drying of pulp and paper", Ind. Eng. Chem. Vol. 22, 1930, pp 132-136
5. Nonhebel, G. and Moss, A.A., "Drying of Solids In the Chemical Industry", The Butter worth Group, London, 1971
6. Fortes, M. "A Non-Equilibrium Thermodynamics Approach to Transport Phenomena in Capillary-porous Media", PhD Thesis, Purdue University, USA, 1978
7. Coulson, J. M. and Richardson, J. F., Chemical Engineering, Vol. 1, 4th Edition, Pergamon Press plc, Oxford, U.K., 1990
8. Sherwood, T.K. and Comings, E.W. "The Drying of Solids V", Ind. Eng. Chem. Vol. 25, 1933, pp 311-316
9. Bories, S.A., "Fundamentals of Drying of Capillary-Porous Bodies", A Chapter in: Convective Heat and Mass Transfer in Porous Media, Editors: Kakac, S. and Kilkis, B., Kluwer Academic Pub., Netherlands, 1990, pp 391-434
10. Keey, R.B. Introduction to Industrial Drying Operations, London, William Clowes & Sons Ltd., 1978, pp 35-37
11. Arrowsmith, A. "External Heat and Mass Transfer to Drying Solids", An Education Course in Industial Solids Drying, University of Birmingham, October 1980, pp 34-45
12. Van Brackel, J. "Mass Transfer in Convective Drying", Advances in Drying, Vol. 1, 1980, pp 217-268
13. Strumillo, C. and Kudra, T. Drying: Principles, Applications and Design, Gordon and Breach Science Publishers, Switzerland, 1986.
14. Gehrmann D. and Kast W. "Drying of Gels", Proceedings of the 1st Int. Symp. on Drying, Montreal, Canada, 1978, pp 239-246
15. Keey, R.B. "Theoretical Foundation of Drying Technology", Advances in Drying, Vol. 1, 1980, pp 1-22
16. Fortes, M. and Okos, M. "Drying theories: Their Bases and limitations as applied to food and grains" Advances in Drying, Vol. 1, 1980, pp 119-150
17. Kisakurek, B. and Gebizlioglug, O. "Capillary mechanism in drying" Proceedings of the 1st Int. Symp. on drying, Canada, 1978, pp 59-65
18. Robbins, M.C. "Drying in capillary-porous media", PhD Thesis, North Carolina State University, Raleigh, USA, 1991

19. Moyne, C. and Perre, P. "Process Related to Drying, Part I, Theoretical Model", Drying Technology, Vol. 5, 1991, pp 1135-1152

20. Newman, A.B. "Diffusion and Surface Emission Equation", Trans. A.I.Ch.E., Vol. 27, 1931, pp 203-220

21. Gilliland, E.R., "Fundamentals of Drying and Air Conditioning", Ind. Eng. Chem., Vol. 30, 1938, pp 506-514

22. Sherwood, T.K., "Application of Theoretical Diffusion Equations to The Drying of Solids " Trans. A.I.Ch.E., Vol. 27, 1931, P190-202

23. Crank, J. The Mathematics of Diffusion, Clarendon, Oxford, 1975

24. Carslaw, H. and Jaeger, J., Conduction of Heat in Solids, 2nd Ed., Clarendon, N.Y., U.S.A., 1958

25. Hougen, O.A.; McCanley, H. and Marshall, W., "Limitation of Diffusion Equations in Drying", Trans. A.I.Ch.E., Vol. 36, 1940, pp 183-208

26. Kamei, S. and Shiomi, S., J., Soc. Chem. Ind., Japan, Supplementary Binding, Vol. 40, 1937, p40

27. Van Arsdel, W.B., Chem. Eng. Progr. Trans. Vol. 43, 1947, pp 13

28. Babbit, J.D. "On the Differential Equations of Diffusion", Can. J. Res. Sect. A., Vol. 18, 1950, pp 419-474

29. Berger, D. and Pei D.C., "Drying of Hygroscopic Capillary Porous Solids - A Theoretical Approach", Int. J. of Heat Mass Transfer, Vol. 16, 1973, pp 293-302

30. Ceaglsk, N.H. and Hougen, O., "The Drying of Granular Solids", Trans. A.I.Ch.E., Vol. 33, 1937, pp 283-312

31. Swanson, B.; MSc Thesis; Illinois Inst. of Tech., Chicago, 1944

32. Peck, R.; Griffith, R. and Rao, N. "Relative Magnitudes of Surface and Internal Resistance in Drying", Ind. Eng. Chem., Vol 44, 1952, pp 664-669

33. Buckingham, E.A. "Studies on The Movement of Soil Moisture", U.S. Dept. Agr. Bulletin No. 38, 1907

34. Gardner, O.W., Soil Sci., Vol. 10, 1920, pp 103

35. Richards, L.A., Physics, Vol. 1, 1931, pp 318

36. Richards, L.A. and Wilson, B., J. Amer. Soc. Agron, Vol. 28, 1936, pp 427

37. Muskat, M., "The Flow of Homogeneous Fluids Through Porous Media", 1st Ed., McGraw Hill, N.Y., 1937

38. Miller, E.E. and Miller, R.D. "Theory of Capillary Flow: I Practical Implications", Proc. Soil Sci., Soci. Am, Vol. 19, 1955, pp 267-271

39. Miller, E.E. and Miller, R.D. "Theory of Capillary Flow: II Experimental Information" Proc. Soil Sci., Soci. Am. Vol. 19, 1955, pp 271-275

40. Van Vorst, W.D. "Remarks on the Drying of Granular Materials", The Boelter Anniversary, Vol. 1 Heat Transfer Thermodynamics and Education Edition, H.A. Johnson, McGraw Hill, N.Y., 1964, pp 378

41. Martynenko, O.; Lerdansky, V. and Pavlyukevich "Kinetics of Mass Transfer in Capillary with Account for Movable Absorbed Layers", Proceedings of the 2nd Int. Symp. in Drying, Vol. 2, Montreal, Canada, 1980, pp 17-20

42. Kisakurek, B., The Preparation of Generalized Drying Curve for Porous Solids, PhD. Thesis, Illinois Inst. of Tech., Chicago, U.S.A., 1972

43. Henry, P.S. " Diffusion in Absorbing Media" Proceedings of Royal Soc., Vol. 171, Series A, London, 1939, pp. 215-241

44. Cassie, A.B, King, G. and Baxter, S., Trans. Faraday Soc., Vol. 36, 1940,445-458

45. Gurr, G.C; Marshal, T.J. and Hutton, J.H. " Movement of Water in Soil Due to A Temperature Gradient" Soil Science, Vol. 74, 1952, pp. 335-345.

46. Kuzmak, J.M and Sereda, P.J " The Mechanism By Which Water Moves Through A Porous Material Subjected to A Temperature Gradient : I Introduction of A Vapour Gap into A Saturated System " Soil Science, Vol. 84, 1957, pp. 291-299

47. Kuzmak, J.M " The Mechanism By Which Water Moves Through A Porous Material Subjected to A Temperature Gradient : II Salt Tracer and Streaming Potential to Detect Flow in The Liquid Phase" Soil Science, Vol. 84, 1957, pp. 419-422

48. Harmathy, T.Z " Simultaneous Moisture and Heat Transfer In Porous System With Particular Reference to Drying " Ind. Eng. Chem. Fund., Vol. 8, 1969, pp. 92-103

49. Garside, J.; Lord, L. and Reagan, R. " The Drying of Granular Fertilizers " Chem. Eng. Sci., Vol. 25, 1970, pp. 1133-1148

50. Luikov, A.V. Heat and Mass Transfer in Capillary Porous Bodies, Pergamon Press, Oxford, U.K., 1966

51. Mikhailov, M.D. "Exact Solution of Temperature and Moisture Distributions in Porous Half-Space with Moving Evaporation Front", Int. J. Heat Mass Transfer, Vol. 18, 1975, pp 797-804

52. Cary, J.W. and Taylor, S.A "The Interaction of The Simultaneous Diffusion of Heat and Water Vapour " Soil Sci. Amer. Proc., 26, 1962, pp. 413-416

53. Taylor, S.A. and Cary, J.W. "Linear Equations For The Simultaneous Flow of Matter and Energy in A Continuous Soil System " Soil Sci. Amer. Proc., 28, 1964, pp.167-172

54. Luikov, A.V. "Application of Irreversible Thermodynamics Methods to Investigation of Heat and Mass Transfer", Int. J. Heat Mass Transfer, Vol. 9, 1966, pp. 139-152

55. Luikov, A.V."Application of Methods of Thermodynamics of Irreversible Processes to Investigation of Heat and Mass Transfer in A Boundary Layer", Int. J. Heat Mass Transfer, Vol. 3, 1961, pp. 167-174

56. Fortes, M. and Okos, M.R. " A Non-Equilibrium Thermodynamics Approach to Transport Phenomena in Capillary Porous Media " Proceedings of the 1st Int. Symp. on Drying , Montreal, Canada, 1978, pp.100-109

57. Krischer, O. Die Wissenschaftlichen Grundlagen der Trocknungstechnik, Springer Verlag, Berlin, 1956

58. Philip, J.R., and De Vries, D.A. "Moisture Movement in Porous Materials under Temperature Gradients", Trans. Amer. Geophys. U., Vol. 38, 1957, pp 222-232

59. De Vries, D.A. "Simultaneous Transfer of Heat and Moisture in Porous Media " Trans Amer. Geophys. U., Vol 39, 1958, pp. 909-916

60. De Vries, D.A. " The Theory of Heat and Moisture Transfer in Porous Media Revisited " Int. J. Heat Mass Transfer Vol. 30, 1987, pp.1343-1350

61. Whitaker, S. " Toward A Diffusion Theory of Drying " Ind. Eng. Chem. Fundam, Vol. 16, 1977, pp. 408-414

62. Whitaker, S. "Simultaneous Heat, Mass and Momentum Transfer in Porous Media : A Theory of Drying " Advances in Heat Transfer, Vol. 13, 1977, pp.119-203

63. Whitaker, S. " Heat and Mass Transfer in Granular Porous Media " Advances in Drying, Vol. 1, 1980, pp. 23-61

64. Whitaker, S. " Moisture Transport Mechanisms During The Drying of Granular Porous Media " Proceedings of the 4th Int. Drying Symp., Kyoto, Japan, 1984, pp. 21-32

65. Whitaker, S. " The Role of Species Momentum Equation in The Drying Processes " Proceedings of the 7th Int. Drying Symp., Prague, Czech., 1990, pp. 97-109

66. Whitaker, S. and Chou, W. " Drying Granular Porous Media, Theory and Experiment " Drying Tech., Vol. 1, 1983, pp.3-33

67. Masters, K. Spray Drying Handbook , 5th ed. , Longman Scientic & Tecknical, England, 1991

68. Gardner, A.W., Industrial Drying , Leonard Hill, London, 1971

69. Mujumdar, A.S., Handbook of Industrial Drying, Marcel Dekker, Inc., New York, 1987

70. Backhurst,J.R.and Harker, J.H., Chemical Engineering,Vol.2, Pergamon Press plc, Oxford, U.K., 1990

71. Sherwood, T.K. "Application of the Theoretical Diffusion Equations in the Drying of Solids", Trans. Am. Inst. Chem. Eng. Vol. 27 1931, pp 190-202

72. Haines, W.B. "The hystereses effect in capillary properties, and The models of Moisture Distribution Association Therewith", J. Agr. Sci. Vol. 20, 1930, pp 97-116

73. Pearse, J; Oliver, T and Newitt, D., "The Mechanism of The Drying of Solids, Part I" Trans. Inst. Chem. Eng., Vol. 27, 1947, pp 1-8

74. Oliver, T. and Newitt, D. "The Mechanism of The Drying of Solids, Part II", Trans. I. Ch. Eng., Vol. 27, 1949, pp 9-18

75. Newitt, D. and Coleman, M. "The Mechanism of Drying of Solids, Part III", Trans. I. Ch. Eng., Vol. 30, 1952

76. King, A.R. and Newitt, D. "The Mechanism of The Drying of Solids, Part VII" Trans. I. Ch. Eng., Vol. 33, 1955, pp 64-71

77. King, A.R. "The Mechanisms of The Drying of Solids by Conduction Heating" PhD. Thesis, Imperial College of Science & Technology, London, 1955

78. Corben, R. and Newitt, D. "The Mechanism of The Drying of Solids, Part VI" Trans I. Ch. Eng., Vol. 33, 1955, pp 52-63

79. Nissan, A., Kaye, W. and Bell, J., "Mechanism of Drying Thick Porous Bodies During The Falling Rate Period", A.I.Ch.E Journal, Vol. 5, 1959, pp 103-110

80. Toei, R.; Hayashi, S.; Hasegawa, J.; Kai, T. and Tanaka, S., "Mechanism of Drying of a Bed of Granular and Powdered Materials During the Second Falling Rate Period." Kagaku Kogaku, Vol. 2 No. 2, 1964, pp 250-254

81. Vyas, K.C., "The Drying of Thick Porous Materials", PhD. Thesis, Illinois Inst. of Tech., Chicago, U.S.A., 1974

82. Toei, R. and Okazaki, M., "Drying Mechanism of Capillary-Porous Bodies", Journal of Eng. Physics, Vol. 19, 1970, pp 1122-1131

83. Peck, R.; Vyas, K. and Toei, R., "Capillary Theory Applied to Drying", A.I.Ch.E. Symp. Series, Vol. 73, 1977, pp 63-70

84. Haertling, M. " Prediction of Drying Rates" Proceedings of the 2nd Int. Symp. In Drying, Vol. 1, Montreal Canada, 1980, pp.88-98

85. Wang, N. and Brennan, T. "Effect of Water Binding on the Drying Behaviour of Potato" Proceedings of 8th Int. Drying Symp., Montreal, Canada, 1992, pp 1350-1359

86. Yusheng, Z. "Diffusion in Potato Drying", Journal of Food Eng. Vol. 7, 1988, pp 249-262

87. Dressel, B. and Militzer, K. "Modelling of Mass Transfer within the Solid as a Basic for The Mathematical Description of Convection Drying" Proceedings of the 4th Int. Drying Symp., Kyoto, Japan, 1984, pp 28-34

88. Strongin, V. and Borde, I. "Theoretical Prediction of Moisture Transfer by Convective Drying for a Flat Plate" Proceedings of the 4th Inst. Drying Symp., Kyoto, Japan, 1984, pp 143-149

89. Schultz, P. "On The Falling-Rate Period" Chem. Eng. Technology. Vol. 14, 1991, pp 234-239

90. Rattanapant, O., Lebert, A. and Laguerre, J. "Simulation of Deep Bed Drying of Particles" Proceedings of the 6th Int. Symp. on Drying, Versailles, France, 1988, pp 565-572

91. Marc Part "Heat and Mass Transfer Predetermination Between A Drying Material and An External Flow" Proceedings of the 5th Int. Symp. on Drying, Massachusetts, U.S.A., 1986, pp 105-111

92. Oliveira, A.C. and Oliveira, E.F. "Simulation of The Convective Drying of Capillary Porous Materials" Proceedings of the 5th Int. Symp. on Drying, Massachusetts, U.S.A., 1986, pp 65-70

93. Cunningham, R. and Kelly, J. "Moisture Concentration Profiles in Drying Packed Beds" Proceedings of the 3rd Int. Drying Symp., Vol. 1, Birmingham, U.K., 1982, pp 178-189

94. Cousin, B., Benet, J. and Auna R. "Experimental Study of The Drying of A Thick Layer of Natural Crumb Rubber" Drying Technology, Vol. 11, 1993, pp 1401-1413

95. Basilico, C. and Moyne, C. "Moisture Transport Analysis During High Temperature Convective Drying of Wood" Drying of Solids,, Editor A. Mujumdar, Wiley Eastern Limited, New Delhi, India, 1986

96. Basilico, C.; Moyne, C. and Martin, M. "High Temperature Convective Drying of Softwood, Moisture Migration Mechanisms" Proceedings of the 3rd Int. Drying Symp., Vol. 1, Birmingham, U.K., 1982, pp 46-55

97. Moyne, C. and Basilico, C. "High Temperature Convective Drying of Softwood and Hardwood" Proceedings of the 4th Int. Drying Symp., Kyoto, Japan, 1984, pp 376-381

98. Moyne, C. and Degiovanni, A. "Importance of Gas Phase Momentum Equation In Drying Above The Boiling Point of Water" Proceedings of the 4th Int. Drying Symp., Kyoto, Japan, 1984, pp 109-116

99. Basilico, C.; Genevaux, J. and Martin, M. "High Temperature Drying of Wood Semi-Industrial Kiln Experiments" Proceedings of the 6th Int. Symp. Vol. 1 on Drying, Versailles, France, 1988, pp 329-335

100. Moyne, C.; Stemmelen, D. and Degiovanni, A. "Asymmetric Drying of Porous Materials at High Temperature. Theoretical Analysis and Experiments" Int. Chem. Eng., Vol. 30, 1990, pp 654-671

101. Schadler, N. and Kast, W. "Experimental Studies and Mathematical Modelling on Convective Drying of Porous Bodies" Drying of Solids, editor A. Mujindar, Wiley Eastern Limited, New Delhi, India, 1986, pp 29-40

102. Schadler, N. and Kast W. "A Complete Model of The Drying Curve for Porous Bodies Experimental and Theoretical Studies" Int. Journal Heat Mass Transfer, Vol. 30, 1987, pp 2031-2044

103. Bories, S.; Bacon, G. and Recan, M. "Experimental and Numerical Study of Coupled Heat and Mass Transfer in Porous Materials" Proceedings of the 4th Int. Drying Symp., Kyoto, Japan, 1984, pp 15-21

104. Bories, S. "Recent Advances in Modelisation of Coupled Heat and Mass Transfer In Capillary-Porous Bodies " Proceedings of the 6th Int. Symp. on Drying, Vol. 1, Versailles, France, 1988, pp 47-60

105. Przesmycki, Z. and Strumillo, C. "The Mathematical Modelling of Drying Process Based on Moisture Transfer Mechanism" Proceedings of the 4th Int. Drying Symp., Kyoto, Japan, 1984, pp 126-134

106. Murthy, S.; Murthy, M. and Ramachandran, A. "Low Intensity Convective Drying of Non-Hygroscopic Porous Materials of High Initial Moisture Content", Chem. Eng. Sci., Vol. 31, 1976, pp 975-983

107. Basilico, C.; Moyne, C. and Martin, M. "High Temperature Convective Drying of Softwood Moisture Migration Mechanisms", Proceedings of the 3rd Int. Drying Symp., Vol. I, Birmingham, U.K., 1982, pp 46-55

108. Haber, S.; Shavit, A. and Dayan, J. "The Effect of Heat Convection on Drying of Porous Semi-Infinite Space", Int. J. Heat Mass Transfer, Vol. 27, 1984, pp 2347-2353

109. Nasrallah, B.S. and Perre, P. "Detailed Study of Model of Heat and Mass Transfer During Convective Drying of Porous Media", Int. Heat Mass Transfer, Vol. 31, 1988, pp 957-967

110. Toei, R. "Drying Mechanism of Capillary Porous Bodies", Advances in Drying, Vol. 2, 1983, pp 269-297

111. Luikove, A.V."System of Differential Equations of Heat and Mass Transfer in Capillary-Porous Bodies", Int. J. Heat Mass Transfer, Vol. 18, 1975, pp 1-14

112. Mikhailov, M.D., "General Solutions of The Diffusion Equations Coupled at Boundary Conditions", Int. J. Heat Mass Transfer, Vol. 16, 1973, pp 2155-2164

113. Ceaglsk, N. and Hougan, O.A. "The Drying of Granular Solids", Ind. Chem., Vol. 29, 1937, pp 805-328

114. Szentgyorgyi, S. "Drying of Capillary Porous Materials in The Second Falling Rate Period" Proceedings of the 3rd Int. Symp. on Drying, Vol. 1, Birmingham, U.K., 1982, pp 100-109

115. Szentgyorgyi, S. and Orvos, M. "An Approximation Method For the Determination of The Distribution of Temperature and Moisture Content in The Falling Rate Period of Drying", Drying Tech., Vol. 3, 1985, pp 399-419

116. Chen, P. and Schmidt, P. "A Model For Drying of Flow-Through Beds of Granular Products with Dielectric Heating" ASME, HTD, Vol. 146, 1990, pp 121-127

117. Chen, P. and Pei, D. "A Mathematical Model of Drying Processes", Int. J. Heat Mass Transfer, Vol. 32, 1989, pp 297-310

118. Ashworth, J.C. "Interpretation of Small-scale Drying Tests", An Education Course in Industrial Solids Drying, University of Birmingham, 1980, pp151-183

119. Lopez, G.F., Convective Drying and Solid-Moisture Interactions, PhD Thesis, University of Reading, Reading, England, 1989

120. Sjoholm, I. "Studies on Convective and Conductive Drying of Foodstuffs in Thin Films", Proceedings of the 3rd Int. Drying Symp., Birmingham, U.K., 1982, pp 451-456

121. Obrien, L.J. and Stutzman, L.F. "Mass Transfer of Pure Liquids From A Plane, Free Surface" Ind. Eng. Chem., Vol. 42, 1950, pp 1181-1187

122. Shepherd, C.; Hadlock, C. and Brewer, R. "Drying Materials in Trays, Evaporation of Surface Moisture" Ind. Eng. Chem., Vol. 30, 1938, pp 388-397

123. McCabe, W.L. and Smith, J.L., Unit Operations of Chemical Engineering, McGraw Hill Book Co. Inc., U.S.A., 1967

124. Lomax, W.R. and Saul, A.J., Laboratory Work in Hydraulics, Granada Publishing Ltd., London, U.K., 1979, pp 73-77

125. Walshaw, A.C. and Jobson, D.A., Mechanics of Fluids, 3rd Edition, Longman Group Ltd., 1979, pp 314-317

126. Perry, R., Green, D. and Maloney, J., Perry's Chemical Engineering Handbook, 5th Edition, McGraw-Hill Book Co., 1973, pp 5. (21-34)

127. Blow, C.M. and Hepburn, C., Rubber Technology and Manufacture, 2nd Edition, Dorstel Press Ltd., Essex, U.K., 1982, pp 48

128. Almubarak, A.A. and Mumford, C.J., "Characteristics of The Receding Evaporation Front in Convective Drying" Proceedings of the 9th Int. Drying Symp., Gold Coast, Australia, 1994, pp 231-238

129. Goodman, T.R., "Application of Integral Methods to Transient Nonlinear Heat Transfer", Advanced in Heat Transfer, Vol. 1, 1964, pp 51-122

130. Benson, R. and Sill, B. "The Use of Integral Methods in Solving Partial Differential Equations", Math. Modelling, An Int. Journal,Vol.8,1987,pp344-347

131. Keey, R.B. "Basic Concepts in Drying", Course Notes, Drying Short Course, Brisbane, Australia, July 1994, pp 7

132. Waananen, K.; Litchfield, J. and Okos, M. "Classification of Drying Models for Porous Solids" Drying Technology, Vol. 11, 1993, pp 1-40

133. Finlayson, B.A., Non-Linear Analysis in Chemical Engineering, McGraw-Hill Inc., U.S.A., 1980

134. Davis, M.E., Numerical Methods and Modelling For Chemical Engineers, John Wiley & Sons, N.Y., U.S.A., 1984

135. Comini, C.B. and Primicerio, A.F. "Numerical Solution of Phase-Change Problems" Int. J. Heat Mass Transfer, Vol. 16, 1973, pp 1825-1832

136. Jenson, V.G. and Jeffreys, G.V., Mathematical Methods in Chemical Engineering, 2nd Edition, Academic Press, London, U.K., 1977

137. Roques, M. and Cornish, A. "Phenomenological Coefficients for Heat and Mass Transfer Equations in Wet Porous Media", Proceedings of the 2nd Int. Symp in Drying, Montreal, Canada, 1980, pp 36-42

138. Geankoplis, C.J., Transport Processes and Unit Operations, Allyn and Bacon Inc., Boston, Massachusetts, U.S.A., 1978

139. Geankoplis, C.J., Mass Transfont Phenomena, 3rd Edition, Edwards Brothers Inc., U.S.A., 1978

140. Treybal, R., Mass-Transfer Operations, 3rd Edition, McGraw-Hill Inc., U.S.A., 1980

141. Rogers, J. and Kaviany, M. "Variation of Heat Transfer Coefficients During Drying of Granular Beds", Trans. of the ASME, Vol. 122, 1990, pp 668-674

142. Okazaki, M. "Heat and Mass Transport Properties of Heterogeneous Materials" Proceedings of the 4th Int. Drying Sump., Kyoto, Japan, 1984, pp 84-96

143. Endrenyi, S. and Szentivanyi, D. "Numerical Evaluation of Transfer Coefficients of Drying Process of Porous Bodies in The Falling Rate Period" Proceedings of the 1st Int. Symp., Montreal, Canada, 1978, pp 48-52

144. Mitura, E.; Kaminski, W. and Michaiowski, S. "Application of Drying Kinetics Investigation To The Determination of Average Heat Transfer Coefficient in

Biosynthesis Materials" Proceedings of the 7th Int. Drying Symp., Prague, Czechoslovakia, 1990, pp 191-195

145. Krupiczka, R. "Analysis of Thermal Conductivity in Granular Materials" Int. Chem. Eng., Vol. 7, 1967, pp 122-144

146. Moyne, C. "Thermal Conductivity of Wet Porous Media", A Chapter in : Heat and Mass Transfer in Porous Media, Editors: Quintard, M. and Todorovic, M., Elsevier Science Publishers B.V., N.Y., U.S.A., 1992, pp 783-794

147. Gerrard, P. "Thermal Conductivity and Drying in Moisture Granular Beds" PhD. Thesis, Birmingham University, Birmingham, U.K., 1973

148. Mnashe, J. "Accurate Measurements of Thermal Conductivity of Liquids", PhD. Thesis, Imperial College of Science and Technology, London, U.K., 1981

149. Okazaki, M.; Ito, I. and Toei, R. "Effective Thermal Conductivities of Wet Granular Materials" A.I.Ch.E. Symp. Series, Vol. 73, 1977, pp 164-176

150. Dulnev, G.; Volkov, D. and Makarev, V. "Thermal Conductivity of Moist Porous Materials" J. of Eng. Physics, Vol. 56, 1989, pp 198-206

151. Saravacos, G.; Drouzas, A.; Marousis, S. and Kostaropoulos, A. "Effective Thermal and Moisture Diffusivities of Granular Starch" Proceedings of the 6th Int. Symp. on Drying, Versailles, France, 1988, pp 379-384

152. Shishido, I.; Suzuki, M. and Ohtani, S. "Determination of The Diffusivity of Moisture Within Wet Material", Proceedings of the 1st Int. Symp. on Drying, Montreal, Canada, 1978, pp 30-35

153. Yamamoto, S.; Hoshika, M. and Sano, Y. "Determination of Concentration Dependent Diffusion Coefficient from Drying Rates" Proceedings of the 4th Int. Drying Symp., Kyoto, Japan, 1984, pp 490-497

154. Yoshida, M.; Miyashita, H. and Okazaki, M. "Estimation of Drying Rate and Determination of Moisture Diffusivity For Non-Hygroscopic Porous Material Based on The Characteristic Function For The Regular Regime" Proceedings of the 8th Int. Drying Symp., Montreal, Canada, 1992, pp 243-252

155. Moyne, C.; Roques, M. and Wolf, W. "A Collaborative Experiment on Drying Beds of Glass Spheres" Chapter 3 in , Physical Properties of Food-2 COAT 90 bis, edited by: Jowitt, R.; Escher, F.; Kent, M.; Mckenna, B. and Roques, M., Elsevier Applied Science Pub., N.Y., 1990, pp 27-54

156. Kechaou, N. and Roques, M. "A Variable Diffusivity Model for Drying of Highly Deformable Materials" Proceedings of the 8th Int. Drying Symp., Montreal, Canada, 1992, pp 403-309

157. Iida, Y. and Ohtani, S. "A New Transient Method For Measuring The Diffusion Coefficient Under Arbitrary Boundary Conditions", Proceedings of the 2nd Int. Symp. in Drying, Montreal, Canada, 1980, pp 149-156

158. Toei, R.; Imakoma, H.; Tamon, H. and Okazaki, M. "Water Transfer Coefficient in Adsorptive Porous Body" J. of Chem. Eng. of Japan, Vol. 16, 1983, pp 364-369

159. Kanevce, G.; Stefanovic, M. and Pavasovic, V. "Experimental Determination of The Diffusivity of Moisture Within Capillary Porous Bodies" Proceedings of the 2nd Int. Symp. in Drying, Montreal, Canada, 1980, pp 128-131

160. Satterfield, C.N., Mass Transfer in Heterogeneous Catalysis, The MIT Press, Cambridge, U.K., 1970, pp 217

161. Ketelaars, A.; Lauf, O.; Coumans, W. and Kerkhof, P. "Determination of Diffusion Coefficient from Experimental Moisture Concentration Profiles in Clay", Proceedings of the 8th Int. Drying Symp, Montreal, Canada, 1992, pp 345-352

162. Blumberg, W. and Schlunder, E. "Simultaneous Vapour and Liquid Diffusion in Partially Wetted Porous Media" Drying Technology, Vol. 11, 1993, pp 41-64

163. Luikov, A.V. "Heat and Mass Transfer in Capillary-Porous Bodies", Advances in Heat Transfer, Vol. 1, 1964, pp 123-184

164. Luikov, A.V., "The Kinetics of Heat Transfer in The Process of Drying Moist Materials" Int. Chem. Eng., Vol. 13, 1973, pp 639-642

165. Shahab, S. and Bruce, D. "Heat Transfer Coefficient in Drying Granular Materials", Proceedings of the 5th Int. Symp. on Drying, Massachusetts, U.S.A., 1986, pp 862-867

166. Almubarak, A.A. and Mumford, C.J., "Variation of Temperature Gradient According To Material Width In Convective Drying" The ICHEME Research Event, First European Conference, Vol. 2, Edinburgh, U.K., 1995, pp 886-888

167. Genskow, L.R., "Considerations in Drying Consumer Products", Proceedings of the 6th Int. Symp. on Drying, Versailles, France, 1988, pp 39-46

168. APV-Mitchell Dryers Ltd., Laboratory and Pilot Scale Dryers, Coolers and Blenders, 1988

169. Almubarak, A.A. and Mumford, C.J. "Mechanisms of Convective and Conductive Drying" The Second Scientific Conference, National Union of Kuwaiti Students, pp 25-27

APPENDIX A

FINITE DIFFERENCE METHOD SOLUTION

A.1 Basic Equations

The non-linear equations which describe the falling rate period with the moving boundary equations can be solved by the finite difference method. A network of grid points is first established to show the locations of the receding evaporation front at any time. This network is shown in Fig. A.1.

The evaporation front was assumed to have receded equal distances Δx for every time interval Δt. The number of front steps must correspond to the number of time steps. The lines, i, indicate the locations of the front and the lines, j, indicate the time levels, taking into account that the distances, Δx, are constant but the intervals, Δt, are not since the velocity of the front varies with time.

The temperature of the evaporation plane varies with time and with position. For practical computational purposes, the temperature of the front can be calculated at the points, n, as shown in the network. Therefore, if the material bed of depth L is divided into k portions where every portion equals $n\Delta x$, the front will have move a distance Δx at the end of each time step Δt and from time to time, the front will have moved a distance $n\Delta x$. The points n, 2n, 3n, ... are main points on the grid. The number of time steps required to complete the whole drying period will be kn.

During the solution of the differential equation, the new value of the temperature obtained at the subsequent instant of time Δt will be represented as T'.

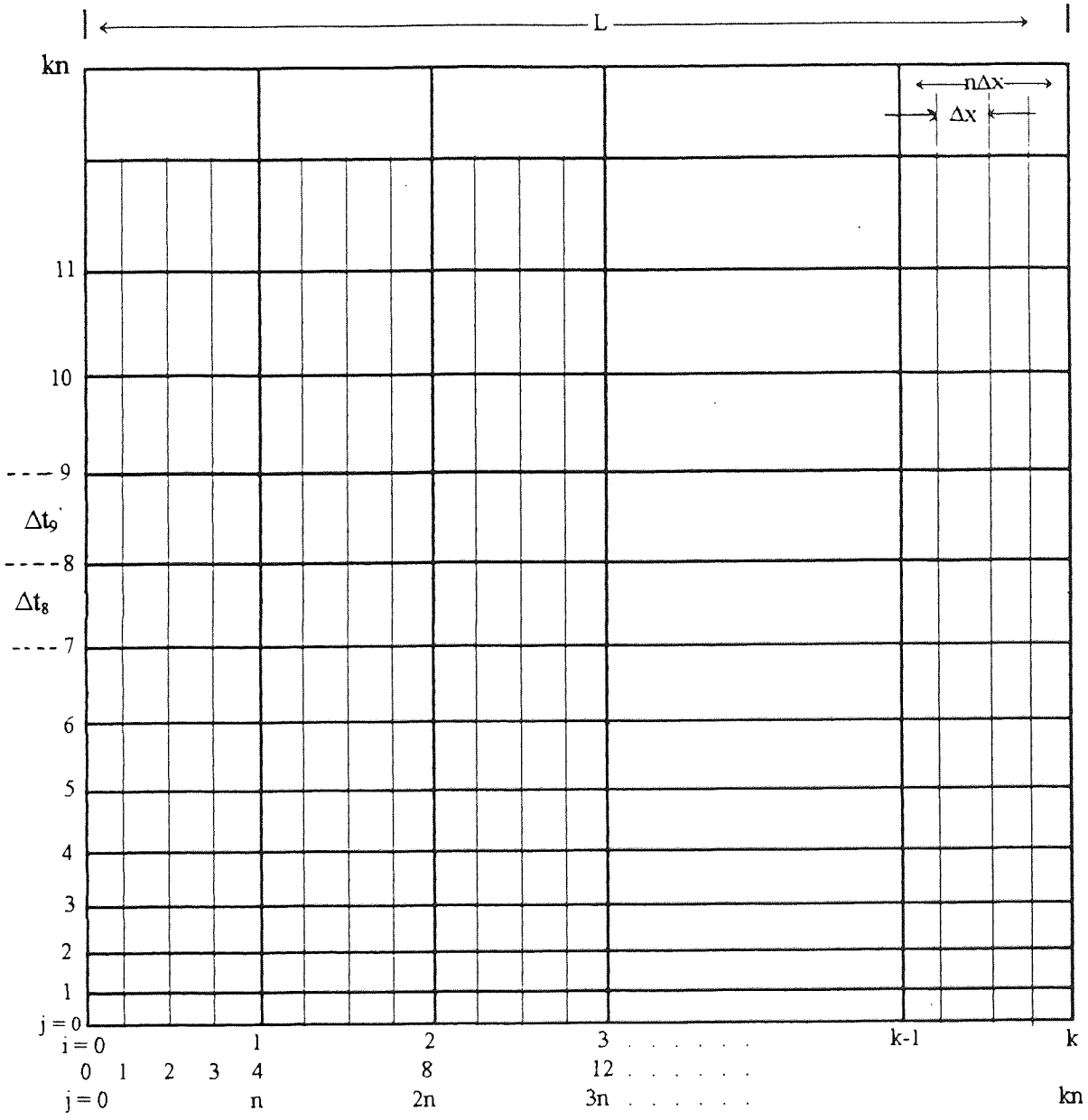

Fgure A.1 The network of grid points

A.1.1 Equation of Main Grid Points With Respect to Location

The derivative of temperature with respect to time and to distance can be defined as follows:

The derivative with respect to time at i,

$$\frac{\partial T}{\partial t} = \frac{T_i' - T_i}{\Delta t} \qquad \text{(A.1-1)}$$

The first derivative with respect to location i,

$$\frac{\partial T}{\partial x} = \frac{T_{i+1} - T_i}{n\Delta x} \qquad \text{(A.1-2)}$$

and the second derivative with respect to location i,

$$\frac{\partial^2 T}{\partial x^2} = \frac{T_{i+1} - 2T_i + T_{i-1}}{(n\Delta x)^2} \qquad \text{(A.1-3)}$$

The temperature gradient is assumed to be parabolic in the form,

$$T = C_o + C_1 x + C_2 x^2 \qquad \text{(A.1-4)}$$

At x = 0 then $T_o' = C_o$. The subsequent temperature T_1' will be,

$$T_1' = T_0' + C_1(n\Delta x) + C_2(n\Delta x)^2 \qquad \text{(A.1-5)}$$

and

$$T_2' = T_0' + C_1\, 2(n\Delta x) + C_2\, 4(n\Delta x)^2 \qquad \text{(A.1-6)}$$

Solving Eq. (A.1-5) and (A.1-6) yields,

$$C_1 = \frac{-3\,T_0' + 4T_1' - T_2'}{2(n\Delta x)} \tag{A.1-7}$$

At the surface x = 0; i = 0 gives

$$\frac{\partial T}{\partial x}\Big|_{x=0} = C_1 = \frac{-3\,T_0' + 4T_1' - T_2'}{2\,(n\Delta x)} \tag{A.1-8}$$

A.1.2 Equations of Non-Main Grid Points

At t=0, the front lies on the surface. At time, t, the front recedes inside the bed. If the receding front lies between the surface and the first main grid point, n, i.e. $0<j<n$, then applying a linear approximation will give

$$\frac{\partial T}{\partial x} = \frac{T_j' - T_0'}{j\Delta x} \tag{A.1-9}$$

If the front lies between the first point, n, and the second point 2n i.e. $n<j\leq 2n$ as shown in Fig. A.2, then a second degree approximation can be applied. Thus, for x = 0, leads to $T_0' = C_0$. The subsequent temperature T_1' will be,

$$T_1' = T_0' + C_1(n\Delta x) + C_2(n\Delta x)^2 \tag{A.1-10}$$

and

$$T_j' = T_0' + C_1(j\Delta x) + C_2(j\Delta x)^2 \tag{A.1-11}$$

Solving Eqs. (A.1-10) and (A.1-11) yields,

$$C_1 = \frac{-(j^2 - n^2)T_0' + j^2 T_1' - n^2 T_j'}{(j-n)\, nj\Delta x} \qquad \text{(A.1-12)}$$

Therefore, the derivative with respect to the boundary surface location can be written as

$$\left.\frac{\partial T}{\partial x}\right|_{x=0} = \frac{-(j^2 - n^2)\, T_0' + j^2\, T_1' - n^2\, T_j'}{(j-n)\, nj\Delta x} \qquad \text{(A.1-13)}$$

If the front lies on the point 2n (i.e. j = 2n), then Eq. (A.1-8) can be applied.

For the case j>2n, the derivative with respect to the boundary surface can be calculated by using equations of main grid points from known values at the locations j=0, n and 2n.

At the bottom of the bed, i.e. x = L and i = kn, then by the same method used to calculate Eq. (A.1-8), the derivative with respect to the boundary condition can be written as:

$$\left.\frac{\partial T}{\partial x}\right|_{x=L} = \frac{3T_k' - 4T_{k-1}' + T_{k-2}'}{2(n\Delta x)} \qquad \text{(A.1-14)}$$

For the case (k-2)n≤j<(k-1)n, the differential equation can be calculated according to Fig. A.3, introducing the term j* as j* = j - (k - 2)n. On the basis of the above consideration, the derivative with respect to the boundary conditions will be,

$$\left.\frac{\partial T}{\partial x}\right|_{L} = \frac{-\left[(2n - j^*)^2 - n^2\right]T_k' + (2n - j^*)^2\, T_{k-1}' - n^2 T_j'}{n(2n - j^*)\,(j^* - n)\Delta x} \qquad \text{(A.1-15)}$$

For the case j = (k-2)n, then $T_j' = T_{(k-2)n} = T_{k-2}$ and j* = 0, then Eq. (A.1-15) turns into Eq. (A.1-14).

Determination of the first derivatives with respect to location for the case of the receding front, can be expressed as follows:

The receding front in general position, i.e. at any grid point, is shown in Fig. A.4.

If

$n < j < 2n$, then $i = n$

$2n < j < 3n$, then $i = 2n$

and

$(k - 2)\, n < j < (k - 1)n$, then $i = (k - 2)n$.

Applying second degree approximation:

$$\left.\frac{\partial T}{\partial x}\right|_{f(t)-} = \frac{(j-i)^2 T'_{i-1} - (j-i+n)^2 T'_i + n[2(j-i)+n]T'_j}{n(j-i+n)\,(j-i)\,\Delta x} \qquad \text{(A.1-16)}$$

and

$$\left.\frac{\partial T}{\partial x}\right|_{f(t)+} = \frac{-n[2(i-j)+3n]T'_j + (i+2n-j)^2 T'_{i+1} - (i+n-j)^2 T'_{i+2}}{n(i+n-j)\,(i+2n-j)\,\Delta x} \qquad \text{(A.1-17)}$$

If the front is situated at internal main grid points, i.e. $j = 2n, 3n, \ldots (k - 2)n$, then the derivatives may be computed by means of main grid equations.

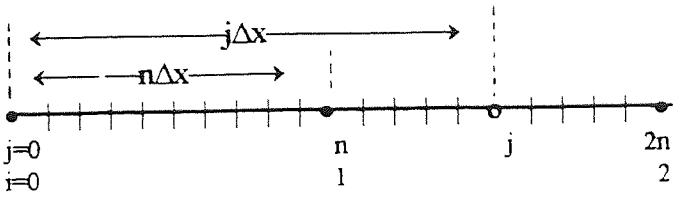

Figure A2 Receding evaporation front between the first point n and the second point 2n

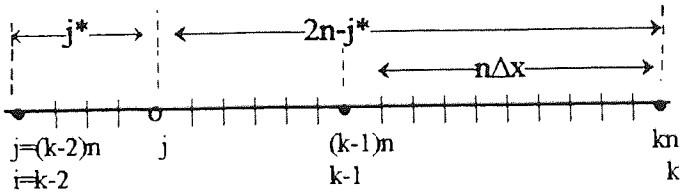

Figure A.3 Receding evaporation front in position $(k-2)n \leq j < (k-1)n$

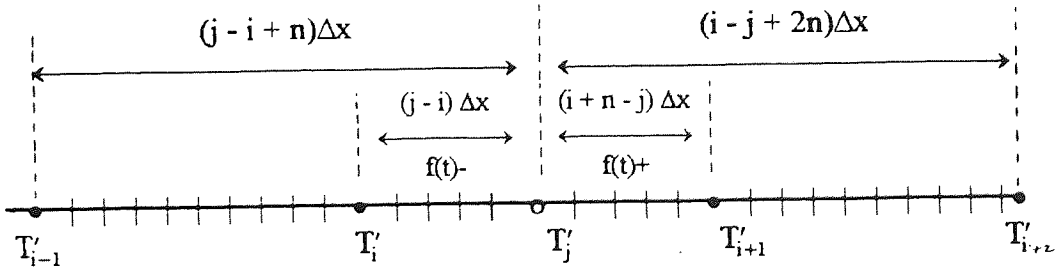

Figure A.4 Receding evaporation front in general position.

A.1.3 Approximation of Second Derivatives With Respect to Location

Figure A.5 shows the two zones. Considering the dry zone, the approximation of second derivatives with respect to location can be written as,

$$\frac{\partial^2 T}{\partial x^2} = 2\frac{(j-1-i)T_{i-1} - (n+j-i-1)T_i + nT_{j-1}}{n(j-1-i)(n-j-1-i)\,\Delta x^2} \qquad \text{(A.1-18)}$$

For the case $0<j<n$, no internal point exists in the dry zone, hence Eq. (A.1-18) cannot be applied;

For the case $j = n + 1$, $i = n$ (main point) the front meets the main grid point, and similarly, at time levels

$$j = 2n + 1,\ 3n + 1,\ \ldots(k - 1)n + 1;$$

Eq. (A.1-18) can be applied for the following cases:

$$n + 2 \le j \le 2n, \qquad i = n;$$

and

$$2n + 2 \le j \le 3n, \qquad i = 2n;$$

and

$$(k - 1)n + 2 \le j \le k\,n, \qquad i = (k - 1)n.$$

A general position within the wet zone is shown in Fig. A.6,

$$\frac{\partial^2 T}{\partial x^2} \approx 2\frac{nT_{j-1} - (i+1-j+n)T_i + (i+1-j)T_{i+1}}{n(n+i+1-j)\,(i+1-j)\,\Delta x^2} \qquad \text{(A.1-19)}$$

For the cases:

$0 < j \le n$,	$i = n$
$n + 2 \le j \le 2n$,	$i = 2n$
$(k-2)n + 2 \le j \le (k - 1)n$,	$i = (k - 1)n$

Eq. (A.1-19) may be applied.

For $j = n + 1, 2n + 1, \ldots (k - 2)n + 1$, the main grid point equations may be applied.

If $j > (k - 1)\, n$, there is no internal point within the wet zone.

A.2 Solution For The Boundary Conditions

A.2.1 Boundary Condition At x = 0

The boundary condition at the surface, $x = 0$, is

$$-\lambda_d \frac{dT_d}{dx} = h(T_a - T_s) \qquad \text{(A.2-1)}$$

1. For the case $0 < j \le n$ and using Eq. (A.1-9), the surface boundary condition becomes as follows,

$$-\lambda_d \frac{T_j' - T_0'}{j\Delta x} = h(T_a - T_0') \qquad \text{(A.2-2)}$$

which yields,

$$T_0' = \frac{j\Delta x\, h T_a + \lambda_d T_j'}{j\Delta x h + \lambda_d} \qquad \text{(A.2-3)}$$

2. For the case $n < j < 2n$, using Eq. (A.1-13) yields,

$$T_0' = \frac{nj(j-n)\Delta x h\, T_a + \lambda_d T_j'\, j^2 - \lambda_d n^2 T_j'}{\lambda_d (j^2 - n^2) + hnj(j-n)\Delta x} \qquad \text{(A.2-4)}$$

3. For the case $2n \le j \le k\, n$, using Eq. (A.1-8) gives,

$$T_0' = \frac{2n\Delta x h T_a + 4\lambda_d T_1' - \lambda_d T_2'}{3\lambda_d + 2n\Delta x h} \qquad \text{(A.2-5)}$$

A.2.2 Boundary Condition At x =L

The boundary condition at the bottom of the bed, x = L, is

$$-\lambda_w \frac{\partial T_w}{\partial x} = 0 \qquad \text{(A.2-6)}$$

The equation to describe the wet zone was given in Chapter 6 as,

$$\frac{\partial T_w}{\partial t} = \alpha_w \frac{\partial^2 T_w}{\partial x^2} \qquad \text{(A.2-7)}$$

Therefore for the case of $0 < j \le (k\text{-}1)n$, the above equations lead to,

$$\frac{T_k' - T_k}{\Delta t j} = \alpha_w \frac{2}{(n\Delta x)^2}(T_{k-1} - T_k) \qquad \text{(A.2-8)}$$

which gives,

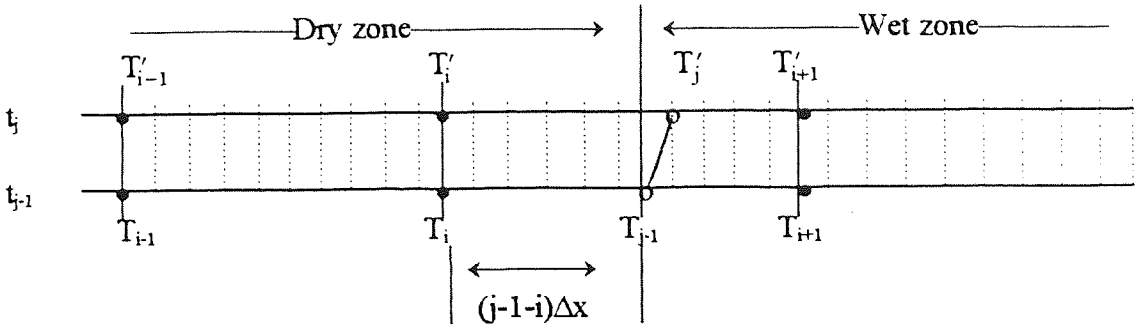

Figure A.5 Dry zone and wet zone within the network grid.

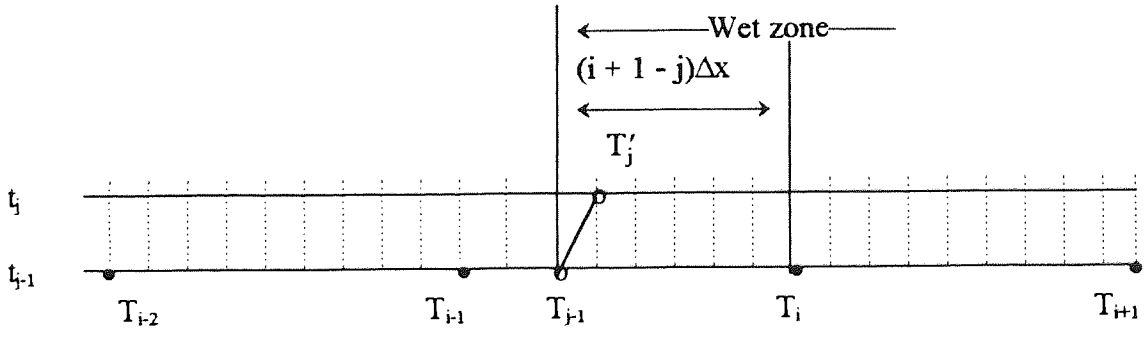

Figure A.6 Network grid shows the wet zone

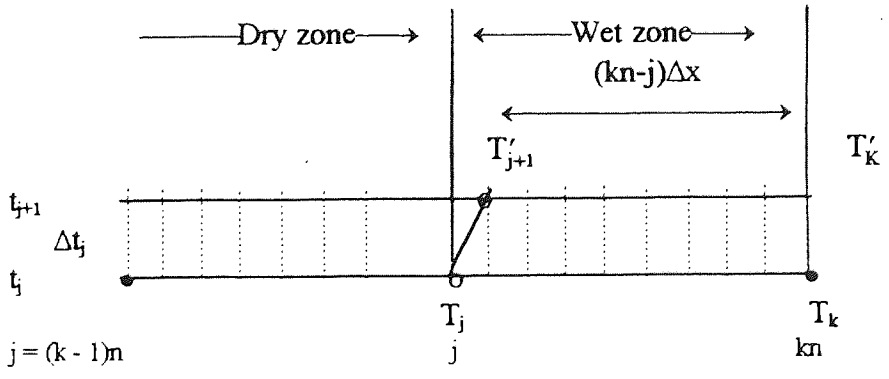

Figure A.7 The receding evaporation front near the bottom of the bed.

$$T_k' = T_k + \frac{2\alpha_w \Delta tj}{(n\Delta x)^2}(T_{k-1} - T_k) \qquad \text{(A.2-9)}$$

For the case (k-1)n < j ≤ kn, according to Fig. A.7 the following equation can be obtained,

$$T_k' = T_k + \frac{2\alpha_w \Delta tj}{(kn - j)^2 \Delta x^2}(T_j - T_k) \qquad \text{(A.2-10)}$$

A.2.3 Boundary Condition At x = f(t)

The moving boundary condition at x = f(t) is

$$-\lambda_d \frac{\partial T_d}{\partial x} = -\lambda_w \frac{\partial T_w}{\partial x} + \mathbf{m}\Delta hv \qquad \text{(A.2-11)}$$

Where **m** is the drying rate and was calculated in Chapter 6.0 as,

$$\mathbf{m} = \frac{Mw}{RT} \frac{s(T_f - T_{dew})}{(\frac{1}{k_c'} + \frac{f(t)}{D_{eff}})} \qquad \text{(A.2-12)}$$

and s is the slope of the saturated curve of water as,

$$s = \frac{P_f - P_{va}}{T_f - T_{dew}} \qquad \text{(A.2-13)}$$

1. For the case 0 < j < n and with using Eq. (A.1-9) and Eq. (A.1-17):

$$-\lambda_d \frac{T'_j - T'_0}{j\Delta x} = -\lambda_w \frac{-n[2(i-j)+3n]T'_j + (i+2n-j)^2 T'_{i+1} - (i+n-j)^2 T'_{i+2}}{n(i+n-j)\,(i+2n-j)\Delta x} + \frac{s(T'_j - T_{dew})\Delta hv}{\frac{RT}{k'_c Mw} + j\Delta x(\frac{RT}{D_{eff} Mw})} \qquad \text{(A.2-14)}$$

and if $j < n$ then $i = 0$; substituting Eq. (A.2-3) for T'_0 gives,

$$T'_j = \frac{\frac{\lambda_d C_0 j\Delta x h T_a}{j\Delta x h + \lambda_d} + \frac{sC_0 j\Delta x \Delta hv}{(\frac{RT}{k'_c Mw}) + j\Delta x(\frac{RT}{D_{eff} Mw})} T_{dew} + \lambda_w j(2n-j)^2 T'_1 - \lambda_w j(n-j)^2 T'_2}{\lambda_d C_0 - \frac{\lambda_w^2 C_0}{j\Delta x h + \lambda_d} + \lambda_w jn(3n-2j) + \frac{sC_0 \Delta hv\, j\Delta x}{(\frac{RT}{k'_c Mw}) + j\Delta x(\frac{RT}{D_{eff} Mw})}} \qquad \text{(A.2-15)}$$

where

$$C_0 = n(n-j)\,(2n-j) \qquad \text{(A.2-16)}$$

2. For the case: $j = n$, i.e. the front lies on the first main grid point, the boundary condition can be written using Eq. (A.1-8) as,

$$-\lambda_d \frac{T'_1 - T'_0}{n\Delta x} = -\lambda_w \frac{-3T'_1 + 4T'_2 - T'_3}{2n\Delta x} + \frac{s(T'_1 - T_{dew})\Delta hv}{(\frac{RT}{k'_c Mw}) + n\Delta x(\frac{RT}{D_{eff} Mw})} \qquad \text{(A.2-17)}$$

and the substitution of T'_0 by Eq. (A.2-3) gives

$$T_1' = \frac{\dfrac{2\lambda_d n\Delta x h T_a}{n\Delta x h + \lambda_d} + \dfrac{2sn\Delta x\Delta hv T_{dew}}{\left(\dfrac{RT}{k_c' Mw}\right) + n\Delta x\left(\dfrac{RT}{D_{eff} Mw}\right)} + 4\lambda_w T_2' - \lambda_w T_3'}{2\lambda_d - \dfrac{2\lambda_d^2}{n\Delta x h + \lambda_d} + 3\lambda_w + \dfrac{2sn\Delta x\Delta hv}{\left(\dfrac{RT}{k_c' Mw}\right) + n\Delta x\left(\dfrac{RT}{D_{eff} Mw}\right)}} \qquad \text{(A.2-18)}$$

3. For the case $n < j < 2n$ with the substitution of Eqs. (A.1-16) and (A.1-17) and considering that $i = n$ and $T_n' = T_1'$, the boundary condition will be:

$$-\lambda_d \frac{(j-n)^2 T_0' - j^2 T_1' + n(2j-n)T_j'}{n(j-n)j\Delta x} = -\lambda_w \frac{-n(5n-2j)T_j' + (3n-j)^2 T_2' - (2n-j)^2 T_3'}{n(2n-j)\,(3n-j)\Delta x} + \frac{s(T_j' - T_{dew})\Delta hv}{\left(\dfrac{RT}{k_c' Mw}\right) + j\Delta x\left(\dfrac{RT}{D_{eff} Mw}\right)} \qquad \text{(A.2-19)}$$

Introducing:

$$C_1 = j(j - n) \qquad \text{(A.2-20)}$$

$$C_2 = (2n - j)\,(3n - j) \qquad \text{(A.2-21)}$$

and substituting Eq. (A.2-4) for T_0', the correlation can be solved and gives

$$T_j' = \frac{1}{b_1}\Bigg\{ \frac{sC_1C_2n\Delta x\Delta hv T_{dew}}{\left(\dfrac{RT}{k_c' Mw}\right) + j\Delta x\left(\dfrac{RT}{D_{eff} Mw}\right)} - \frac{\lambda_d C_1 C_2 n(j-n)^2 \Delta x h T_a}{\lambda_d(j^2 - n^2) + hnC_1\Delta x} + \left[\lambda_d j^2 C_2 - \frac{\lambda_d^2 C_2 (j-n)^2 j^2}{\lambda_d(j^2 - n^2) + hnC_1\Delta x}\right] T_1' + \lambda_w C_1 (3n-j)^2 T_2' - \lambda_w C_1 (2n-j)^2 T_3' \Bigg\} \qquad \text{(A.2-22)}$$

where

$$b_1 = \lambda_d C_2 n(2j-n) - \frac{\lambda_d^2 C_2 n^2 (j-n)^2}{\lambda_d (j^2 - n^2) + hnC_1 \Delta x} +$$

$$\lambda_w C_1 n(5n-2j) + \frac{sC_1 C_2 n \Delta x \Delta hv}{(\frac{RT}{k_c' Mw}) + j\Delta x(\frac{RT}{D_{eff} Mw})} \qquad \text{(A.2-23)}$$

4. For the case j - 2n, on the basis of Esq. (A.1-8) and (A.1-14), the boundary condition becomes:

$$-\lambda_d \frac{T_0' - 4T_1' + 3T_2'}{2n\Delta x} = -\lambda_w \frac{-T_4' + 4T_3' - 3T_2'}{2n\Delta x} + \frac{s(T_2' - T_{dew})\Delta hv}{(\frac{RT}{k_c' Mw}) + 2n\Delta x(\frac{RT}{D_{eff} Mw})} \qquad \text{(A.2-24)}$$

substituting T_0' in Eq. (A.2-5) and rearranging:

$$T_2' = \frac{1}{b_2}\Big\{ \frac{2sn\Delta x \Delta h_v T_{dew}}{(\frac{RT}{k_c' Mw}) + 2n\Delta x(\frac{RT}{D_{eff} Mw})} - \frac{2\lambda_d n \Delta x h T_a}{3\lambda_d + 2n\Delta x h} +$$

$$\left[4\lambda_d - \frac{4\lambda_d^2}{3\lambda_d + 2n\Delta x h}\right] T_1' + 4\lambda_w T_3' - \lambda_w T_4' \Big\} \qquad \text{(A.2-25)}$$

where

$$b_2 = 3\lambda_d - \frac{\lambda_d^2}{3\lambda_d + 2n\Delta x h} + 3\lambda_w + \frac{2sn\Delta x \Delta hv}{(\frac{RT}{k_c' Mw}) + 2n\Delta x(\frac{RT}{D_{eff} Mw})} \qquad \text{(A.2-26)}$$

5. For the case $2n < j < (k-2)n$, applying Eqs. (A.1-16) and (A.1-17) and with the following considerations,

$2n < j < 3n$, then $i = 2n$

$3n < j < 4n$, then $i = 3n$

$$\vdots \qquad\qquad \vdots$$

$$(k-3)n < j < (k-2)n \qquad\qquad i = (k-3)n$$

the boundary condition becomes:

$$-\lambda_d \frac{(j-i)^2 T'_{i-1} - (j-i+n)^2 T'_i + n[2(j-i)+n]T'_j}{n(j-i+n)\,(j-i)\Delta x} =$$

$$-\lambda_w \frac{-n[2(i-j)+3n]T'_j + (i+2n-j)^2 T'_{i+1} - (i+n-j)^2 T'_{i+2}}{n(i+n-j)\,(i+2n-j)\Delta x} +$$

$$\frac{s(T'_j - T_{dew})\Delta hv}{(\frac{RT}{k'_c Mw}) + j\Delta x(\frac{RT}{D_{eff} Mw})} \qquad \text{(A.2-27)}$$

with introducing

$$C_3 = (j-i+n)\,(j-i) \qquad \text{(A.2-28)}$$

$$C_4 = (i+n-j)\,(i+2n-j) \qquad \text{(A.2-29)}$$

and solving with respect to T'_j yields:

$$T'_j = \frac{1}{b_3}\Big\{ \frac{sC_3C_4n\Delta x\Delta hv}{(\frac{RT}{k'_c Mw}) + j\Delta x(\frac{RT}{D_{eff} Mw})} T_{dew} - \lambda_d C_4 (j-i)^2 T'_{i-1} + \lambda_d C_4 (j-i+n)^2 T'_i +$$

$$\lambda_w C_3 (i+2n-j)^2 T'_{i+1} - \lambda_w C_3 (i+n-j)^2 T'_{i+2}\Big\} \qquad \text{(A.2-30)}$$

where

$$b_3 = \lambda_d C_4 n[2(j-i)+n] + \lambda_w C_3 n[2(i-j)+3n] + \frac{sC_3C_4n\Delta x\Delta hv}{(\frac{RT}{k'_c Mw}) + j\cdot\Delta x(\frac{RT}{D_{eff} Mw})} \qquad \text{(A.2-31)}$$

6. For the case $(k - 2)n < j < (k - 1)n$, $i = (k-2)n$, thus $T'_{i+2} = T'_k$. The unknown term T'_j may be calculated on the basis of Eq. (A.2-30); but first T'_k must be determined on the basis of Eq. (A.2-9).

7. For the case $(k - 1)n < j < kn$,taking into account Fig. A.7 and the second degree approximation for the temperature distribution give,

$$\left.\frac{\partial T_w}{\partial x}\right|_{f(t)+} \approx 2\frac{T'_k - T'_j}{(kn - j)\Delta x} \tag{A.2-32}$$

and since $i = (k - 1)n$, further by using Eq. (A.1-16), the boundary condition can be written as

$$-\lambda_d \frac{(j-i)^2 T'_{i-1} - (j-i+n)^2 T'_i + n[2(j-i)+n]T'_j}{n(j-i+n)(j-i)\Delta x} =$$

$$-\lambda_w \frac{2(T'_k - T'_j)}{(kn - j)\Delta x} + \frac{s(T'_j - T_{dew})\Delta hv}{(\frac{RT}{k'_c Mw}) + j\Delta x(\frac{RT}{D_{eff} Mw})} \tag{A.2-33}$$

and T'_k may be calculated on the basis of the second boundary condition, according to Eq. (A.2-10) which gives,

$$T'_j = \frac{1}{b_4}\Big\{ \frac{sC_3 n\Delta x(kn - j)\Delta hv}{(\frac{RT}{k'_c Mw}) + j\Delta x(\frac{RT}{D_{eff} Mw})} T_{dew} - \lambda_d (kn - j)(j-i)^2 T'_{i-1} +$$

$$\lambda_d (kn - j)(j-i+n)^2 T'_i + 2\lambda_w n C_3 T'_k \tag{A.2-34}$$

where

$$b_4 = \lambda_d (kn - j)n[2(j-i)+n] + 2\lambda_w n C_3 + \frac{sC_3 n(kn - j)\Delta x\,\Delta hv}{(\frac{RT}{k'_c Mw}) + j\Delta x(\frac{RT}{D_{eff} Mw})} \tag{A.2-35}$$

8. For the case j = 3n, 4n, ... (k - 2)n, the drying front will coincide with a main grid point, therefore the main grid points equations can be applied. Thus,

if $j = 3n \rightarrow i = 3n$

$j = 4n \rightarrow i = 4n$

etc. ⋮ ⋮

$j = (k - 2)n \rightarrow i = (k - 2)n$

and the boundary condition can be written as:

$$-\lambda_d \frac{T'_{i-2} - 4T'_{i-1} + 3T'_i}{2n\Delta x} = -\lambda_w \frac{-3T'_i + 4T'_{i+1} - T'_{i+2}}{2n\Delta x} + \frac{s(T'_i - T_{dew})\Delta hv}{(\frac{RT}{k'_c Mw}) + j\Delta x(\frac{RT}{D_{eff} Mw})} \quad \text{(A.2-36)}$$

which leads to,

$$T'_i = \frac{\frac{2sn\Delta x\Delta hv}{(\frac{RT}{k'_c Mw}) + j\Delta x(\frac{RT}{D_{eff} Mw})} T_{dew} - \lambda_d T'_{i-2} + \lambda_d 4T'_{i-1} + 4\lambda_w T'_{i+1} - \lambda_w T'_{i+2}}{3\lambda_d + 3\lambda_w + \frac{2sn\Delta x\Delta hv}{(\frac{RT}{k'_c Mw}) + j\Delta x(\frac{RT}{D_{eff} Mw})}} \quad \text{(A.2-37)}$$

9. In the case j = (k - 1)n, the drying front will meet the last internal main grid point. Thus on the basis of Fig. A.8 and since i = (k - 1)n and $T'_i = T'_{k-1}$; the boundary condition can be written as:

$$-\lambda_d \frac{T'_{k-3} - 4T'_{k-2} + T'_{k-1}}{2n\Delta x} = -\lambda_w 2\frac{T'_k - T'_{k-1}}{n\Delta x} + \frac{s(T'_{k-1} - T_{dew})\Delta hv}{(\frac{RT}{k'_c Mw}) + j\Delta x(\frac{RT}{D_{eff} Mw})} \quad \text{(A.2-38)}$$

which leads to,

$$T'_{k-1} = \frac{\dfrac{2snA\Delta x\Delta hv}{(\dfrac{RT}{k'_c Mw}) + j\Delta x(\dfrac{RT}{D_{eff} Mw})} T_{dew} - \lambda_d T'_{k-3} + \lambda_d 4T'_{k-2} + 4\lambda_w T'_k}{3\lambda_d + 4\lambda_w + \dfrac{2snA\Delta x\Delta hv}{(\dfrac{RT}{k'_c Mw}) + j\Delta x(\dfrac{RT}{D_{eff} Mw})}} \qquad \text{(A.2-39)}$$

A.3 Solution For The Dry Zone

In Chapter 6, dry and wet zone equations were described as follows,

$$\frac{\partial T_d}{\partial t} = \alpha_d \frac{\partial^2 T_d}{\partial x^2} \qquad \text{(A.3.1)}$$

and

$$\frac{\partial T_w}{\partial t} = \alpha_w \frac{\partial^2 T_w}{\partial x^2} \qquad \text{(A.3-2)}$$

The differential equation for the dry zone can be determined numerically.

1. For the case $0 < j \leq n$, there is no internal point (main grid point) for the dry zone;

2. For the case $j = n + 1$, only two points occur within the dry zone, thus the approximation of the second derivative with respect to location cannot be applied in the usual way.

The temperature change at x:

$$dT_x = \left(\frac{\partial T}{\partial t}\right)_x dt + \left(\frac{\partial T}{\partial x}\right)_x dx \qquad \text{(A.3-3)}$$

Therefore,

$$\frac{dT_x}{dx} = \left(\frac{\partial T}{\partial t}\right)_x \frac{1}{\frac{dx}{dt}} + \left(\frac{\partial T}{\partial x}\right)_x \tag{A.3-4}$$

At the front, location x may be considered as the common point of both the dry region and the wet region. Thus, the temperature of the dry zone equals the temperature of the wet zone, which gives,

$$\frac{\partial T_d}{\partial x} = \frac{\partial T_w}{\partial x} \tag{A.3-5}$$

By using Eq. (A.3-4), and substituting Eq. (A.3-1) and (A.3-2) for the two regions gives,

$$\left(\alpha_d \frac{\partial^2 T_d}{\partial x^2}\right) \frac{1}{\frac{dx}{dt}} + \frac{\partial T_d}{\partial x} = \alpha_w \frac{\partial^2 T_w}{\partial x^2} \frac{1}{\frac{dx}{dt}} + \frac{\partial T_w}{\partial x} \tag{A.3-6}$$

Therefore,

$$\frac{\partial^2 T_d}{\partial x^2} = \frac{\alpha_w}{\alpha_d} \frac{\partial^2 T_w}{\partial x^2} + \frac{dx}{dt}\left[\frac{\partial T_w}{\partial x} - \frac{\partial T_d}{\partial x}\right] \frac{1}{\alpha_d} \tag{A.3-7}$$

and the substitution of Eq. (A.3-7) into Eq. (A.3-1) gives:

$$\frac{\partial T_d}{\partial t} = \alpha_w \frac{\partial^2 T_w}{\partial x^2} + \frac{dx}{dt}\left[\frac{\partial T_w}{\partial x} - \frac{\partial T_d}{\partial x}\right] \tag{A.3-8}$$

Transcribing Eq. (A.3-8) to a differential equation, at the instant of time j = n + 1 and at the location i = n at the first main grid point, the temperature variation can be expressed by

$$\frac{T_i' - T_i}{\Delta t_j} = \alpha_w \frac{T_i - 2T_{i+1} + T_{i+2}}{(n\Delta x)^2} + v_{j-1}\left(\frac{T_{i+1} - T_i}{n\Delta x} - \frac{T_i - T_{i-1}}{n\Delta x}\right) \qquad \text{(A.3-9)}$$

where v is velocity of the front, can be defined as $v_{j-1} = \Delta x/\Delta tj$.

Substituting Eq. (A.3-9) and rearranging gives

$$T_i' = \frac{1}{n}T_{i-1} + \left[\frac{\alpha_w \Delta t_j}{(n\Delta x)^2} + 1 - \frac{2}{n}\right]T_i + \left[\frac{1}{n} - \frac{2\alpha_w \Delta t_j}{(n\Delta x)^2}\right]T_{i+1} + \frac{\alpha_w \Delta t_j}{(n\Delta x)^2}T_{i+2} \qquad \text{(A.3-10)}$$

Similarly, if j = (k - 1)n + 1, then at i = (k - 1)n and because of the symmetry condition $T_i = T_{i+2}$, we obtain

$$T_i' = \frac{1}{n}T_{i-1} + \left[\frac{2\alpha_w \Delta t_j}{(n\Delta x)^2} + 1 - \frac{2}{n}\right]T_i + \left[\frac{1}{n} - \frac{2\alpha_w \Delta t_j}{(n\Delta x)^2}\right]T_{i+1} \qquad \text{(A.3-11)}$$

3. The points, determinable by the equations of main grid points, with respect to location, applying Eqs. (A.1-1) - (A.1-3) are as follows:

- for the time steps $2n + 1 \le j \le 3n$, at i = n;
- for the time steps $3n + 1 \le j \le 4n$, at i = n, 2n, etc.

⋮

- for the time steps $(k - 1)n + 1 \le j \le k\,n$, at i = n, 2n, 3n, ... (k - 2)n;

respectively, Eq. (A.3-1) can be rewritten as

$$\frac{T_i' - T_i}{\Delta t_j} = \alpha_d \frac{T_{i+1} - 2T_i + T_{i-1}}{(n\Delta x)^2} \qquad \text{(A.3-12)}$$

Rearranging yields:

$$T_i' = \frac{\alpha_d \Delta t_j}{(n\Delta x)^2} T_{i-1} + \left[1 - \frac{2\alpha_d \Delta t_j}{(n\Delta x)^2}\right] T_i + \left[\frac{\alpha_d \Delta t_j}{(n\Delta x)^2}\right] T_{i+1} \qquad \text{(A.3-13)}$$

4. The points determinable by the equations of non-main grid points, applying Eqs. (A.1-1), (A.1-2) and (A.1-18), are as follows:

- for time steps $n + 2 \le j \le 2n$, at $i = n$
- for time steps $2n + 2 \le j \le 3n$, at $i = 2n$

$$\vdots$$

- for time steps $(k - 1)n + 2 \le j \le kn$, at $i = (k - 1)n$, respectively, Eq. (A.3-1) becomes:

$$\frac{T_i' - T_i}{\Delta t_j} = 2\alpha_d \frac{(j-1-i)T_{i-1} - (n+j-i-1)T_i + nT_{j-1}}{n(j-1-i)(n+j-1-i)\Delta x^2} \qquad \text{(A.3-14)}$$

Rearranging gives:

$$T_i' = \frac{2\alpha_d \Delta t_j}{n(n+j-1-i)\Delta x^2} T_{i-1} + \left[1 - \frac{2\alpha_d \Delta t_j}{n(j-1-i)\Delta x^2}\right] T_i + \left[\frac{2\alpha_d \Delta t_j}{(j-1-i)(n+j-1-i)\Delta x^2}\right] T_{j-1} \qquad \text{(A.3-15)}$$

5. For time step $j - 2n + 1$, at $i = 2n$ Eq. (A.3-10) can be applied; 2 grid points being already provided at the former time step, the main grid formula could be applied too.

The equations to be applied in different cases are as follows:

- For the time step $0 < j \le n$ no internal main grid point occurs;
- for the time step $j = n + 1$, at $i = n$

  $T_{n,j}'$ can be computed according to Eq. (A.3-10)
- for the time step $n + 2 \le j \le 2n$, at $i = n$

T_i' can be computed according to Eq. (A.3-15)

- for the time step $j = 2n + 1$, at $i = 2n$

  T_i' can be computed according to Eq. (A.3-10)

- for the time step $2n + 2 \leq j \leq 3n$, at $i = 2n$

  T_i' can be computed according to Eq. (A.3-15)

  ⋮

- for the time step $j = (k - 1)n + 1$, at $i = (k - 1)n$

  T_i' can be computed according to Eq. (A.3-11)

- for the time step $(k - 1)n + 2 \leq j \leq kn$, at $i = (k - 1)n$

  T_i' can be computed according to Eq. (A.3-15)

- for the time step $2n + 1 \leq j \leq 3n$, at $i = n$

  T_i' can be computed according to Eq. (A.3-13)

- for the time step $3n + 1 \leq j \leq 4n$, at $i = n, 2n$

  T_i' can be computed according to Eq. (A.3-13)

  ⋮

- for the time step $(k - 1)n + 1 \leq j \leq kn$,

  at $i = n, 2n, 2n \ldots (k - 2)n$

  T_i' can be computed according to Eq. (A.3-13).

A.4 Solution For The Wet Zone

The differential equations for the wet zone can be calculated numerically.

1. The internal points, computable by the equation of main grid points with respect to location, are as follows:

- for time levels $0 < j \leq n + 1$,

  at $i = 2n, 3n \ldots (k - 1)n$

- for time levels $n + 2 \leq j \leq 2n + 1$,

  at $i = 3n, 4n, \ldots (k - 1)\, n$

⋮

- for time levels $(k-3)n + 2 \le j \le (k - 2)n + 1$,

  at $i = (k - 1)n$

$$\frac{T_i' - T_i}{\Delta t_j} = \alpha_w \frac{T_{i+1} - 2T_i + T_{i-1}}{(n\Delta x)^2} \tag{A.4-1}$$

Therefrom

$$T_i' = \frac{\alpha_w \Delta t_j}{(n\Delta x)^2} T_{i-1} + \left[1 - \frac{2\alpha_w \Delta t_j}{(n\Delta x)^2}\right] T_i + \frac{\alpha_w \Delta t_j}{(n\Delta x)^2} T_{i+1} \tag{A.4-2}$$

may be obtained.

2. The internal points - first points after the front - computable by non-main grid points with respect to location, are as follows:

- for the time levels $0 < j \le n + 1$, at $i = n$
- for the time levels $n + 2 \le j \le 2n + 1$, at $i = 2n$

⋮

- for the time levels $(k - 2)n + 2 \le j \le (k - 1)n$,

  at $i = (k - 1)n$

while after time step $j > (k - 1)n$, no internal main grid point will occur in the wet zone.

With the application of Eq. (A.1-19) the following correlation can be obtained:

$$\frac{T_i' - T_i}{\Delta t_j} = 2\alpha_w \frac{nT_{j-1} - (i + 1 - j + n)T_i + (i + 1 - j)T_{i-1}}{n(n + i + 1 - j)(i + 1 - j)\Delta x^2} \tag{A.4-3}$$

whereas

$$T_i' = \frac{2\alpha_w \Delta t_j}{(n+i+1-j)(i+1-j)\Delta x^2} T_{j-1} + T_i \left[1 - \frac{2\alpha_w \Delta t_j}{n(i+1-j)\Delta x^2} \right] +$$

$$\frac{2\alpha_w \Delta t_j}{n(n+i+1-j)\Delta x^2} T_{i+1} \qquad \text{(A.4-4)}$$

APPENDIX B

COMPUTER PROGRAM

A complete computer program for solving the temperature distribution in a thick bed of solids is shown in this appendix. The program can calculate the temperature at any desired depth. In the current research, a bed of 0.032 m depth was divided into eight portions, i.e. k = 8. Each portion has a thickness of 0.004 m, i.e. $n\Delta x = 0.004$ m. Thus, the program will calculate temperatures at nine levels.

Δn and n can be chosen as any small numbers. These however can be approximated as follows:

The velocity of the evaporation front decelerates with time. Thus, the final movement of the front is assumed to be very small and represents the minimum movement as

$$\Delta x^* = v^* \cdot \Delta t^* \tag{B.1}$$

where Δt^* is the time required for the front to move distance Δx^*. This interval, Δt^*, can be correlated by the finite difference method as a main grid point near the bottom of the bed which gives,

$$\frac{2\alpha_w}{(n\Delta x)^2} \cong \frac{1}{\Delta t^*} \tag{B.2}$$

rearranging Eq. (B.2) as

$$\Delta t^* \leq \frac{(n\Delta x)^2}{2\alpha_w} \tag{B.3}$$

The velocity of the front v* can be calculated by using Eq. (6.4-20) with replacing T_f by T_a, since at the end of the drying process, the temperature of the front can be assumed equal to T_a. (At the beginning of the falling rate period, the evaporation front is at the surface, hence $T_f = T_{wb}$). Thus, Eq. (B.1) can be solved, giving an approximate value for Δx^*. For example, the calculated Δx^* for the 100 μm glass beads will be 1.53×10^{-6} m. Therefore, the approximation value for n* can be written as,

$$n^* = \frac{n\Delta x}{\Delta x^*} = \frac{0.004}{1.53 \times 10^{-6}} = 2614.38 \qquad \text{(B.4)}$$

Therefore, any number around 2614.38 can give a suitable solution. For practical computational purposes, the distribution of grid point n = 2000 was considered which gave $\Delta x = 2 \times 10^{-6}$ m.

```
{ A Computer Program For The Model of Thick Beds Solids}
{..Written by: A.A.Almubarak, 1995  }

program drying;

const k=8; n=2000;
      dx=0.000002; p=10;
      tp=52; tcr=150;

var   ii,ll,m,tj,y,z:integer;
      j,i,l   :longint;
      c0,c1,c2,c4 :double;
      Twb,Ta,Td,T0,h,G,alfd,alfw,Lad,Law,dhv,R,s,Lam,
      alfm,u1,taa,tbb,tcc,v,dt,tk,tk2,Ts,q,qq,si,sf,
      dlw,por,mp:double;

TT:array[0..k,1..2]  of real;
x:array[0..k,1..2]   of real;
zz:array[0..k,1..2]  of real;
TTT:array[0..k,1..2] of real;
t:array[0..k+1,1..2] of double;

input: text ;
result: text;
label y1,y2,y3,y4,y5,y6,y7,y8,y9,y10,y20;

begin
  assign (input,  'a:dryinput.dat' );
  assign (result, 'c:dryresult.dat');
  reset (input);
  rewrite (result);

readln (input,Twb,Ta,Td,T0,si,sf,h,G,alfd,alfw,Lad,Law,
        dhv,R,s,dlw,por,mp,Lam,alfm);

{Twb: wet bulb temperature (C)}
{Ta: air temperature (C)}
{Td:dew-point temperature (C)}
{T0:initial temperature (C)}
{si:initial slop=(ps-pva)/(Twb-Td) (atm/C)}
{sf:final slop=(pa-pva)/(Ta-Td)    (atm/C)}
{h:heat transfer coefficient (kcal/sq.m C)}
{G: G=RT/MwDeff.(atm.m.hr/kg)}
{alfd:eff. thermal diffusivity of dry zone(sq.m/hr)}
{alfw:eff. thermal diffusivity of wet zone(sq.m/hr)}
{Lad:eff. thermal cond. of dry zone(kcal/mhrC)}
{Law:eff. thermal cond. of wet zone(kcal/mhrC)}
{dhv:latent heat of evaporation (kcal/kg)}
{R: R=RT/Mwkc (atm.hr.sq.m/kg) }
{s:average slop=(si+sf)/2  (atm/C)}
{dlw:density of liguid water(kg/cu.m)}
{por:porosity}
{mp:drying rate of pre-constant rate period(kg/hr-sq.m)}
{Lam:eff. thermal cond. of wet material(kcal/mhrC)}
{alfm:eff. thermal diffusivity of wet material(sq.m/hr)}
```

```
{.....Pre-Constant Rate Period...}

x[0,1]:= 0.0     ;
zz[0,1]:= 0.0 ;

writeln(result);writeln(result);
writeln(result);writeln(result);
for z:=0 to k do begin
zz[z+1,1]:=zz[z,1]+(n*dx);
writeln(result,'                          T',z, ' : Temp. at  x= ',
         zz[z,1]*100:3:2,'  cm');
end;
writeln(result);writeln(result);
writeln(result);

writeln(result,'            The predicted results are:');
writeln(result);
for tj:=1 to tp  do begin
taa:=tj;
if tj=tp then goto y10;
if tj/p=int(tj/p) then

y10:
begin
writeln(result);
writeln(result,'              Time: ',taa:3:2,'  min.');

for y:=0 to k   do begin

x[y+1,1]:=x[y,1]+(n*dx) ;
Ts:=(T0+Twb)/2 ;
q:=h*(Ta-Ts)-mp*dhv ;
qq:=sqrt(6*alfm*tj/60)-x[y,1]*2+x[y,1]*x[y,1]/
    sqrt(6*alfm*tj/60) ;
TT[y,1]:=T0+q*qq*0.5/Lam ;
write(result,'              T',y,'=',TT[y,1]:3:2);
end; writeln(result);

end;
end;

{.....Constant Rate Period.....}

for tj:=tp to tcr   do begin

tbb:=tj;
if tj=tcr then goto  y20;
if tj/(2*p)=int(tj/(2*p)) then
y20:
begin
writeln(result);
writeln(result,'              Time: ',tbb:3:2,'  min.');
```

```
for y:=0 to 2   do begin
TTT[y,1]:=TT[y,1];
write(result,'                T',y,'=',TTT[y,1]:3:2);
end;
writeln(result);

for y:=3 to 5   do begin
TTT[y,1]:=TT[y,1];
write(result,'                T',y,'=',TTT[y,1]:3:2);
end;
writeln(result);

for y:=6 to k   do begin
TTT[y,1]:=TT[y,1];
write(result,'                T',y,'=',TTT[y,1]:3:2);
end;
writeln(result);

end;
end;

{.....Falling Rate period.....}

v:=(Twb-Td)*si/(dlw*por*R);
for ii:=0 to k do
begin t[ii,1]:=TTT[ii,1];
end;
j:=0; tcc:=tcr;

y6:
dt:=dx/v;
tcc:=tcc+(dt*60);
i:=0;
ii:=0;
j:=j+1;

y8:
ii:=ii+1;
i:=ii*n;
if i=k*n then goto y7;
if i<j then

{.....Dry Zone..... }

if j=i+1 then
if j=(k-1)*n+1 then
begin
tk:=t[ii-1,1]/n+(2*alfw*dt/sqr(n*dx)+1-2/n)*t[ii,1];
t[ii,2]:=tk+(1/n-2*alfw*dt/sqr(n*dx))*t[ii+1,1];
goto y8;
end
else
```

```
begin
tk:=t[ii-1,1]/n+(alfw*dt/sqr(n*dx)+1-2/n)*t[ii,1];
t[ii,2]:=tk+(1/n-2*alfw*dt/sqr(n*dx))*t[ii+1,1]+alfw*dt/
         sqr(n*dx)*t[ii+2,1];
goto y8;
end
else
if i<j-n then
begin
tk:=alfd*dt/sqr(n*dx)*t[ii-1,1];
tk:=tk+(1-2*alfd*dt/sqr(n*dx))*t[ii,1];
t[ii,2]:=tk+(alfd*dt/sqr(n*dx))*t[ii+1,1];
goto y8;
end
else
begin
c1:=n+j-1-i;       c2:=j-1-i;
tk:=2*alfd*dt/(sqr(dx)*c1*n)*t[ii-1,1];
tk:=tk+(1-2*alfd*dt/(sqr(dx)*n*c2))*t[ii,1];
t[ii,2]:=tk+(2*alfd*dt/(sqr(dx)*c2*c1))*t[k+1,1];
goto y8;
end
else

{.....Wet Zone .....}

if i<>j then
begin
if i>=j+n-1 then
begin
tk:=alfw*dt/sqr(n*dx)*t[ii-1,1]+(1-2*alfw*dt/sqr(n*dx))*
    t[ii,1];
t[ii,2]:=tk+alfw*dt/sqr(n*dx)*t[ii+1,1];
goto y8;
end
else
begin
tk:=2*alfw*dt/(sqr(dx)*(n+i+1-j)*(i+1-j))*t[k+1,1];
tk:=tk+(1-2*alfw*dt/(sqr(dx)*n*(i+1-j)))*t[ii,1];
t[ii,2]:=tk+2*alfw*dt/(sqr(dx)*n*(n+i+1-j))*t[ii+1,1];
goto y8;
end;
end
else
begin
tk:=alfw*dt/sqr(n*dx)*t[ii-1,1]+(1-2*alfw*dt/sqr(n*dx))*
    t[ii,1];
t[ii,2]:=tk+alfw*dt/sqr(n*dx)*t[ii+1,1];
goto y8;
end;
```

```
{.....Boundary Conditions .....}

y7:
if j<=(k-1)*n then
t[ii,2]:=t[ii,1]+2*alfw*dt/sqr(n*dx)*
         (t[ii-1,1]-t[ii,1])
else
t[ii,2]:=t[ii,1]+2*alfw*dt/sqr((k*n-j)*dx)*
         (t[k+1,1]-t[ii,1]);
l1:=j div n;
l:=l1*n;
if l1=0 then goto y1;
if l1=1 then goto y2;
if l1=2 then goto y3;
if l1=k-1 then goto y5
else goto y4;

y1:
begin
c0:=2*n-j;
c0:=c0*n*(n-j);
tk:=Lad*c0*j*dx*h*Ta/(dx*j*h+Lad)+s*c0*j*dx*dhv/
    (R+dx*j*G)*Td;
tk:=tk+Law*j*sqr(2*n-j)*t[1,2]-Law*j*sqr(n-j)*t[2,2];
tk2:=Lad*c0-Lad*Lad*c0/(dx*j*h+Lad)+Law*j*n*(3*n-2*j);
tk2:=tk2+s*c0*dhv*j*dx/(R+dx*j*G);
t[k+1,2]:=tk/tk2;
end;
goto y9;

y2:
if j=n then
begin
tk:=2*Lad*n*dx*h*Ta/(n*dx*h+Lad)+2*s*n*dx*dhv*Td/
    (R+n*dx*G);
tk:=tk+4*Law*t[2,2]-Law*t[3,2];
tk2:=2*Lad-2*Lad*Lad/(n*dx*h+Lad)+3*Law+2*s*n*dx*dhv/
     (R+n*dx*G);
t[k+1,2]:=tk/tk2;
t[1,2]:=t[k+1,2];
end
else
begin
c1:=j;     c1:=c1*(j-n);
c2:=2*n-j;      c2:=c2*(3*n-j);
tk:=s*c1*c2*n*dx*dhv*Td/(R+dx*j*G);
tk:=tk-Lad*c1*c2*n*sqr(j-n)*dx*h*Ta/(Lad*(j*j-n*n)+
    h*n*c1*dx);
tk:=tk+(Lad*j*j*c2-c2*sqr(Lad*(j-n)*j)/(Lad*(j*j-n*n)+
    h*n*c1*dx))*t[1,2];
tk:=tk+Law*c1*sqr(3*n-j)*t[2,2]-Law*c1*sqr(2*n-j)*t[3,2];
u1:=Lad*c2*n*(2*j-n)-c2*sqr(Lad*n*(j-n))/(Lad*(j*j-n*n)+
    h*n*c1*dx);
u1:=u1+Law*c1*n*(5*n-2*j)+s*c1*c2*n*dx*dhv/(R+dx*j*G);
t[k+1,2]:=tk/u1;
end;
goto y9;
```

```
y3:
if j=2*n then
begin
u1:=3*Lad-Lad*Lad/(3*Lad+2*n*dx*h)+3*Law+2*s*n*dx*dhv/
    (R+2*n*dx*G);
tk:=2*s*n*dx*dhv*Td/(R+2*n*dx*G)-2*Lad*n*dx*h*Ta/
    (3*Lad+2*n*dx*h);
tk:=tk+(4*Lad-4*Lad*Lad/(3*Lad+2*n*dx*h))*t[1,2]+4*Law*
    t[3,2]-Law*t[4,2];
t[k+1,2]:=tk/u1;
t[2,2]:=t[k+1,2];
goto y9;
end
else
begin
c1:=j; c1:=c1-1+n;  c1:=c1*(j-1);
c4:=1; c4:=c4+n-j;  c2:=c4*1+c4*2*n-c4*j;
u1:=Lad*c2*n*(2*(j-1)+n)+Law*c1*n*(2*(1-j)+3*n)+
    s*c1*c2*n*dx*dhv/(R+dx*j*G);
tk:=s*c1*c2*n*dx*dhv/(R+dx*j*G)*Td-Lad*c2*sqr(j-1)*
    t[11-1,2];
tk:=tk+Lad*c2*sqr(j-1+n)*t[11,2]+Law*c1*sqr(1-j+2*n)*
    t[11+1,2];
t[k+1,2]:=(tk-Law*c1*sqr(1-j+n)*t[11+2,2])/u1;
end;
goto y9;

y4:
if j/n=j div n then
begin
tk:=2*s*n*dx*dhv/(R+dx*j*G)*Td-Lad*t[11-2,2]+Lad*4*
    t[11-1,2]+4*Law*t[11+1,2];
t[k+1,2]:=(tk-Law*t[11+2,2])/(3*Lad+3*Law+2*s*n*dx*dhv/
          (R+dx*j*G));
t[11,2]:=t[k+1,2];
end
else
begin
c1:=j; c1:=c1-1+n;  c1:=c1*(j-1);
c4:=1; c4:=c4+n-j;  c2:=c4*1+c4*2*n-c4*j;
u1:=Lad*c2*n*(2*(j-1)+n)+Law*c1*n*(2*(1-j)+3*n)+s*c1*
    c2*n*dx*dhv/(R+dx*j*G);
tk:=s*c1*c2*n*dx*dhv/(R+dx*j*G)*Td-Lad*c2*sqr(j-1)*
    t[11-1,2];
tk:=tk+Lad*c2*sqr(j-1+n)*t[11,2]+Law*c1*sqr(1-j+2*n)*
    t[11+1,2];
t[k+1,2]:=(tk-Law*c1*sqr(1-j+n)*t[11+2,2])/u1;
end;
goto y9;

y5:
if j=(k-1)*n then
```

```
begin
tk:=2*s*n*dx*dhv/(R+dx*j*G)*Td-Lad*t[k-3,2]+Lad*4*
    t[k-2,2]+4*Law*t[k,2];
t[k+1,2]:=tk/(3*Lad+4*Law+2*s*n*dx*dhv/(R+dx*j*G));
t[k-1,2]:=t[k+1,2];
goto y9;
end
else
begin
c1:=j;    c1:=c1-1+n;    c1:=c1*(j-1);
u1:=Lad*(k*n-j)*n*(2*(j-1)+n)+2*Law*n*c1+s*c1*n*
    (k*n-j)*dx*dhv/(R+dx*j*G);
tk:=s*c1*n*dx*(k*n-j)*dhv/(R+dx*j*G)*Td-Lad*(k*n-j)*
    sqr(j-1)*t[11-1,2];
t[k+1,2]:=(tk+Lad*(k*n-j)*sqr(j-1+n)*t[11,2]+2*Law*n*
          c1*t[k,2])/u1;
end;

y9:
if j<=n then
t[0,2]:=(dx*j*h*Ta+Lad*t[k+1,2])/(dx*j*h+Lad)
else
if j<2*n then
begin
tk:=dx*n*j*(j-n)*h*Ta+Lad*j*j*t[1,2]-Lad*n*n*t[k+1,2];
t[0,2]:=tk/(Lad*(j*j-n*n)+h*n*j*(j-n)*dx);
end
else
begin
tk:=n*2*dx*h*Ta+4*Lad*t[1,2]-Lad*t[2,2];
t[0,2]:=tk/(3*Lad+2*h*n*dx);
end;
v:=(T[k+1,2]-Td)*s/(dlw*por*(R+dx*j*G));
for ii :=0 to k+1 do
t[ii,1]:=t[ ii,2];
if 2*j/n=int(2*j/n) then
begin
writeln(result);
writeln (result,'              Time: ', tcc:4:2,' min.');
writeln ('j=',j);

for ii:=0 to 2 do begin
write(result,'              T',ii,'=' , t[ ii,1]:3:2);
end;
writeln(result);

for ii:=3 to 5 do begin
write(result,'              T',ii,'=' , t[ii,1]:3:2)
end;
writeln(result);
```

```
for ii:=6 to k do begin
write(result,'                T',ii,'=' , t[ii,1]:3:2);
end;
writeln(result);
end;

if j<k*n-1 then goto y6;
writeln(result);
writeln (result,'             Total time:',tcc:4:2,'min.');
writeln ('j=',j);
close (input);
close (result);
end.
```

APPENDIX C

PREDICTED RESULTS

1. Glass beads, 100 μm, air temperature 84°C

2. Polystyrene pellets, air temperature 84°C

3. Activated alumina, air temperature 84°C

4. Wood powder, air temperature 84°C

5. Glass beads, 100 μm, air temperature 64°C

6. Glass beads, 100 μm, air temperature 54°C

((Glass beads 100 μm, 84 °C))

T0 : Temp. at x= 0.00 cm
T1 : Temp. at x= 0.40 cm
T2 : Temp. at x= 0.80 cm
T3 : Temp. at x= 1.20 cm
T4 : Temp. at x= 1.60 cm
T5 : Temp. at x= 2.00 cm
T6 : Temp. at x= 2.40 cm
T7 : Temp. at x= 2.80 cm
T8 : Temp. at x= 3.20 cm

The predicted results are:

Time: 10.00 min.

T0=28.05	T1=27.31	T2=26.62
T3=25.97	T4=25.38	T5=24.83
T6=24.33	T7=23.88	T8=23.48

Time: 20.00 min.

T0=30.56	T1=29.81	T2=29.09
T3=28.41	T4=27.77	T5=27.16
T6=26.58	T7=26.04	T8=25.53

Time: 30.00 min.

T0=32.48	T1=31.73	T2=31.00
T3=30.31	T4=29.64	T5=29.00
T6=28.39	T7=27.81	T8=27.25

Time: 40.00 min.

T0=34.10	T1=33.35	T2=32.62
T3=31.91	T4=31.23	T5=30.58
T6=29.94	T7=29.34	T8=28.75

Time: 50.00 min.

T0=35.53	T1=34.77	T2=34.04
T3=33.33	T4=32.64	T5=31.97
T6=31.33	T7=30.70	T8=30.10

Time: 52.00 min.

T0=35.80	T1=35.04	T2=34.31
T3=33.60	T4=32.90	T5=32.24
T6=31.59	T7=30.96	T8=30.35

Time: 60.00 min.

T0=35.80	T1=35.04	T2=34.31
T3=33.60	T4=32.90	T5=32.24
T6=31.59	T7=30.96	T8=30.35

Time: 80.00 min.

T0=35.80	T1=35.04	T2=34.31
T3=33.60	T4=32.90	T5=32.24
T6=31.59	T7=30.96	T8=30.35

Time: 100.00 min.

T0=35.80	T1=35.04	T2=34.31
T3=33.60	T4=32.90	T5=32.24
T6=31.59	T7=30.96	T8=30.35

Time: 120.00 min.

T0=35.80	T1=35.04	T2=34.31
T3=33.60	T4=32.90	T5=32.24
T6=31.59	T7=30.96	T8=30.35

Time: 140.00 min.

T0=35.80	T1=35.04	T2=34.31
T3=33.60	T4=32.90	T5=32.24
T6=31.59	T7=30.96	T8=30.35

Time: 150.00 min.

T0=35.80	T1=35.04	T2=34.31
T3=33.60	T4=32.90	T5=32.24
T6=31.59	T7=30.96	T8=30.35

Time: 157.38 min.

T0=38.54	T1=35.42	T2=34.57
T3=33.87	T4=33.27	T5=32.77
T6=32.35	T7=32.00	T8=31.73

Time: 172.90 min.

T0=43.25	T1=38.51	T2=37.48
T3=36.57	T4=35.78	T5=35.10
T6=34.53	T7=34.07	T8=33.70

Time: 196.61 min.

T0=43.41	T1=40.12	T2=38.23
T3=37.67	T4=37.16	T5=36.68
T6=36.25	T7=35.86	T8=35.50

Time: 228.52 min.

T0=46.86	T1=42.97	T2=39.94
T3=39.40	T4=38.90	T5=38.44
T6=38.01	T7=37.61	T8=37.25

Time: 268.62 min.

T0=53.20	T1=49.68	T2=46.28
T3=44.26	T4=43.54	T5=42.89
T6=42.30	T7=41.77	T8=41.30

Time: 316.91 min.

T0=56.68	T1=53.54	T2=50.48
T3=47.50	T4=46.86	T5=46.25
T6=45.67	T7=45.14	T8=44.64

Time: 373.39 min.

T0=59.28	T1=56.43	T2=53.63
T3=50.89	T4=49.25	T5=48.68
T6=48.14	T7=47.61	T8=47.12

Time: 438.06 min.

T0=61.33	T1=58.71	T2=56.13
T3=53.59	T4=51.09	T5=50.55
T6=50.04	T7=49.53	T8=49.05

Time: 510.93 min.

T0=63.00	T1=60.57	T2=58.17
T3=55.80	T4=53.46	T5=52.05
T6=51.56	T7=51.08	T8=50.62

Time: 591.99 min.

T0=64.42	T1=62.15	T2=59.90
T3=57.68	T4=55.48	T5=53.31
T6=52.84	T7=52.38	T8=51.94

Time: 681.24 min.

T0=65.63	T1=63.50	T2=61.39
T3=59.29	T4=57.22	T5=55.17
T6=53.93	T7=53.50	T8=53.07

Time: 778.69 min.

T0=66.70	T1=64.69	T2=62.70
T3=60.72	T4=58.76	T5=56.81
T6=54.89	T7=54.47	T8=54.06

Time: 884.32 min.

T0=67.64	T1=65.74	T2=63.85
T3=61.98	T4=60.11	T5=58.27
T6=56.44	T7=55.33	T8=54.94

Time: 998.15 min.

T0=68.48	T1=66.68	T2=64.88
T3=63.10	T4=61.33	T5=59.57
T6=57.83	T7=55.95	T8=55.72

Time: 1120.18 min.

T0=73.30	T1=72.07	T2=70.88
T3=69.72	T4=68.60	T5=67.53
T6=66.50	T7=65.51	T8=65.03

Total time:1250.26min.

((Polystyrene pellets, 84°C))

T0 : Temp. at x= 0.00 cm
T1 : Temp. at x= 0.40 cm
T2 : Temp. at x= 0.80 cm
T3 : Temp. at x= 1.20 cm
T4 : Temp. at x= 1.60 cm
T5 : Temp. at x= 2.00 cm
T6 : Temp. at x= 2.40 cm
T7 : Temp. at x= 2.80 cm
T8 : Temp. at x= 3.20 cm

The predicted results are :

Time: 10.00 min.
T0=26.06 T1=24.70 T2=23.44
T3=22.26 T4=21.17 T5=20.17
T6=19.26 T7=18.43 T8=17.70

Time: 20.00 min.
T0=30.64 T1=29.27 T2=27.97
T3=26.72 T4=25.54 T5=24.43
T6=23.37 T7=22.38 T8=21.45

Time: 30.00 min.
T0=34.15 T1=32.78 T2=31.46
T3=30.19 T4=28.97 T5=27.80
T6=26.68 T7=25.61 T8=24.60

Time: 40.00 min.
T0=37.12 T1=35.74 T2=34.41
T3=33.12 T4=31.88 T5=30.68
T6=29.52 T7=28.41 T8=27.34

Time: 45.00 min.
T0=38.46 T1=37.08 T2=35.75
T3=34.45 T4=33.20 T5=31.99
T6=30.82 T7=29.69 T8=28.60

Time: 60.00 min.
T0=38.46 T1=37.08 T2=35.75
T3=34.45 T4=33.20 T5=31.99
T6=30.82 T7=29.69 T8=28.60

Time: 80.00 min.
T0=38.46 T1=37.08 T2=35.75
T3=34.45 T4=33.20 T5=31.99
T6=30.82 T7=29.69 T8=28.60

Time: 100.00 min.
T0=38.46 T1=37.08 T2=35.75
T3=34.45 T4=33.20 T5=31.99
T6=30.82 T7=29.69 T8=28.60

Time: 120.00 min.
T0=38.46 T1=37.08 T2=35.75
T3=34.45 T4=33.20 T5=31.99
T6=30.82 T7=29.69 T8=28.60

Time: 140.00 min.
T0=38.46 T1=37.08 T2=35.75
T3=34.45 T4=33.20 T5=31.99
T6=30.82 T7=29.69 T8=28.60

Time: 160.00 min.
T0=38.46 T1=37.08 T2=35.75
T3=34.45 T4=33.20 T5=31.99
T6=30.82 T7=29.69 T8=28.60

Time: 180.00 min.
T0=38.46 T1=37.08 T2=35.75
T3=34.45 T4=33.20 T5=31.99
T6=30.82 T7=29.69 T8=28.60

Time: 186.00 min.
T0=38.46 T1=37.08 T2=35.75
T3=34.45 T4=33.20 T5=31.99
T6=30.82 T7=29.69 T8=28.60

Time: 193.92 min.
T0=41.73 T1=34.78 T2=34.16
T3=33.62 T4=33.14 T5=32.70
T6=32.32 T7=31.99 T8=31.72

Time: 208.79 min.
T0=48.04 T1=36.79 T2=36.02
T3=35.34 T4=34.73 T5=34.21
T6=33.75 T7=33.38 T8=33.07

Time: 230.66 min.
T0=50.69 T1=41.74 T2=37.14
T3=36.61 T4=36.12 T5=35.68
T6=35.27 T7=34.91 T8=34.59

Time: 259.56 min.
T0=54.97 T1=46.34 T2=38.63
T3=38.13 T4=37.67 T5=37.24
T6=36.84 T7=36.47 T8=36.14

Time: 295.46 min.
T0=59.29 T1=51.67 T2=44.25
T3=40.38 T4=39.88 T5=39.41
T6=38.97 T7=38.57 T8=38.20

Time: 338.38 min.
T0=61.96 T1=55.14 T2=48.45
T3=41.94 T4=41.49 T5=41.05
T6=40.64 T7=40.25 T8=39.88

Time: 388.32 min.

T0=64.06	T1=57.87	T2=51.78
T3=45.81	T4=42.67	T5=42.26
T6=41.87	T7=41.50	T8=41.14

Time: 445.26 min.

T0=65.77	T1=60.10	T2=54.50
T3=49.00	T4=43.59	T5=43.21
T6=42.85	T7=42.49	T8=42.15

Time: 509.22 min.

T0=67.19	T1=61.96	T2=56.78
T3=51.67	T4=46.63	T5=43.97
T6=43.63	T7=43.29	T8=42.96

Time: 580.20 min.

T0=68.40	T1=63.54	T2=58.72
T3=53.96	T4=49.25	T5=44.62
T6=44.29	T7=43.97	T8=43.66

Time: 658.19 min.

T0=69.44	T1=64.90	T2=60.40
T3=55.93	T4=51.52	T5=47.16
T6=44.85	T7=44.54	T8=44.24

Time: 743.19 min.

T0=70.35	T1=66.09	T2=61.86
T3=57.67	T4=53.51	T5=49.40
T6=45.33	T7=45.04	T8=44.76

Time: 835.20 min.

T0=71.15	T1=67.14	T2=63.15
T3=59.19	T4=55.26	T5=51.37
T6=47.52	T7=45.48	T8=45.21

Time: 934.23 min.

T0=71.86	T1=68.07	T2=64.30
T3=60.55	T4=56.83	T5=53.14
T6=49.49	T7=45.75	T8=45.61

Time: 1040.27 min.

T0=74.15	T1=71.09	T2=68.07
T3=65.10	T4=62.18	T5=59.33
T6=56.54	T7=53.82	T8=52.49

Total time: 1153.21 min.

((Activated alumina, 84 °C))

T0 : Temp. at x= 0.00 cm
T1 : Temp. at x= 0.40 cm
T2 : Temp. at x= 0.80 cm
T3 : Temp. at x= 1.20 cm
T4 : Temp. at x= 1.60 cm
T5 : Temp. at x= 2.00 cm
T6 : Temp. at x= 2.40 cm
T7 : Temp. at x= 2.80 cm
T8 : Temp. at x= 3.20 cm

The predicted results are :

Time: 10.00 min.
T0=32.67 T1=32.10 T2=31.57
T3=31.07 T4=30.61 T5=30.19
T6=29.80 T7=29.45 T8=29.14

Time: 20.00 min.
T0=34.61 T1=34.03 T2=33.48
T3=32.96 T4=32.46 T5=31.98
T6=31.54 T7=31.12 T8=30.73

Time: 30.00 min.
T0=36.10 T1=35.51 T2=34.96
T3=34.42 T4=33.90 T5=33.41
T6=32.94 T7=32.49 T8=32.06

Time: 31.00 min.
T0=36.23 T1=35.65 T2=35.09
T3=34.55 T4=34.03 T5=33.54
T6=33.06 T7=32.61 T8=32.18

Time: 40.00 min.
T0=36.23 T1=35.65 T2=35.09
T3=34.55 T4=34.03 T5=33.54
T6=33.06 T7=32.61 T8=32.18

Time: 60.00 min.
T0=36.23 T1=35.65 T2=35.09
T3=34.55 T4=34.03 T5=33.54
T6=33.06 T7=32.61 T8=32.18

Time: 80.00 min.
T0=36.23 T1=35.65 T2=35.09
T3=34.55 T4=34.03 T5=33.54
T6=33.06 T7=32.61 T8=32.18

Time: 100.00 min.
T0=36.23 T1=35.65 T2=35.09
T3=34.55 T4=34.03 T5=33.54
T6=33.06 T7=32.61 T8=32.18

Time: 120.00 min.
T0=36.23 T1=35.65 T2=35.09
T3=34.55 T4=34.03 T5=33.54
T6=33.06 T7=32.61 T8=32.18

Time: 140.00 min.
T0=36.23 T1=35.65 T2=35.09
T3=34.55 T4=34.03 T5=33.54
T6=33.06 T7=32.61 T8=32.18

Time: 160.00 min.
T0=36.23 T1=35.65 T2=35.09
T3=34.55 T4=34.03 T5=33.54
T6=33.06 T7=32.61 T8=32.18

Time: 180.00 min.
T0=36.23 T1=35.65 T2=35.09
T3=34.55 T4=34.03 T5=33.54
T6=33.06 T7=32.61 T8=32.18

Time: 200.00 min.
T0=36.23 T1=35.65 T2=35.09
T3=34.55 T4=34.03 T5=33.54
T6=33.06 T7=32.61 T8=32.18

Time: 215.00 min.
T0=36.23 T1=35.65 T2=35.09
T3=34.55 T4=34.03 T5=33.54
T6=33.06 T7=32.61 T8=32.18

Time: 224.39 min.
T0=39.51 T1=34.51 T2=34.12
T3=33.78 T4=33.46 T5=33.16
T6=32.85 T7=32.55 T8=32.25

Time: 240.13 min.
T0=44.61 T1=36.14 T2=35.51
T3=34.95 T4=34.44 T5=34.00
T6=33.61 T7=33.27 T8=32.98

Time: 262.34 min.
T0=46.51 T1=39.75 T2=36.20
T3=35.75 T4=35.34 T5=34.96
T6=34.61 T7=34.30 T8=34.01

Time: 290.99 min.
T0=50.38 T1=43.54 T2=37.46
T3=37.02 T4=36.61 T5=36.22
T6=35.87 T7=35.54 T8=35.25

Time: 326.10 min.
T0=55.02 T1=48.84 T2=42.77
T3=39.52 T4=39.02 T5=38.56
T6=38.13 T7=37.74 T8=37.39

Time: 367.67 min.
T0=57.73 T1=52.12 T2=46.57
T3=41.11 T4=40.66 T5=40.23
T6=39.82 T7=39.43 T8=39.07

Time: 415.69 min.
T0=59.89 T1=54.73 T2=49.62
T3=44.58 T4=41.87 T5=41.46
T6=41.07 T7=40.70 T8=40.34

Time: 470.17 min.
T0=61.69 T1=56.92 T2=52.18
T3=47.48 T4=42.84 T5=42.46
T6=42.09 T7=41.72 T8=41.37

Time: 531.10 min.
T0=63.23 T1=58.78 T2=54.36
T3=49.97 T4=45.62 T5=43.28
T6=42.93 T7=42.58 T8=42.24

Time: 598.48 min.
T0=64.56 T1=60.39 T2=56.25
T3=52.13 T4=48.05 T5=44.00
T6=43.66 T7=43.32 T8=43.00

Time: 672.33 min.
T0=65.73 T1=61.81 T2=57.91
T3=54.03 T4=50.17 T5=46.35
T6=44.29 T7=43.97 T8=43.66

Time: 752.62 min.
T0=66.76 T1=63.06 T2=59.38
T3=55.71 T4=52.07 T5=48.44
T6=44.85 T7=44.54 T8=44.24

Time: 839.37 min.
T0=67.68 T1=64.17 T2=60.68
T3=57.21 T4=53.75 T5=50.31
T6=46.90 T7=45.05 T8=44.76

Time: 932.58 min.
T0=68.50 T1=65.18 T2=61.86
T3=58.56 T4=55.27 T5=52.00
T6=48.74 T7=45.39 T8=45.23

Time: 1032.24 min.
T0=71.26 T1=68.53 T2=65.81
T3=63.12 T4=60.45 T5=57.80
T6=55.18 T7=52.59 T8=51.30

Total time: 1138.25 min.

((Wood powder, 84°C))

T0 : Temp. at x= 0.00 cm
T1 : Temp. at x= 0.40 cm
T2 : Temp. at x= 0.80 cm
T3 : Temp. at x= 1.20 cm
T4 : Temp. at x= 1.60 cm
T5 : Temp. at x= 2.00 cm
T6 : Temp. at x= 2.40 cm
T7 : Temp. at x= 2.80 cm
T8 : Temp. at x= 3.20 cm

The predicted results are :

Time: 10.00 min.
T0=31.80 T1=30.12 T2=28.61
T3=27.25 T4=26.04 T5=24.99
T6=24.10 T7=23.37 T8=22.79

Time: 20.00 min.
T0=35.86 T1=34.16 T2=32.57
T3=31.10 T4=29.73 T5=28.48
T6=27.34 T7=26.30 T8=25.38

Time: 30.00 min.
T0=38.97 T1=37.26 T2=35.65
T3=34.12 T4=32.68 T5=31.34
T6=30.08 T7=28.92 T8=27.85

Time: 33.00 min.
T0=39.80 T1=38.09 T2=36.47
T3=34.93 T4=33.48 T5=32.11
T6=30.84 T7=29.64 T8=28.54

Time: 40.00 min.
T0=39.80 T1=38.09 T2=36.47
T3=34.93 T4=33.48 T5=32.11
T6=30.84 T7=29.64 T8=28.54

Time: 60.00 min.
T0=39.80 T1=38.09 T2=36.47
T3=34.93 T4=33.48 T5=32.11
T6=30.84 T7=29.64 T8=28.54

Time: 100.00 min.
T0=39.80 T1=38.09 T2=36.47
T3=34.93 T4=33.48 T5=32.11
T6=30.84 T7=29.64 T8=28.54

Time: 140.00 min.
T0=39.80 T1=38.09 T2=36.47
T3=34.93 T4=33.48 T5=32.11
T6=30.84 T7=29.64 T8=28.54

Time: 160.00 min.
T0=39.80 T1=38.09 T2=36.47
T3=34.93 T4=33.48 T5=32.11
T6=30.84 T7=29.64 T8=28.54

Time: 200.00 min.
T0=39.80 T1=38.09 T2=36.47
T3=34.93 T4=33.48 T5=32.11
T6=30.84 T7=29.64 T8=28.54

Time: 220.00 min.
T0=39.80 T1=38.09 T2=36.47
T3=34.93 T4=33.48 T5=32.11
T6=30.84 T7=29.64 T8=28.54

Time: 260.00 min.
T0=39.80 T1=38.09 T2=36.47
T3=34.93 T4=33.48 T5=32.11
T6=30.84 T7=29.64 T8=28.54

Time: 280.00 min.
T0=39.80 T1=38.09 T2=36.47
T3=34.93 T4=33.48 T5=32.11
T6=30.84 T7=29.64 T8=28.54

Time: 300.00 min.
T0=39.80 T1=38.09 T2=36.47
T3=34.93 T4=33.48 T5=32.11
T6=30.84 T7=29.64 T8=28.54

Time: 308.17 min.
T0=43.17 T1=34.58 T2=34.09
T3=33.64 T4=33.22 T5=32.82
T6=32.46 T7=32.13 T8=31.85

Time: 322.96 min.
T0=49.98 T1=36.12 T2=35.47
T3=34.89 T4=34.38 T5=33.92
T6=33.52 T7=33.18 T8=32.90

Time: 344.45 min.
T0=53.01 T1=41.92 T2=36.33
T3=35.87 T4=35.45 T5=35.06
T6=34.71 T7=34.38 T8=34.10

Time: 372.63 min.
T0=57.33 T1=46.94 T2=37.50
T3=37.07 T4=36.67 T5=36.30
T6=35.95 T7=35.63 T8=35.34

Time: 407.50 min.
T0=61.31 T1=52.19 T2=43.31
T3=38.77 T4=38.35 T5=37.95
T6=37.59 T7=37.24 T8=36.93

Time: 449.07 min.
T0=63.83 T1=55.69 T2=47.71
T3=39.94 T4=39.56 T5=39.19
T6=38.85 T7=38.52 T8=38.20

Time: 497.33 min.
T0=65.80 T1=58.44 T2=51.20
T3=44.09 T4=40.43 T5=40.10
T6=39.77 T7=39.46 T8=39.16

Time: 552.29 min.
T0=67.41 T1=60.69 T2=54.06
T3=47.53 T4=41.12 T5=40.81
T6=40.50 T7=40.21 T8=39.92

Time: 613.94 min.
T0=68.75 T1=62.56 T2=56.44
T3=50.40 T4=44.45 T5=41.37
T6=41.09 T7=40.80 T8=40.53

Time: 682.28 min.
T0=69.88 T1=64.15 T2=58.47
T3=52.85 T4=47.31 T5=41.85
T6=41.58 T7=41.31 T8=41.05

Time: 757.32 min.
T0=70.85 T1=65.51 T2=60.21
T3=54.96 T4=49.77 T5=44.65
T6=41.99 T7=41.73 T8=41.49

Time: 839.05 min.
T0=71.70 T1=66.70 T2=61.74
T3=56.81 T4=51.93 T5=47.11
T6=42.35 T7=42.11 T8=41.87

Time: 927.48 min.
T0=72.44 T1=67.74 T2=63.07
T3=58.43 T4=53.83 T5=49.27
T6=44.77 T7=42.43 T8=42.20

Time: 1022.60 min.
T0=73.10 T1=68.67 T2=64.26
T3=59.87 T4=55.52 T5=51.21
T6=46.94 T7=42.62 T8=42.50

Time: 1124.42 min.
T0=74.82 T1=71.10 T2=67.42
T3=63.79 T4=60.21 T5=56.69
T6=53.25 T7=49.87 T8=48.21

Total time: 1232.82 min.

((Glass beads 100 μm, 64°C))

T0 : Temp. at x= 0.00 cm
T1 : Temp. at x= 0.40 cm
T2 : Temp. at x= 0.80 cm
T3 : Temp. at x= 1.20 cm
T4 : Temp. at x= 1.60 cm
T5 : Temp. at x= 2.00 cm
T6 : Temp. at x= 2.40 cm
T7 : Temp. at x= 2.80 cm
T8 : Temp. at x= 3.20 cm

The predicted results are :

Time: 10.00 min.		
T0=25.18	T1=24.79	T2=24.43
T3=24.09	T4=23.78	T5=23.49
T6=23.23	T7=22.99	T8=22.78
Time: 20.00 min.		
T0=26.50	T1=26.11	T2=25.73
T3=25.38	T4=25.04	T5=24.71
T6=24.41	T7=24.13	T8=23.86
Time: 30.00 min.		
T0=27.52	T1=27.12	T2=26.74
T3=26.37	T4=26.02	T5=25.69
T6=25.36	T7=25.06	T8=24.76
Time: 40.00 min.		
T0=28.37	T1=27.97	T2=27.59
T3=27.22	T4=26.86	T5=26.51
T6=26.18	T7=25.86	T8=25.55
Time: 50.00 min.		
T0=29.12	T1=28.72	T2=28.34
T3=27.96	T4=27.60	T5=27.25
T6=26.91	T7=26.58	T8=26.26
Time: 60.00 min.		
T0=29.80	T1=29.40	T2=29.02
T3=28.64	T4=28.27	T5=27.92
T6=27.57	T7=27.24	T8=26.91
Time: 70.00 min.		
T0=30.43	T1=30.03	T2=29.64
T3=29.26	T4=28.89	T5=28.53
T6=28.18	T7=27.84	T8=27.51
Time: 80.00 min.		
T0=31.01	T1=30.61	T2=30.22
T3=29.84	T4=29.47	T5=29.11
T6=28.75	T7=28.41	T8=28.07

Time: 100.00 min.
T0=31.01 T1=30.61 T2=30.22
T3=29.84 T4=29.47 T5=29.11
T6=28.75 T7=28.41 T8=28.07

Time: 120.00 min.
T0=31.01 T1=30.61 T2=30.22
T3=29.84 T4=29.47 T5=29.11
T6=28.75 T7=28.41 T8=28.07

Time: 140.00 min.
T0=31.01 T1=30.61 T2=30.22
T3=29.84 T4=29.47 T5=29.11
T6=28.75 T7=28.41 T8=28.07

Time: 160.00 min.
T0=31.01 T1=30.61 T2=30.22
T3=29.84 T4=29.47 T5=29.11
T6=28.75 T7=28.41 T8=28.07

Time: 180.00 min.
T0=31.01 T1=30.61 T2=30.22
T3=29.84 T4=29.47 T5=29.11
T6=28.75 T7=28.41 T8=28.07

Time: 200.00 min.
T0=31.01 T1=30.61 T2=30.22
T3=29.84 T4=29.47 T5=29.11
T6=28.75 T7=28.41 T8=28.07

Time: 218.06 min.
T0=34.67 T1=32.63 T2=32.04
T3=31.56 T4=31.17 T5=30.88
T6=30.67 T7=30.53 T8=30.46

Time: 257.20 min.
T0=37.47 T1=36.61 T2=35.99
T3=35.42 T4=34.91 T5=34.46
T6=34.07 T7=33.73 T8=33.45

Time: 317.45 min.
T0=38.24 T1=36.49 T2=35.49
T3=35.23 T4=34.98 T5=34.74
T6=34.50 T7=34.28 T8=34.06

Time: 398.80 min.
T0=40.49 T1=38.11 T2=36.44
T3=36.18 T4=35.94 T5=35.70
T6=35.47 T7=35.25 T8=35.05

Time: 501.26 min.
T0=47.11 T1=45.16 T2=43.25
T3=42.09 T4=41.65 T5=41.23
T6=40.83 T7=40.46 T8=40.11

Time: 624.82 min.

T0=49.29	T1=47.59	T2=45.90
T3=44.24	T4=43.84	T5=43.46
T6=43.09	T7=42.72	T8=42.37

Time: 769.49 min.

T0=50.68	T1=49.14	T2=47.60
T3=46.08	T4=45.14	T5=44.78
T6=44.43	T7=44.09	T8=43.75

Time: 935.27 min.

T0=51.77	T1=50.35	T2=48.94
T3=47.54	T4=46.14	T5=45.81
T6=45.48	T7=45.15	T8=44.83

Time: 1122.15 min.

T0=52.68	T1=51.37	T2=50.06
T3=48.76	T4=47.46	T5=46.66
T6=46.35	T7=46.04	T8=45.74

Time: 1330.14 min.

T0=53.46	T1=52.24	T2=51.02
T3=49.81	T4=48.60	T5=47.39
T6=47.10	T7=46.81	T8=46.52

Time: 1559.23 min.

T0=54.14	T1=52.99	T2=51.85
T3=50.71	T4=49.58	T5=48.45
T6=47.75	T7=47.47	T8=47.20

Time: 1809.43 min.

T0=54.73	T1=53.66	T2=52.58
T3=51.51	T4=50.44	T5=49.38
T6=48.32	T7=48.06	T8=47.80

Time: 2080.74 min.

T0=55.26	T1=54.24	T2=53.23
T3=52.21	T4=51.21	T5=50.20
T6=49.20	T7=48.57	T8=48.33

Time: 2373.15 min.

T0=55.72	T1=54.76	T2=53.80
T3=52.84	T4=51.89	T5=50.93
T6=49.98	T7=48.95	T8=48.80

Time: 2686.67 min.

T0=59.66	T1=59.15	T2=58.65
T3=58.16	T4=57.66	T5=57.18
T6=56.70	T7=56.22	T8=55.98

Total time: 3021.13 min.

((Glass beads 100μm, 54 °C))

T0 : Temp. at x= 0.00 cm
T1 : Temp. at x= 0.40 cm
T2 : Temp. at x= 0.80 cm
T3 : Temp. at x= 1.20 cm
T4 : Temp. at x= 1.60 cm
T5 : Temp. at x= 2.00 cm
T6 : Temp. at x= 2.40 cm
T7 : Temp. at x= 2.80 cm
T8 : Temp. at x= 3.20 cm

The predicted results are :

Time: 10.00 min.
T0=24.24 T1=23.96 T2=23.71
T3=23.47 T4=23.25 T5=23.05
T6=22.86 T7=22.69 T8=22.55

Time: 20.00 min.
T0=25.16 T1=24.88 T2=24.62
T3=24.37 T4=24.13 T5=23.91
T6=23.69 T7=23.49 T8=23.30

Time: 30.00 min.
T0=25.87 T1=25.59 T2=25.33
T3=25.07 T4=24.82 T5=24.59
T6=24.36 T7=24.15 T8=23.94

Time: 40.00 min.
T0=26.47 T1=26.19 T2=25.92
T3=25.66 T4=25.41 T5=25.17
T6=24.94 T7=24.71 T8=24.49

Time: 50.00 min.
T0=27.00 T1=26.72 T2=26.45
T3=26.19 T4=25.93 T5=25.68
T6=25.45 T7=25.22 T8=24.99

Time: 60.00 min.
T0=27.48 T1=27.20 T2=26.92
T3=26.66 T4=26.40 T5=26.15
T6=25.91 T7=25.68 T8=25.45

Time: 70.00 min.
T0=27.91 T1=27.63 T2=27.36
T3=27.10 T4=26.84 T5=26.59
T6=26.34 T7=26.10 T8=25.87

Time: 80.00 min.
T0=28.32 T1=28.04 T2=27.77
T3=27.50 T4=27.24 T5=26.99
T6=26.74 T7=26.50 T8=26.26

Time: 82.00 min.
T0=28.40 T1=28.12 T2=27.85
T3=27.58 T4=27.32 T5=27.07
T6=26.82 T7=26.57 T8=26.34

Time: 100.00 min.
T0=28.40 T1=28.12 T2=27.85
T3=27.58 T4=27.32 T5=27.07
T6=26.82 T7=26.57 T8=26.34

Time: 120.00 min.
T0=28.40 T1=28.12 T2=27.85
T3=27.58 T4=27.32 T5=27.07
T6=26.82 T7=26.57 T8=26.34

Time: 160.00 min.
T0=28.40 T1=28.12 T2=27.85
T3=27.58 T4=27.32 T5=27.07
T6=26.82 T7=26.57 T8=26.34

Time: 180.00 min.
T0=28.40 T1=28.12 T2=27.85
T3=27.58 T4=27.32 T5=27.07
T6=26.82 T7=26.57 T8=26.34

Time: 200.00 min.
T0=28.40 T1=28.12 T2=27.85
T3=27.58 T4=27.32 T5=27.07
T6=26.82 T7=26.57 T8=26.34

Time: 240.00 min.
T0=28.40 T1=28.12 T2=27.85
T3=27.58 T4=27.32 T5=27.07
T6=26.82 T7=26.57 T8=26.34

Time: 260.00 min.
T0=28.40 T1=28.12 T2=27.85
T3=27.58 T4=27.32 T5=27.07
T6=26.82 T7=26.57 T8=26.34

Time: 290.00 min.
T0=32.72 T1=31.24 T2=30.82
T3=30.48 T4=30.22 T5=30.02
T6=29.90 T7=29.84 T8=29.84

Time: 355.64 min.
T0=37.31 T1=35.37 T2=34.99
T3=34.64 T4=34.32 T5=34.05
T6=33.80 T7=33.60 T8=33.42

Time: 456.94 min.
T0=39.77 T1=36.72 T2=35.15
T3=35.06 T4=34.98 T5=34.89
T6=32.81 T7=32.72 T8=32.64

Time: 593.92 min.

T0=43.36	T1=37.64	T2=36.59
T3=36.50	T4=33.41	T5=33.32
T6=33.24	T7=33.16	T8=33.08

Time: 766.56 min.

T0=43.48	T1=42.27	T2=41.07
T3=40.35	T4=40.11	T5=39.88
T6=39.66	T7=39.45	T8=39.25

Time: 974.88 min.

T0=45.03	T1=43.99	T2=42.95
T3=41.93	T4=41.72	T5=41.51
T6=41.31	T7=41.11	T8=40.92

Time: 1218.88 min.

T0=45.95	T1=45.02	T2=44.09
T3=43.16	T4=42.61	T5=42.42
T6=42.23	T7=42.05	T8=41.87

Time: 1498.54 min.

T0=46.69	T1=45.84	T2=44.99
T3=44.14	T4=43.31	T5=43.13
T6=42.96	T7=42.79	T8=42.62

Time: 1813.87 min.

T0=47.29	T1=46.51	T2=45.73
T3=44.96	T4=44.18	T5=43.72
T6=43.56	T7=43.40	T8=43.24

Time: 2164.88 min.

T0=47.80	T1=47.08	T2=46.36
T3=45.64	T4=44.93	T5=44.21
T6=44.06	T7=43.91	T8=43.76

Time: 2551.56 min.

T0=48.23	T1=47.56	T2=46.89
T3=46.23	T4=45.56	T5=44.90
T6=44.50	T7=44.35	T8=44.21

Time: 2973.91 min.

T0=48.61	T1=47.99	T2=47.36
T3=46.74	T4=46.11	T5=45.49
T6=44.87	T7=44.74	T8=44.61

Time: 3431.93 min.

T0=48.94	T1=48.36	T2=47.77
T3=47.18	T4=46.60	T5=46.01
T6=45.43	T7=45.08	T8=44.95

Total time: 3925.62 min.

APPENDIX D

EXPERIMENTAL RESULTS

Tables (D.1 to D.11) and (D.22 to D.24) :

T_0 represents temperature at x = 0 cm
T_1 represents temperature at x = 0.7 cm
T_2 represents temperature at x = 1.2 cm
T_3 represents temperature at x = 1.7 cm
T_4 represents temperature at x = 2.4 cm
T_5 represents temperature at x = 3.2 cm

Tables (D.12 to D.18) and (D.25 to D.29) :

T_0 represents temperature at x = 0 cm
T_1 represents temperature at x = 0.7 cm
T_2 represents temperature at x = 1.7 cm
T_3 represents temperature at x = 2.4 cm
T_4 represents temperature at x = 3.2 cm

Tables D.19 and D.21 :

T_0 represents temperature at x = 0 cm
T_1 represents temperature at x = 0.8 cm
T_2 represents temperature at x = 1.6 cm
T_3 represents temperature at x = 2.4 cm
T_4 represents temperature at x = 3.2 cm
T_5 represents temperature at x = 4 cm
T_6 represents temperature at x = 4.7 cm

Table D.20 :

T_0 represents temperature at x = 0 cm
T_1 represents temperature at x = 3 cm
T_2 represents temperature at x = 6.5 cm

Table D.1 Glass beads 100 μm

T_a = 84°C T_{wb} = 38°C
tray d = 8.3 cm L = 3.2 cm
W_w = 53.5 gm W_s = 266.5 gm

t min.	W_t gm	T_0 °C	T_1 °C	T_2 °C	T_3 °C	T_4 °C	T_5 °C
0	1050.6	21	21	21	22	22	22
4	1049.8	29	28	24	23.5	22	22
10	1048.6	32	29	27	26	24	24
15	1047.5	33	31	29	28	26	25
20	1046.7	34	32	30	28	27	26
30	1044.5	35	33	31	30	29	28.5
47	1041.2	36	34	33	32	31	30
65	1037.5	37	35	33	33	32	31
85	1033.5	37.5	36	35	34	33	32
105	1029.5	38	36	35	34	32.5	32
130	1024.5	37.5	36.5	35	34	33	32
150	1020.9	37.5	36	35.5	34	33	32
165	1018.2	39	36	35	34	33	32
180	1015.4	39	37	36	35	34	33
210	1010.7	42	39	37	36	35	34
240	1007.7	51	44	41	40	37	36
265	1005.0	57	47	43	41	39	38
290	1004.3	57	51	45	43	40	39
305	1003.8	61	51	47	44	41	40
315	1003.6	63	51	48	45	42.5	41
330	1003.4	64	59	50	46	43	42
345	1003.0	65	59	50	46	43	42
360	1002.6	66	61	53	46	43	42
375	1002.4	66.5	62.5	55	49	43	42
400	1002.0	68	64	58	54.5	43	42
430	1001.7	69	65	60	55	45	42
460	1001.4	69	65	61	56	47	42
490	1001.1	70	66	62	57	49	42
520	1000.9	71	66	62	58	51	42
550	1000.7	71	67	63	59.5	53	43
580	1000.6	72	67	63	59	54	44
600	1000.5	73	68	64	60	54	46

Table D.2 Glass beads 400 μm

T_a = 84°C T_{wb} = 38°C
tray d = 8.3 cm L = 3.2 cm
W_w = 61 gm W_s = 267 gm

t min.	W_t gm	T_0 °C	T_1 °C	T_2 °C	T_3 °C	T_4 °C	T_5 °C
0	1063.0	23	23	23	23	23	23
4	1062.2	29	26	24	23	22	22
10	1060.7	33	31	29	27	26.5	25
20	1058.7	35	33	32	31	29	28
30	1056.9	36	35	34	33	31	30
45	1053.7	37	36	35	34	33	32
60	1051.2	37	36.5	36	35	34	33
92	1044.9	38	37	36	35	34	33
123	1039.3	38	37	36	35	34	34
155	1032.2	38	37	36	35	34	33
195	1025.1	40	39	38	37	36	35
225	1019.0	41	40	39	38	37	36
245	1015.2	46	43	40	39	38	37
270	1011.3	46	46	41	40	39	38
300	1007.5	54	46.5	47	43	41	39
334	1005.4	63	52	48	46	44	42
360	1005.0	66	59	52	47	45	43
390	1004.1	68	62	56	48	45	43
420	1003.6	69	63	57	52	45	43
450	1003.4	70.5	64	58	53	45	43
480	1003.2	71	65	60	54	48	43
510	1003.1	71	67	62.5	55	50	46
540	1003.0	72	68	63	57	53	49
570	1003.0	73	70	65	59	54	51
600	1002.9	74	70	65	61	56	52

Table D.3 Glass beads 4000 μm

T_a = 84°C T_{wb} = 38°C
tray d = 8.3 cm L = 3.2 cm
W_w = 95 gm W_s = 210 gm

t min.	W_t gm	T_0 °C	T_1 °C	T_2 °C	T_3 °C	T_4 °C	T_5 °C
0	1013.9	21	22	22	22	22	22
10	1011.8	26	25	24	23	23	22
20	1009.7	30	29	28	27	26	25
30	1007.7	37	36	35	34	33	32
60	1001.5	37	36	35	34	33	32
75	998.4	37	36	35	34	33	32
100	994.5	41	39	37	36	35	33
120	992.5	46	41	39	37	36	35
150	988.1	46	43	41	39	38	36
180	983.8	47	44	43	40	40	37
210	980.7	51	44	43	41	40	39
240	977.7	55	46	43	41	40	39
270	974.8	60	49	43	42	40	39
300	971.9	63	54	45	43	41	39
330	969.0	65	55	48	43	41	39
360	966.2	68	57	50	46	40	39
390	963.5	70	59	52	48	40	39
410	961.0	72	60	53	49	40	39
440	958.3	73	61	54	50	40	39
470	955.8	74	63	54	51	43	39
500	953.3	75	65	56	52	45	39
530	950.9	76	67	58	54	46	39
560	948.6	77	68	60	55	47	39
600	946.3	78	70	61	56	48	42

Table D.4 Polystyrene pellets

T_a = 84°C T_{wb} = 39°C
tray d = 8.3 cm L = 3.2 cm
W_w = 71.5 gm W_s = 92.4 gm

t min.	W_t gm	T_0 °C	T_1 °C	T_2 °C	T_3 °C	T_4 °C	T_5 °C
0	887.5	15	15	15	15	15	15
4	886.3	28	16	19	16	15	15
10	883.9	33	30	26	22	18	16
15	882.6	34	31	28	25	21	18
20	881.4	35	32	30	26	22	19
30	879.4	36	34	32	29	25	22
40	877.4	36	35	34	31	27	24
50	875.4	36	35	34	32	29	25
60	873.5	36	36	35	33	30	26
70	871.6	37	36	35	34	31	28
82	869.6	37	36	35	34	31	28
90	868.1	37	36	35	34	31	28
100	866.4	37	36	35	34	31	28
110	865.0	38	37	36	35	31	29
120	863.6	38	36	36	35	32	29
135	861.6	38	37	37	35	33	30
150	859.6	39	38	38	36	33	31
180	856.3	41	39	39	38	35	32
210	853.3	42	41	40	38	35	33
240	850.8	48	42	41	38	35	33
260	849.1	52	42	41	39	36	33
290	846.7	57	48	42	40	36	33
322	844.3	57	51	43	40	37	34
340	843.0	59	54	43	40	36	33
370	841.1	61	55	43	40	37	34
405	839.0	62	56	48	41	37	34
436	837.0	63	56	49	41	37	34
460	835.8	63	56	49	41	37	34
480	834.7	64	57	50	41	37	34
510	833.3	65	59	51	41	38	34
540	831.9	65	59	52	41	38	35
570	830.7	66	60	53	43	38	35
600	830.0	68	62	55	45	38	35

Table D.5 Activated alumina, 150 mesh

T_a = 84°C T_{wb} = 38°C
tray d = 8.3 cm L = 3.2 cm
W_w = 100 gm W_s = 110 gm

t min.	W_t gm	T_0 °C	T_1 °C	T_2 °C	T_3 °C	T_4 °C	T_5 °C
0	890.7	27	30	31	31	30	29
6	888.2	30	33	32	31	31	30
10	887.4	31	33	33	32	31	31
15	885.2	31	34	34	33	32	31
20	884.0	34.5	34	34	33	32	32
30	881.5	35	34.5	34	34	34	32
45	877.5	35.5	35	35	34	34	33
60	873.7	36	35.5	35	35	34.5	34
80	868.3	36.5	36	35.5	35	34.5	34
90	865.9	36	36	36	35	34	34
105	861.9	36.5	35	35	35	34	34
140	853.6	36.5	35	35.5	35	34.5	34
150	851.0	37	36	35	35	34.5	34
165	847.4	36.5	36	35.5	35	34	34
180	843.7	36.5	36	35	35	34	34
195	840.0	36.5	36	35.5	35	34.5	34
210	836.8	38	37	36	35.5	34	34
233	832.2	39	37.5	36.5	35.5	35	34
240	831.5	40	38	37	36	35.5	34.5
255	829.8	49	38.5	38	36.5	36	35
270	828.2	54	39	38.5	38	36	35
285	826.3	58	40.5	39	38	36.5	35.5
300	824.6	60	41	40	39	38	36
320	823.0	63	41	41	39	38	36.5
340	822.3	65	44	42	40	39	37
360	821.3	66	46	42	40	38	37
380	820.6	66.5	47	41.5	40	38	37
400	820.0	67	48	42	40	38	37
420	819.5	68	49	42	40	38	37
440	818.2	68	50	42	40	38	37
460	818.1	68	51	44	39	38	36
480	817.6	69	52	45	40	38	36.5
500	817.2	69	54	46	40	38	37
520	816.8	70	56	48	40	38	37
540	816.5	71	57	49	40	38	37
560	816.3	71	59	51	43	38	37
580	816.1	72	60	53	44	38	37
600	816.0	72	61	55	46	38	37

Table D.6 Wood powder

T_a = 84°C T_{wb} = 39°C
tray d = 8.3 cm L = 3.2 cm
W_w = 78 gm W_s = 25.5 gm

t min.	W_t gm	T_0 °C	T_1 °C	T_2 °C	T_3 °C	T_4 °C	T_5 °C
0	838.0	21	22	22	22	22	22
5	837.2	31	30	26	23	23	22
10	836.2	35	33	30	30	28	29
15	835.5	38	37	34	31	30	30
20	834.6	39	38	35	33	32	30
25	833.9	40	38	36	34	33	31
30	833.1	40	38	37	35	34	32
35	832.6	40	38	37	36	35	33
40	831.8	40	38	38	36	35	34
50	829.9	40	39	38	37	36	34
60	828.4	41	39	38	37	37	35
75	825.8	41	39	38	37	36	36
90	823.7	41	40	39	38	37	36
105	821.4	41	40	39	38	37	36
120	819.2	41	40	39	38	37	36
140	816.0	41	40	39	38	37	36
150	814.4	41	40	39	37	37	35
165	812.0	41	40	39	37	36	35
180	809.7	41	40	39	37	36	35
195	807.5	42	40	39	37	36	35
210	805.1	44	41	38	37	36	35
240	801.0	45	41.5	38	37	36	35
255	799.1	46	42	39	37	36	35
270	797.0	46	43	39	38	36	35
285	794.9	48	45	39	38	37	35
300	792.4	50	45	40	38	37	35
330	790.0	57	45	40	38.5	37	35
345	787.9	61	45	40.5	38.5	37	36
360	787.2	65	48	41	39	37	36
375	785.7	66	49	41	39	37	36
390	784.9	67	50	41	39	37	36
405	783.8	68	51	41	39	37	36
420	782.8	69	52	41	39	37	36
435	782.2	69	54	41	39	37	36
460	781.2	69	55	41	39	37	36
480	780.2	69	56	42	39	37	36
510	779.2	70	57	44	39	37	36
540	777.7	71	58	48	39	37	36
570	777.4	71	59	49	39	37	36
600	776.9	71	60	50	42	37	36
630	776.8	72	61	52	44	37	36
660	776.7	72	63	54	45	37	36

Table D.7 Glass beads 400 μm

T_a = 74°C T_{wb} = 36°C
tray d = 8.3 cm L = 3.2 cm
W_w = 60 gm W_s = 266 gm

t min.	W_t gm	T_0 °C	T_1 °C	T_2 °C	T_3 °C	T_4 °C	T_5 °C
0	1049.2	21	21	21	21	21	21
5	1048.5	28	26	24	23	22	21
10	1047.8	30	28	26	24	23	22
15	1047.1	32	30	28	26	25	24
30	1045.0	34	33	31	30	29	27
45	1042.5	35	34	33	32	31	30
60	1040.4	36	36	35	34	33	32
90	1035.4	36.5	36	35	34	33	33
120	1030.8	36	36	35.5	35	34.5	34
150	1026.5	36.5	36	35.5	35	34	34
180	1021.9	36.5	36	35.5	35	34.5	34
210	1016.9	36	36	35	35	34	34
240	1012.4	36.5	36	36	35	34.5	34
270	1007.9	37.5	37	35	35.5	35	34
300	1003.3	40	39	36	36	36	34.5
330	999.3	42.5	41	37	37	38	35
360	995.6	45	43	39	38	39	36
380	993.8	48	45	42	41	40	36.5
400	993.2	48	46	43	42	40	37
420	992.5	52	46	44	43	40	37
450	991.2	56	52	45	44	40	38
480	991.1	58	53	50	44	41	38
510	991.0	59	55	51	47	41	38
540	990.6	60	56	52	48	41	38
570	990.4	61	57	53	49.5	44	38
600	990.3	62	58	54	50	45	38
630	990.1	63.5	59	55	50	45	38
660	990.0	64	59	55	51	46	38
690	990.0	66	61	56	52	47	41

Table D.8 Glass beads 100 μm

T_a = 64°C T_{wb} = 33°C
tray d = 8.3 cm L = 3.2 cm
W_w = 53.5 gm W_s = 266.5 gm

t min.	W_t gm	T_0 °C	T_1 °C	T_2 °C	T_3 °C	T_4 °C	T_5 °C
0	1039.0	22	22	22	22	22	22
10	1037.0	24.5	24	24	23	23	23
20	1035.4	26.5	26	25.5	25	24.5	24
25	1034.8	27	27	26	25	25	24.5
30	1033.8	28	27.5	27	26	25.5	25
40	1031.9	29	28	27.5	26.5	26.5	26
50	1030.0	30	29	29	28	27.5	27
60	1028.2	31	30	30	29	28.5	28
76	1025.0	31.5	31	30.5	30	29.5	29
90	1022.2	31.5	31	31	30	30	29.5
105	1019.4	31	31	31	30.5	30	29
120	1016.6	31.5	31	31	30	30	29.5
135	1014.1	32	31.5	31	30.5	30	29
150	1011.2	32	31	31	30	30	29
180	1006.0	31.5	31	31	30	30	29.5
210	1001.8	31.5	31.5	31	30	31	30
240	998.1	32	32	31	31	32	31
270	995.1	37	35	34.5	34	33	31
300	993.7	39	37	36	35	33	32
330	992.8	39	39	37	36	34	33
360	991.9	46	40	38	37	35	34
390	991.0	47	43	38.5	37	35	34
420	990.7	48	45	39	38	36	35
450	990.4	49	47	44	39	36	35
480	990.2	50	47	44	42	37	35
510	990.1	50	48	45	42	37	34
540	989.9	51	48	45	42	39.5	35
570	989.8	52	49.5	46	43	39	35
600	989.7	52	49	46	43	40	35
620	989.7	53	50	47	44	41	35
660	989.6	55	51	48	45	42	37

Table D.9 Glass beads 100 μm

T_a = 54°C T_{wb} = 30°C
tray d = 8.3 cm L = 3.2 cm
W_w = 53.5 gm W_s = 268 gm

t min.	T_0 °C	T_1 °C	T_2 °C	T_3 °C	T_4 °C	T_5 °C
0	22	22	22	22	22	22
10	26	26	25	24	24	24
20	27	27	26	26.5	27	25
30	28	28	27	26	26	26
40	28	28	28	27	27	26
50	29	28.5	28	28	27	27
60	29	28	28	28	27.5	27.5
70	29	28.5	28	28	28	28
80	29	29	28.5	28	28	28
90	29	29	28.5	28.5	28	28
105	29	29	28.5	28	28	28
120	29	29	28.5	28	28	28
135	29	29	29	28.5	28	28
150	29	29.5	29	29	28.5	28
165	29.5	29	29	29	28	28
187	29.5	29	29	29	28.5	28
195	29	29.5	29	29	28.5	28.5
210	29.5	29	29	29	28.5	29
240	29	29.5	29	29	28.5	29
260	29.5	29.5	29	29	28.5	29
280	34	33	32	31	30	29
300	36	35	33	32	31	30
330	37	36	34	33	31	30
360	38	37	35	33	32	31
390	38	37	35	34	32	31
420	39	38	36	34	32	32
450	44	39	36	34	33	32
480	44	42	37	34	33	32
510	45	42	37	34	33	32
540	45	42	39	35	34	32
570	46	43	39	35	34	32
600	46	43	40	35	34	32
630	47	44	41	36	34	32

Table D.10 Pure distilled water

T_a = 84°C T_{wb} = 38°C
tray d = 8.3 cm L = 3.2 cm
W_w = 155 gm

t min.	W_t gm	T_0 °C	T_1 °C	T_2 °C	T_3 °C	T_4 °C	T_5 °C
0	877.7	21	21	21	21	21	21
5	876.4	32	29	26	24	24	22
8	875.7	35	30	28	25	25	23
10	875.0	36	32	29	26	26	23
15	873.7	36	33	31	28	27	24
20	872.3	37	33	31	29	27	25
25	871.0	38	33	32	31	29	27
30	869.8	39	34	33	31	30	28
40	867.8	42	35	34	32	31	29
45	866.8	43	35	34	33	31	30
50	865.6	44	37	34	33	32	30
60	863.4	55	37	34	33	32	31
70	861.1	60	37	35	34	33	32
75	860.0	62	37	35	34	33	33
83	857.9	65	37	35	34	34	33
85	857.4	66	40	36	35	35	33
90	856.6	67	40	35	35	34	33
110	852.5	68	43	36	36	35	34
120	850.5	69	44	37	37	36	35
140	846.6	70	46	37	37	36	35
150	844.4	71	50	37	37	36	35
160	842.3	71	55	37	37	36	35
170	840.3	71	60	37	37	36	35
180	838.3	72	65	37	37	36	35
185	837.5	73	70	37	37	36	35
195	835.5	75	73	39	37	36	35
200	834.6	76	74	40	37	37	36
220	831.1	77	75	41	37	37	36
240	827.6	77	75	43	37	37	36
270	822.7	78	76	44	37	37	36
280	821.2	78	77	48	37	37	36
300	817.8	78	77	57	37	37	36
315	815.3	78	77	70	37	37	36
330	813.2	78	78	76	37	37	36
340	811.6	78	78	76	37	37	36
350	809.9	79	78	77	38	37	37
360	808.2	79	79	77	40	37	37
375	805.8	80	79	77	41	37	37
400	802.2	80	79	78	43	37	37
430	797.7	80	79	78	46	37	37
460	793.1	80	79	78	50	37	37
480	789.8	81	80	79	54	37	37
510	785.7	81	80	79	60	37	37
540	781.4	81	80	79	62	37	37
570	777.1	82	80	79	65	37	37
600	772.8	83	81	80	66	39	37
630	768.5	83	81	80	67	41	37
660	764.2	84	82	81	68	45	37

Table D.11 Dry bed of glass beads 100 μm

T_a = 84°C
tray d = 8.3 cm
T_{wb} = 39°C
L = 3.2 cm
W_s = 278.2 gm

t min.	T_0 °C	T_1 °C	T_2 °C	T_3 °C	T_4 °C	T_5 °C
0	24	24	24	24	24	24
5	52	42	33	33	27	27
10	59	50	43	42	34	28
15	60	52	46	45	37	30
20	62	55	51	48	41	33
30	65	59	55	52	46	38
40	68	60	58	56	49	40
60	72	68	64	61	52	47
80	75	70	67	63	55	49
100	78	75	69	63	55	50
120	80	76	70	63	56	51
150	80	76	71	63	56	52
180	82	77	71	63	56	52
210	82	77	72	63	56	52
240	83	78	72	63	56	52
270	83	78	72	64	56	52
285	83	78	72	64	57	53
300	83	78	72	64	57	53
330	83	78	71	63	56	52
360	83	78	72	64	57	53
390	83	79	72	64	57	53
420	83	79	72	64	57	53
450	83	79	72	64	57	53
480	83	79	72	64	57	53
510	83	79	72	64	57	53
540	83	79	72	64	57	53
570	83	79	72	64	57	53
600	83	79	72	64	57	53

Table D.12 Glass beads 100 μm

T_a = 84°C
tray d = 5.3 cm
W_w = 22.5 gm
T_{wb} = 38°C
L = 3.2 cm
W_s = 108.5 gm

t min.	W_t gm	T_0 °C	T_1 °C	T_2 °C	T_3 °C	T_4 °C
0	728.8	20	20	21	21	21
6	728.1	31	28	28	28	27
10	727.7	34	34	35	35	34
15	726.9	38	40	43	44	43
20	726.3	40	45	49	50	50
30	725.1	40	46	52	54	55
40	723.6	41	49	53	55	56
45	723.0	42	49	54	56	57
50	722.4	41	50	54	56	57
60	720.9	42	50	55	56	57
75	718.9	42	51	54	57	57
90	716.9	42	52	54	56	57
105	714.8	44	52	54	57	58
120	713.0	48	52	55	58	59
135	711.2	49	53	57	59	60
150	709.9	52	55	57	60	60
165	708.8	55	57	58	61	61
180	708.0	57	58	58	60	61
195	707.7	60	60	60	61	61
210	707.4	71	64	63	64	61
225	707.2	75	72	67	64	60
230	707.2	77	74	69	65	61
235	707.1	77	74	70	66	63
240	706.9	77	75	71	67	64
255	706.9	77	76	72	69	66
270	706.8	78	76	73	69	66
285	706.7	79	76	73	69	67
300	706.7	80	77	73	70	67
330	706.6	81	78	73	70	67
350	706.6	81	78	73	70	67

Table D.13 Glass beads 400 μm

T_a = 84°C T_{wb} = 39°C
tray d = 5.3 cm L = 3.2 cm
W_w = 30 gm W_s = 123 gm

t min.	W_t gm	T_0 °C	T_1 °C	T_2 °C	T_3 °C	T_4 °C
0	656.2	21	22	23	23	23
10	654.3	38	40	42	41	39
20	652.6	43	49	52	52	51
30	651.0	45	51	55	56	57
60	646.7	45	53	55	57	58
90	642.8	45	53	55	57	58
120	638.7	45	53	55	57	59
150	635.0	46	54	55	58	59
182	630.9	47	54	55	59	59
210	628.0	54	56	58	61	61
240	626.6	76	68	62	63	62
274	626.4	79	76	74	71	70
300	626.3	80	78	76	73	72
330	626.3	80	78	76	73	72
360	626.2	81	78	76	73	72
375	626.2	82	79	76	73	72
400	626.2	82	79	77	73	72

Table D.14 Polystyrene pellets

T_a = 84°C T_{wb} = 39°C
tray d = 5.3 cm L = 3.2 cm
W_w = 36 gm W_s = 46 gm

t min.	T_0 °C	T_1 °C	T_2 °C	T_3 °C	T_4 °C
0	20	20	20	20	20
10	40	41	39	40	36
15	44	44	42.5	41	42
20	46	45	43	41	45
30	47	45	47	45	49
40	47	47	50	47	53
50	46	50	50	50	55
60	46	50	53	56	57
75	46	50	52	57	57
80	46	50	53	56	57
85	46	50	53	56	57
90	46	50	53	56	57
100	46	50	52	56	57
105	46	50	53	56	56
110	46.5	52	53	55	56.5
120	47	52	54	57	57.5
130	47	52	53.5	57	57
155	48	52	54	57	57
170	49	51	53.5	56	56
180	49	58	58	58	57
200	60	59	58	58	57
225	61	59	59	58	57.5
250	62	60	60	59	58
275	63	60	60.5	59	58
300	65	61.5	61	59	58
325	67	62	61	59	58
350	70	62	61	59	58

Table D.15 Activated alumina, 150 mesh

T_a = 84°C T_{wb} = 38°C
tray d = 5.3 cm L = 3.2 cm
W_w = 40 gm W_s = 43.5 gm

t min.	W_t gm	T_0 °C	T_1 °C	T_2 °C	T_3 °C	T_4 °C
0	594.50	24	25	24	25	24
6	594.06	34	33	33.5	34	34
10	593.70	37	38	39	40	39
15	592.98	40	44	46	48	47
20	592.32	42	47	51	53	52
30	590.00	44	51	55	58	57
45	588.60	44	53	58	59	60
60	586.42	44	53	58	59	60
75	584.25	44	54	58	59.5	60
90	581.95	44	54	58	59	60
105	579.64	44	54	58	59	60
120	577.52	44	54	58	59	60
142	574.42	44	54	58	59.5	60
150	573.40	44	54	58	59	60
165	571.54	46	54	58	59	60
180	570.15	48	54	58	59	60
195	569.00	53	54	58	59	60
210	568.10	53	50	55	58	59
225	567.40	58	52	55	58	59
240	566.54	63	55	55	59	59
255	565.95	65	55	57	60	59
270	565.28	70	57	59	60	60
285	564.80	73	63	60	62	61
300	564.48	75	66	61	63	61
315	563.86	75	67	61	63	61
330	563.66	76	68	61	63	62
345	563.40	77	69	62	63	62
360	563.06	77	69	62	63	62
375	562.90	77.5	70	62	63	62
390	562.83	77	70	62	63	62
405	562.54	77	70	62	63	62
420	562.50	78	71	63	63	62
435	562.30	78	72	64	64	62
450	562.10	78	72	65	64	62
465	562.08	79	73	65	64	62
480	562.07	79	73	65	64	62
495	562.07	79	74	66	64	62
510	562.06	79.5	75	67	64	62
525	562.06	80	75.5	68	64	62
540	562.06	80	76	68.5	64	62
555	562.05	81	76.5	69	64	62
570	562.05	81	77	70	65	62
585	562.05	81.5	77	71	66	62
600	562.05	82	77.5	71.5	67	62

Table D.16 Wood powder

T_a = 84°C T_{wb} = 39°C
tray d = 5.3 cm L = 3.2 cm
W_w = 43 gm W_s = 14 gm

t min.	W_t gm	T_0 °C	T_1 °C	T_2 °C	T_3 °C	T_4 °C
0	193.8	21	22	22	22	22
10	192.5	33	33	38	36	33
20	190.98	38	43	49	47	45
30	189.6	40	48	54	53	51
45	187.12	42	50	57	55	56
60	185.0	43	51	55	57	56
90	180.46	42	51	55	57	56
120	176.11	42	51	55	57	56
150	172.1	43	51	55	57	56
180	168.32	43	51	55	57	56
210	164.7	43	51	55	57	56
240	161.5	45	51	57	57	56
270	159.32	51	49	57	56	53
300	157.5	58	49	56	55	52
345	155.33	66	49	53	54	51
360	155.06	67	50	53	53	51
390	154.17	69	54	53	52	51
420	153.5	72	58	54	52	52
450	153.06	73	62	56	53	51
485	152.38	75	66	58	56	54
520	151.3	74	67	59	57	54
600	151.04	76	72	60	62	57

Table D.17 Glass beads 100 μm

T_a = 84°C T_{wb} = 39°C
tray d = 2.6 cm L = 3.2 cm
W_w = 7 gm W_s = 35 gm

t min.	T_0 °C	T_1 °C	T_2 °C	T_3 °C	T_4 °C
0	21	21	22	21	22
5	25	24	24	23.5	23
10	27	27	26.5	25	25
15	30	28	28	27	26
25	35	34	32	31	30
35	39	39	38	37	37
45	39	40	40	41	42
55	43	44	45	46	50
65	43	46	51	53	56
75	43	46.5	52	57	59
85	43	47	52	57.5	59
95	45	49	52	57	59.5
105	50	51	53	57.5	59
115	63	60	55	58.5	60
125	68	60	62.5	61	60
135	71	62	64	62	60
150	73	66	64	63	61
165	75	70	64	63	61
180	76	72	68	63	61
200	76	74	70	63	61

Table D.18 Glass beads 100 μm

T_a = 84°C T_{wb} = 38°C
tray d = 6.2 cm L = 3.2 cm
W_w = 51 gm W_s = 250 gm

t min.	W_t gm	T_0 °C	T_1 °C	T_2 °C	T_3 °C	T_4 °C
0	505.5	20	21	21	21	21
5	504.7	25	25	24	25	26
10	503.6	29	30	30	31	31
15	502.0	34	35	35	36	36
20	501.2	37	38	39	39	41
30	498.4	40	42	45	43	47
45	494.4	40	42	47	48	49
60	490.3	40	43	47	48	50
75	486.6	41	43	47	48	50
90	482.9	41	43	47	49	50
120	475.9	41	43	47	49	50
150	469.8	41	44	48	49	50
165	465.4	41	45	48	50	51
184	461.0	45	47	49	52	53
215	455.0	55	56	56	56	56
240	454.8	64	62	58	57	57
280	454.7	74	68	65	61	58
300	454.6	75	71	69	61	58

Table D.19 Glass beads 100 μm

T_a = 84°C T_{wb} = 38°C
tray d = 5.3cm L = 4.7 cm
W_w = 30 gm W_s = 150 gm

t min.	T_0 °C	T_1 °C	T_2 °C	T_3 °C	T_4 °C	T_5 °C	T_6 °C
0	21	21	21	22	22	22	22
5	27	25	24	23	23	23	23
10	30	29	28	26.5	26	26	26
15	32	33	32	30	30	30	29
20	34	34	34	33	34	34	32
30	36	38	38	37	38	38	38
40	37	40	41	40	41	41	41
50	38	41	42	42	43	43	43
60	38	41	43	43	45	45	45
75	39.5	42.5	44	44	45	46	46
90	39.5	42.5	44	44.5	45.5	46	46
105	40	42.5	44	44.5	45.5	46	45
120	39.5	43	44	44.5	45	46	46
135	39.5	42.5	44	44.5	45	46	46
150	40	42.5	44	44.5	45.5	47	46
165	41	44	45	46	46	47	46.5
180	42	44	45.5	46	46.5	47	47
210	44	45	46	46	46	47	47
225	44	46	47	47	47	48	47
240	45	47	48	47	47.5	48	47
255	47	48	48	48	48	48	47.5
270	49	49	49	49	49	49	48
285	51.5	50	50	49	49	49	48
300	51.5	51	51	50	50.5	49	47
315	54	52	51.5	51	50.5	50	48
330	56	52	51.5	51	50	50	48
345	57	52	52	51	50	50	48
360	59	52.5	52	51	51	50	47
375	62	53	51	51	50	50	48
390	63	55	52	51	50	50	48
405	65	58	52	51	50.5	49	48
420	67	61	55	51	50	50	48
435	68	62	58	51	50.5	50	47
450	69	64	60	54	50.5	50	48
465	69	65	61	56	54	52	48
480	70	67	64	58	56	54	48
495	71	66	62	57	57	54	48
510	71	66	62	58	57	53	49
525	71	66	62	58	57	54	50
540	71	66	62	58	57	53.5	50
555	71.5	66	62	57.5	57	54	50.5
570	72	66.5	62	58	57	54	51
585	72.5	67	62.5	58	57	54	50.5
600	73	67.5	63	58.5	57	54	50.5

Table D.20 Glass beads 100 μm

T_a = 84°C T_{wb} = 37°C
tray d = 2.6 cm L = 6.5 cm
W_w = 12 gm W_s = 50 gm

t min.	T_0 °C	T_1 °C	T_2 °C
0	24	23	23
15	31	30	32
30	34	36	37
45	36	40	42
60	37	42	45
75	37	43	46
90	38	43	46
105	38	43	48
120	38	44	48
135	39	44	48
150	39	44	49
165	39	44	49
180	40	45	49
195	40	45	49
210	41	45	49
225	41	45	50
240	42	45	50
255	43	46	50
270	45	51	50
285	48	52	51
300	49	53	51
315	51	53	51
330	53	54	52
345	55	55	52
360	56	55	52
375	57	56	52
390	58	56	52
405	59	56	52
420	60	57	53
435	62	57	53
450	65	57	53
465	67	57	53
480	69	56	52
495	71	56	52

Table D.21 Glass beads 100 μm

T_a=84 C T_{wb}=37°C
tray: d=8.3 L=4.7 cm
W_w=80 gm W_s=400 gm

t min.	T_0 °C	T_1 °C	T_2 °C	T_3 °C	T_4 °C	T_5 °C	T_6 °C
0	20	20	20	20	20	20	20
5	27	25	23	21	21	21	21
10	29	27	26	24	23	22	21
15	30	29	28.5	25	24	23	21
20	31	30	29	26	26	24	22
30	31	30	30	28	27	25	23
45	32	31	31	29	29	27	24
60	32.5	32	31	30	29	28	25
77	33	32.5	32	30	30	28	26
90	33.5	33	32.5	31	30	29	27
105	34	33	32.5	32	30	29.5	28
120	34	33	33	32	30.5	30	28
135	34	32	33	32	31	30	28
150	33	33	33	32	30	30	29
165	33.5	33	33	32	31	30	28
180	34	33	32	32	31	30	29
195	34	33.5	33	32	31	30	28
210	35	34	33	32	31	31	28
225	35	35	34	32	32	30	28
240	35.5	35	34	33	32	30	28
255	36	35.5	35	33	32	31	28.5
270	36.5	36	35	33.5	32	31	29
285	37	36	36	34	33	31.5	29
300	37	37	36	34	33	32	29
315	38	37	36.5	34	33	32	29
330	39	37	37	35	34	32	29.5
345	39	38	37	35	34	33	30
360	39.5	38	37	35.5	34	33	30
375	41	38	37	36	35	33	31
390	42	38.5	38	36	35	33.5	30
405	43	40.5	38.5	36	35	34	30.5
420	44	41	38.5	37	36	34	30.5
435	46	41.5	39	37	36.5	35	31
450	48	42	40.5	38	37	35	31
465	51	43	41	39	37	35	31
480	53	44	42	40	37	34	32
495	54	45	43	39.5	38	35	32
510	55	46	44	40	38	35	31
525	56	47	45	41	38	35	31
540	57	48	46	42	38	34	32
555	58	49	46.5	42	38	35	32
570	58.5	50	47	43	38.5	35	32
585	59	50	47	43.5	40	35	32
600	60	51	48	44	42	35	32

Table D.22 Glass beads 100 μm

air flow parallel to the length
T_a=84 C T_{wb}=38°C
rect. tray:l=8.3 cm, w=3.7 cm, L=3.2 cm
W_w=34 gm W_s=163 gm

t min.	T_0 °C	T_1 °C	T_2 °C	T_3 °C	T_4 °C	T_5 °C
0	22	22	22	22	22	22
5	29	28	24	23	22.5	22
10	32	29	27	26	24	24
15	33	31	29	28	26	25
20	34	32	30	28	27	26
30	35	33	31	30	29	28
45	36	34	33	32	31	30
60	36	35	34	33	32	31
80	37	36.5	35	34	33.5	33
105	37.5	36	35	34.5	34	33.5
130	38	36.5	35	34.5	34	33
155	38	36	35	34.5	34	34
165	38	36.5	35	34.5	35	34.5
180	39	37.5	36	35.5	35.5	35
215	42	39	37	36	36.5	36
240	51	44.5	41	40	38	37
260	55.5	47	43	41	40	39
280	58	51	45	43	40.5	40
300	61	52	47	44	41.5	41
315	63	52.5	48	45	43	42
330	64	58	49	45.5	44	43
345	65.5	59	50	46	44	43
355	66	61	53	46.5	44	43
370	67	62	55	49	44	43
395	68	65	58	55	44	43
425	70	66	61	56	45	43
450	72	67	63	58	48	43.5
480	73	70	65	60	51	43
510	76	72	68	62	55	43

Table D.23 Glass beads 100 μm

air at right angle to length
T_a = 84°C T_{wb} = 37°C
rect. tray:l = 8.3 cm w = 3.7 cm, L = 3.2 cm
W_w = 34.5 gm W_s = 163 gm

t min.	T_0 °C	T_1 °C	T_2 °C	T_3 °C	T_4 °C	T_5 °C
0	22	22	22	22	22	22
5	29	28	24	23	22.5	22
10	32	29	27	26	24	24
15	33	30	29	28	25.5	25
20	34	32	30	28	27	26
30	35.5	33	31	30	29	27
45	36	33.5	33	31.5	31	30
60	36	35	34	33	32	33
80	37	36	34.5	34	33	34
105	37.5	36	35	34.5	34	35.5
130	38	36	36	34.5	34	35
155	38	36	35	34	34	35
165	38	36.5	36	35	35	34
180	39	37.5	36	35	35.5	35
215	44.5	38	37	36.5	36.5	36
240	51	44.5	41	40	38	38
260	57	47	43	41	40	39
280	57.5	50.5	45	42.5	40.5	40
300	61	53	47	44	41.5	41
315	62.5	54	47.5	45	43	42.5
330	64	57	49	46	44	43
345	65.5	59	50	47	44	43
355	66	61	52.5	48	44	42
370	67	62	55	49	44	43.5
395	68	65	58	55	44	43
425	70	66	60	56	45	42.5
450	71	67	63	58	48	43
480	73	70	65	60	51	43
510	75	72	67.5	62	55	43

Table D.24 Glass beads 100 μm

T_a = 84°C T_w = 38°C
rect. tray: l = 5.3 w = 3.7 cm, L = 3.2cm
air flow parallel to the the length
W_w = 19.5 gm W_s = 98 gm

t min.	T_0 °C	T_1 °C	T_2 °C	T_3 °C	T_4 °C	T_5 °C
0	22	22	21	21	21	21
5	31	28	28	29	28	28
10	34	34	35	36	35	35
15	38	41	42	43.5	45	43
20	40	45	47	49	50	51
30	40	46	48	52	54	55
40	41	49	50	53	55	57
50	42	50	52	55	57	58
60	43	50	52	56	57	58
75	43	50	52	55	57	57
90	43	51	52	56	57	58
100	43	51	52	56	57	59
110	47.5	52	53	57	58.5	59
120	48	52	54	57	58	60
135	49	52	55	58	59	61
150	52.5	54	55	58	61	60
160	55	57	58	58	61	61
180	59	58	59	59	60	62
200	61	60	60	61	61	62
210	71	65	65	64	64	61
220	75	72	70	68	65	61
230	76	74	72	69	65	62
240	76	75	73	72	67	65
260	76	75	73	72	69	67
270	76	75	74	73.5	69	67
285	77	76	74	73.5	69	67
300	78	77	74	73	71	67
330	78	78	75	74	71	68
350	79	78	75	74	71	68
380	79	77	75	74	71	67
410	79.5	78	76	75	72	68
440	79.5	78	76	75	73	68

Table D.25 Glass beads 100 μm

T_a= 64°C T_{wb}= 33°C
tray d = 5.3 cm L=3.2 cm
W_w= 22 gm W_s= 108 gm

t min.	T_0 °C	T_1 °C	T_2 °C	T_3 °C	T_4 °C
0	20	21	20	21	20
6	27	26	27	27	26
10	30	31	33	34	33
15	32	34	38	39	38
20	34	37	40	42	41
30	36	40	42	43	44
45	38	42	44	45	46
60	38	42	44	45	46
90	39	43	45	46	47
105	39	43	45	46	47
120	39	43	45	46	47
150	39	44	45	46	47
165	39	44	45	46	47
180	40	44	45	46	47
195	40	45	46	47	47
210	41	45	46	47	48
225	43	47	47	48	48
240	44	48	47	47	48
255	45	48	47	48	48
270	48	49	47	48	49
285	53	50	48	49	49
300	56	52	48	49	49
315	59	56	51	50	48
330	60	58	55	54	48
345	60	59	57	56	49
360	61	60	57	56	49
375	61	60	58	57	50
390	61	60	58	56	50

Table D.26 Glass beads 100 μm

T_a= 54°C T_{wb} = 31°C
tray d = 5.3 cm L = 3.2cm
W_w= 22.5 gm W_s = 108 gm

t min.	T_0 °C	T_1 °C	T_2 °C	T_3 °C	T_4 °C
0	20	21	20	21	20
5	24	26	27	27.5	25
10	27	30	31	32	30
15	29	33	34	35	35
30	30	34	35	36	38
45	32	35	36	37	39
60	34	35	34	37	39
75	35	36	37	38	40
90	36	37	38	39	40
105	37	38	39	39	40
130	37	37	39	39	40
150	38	38	39.5	39	40
170	37	38	39	39	41
190	37	38	39	39.5	40
215	37.5	38	38	39	40.5
235	37	38	39	39	40
255	38	38	39	39	41
270	39	38	39	40	41
285	38	39	40	40	42
300	39	40	41	41	42
320	40	40	41	41.5	42
330	41	40	41	41	42
345	44	43	42	41	42
360	45	45.5	44	44	43
375	47	46	45.5	45	43
390	50	46	45	45	44
420	51	48	46	45	43
440	52	49	46	45	44

Table D.27 Pool of distilled water

T_a= 84°C T_{wb}= 39°C
tray d = 2.6 cm L = 3.2 cm
W_w= 25 gm

t min.	T_0 °C	T_1 °C	T_2 °C	T_3 °C	T_4 °C
0	18	18	18	18	18
5	27	23	20	19	19
10	39	36	33	30	29
15	49	40	39	39	39
25	51	46	39	39	39
35	54	50	41	39	39
40	55	55	49	40	40
50	58	57	54	40	40
60	58	58	55	40	40
70	59	59	58	40	40
75	61	61	60	40	40
85	68	62	62	42	40
100	72	65	63	58	41
115	76	69	65	59	41
130	79	73	67	62	41
150	81	78	70	67	41
160	80	78	72	68	50
170	81	80	74	70	56
200	81	80	77	75	64
230	82	81	77	76	65
260	82	81	77	76	65

Table D.28 Pool of distilled water

T_a= 84°C T_{wb} = 39°C
tray d = 5.3 cm L = 3.2cm
W_w= 78 gm

t min.	T_0 °C	T_1 °C	T_2 °C	T_3 °C	T_4 °C
0	22	22	21	21	21
10	41	39	38	37	37
20	41	41	40	40	40
30	42.5	42	42	43	43
45	42.5	42	42	43	43
51	42	42	43	43	43
70	43	42	43	43	43
90	49	43	43	44	43
120	52	43	43	44	44
155	57	47	44	43	44
180	61	62	43	43	44
190	61	62	45	44	44
210	63	65	45.5	44	44
220	63	65	46	44	44.5
240	66	66	47	44	43
260	72	70	52	45	43
300	76	74	60	49	44

Table D.29 Bed of dry glass beads 100 μm

T_a = 84°C T_{wb} = 38°C
tray d = 5.3 cm L = 3.2 cm

t min.	T_0 °C	T_1 °C	T_2 °C	T_3 °C	T_4 °C
0	21	21	20	21	22
5	52	39	28	28	31
10	62	52	42	41	39
15	68	61	52	49	45
20	71	66	59	55	49
30	75	72	66	62	54
40	76	74	69	64	56
50	76	74	70	65	57
60	77	75	70	66	58
70	78	75	70	66	58
80	78	75	70	66	59
90	79	75	70	66	60
105	79	76	70	66	60
120	80	76	70	66	60
135	80	76	70	66	60
150	81	76	70	66	60
165	81	76	70	65	60
180	81	76	70	66	60
195	81	76	70	66	60
210	81	76	70	66	60
225	81	76	69	66	60
240	81	76	70	66	60
260	81	76	70	66	60
280	81	76	70	66	60
320	81	76	70	66	60
360	81	76	70	66	60
380	81	76	70	66	60

APPENDIX E

PUBLICATIONS

1. "Variation of Temperature Gradient According to Material Width in Convective Drying", Proceedings of The 1995 ICHEME Research Event, First European Conference, Vol. 2, pp 886-888, Edinburgh, U.K., January 4-6, 1995.

2. "Characteristics of The Receding Evaporation Front in Convective Drying", Proceedings of The 9th International Drying Symposium, Volume A, pp 231-238, Gold Coast, Australia, August 1-4, 1994.

3. "Mechanisms of Convective and Conductive Drying", Proceedings of The Second Scientific Conference, National Union of Kuwaiti Students, pp 25-27, London, U.K., April 24-25, 1993.

THE 1995 ICHEME RESEARCH EVENT / FIRST EUROPEAN CONFERENCE

VARIATION OF TEMPERATURE GRADIENT ACCORDING TO MATERIAL WIDTH IN CONVECTIVE DRYING

A.A.ALMUBARAK & C.J.MUMFORD
Department of Chemical Engineering &Apllied Chemistry , Aston University

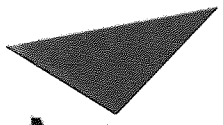

Aston University

CHARACTERISTICS OF THE RECEDING EVAPORATION FRONT IN CONVECTIVE DRYING

A. A. ALMUBARAK and C. J. MUMFORD
Department of Chemical Engineering and Applied Chemistry
Aston University, Birmingham, U.K.